The Role of the Nuclear Factor-kappa B Subunit, p52, in Ribosomal Stress

EMMA KIM CORBIN

Submitted for Doctor of Philosophy

Submission: March 2023

Biosciences Institute

Faculty of Medical Sciences

Newcastle University

Abstract

Activation of the NF-κB transcription factor family forms one of the first lines of defence against environmental threats to the organism and helps programme an appropriate cellular response. Although best known as critical regulators of the inflammatory response, the NF-κB family of transcription factors are also activated by cellular stresses such as hypoxia, DNA damage and play an important role in ageing. Aberrant activation of NF-κB is associated with many inflammatory diseases and cancer.

In work leading up to this thesis, the p52 NF-κB subunit was found to interact with the ribosomal protein RPL11. RPL11 is a component of the 5S RNP, an essential ribosomal subcomplex, comprised of the 5S ribosomal (r)RNA and the ribosomal proteins RPL5 and RPL11. Under conditions of ribosomal stress, free 5S RNP accumulates, carrying out a pivotal role in the stress response by binding to MDM2 and activating p53 tumour suppressor activity.

In this thesis I have further investigated the p52/RPL11 interaction and the role of p52 during ribosomal stress. I found that depletion of p52 from cancer cell lines led to increased cell death in response to ribosomal stress. A combination of *in silico* analysis and co-immunoprecipitation experiments indicated that the MDM2/RPL11 and p52/RPL11 interactions are mutually exclusive. I propose that competition between MDM2 and p52 contributes to the differences in p53-dependent cellular fate during ribosomal stress. Finally, residue glutamate 86 (E86) of p52 was predicted *in silico to* be critical within the p52/RPL11 interface. Through mutation of E86 to alanine, this was later confirmed. Interestingly, the disruption of the RPL11 interaction caused by of the p52-E86A mutation was dependent upon DNA binding. In summary, I propose that p52 plays a cell survival and tumour promoting role following ribotoxic stress through direct binding to RPL11 that facilitates the modulation of p53 target gene expression.

Declaration and Acknowledgements

I certify that the work presented in this thesis is my own, except where acknowledged. I would firstly like to extend a thank you to my undergraduate student, Aleksandra Sukova and my Masters and Research student, Kirsten Ramsay, for their exceptional work under my supervision.

I am grateful to my supervisors, Prof. Neil Perkins, Dr Nick Watkins and Dr Alessio Iannetti for the opportunity, and my progression panel Prof. Jon Higgins and Dr Elaine Wilmore. A big thank you to Prof Perkins for seeing my potential as an undergraduate and supporting me all the way.

A special thank you to the members of the Perkins laboratory, past and present. Namely, Dr Jill Hunter, Dr Iglika Ivanova and Nikita Dhillon. Without the support from these three incredible women in science, this thesis simply would not have been possible. Thank you for helping me through some extremely difficult times. I feel incredibly lucky to have been part of such a great team.

I would also like to thank members of the Watkins laboratory, past and present, specifically Dr Justine Lee and Isabella Lawrence for patiently teaching me techniques.

A big thank you to Dr Niall Kenneth, my mentor, for giving the best pep talks. Thank you for introducing me to the world of research and always helping me, even from afar.

I cannot begin to express the gratitude for the team at Yoga X Life for keeping me sane and providing me with the tools I needed to make my way through the latter stages of the PhD. Thank you for helping me become who I am today.

Finally, I'd like to thank my family and friends for putting up with me through the years, for picking me up when I was down and, at times, piecing me back together.

Contents

x

List of Figures

List of Tables

Chapter 1   Introduction

1.1. Transcription factors

Transcription factors (TF) carry out a critical role in the decoding of the information contained in the genome. These proteins regulate the transcription of DNA to RNA that ultimately leads to the production of proteins. The most recent estimate counted 1639 human TFs (Göös et al., 2022). Their primary function is to bind to, and regulate the expression of, target genes through specific DNA recognition sequences (Vaquerizas et al., 2009). Previously, any protein involved in transcription was called a TF, however now only proteins that can carry out both roles is attached to the name. Target genes of TFs usually fall into categories that allow the regulation of specific pathways, cellular responses or even cell types (Lambert et al., 2018). Interestingly, in different cell types the same TF can regulate different target genes allowing co-ordination of cell-specific responses (Gertz et al., 2012). The amino acid sequences of TFs are often highly conserved between species (Bejerano et al., 2004). Mutations in TFs are frequently linked to the onset of disease (Lee and Young, 2013). For example, mutations in the tumour suppressor protein p53 is found to be present in various cancers. Further, mutant TFs are linked to neurological diseases, such as Huntington's disease, as well as developmental disorders, such as autism.

A vital counterpart to the TF is the DNA sequence to which it binds. TFs can have at least a 1000-fold greater affinity for their sequence in comparison to other DNA motifs (Geertz et al., 2012). Identifying motifs that serve as TF binding sites is key to facilitating the understanding of TF mechanisms, their target genes and therefore their role in cellular biology. Once a TF makes contact with its preferred motif, gene regulation can be induced in a variety of ways. For example, some work by recruiting the transcription machinery, such as RNA polymerase, while others work by creating a steric block that prevents the assembly of transcription machinery (Lambert et al., 2018). The majority of eukaryotic TFs are known to recruit cofactors that act as transcriptional coactivators, or corepressors. Thus, it is thought that TFs act to assemble multi-subunit protein complexes to carry out the regulation of target genes (Reiter et al., 2017). Some famous transcription factors include, the master regulator of inflammation, NF-κB (Gilmore, 2006), and the guardian of the genome, tumour suppressor p53 (Vousden and Prives, 2009).

1.2. The NF-κB family of transcription factors

The Nuclear Factor kappa B (NF-κB) family of transcription factors was originally discovered in 1986 (Sen and Baltimore, 1986). In almost 40 years of research, there have been over 100,000 publications across the breadth of the field and it is clear to say that the NF-κB family play an important cellular role. The family consists of five members, the Rel proteins: RelA (p65), RelB and c-Rel, and the NFKB proteins; NFKB1 (p50/p105) and NFKB2 (p100/p52) (Perkins and Gilmore, 2006). These protein subunits respond to specific cellular stimuli to form homo- and heterodimers in order to regulate the transcription of a large set of target genes. The regulation of target genes can be specific to the original, pathway activating, stimulus and the dimer subsequently formed (Chen et al., 1998, Ghosh et al., 1995, Cramer et al., 1997). Most famously, the NF-κB signalling pathway is described as a cellular defence mechanism in response to infection and stress. In addition, it has been demonstrated that the NF-κB pathway responds to various stimuli, such as DNA damage and hypoxia (van Uden et al., 2008, Campbell et al., 2001). Furthermore, it has been found that the NF-κB family is involved in a vast and complex cellular signalling web and plays a role in processes such as cellular senescence (Rovillain et al., 2011), ageing (García-García et al., 2021) and even in coral bleaching (Mansfield et al., 2017).

NF-κB activation usually occurs through either the canonical or non-canonical signalling pathways; with rare occasions leading to the activation of atypical signalling pathways (Liu et al., 2022a). The canonical pathway is closely associated with genes regulating the inflammatory response, more specifically the upregulation of pro-inflammatory genes. Whereas, the non-canonical pathway is mostly connected with the immune response and genes involved in B- and T- cell development (Perkins and Gilmore, 2006).

The correct execution of the NF-κB pathway relies upon the action of two further protein families, the IκB family and the IKK family (Liu et al., 2022a). The former are a family of repressor proteins that ensure the NF-κB pathway is not able to be constitutively active. The latter is involved in the activation of the NF-κB dimers by phosphorylating and inactivating IκB proteins, allowing active dimers to travel to the nucleus.(Karin, 1999). Constitutively active NF-κB has been implicated in various diseases demonstrating the importance of tightly controlling the process of NF-kB activation (Yu et al., 2020, Gilmore, 2021) .

1.2.1. Evolution of the NF-κB family

The NF-κB family has been found to be highly conserved across a range of species, from single-cell protoists to sea sponges, coral and jellyfish; and finally flies and vertebrates (Ghosh et al., 1998, Mansfield et al., 2017). This further highlights the important role of this signalling cascade to serve as a cellular defence mechanism. Additionally, many of the NF-κB inducing receptors are conserved across species. The most conserved domain in the NF-κB subunits is the Rel Homology Domain (discussed in section 1.2.2) with the region determining DNA binding being the most conserved amino acid sequence. Studies in sea sponges have shown that the NF-κB pathway is involved in early development and later in sponge immunity. NF-κB has also been found to play a role in the early development of coral, jellyfish and sea anemone (Williams and Gilmore, 2020). It is clear the family of transcription factors have evolved to play a pivotal role in cellular signalling.

The development and increasing complexity of innate immunity created a demand for a more complex regulatory system that drove the evolution of NF-κB from a single subunit to a family of proteins with roles still being discovered. The manner in which NF-κB evolved over the years was initially unclear; due to the lack of NF-κB subunits in yeast and *Caenorhabditis elegans* it was assumed the origin was no earlier than arthropods (Irazoqui et al., 2010). Through the discovery of NF-κB in *Cnidarians* (coral, sea anemones and hydra) as well as *Capsaspora owczarzaki*, a single cell metazoan isolated from freshwater snails, the beginnings of the NF-κB family can be placed at about 1000 million years ago in *Opisthokonta*, a eukaryotic group including metazoa and fungi (Gauthier and Degnan, 2008). The true origin of the Rel Homology Domain is still unknown (Figure 1.1). It has now been demonstrated, however, that NF-κB within evolutionarily basal organisms resembles that of more complex organisms in terms of structure, biological relevance and regulatory function (Gauthier and Degnan, 2008). These early forms of NF-κB particularly resemble the NFKB proteins p105 and p100, or the *Drosophila* Relish protein, due to the inclusion of an ankyrin repeat domain alongside the RHD (Williams et al., 2018). The single cell protist, *Capsaspora* was found to contain a protein resembling that of the modern mammalian NFKB1 or NFKB2 protein, containing a fusion of a RHD and ANK domain (Suga et al., 2013). It is believed that during eukaryotic evolution a primitive protein containing solely the Rel Homology Domain evolved to be able to interact with an ankyrin repeat protein, as seen in *Capsaspora*

(Jernigan and Bordenstein, 2014). These genes eventually fused to create a protein containing both domains, resembling that of the mammalian NFKB1 and NFKB2 genes (Williams and Gilmore, 2020).

It is likely that regulatory mechanisms with the capability to remove whole repressor proteins had not yet evolved in the cell to activate NF-κB properties (Sullivan et al., 2007). Therefore, the basal eukaryotes favoured the expression of a protein containing both the active and repressor domain. Alternatively, the IκB protein and Rel Homology Domain could have had entirely different roles within the cell, but as higher organisms emerged the need for transcriptional regulation and a more complex immune system became apparent, the development of the Rel and IκB proteins was required (Williams and Gilmore, 2020). It is proposed that the NF-κB family evolved to be the multi-member family through gene splitting, duplication and divergence, depicted in Figure 1.1. The evolution of the NF-κB subunits and the mechanism of gene splitting, duplication and divergence is not well documented in the literature.

The gene splitting hypothesis describes the event in which a copied gene splits into two or more sections (Oakley and Rivera, 2008). Each section of the gene would be able to duplicate and diverge independently. Through studying unicellular eukaryotes, it emerged that some species had a C terminal ankyrin repeat domain in NF-κB whilst others did not; this was the basis of the gene splitting hypothesis (Gilmore and Wolenski, 2012).

The earliest evidence of diversification of RHD proteins is in Choanoflagellates, a unicellular eukaryote. Analysis of this biological group identified a large range of NF-κB-like proteins, which varied between species. This speaks to the differences that can arise from each singular evolutionary pathway, even within species in the same group. (Williams and Gilmore, 2020). Furthermore, no proteins resembling the Rel family members were found until the search in sea urchins and vertebrates suggesting the gene duplication and divergence of the Rel subfamily occurred 600-550 million years ago (Pancer et al., 1999).

Overall, the apparent reliance of species, from unicellular eukaryotes to complex vertebrates, upon NF-κB proteins displays the huge importance of this family in the development and innate immunity of a vast range of living organisms.
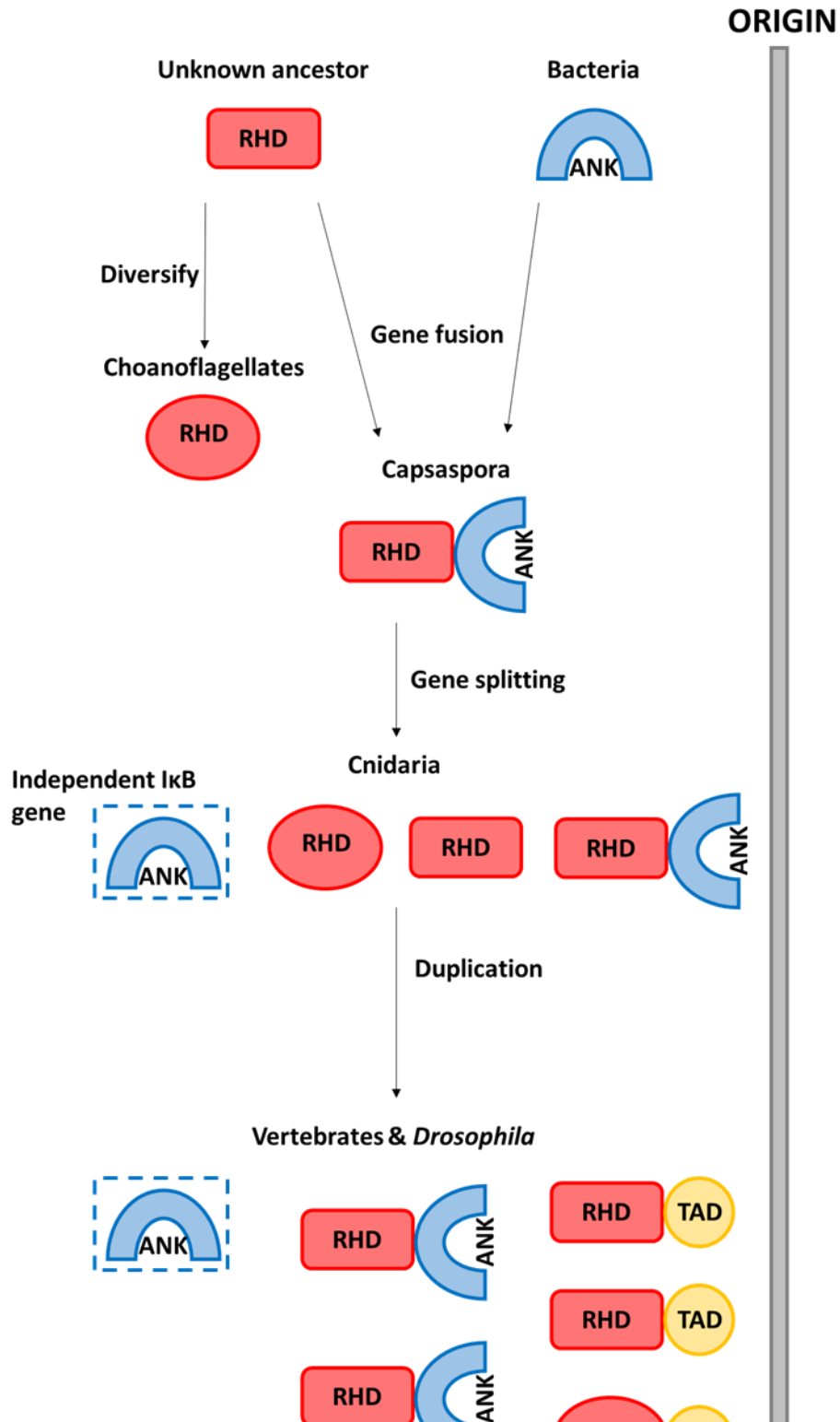
Figure 1.1 The evolution of the NF-κB family. Starting with the origin of the family, represented by a single RHD (Rel Homology Domain) protein. Separately, bacteria contained ankyrin repeat proteins (ANK). As time progressed these domains diversified, fused and duplicated to form the NF-κB family as it is known in Vertebrates and Drosophila. The evolution of the independent IκB gene occured through gene splitting events. Similarly, it is believed that the gene duplicated to form the members of the repressor family that are known today. Figure adapted from Williams and Gilmore, 2020.

1.2.2. Mammalian NF-κB family

As discussed above, the members of the NF-κB family can be placed into two groups. The Rel proteins (RelA, RelB and c-Rel) and the NFKB proteins (p105/p50 and p100/p52). The proteins are grouped in this manner based on their structural homology. Whilst all of the members contain a set of structural domains which define their association with the NF-κB family, the Rel proteins have a different subset of domains to the NFKB proteins (Figure 1.2). The structural domain that defines an NF-κB subunit, is the Rel Homology Domain (RHD). This domain possesses the ability to bind to DNA, to dimerise with other subunits, interact with negative regulators and the nuclear localisation sequence (NLS). The NLS allows the proteins to be imported into the nucleus. (Chen et al., 1998). It can be seen in Figure 1.2 that all of the NF-κB subunits possess this domain. The differences in the structures between the Rel and NF-κB proteins lie within the C terminus. The Rel proteins have a transactivation domain (TAD). The TAD functions to allow transcriptional activation upon binding to DNA. The NF-κB proteins, however, are lacking this domain (Gilmore, 2006). Therefore, dimers including solely p50 or p52 proteins require interactions with co-activator and co-repressor proteins to enable the regulation of target genes. The C termini of the NF-κB proteins contain ankyrin repeat domains, also found in the IkB proteins (Cartwright et al., 2018). These serve an inhibitory function, sequestering dimers in an inactive form. Downstream of the ankyrin repeat region, p100 and p105 contain a PEST domain. This is a domain rich in proline, glutamate, serine and threonine amino acids and is a region that can be highly modified. It is within that domain that phosphorylation events occur that lead to the subsequent proteasomal processing of the longer forms of the proteins (Ghosh et al., 1998). Upstream of the ankyrin repeat domains is the glycine rich region (GRR). During proteasomal processing of the longer, inactive, forms of the proteins, p105 and p100, the GRR signals processing machinery to stop allowing the generation of the shorter, active, forms of the proteins, p50 and p52, respectively (Gilmore, 2006).

Through crystallographic studies it can be seen that the secondary structures of the RHD regions of the five subunits are generally very similar. However, the NF-κB proteins also possess a short, flexible, linker region within the RHD that separates the dimerisation domain and the DNA binding domain (Cramer et al., 1997, Ghosh et al., 1995). This gives

insight into the degree of variation given by each dimer toward their preferential DNA

binding sequence, referred to as a κB site.
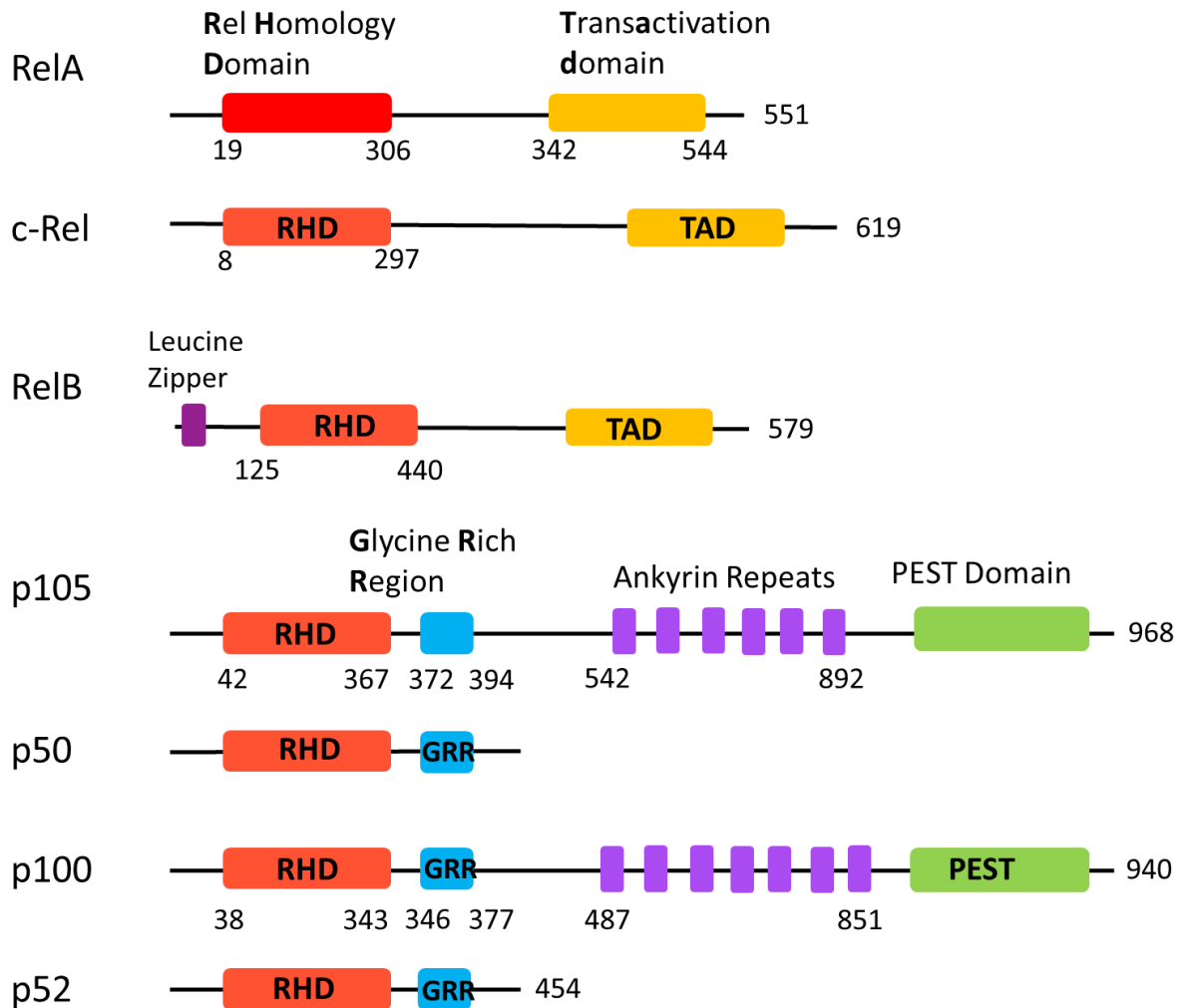
Figure 1.2 The mammalian NF-κB family. Schematics to represent the structural domains of the mammalian NF-κB family. Including the five members, RelA, c-Rel, RelB, p105/p50 and p100/p52. Residue numbers are indicated underneath some structural domains and at the end of the proteins. The structures are depicted from the N terminus (left) to the C terminus (right).

1.2.3. Dimerisation and DNA binding

The five members of the NF-κB family form dimers in order to function. In theory, most dimer combinations can occur with the exception being RelB homodimers. In the cellular environment not all dimer combinations have been able to be observed experimentally and preferential dimer combinations exist (Karin et al., 2002). The most well-known heterodimer is the RelA/p50 dimer. It was suggested that RelB has a preference for p52 and p50 for stabilisation, however RelB/p52 heterodimers are more commonly described. The c-Rel subunit is mostly found in a heterodimer with p50 or RelA as well as forming homodimers. These different dimer combinations can form as a result of different cellular stimuli leading to the activation of different NF-κB pathways (Figure 1.3). It is important to note that dimer formation can be influenced by cellular environments, such as tissue specificity to facilitate the co-ordination of a specific response (Wang et al., 2012). Furthermore, different techniques used in different cellular conditions can misrepresent the abundance NF-κB dimers have in the cell. It is clear, however, different NF-κB dimers hold preferences toward different DNA sequences.

Active NF-κB dimers translocate to the nucleus of cells in order to bind to and regulate the expression of target genes. This is mediated by a highly conserved ~300 residue long section of the RHD, mostly residing in the N-terminus of the domain (Wang et al., 2012). The solved crystal structure of RelA/p50 bound to DNA allowed further insight into understanding the mechanism behind the NF-κB signalling cascade. The published structure revealed the now well documented butterfly structure formed by NF-κB dimers when in the DNA bound form (Chen et al., 1998). Since the RelA/p50 structure was solved (Chen et al., 1998), the crystal structure of the p52 homodimer bound to DNA (Cramer et al., 1997), the p50 homodimer bound to DNA (Ghosh et al., 1995) and c-Rel bound to DNA have been solved (Huang et al., 2001). The release of the aforementioned solved crystal structures bound to different sequences of DNA revealed that, across the different dimers, each monomer contacted DNA in a base-specific manner (Wang et al., 2012).
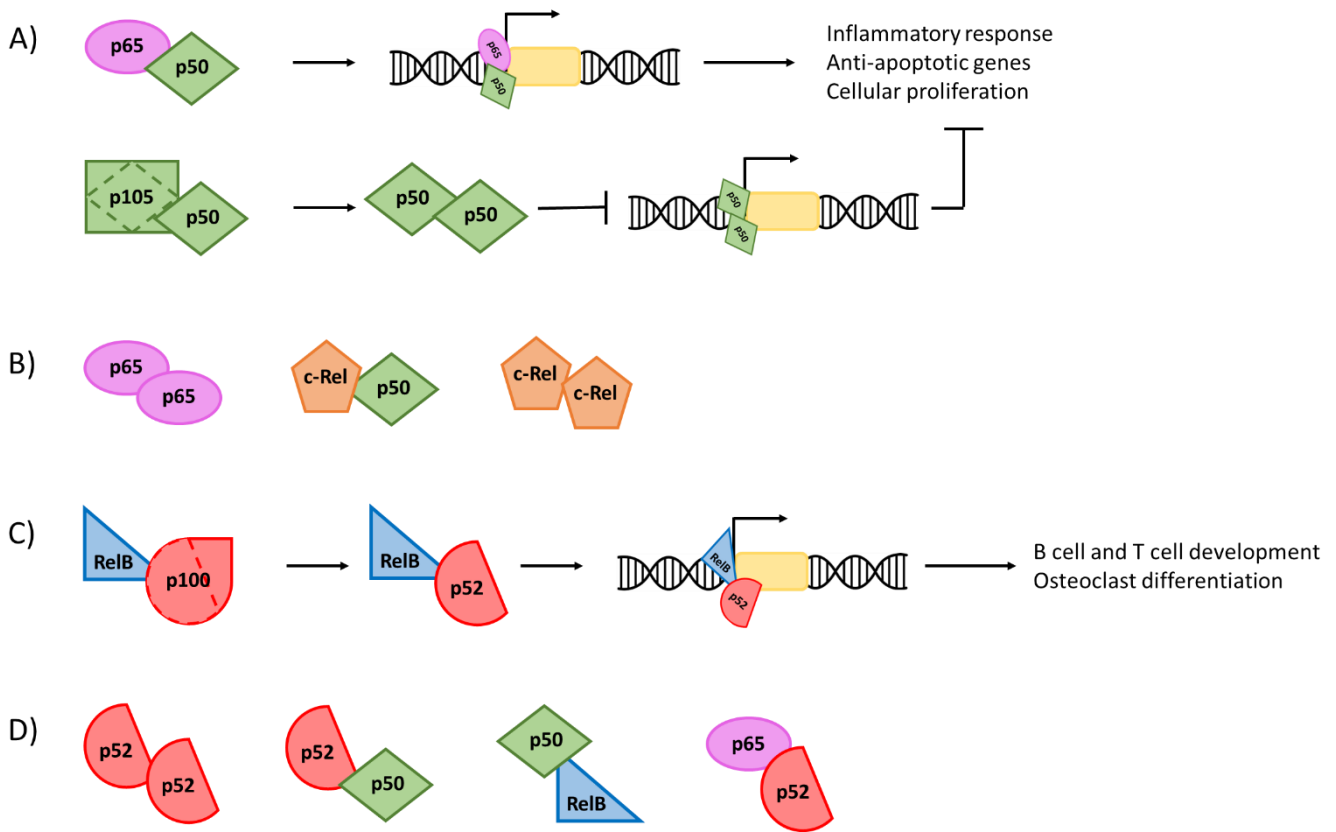
Figure 1.3 Examples of NF-κB dimers. A) The most researched canonical NF-κB dimer is the p65/p50 heterodimer. The activation of this dimer usually leads to the regulation of pro-inflammatory genes, as well as anti-apoptotic genes and genes involved in cellular proliferation. The p105/p50 dimer is activated through the proteolytic processing of p105 to p50. The then active p50 homodimer is usually repressive. B) Other dimers known to signal through the canonical signalling pathway. C) The RelB/p100 heterodimer is subject to proteasomal processing to activate the non-canonical pathway. The active RelB/p52 heterodimer regulates genes involved in immune cell development and osteoclast differentiation. D) Alternative non-canonical pathway-associated dimers.

The short sequences of DNA that the dimers interact with are called κB sites, or κB elements. It has been shown through genomic analysis that these sites are present in the promoter regions of hundreds of genes. All of the solved structures of NF-κB dimers in a DNA bound state display the unique 'butterfly structure' conformation. The dimers are described to 'straddle' DNA. (Chen et al., 1998, Ghosh et al., 1995, Cramer et al., 1997). Moreover, NF-κB dimers use flexible loops to contact DNA where most other TFs use α helices (Chen and Ghosh, 1999). Whilst there is a consensus sequence for the κB elements (5'-GGGRNYYYCC-3'; where R = purine, Y = pyrimidine and N = any nucleotide), there is a level of redundancy due to each dimer preferentially binding to a variant of the consensus (Perkins and Gilmore, 2006). Originally, p65 was not believed to have a role in direct DNA binding due to the inability to capture p65-DNA interactions in the laboratory. However, it was determined that p65 bound to specific sequences of κB sites that had not yet been determined (Chen and Ghosh, 1999). Early studies of different dimer-κB preferences determined the classical κB sites and the variations of which the different dimers could bind to (Kunsch et al., 1992, Perkins et al., 1992).Homo- and heterodimers including the subunits p65, p50 and c-Rel were analysed for DNA binding affinities within a random pool of oligonucleotides. The sequences were then aligned to determine a consensus. The study was also able to determine the sequence specificity of the different subunits and dimer combinations.

The exceptions are p52 homodimers, which do not bind 'classical' NF-κB sites, such as the kappa Ig enhancer and HIV LTR, and prefer palindromic sequences (Perkins et al., 1992). In addition, the c-Rel subunit was shown to have the optimum binding sequence of 5'-NGGRN(A/T)TTCC-3', which is distinctly different to other subunits (Gilmore and Gerondakis, 2011). Furthermore, it has been proposed that the sequence of the κB sites, specifically, the central base pair, can dictate whether a gene is repressed or expressed by an NF-κB dimer (Wang et al., 2012) . Dimers involving RelA preferentially bind to sequences with A/T at the centre and function to activate transcription when bound to these sites. Interestingly, an *in vitro* experiment revealed that RelA dimers are unable to form a strong bond with G/C centric κB sites. When studying the sequence of the κB sites that RelA dimers bind and induce transcriptional repression, there is a significant difference compared to the consensus sequence. On the other hand, p52 homodimers are able to form tight bonds with

G/C at the centre of the sequence (Wang et al., 2012). These homodimers are unique as they first, have a consensus sequence of 5'-GGRRNNYYCC-3', and secondly require cofactors to regulate gene expression (Cramer et al., 1997). It has been documented that p52 homodimers complexed with Bcl-3 upregulate gene expression when bound to G/C centric κB elements, however, when the sequence is A/T centric, the homodimer complex is repressive (Wang et al., 2012). The variation in κB site preference can also be regulated by post-translational modifications. This has been particularly studied in the p50 subunit (Wang et al., 2017). Phosphorylation of the protein at serine 337 is required for DNA binding, whilst serine 242 inhibits DNA binding capabilities. Further studies found that phosphorylation patterns led to the regulation of different subsets of target genes. For example, TNFα leads to phosphorylation of serine 80 of p50 by IKKβ led to p50/p65 heterodimers to bind kB sites with adenine at position -1 with a lower affinity (Smith et al., 2019). Many genes encoding inflammatory cytokines have such κB sites. Therefore, post translational modifications are a way that cellular mechanisms regulate the action of transcription factors to facilitate an appropriate response to specific stress.

1.2.4. The IκB family of repressors

The IκB repressor protein family consists of three canonical members: IκBα, IκBβ, IκBε and two atypical members; Bcl-3 and IκBξ (Figure 1.4). The canonical IκBs repress NF-κB signalling by interacting with members of the family through the Rel Homology domain and sequestering the dimers in an inactive form (Hoffmann et al., 2002). This action is mediated by ankyrin repeat domains. Upon activation of the signalling cascade, these proteins are targeted for phosphorylation, which is followed by K48-linked ubiquitination leading to degradation via the 26S proteasome. The canonical IκBs contain conserved phosphosites that serve as markers for subsequent ubiquitination and degradation. For example, serine 32 and serine 36 of IκBα (Brown et al., 1995). Initially, it was believed that IκB proteins kept NF-κB dimers localised in the cytosol. However, it has since been suggested that dimers bound by IκBα can shuttle between the nucleus and the cytosol due to the presence of a nuclear export sequence in IκBα. Upon degradation of the repressor protein, the shuttling is lost and the active dimer then translocates to the nucleus (Huang et al., 2000, Tam et al.,

2000). Whilst canonical IκB proteins preferentially bind dimers containing RelA or c-Rel, Bcl-3 has a high affinity for p52 or p50 homodimers (Wang et al., 2017).

The members of this protein family are characterised by the ankyrin repeat elements that fold to create the ankyrin repeat domain. The primary function of this domain is to mediate protein-protein interactions. This was visualised in the crystal structure of IκBα bound to a RelA-p50 heterodimer (Huxford et al., 1998). It can be seen that the first two ankyrin repeats of IκBα bury the nuclear localisation sequence of the NF-κB heterodimer, keeping it inactive. Additionally IκBα and IκBβ both possess a PEST domain in the C terminal end, which becomes phosphorylated prior to proteasomal degradation (Hayden and Ghosh, 2008). Interestingly, Bcl-3 possesses a nuclear localisation sequence in the N terminal region of the protein structure and a transactivation domain, resulting in the protein carrying out different functions compared to the canonical members (Zhang et al., 1994).

Bcl-3 is an important regulator of NF-κB signalling and functions as a nuclear transcription cofactor (Collins et al., 2014). The protein was discovered through cloning the breakpoint of a chromosomal translocation in B-cell chronic lymphocytic leukemia. The translocation resulted in the overexpression of Bcl-3, resulting in dysregulation of target genes. Bcl-3 is said to have target genes involved in cellular proliferation and apoptosis, therefore overexpression has been implicated in various cancers. Sensitive to varying types of stimulation and cellular environments, the protein can act to aid the expression of NF-κB target genes or facilitate their repression (Collins et al., 2015). The transactivation domain within the C terminal region of the protein results in p50 or p52 homodimers being reliant upon Bcl-3 for transcriptional regulation, as the NF-κB subunits do not have a transactivation domain of their own (Collins et al., 2014). Interestingly, it has been found that in the presence of RelB, it is unlikely that a p52 homodimer will form. However, the presence of Bcl-3 markedly increases the number of p52 homodimers formed in a given population (Pan et al., 2022).

Bcl-3 has the capability to function as a classical NF-κB inhibitor through removal of p50 and p52 homodimers from DNA. In the context of p50 homodimers, Bcl-3 can remove the repressive dimers from κB sites facilitating transcriptional activation (Franzoso et al., 1993). On the other hand, Bcl-3 can mediate repression of target genes through the inhibition of p50 homodimer degradation (Viatour et al., 2004b). The latter relies upon phosphorylation.

Post-translational modifications have been linked to the functionality of Bcl-3 as a transcriptional cofactor (Viatour et al., 2004a). Serine 394 and serine 398 are phosphorylated to mark Bcl-3 for proteasomal degradation (Wang et al., 2017). Little to no phosphorylation of the protein is linked to classical NF-κB inhibitor functions. Bcl-3 can be phosphorylated by Akt, Erk2 and IKK. Serine 33 is phosphorylated by Akt which stabilises the protein by facilitating the switch from a degradative ubiquitination, to a non-degradative ubiquitination. This allows nuclear import. Further phosphorylation on serine 144 and serine 446 by Erk2 and IKK allows recruitment of the protein to target DNA sequences. Bcl-3 is known for mediating the activation of genes involved in cell migration, and repressing genes involved in cellular death pathways (Massoumi et al., 2006, Wakefield et al., 2013). When the phosphosites S114 and S446 were mutated, significant defects in cell migration and cellular proliferation were seen (Wang et al., 2017).
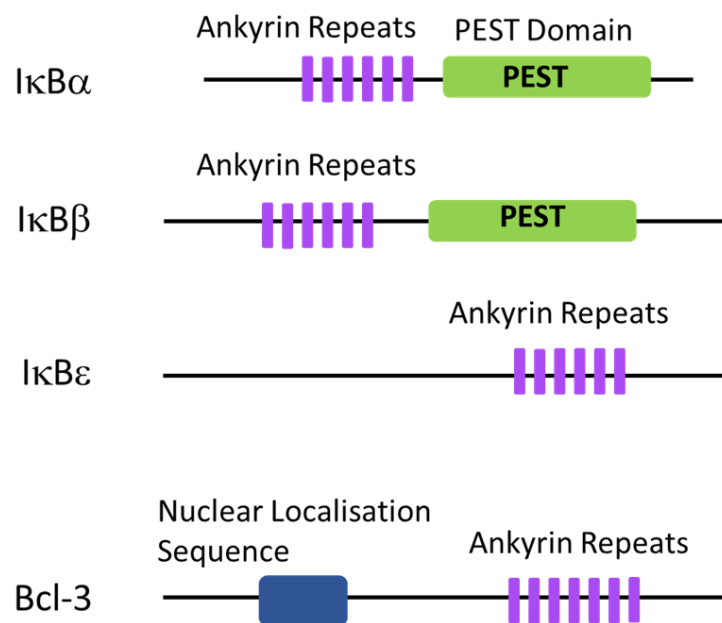
Figure 1.4 The mammalian IκB family. Schematic diagrams to visualise the structural domains of the family of repressors. Most importantly, the presence of ankyrin repeats, which are the defining feature of the proteins.

1.2.5. The IKK complex

The IκB kinase (IKK) complex is a critical regulator of the NF-κB pathway (Hinz and Scheidereit, 2014). The IKK complex is composed of two catalytic subunits, IKKα and IKKβ, along with the regulatory subunit, IKKγ (NEMO) (Figure 1.5). The two kinases share a high sequence homology, however are functionally different. This is reflected in the differences between *ikka*$^{-/-}$ and *ikkb*$^{-/-}$ knockout mouse phenotypes (Gerondakis et al., 2006). The *ikka*$^{-/-}$ mouse displayed developmental defects which led to early neonatal death, resembling the phenotype of mice lacking the IκBα protein (Hu et al., 2001). The *ikkb*$^{-/-}$ murine phenotype is embryonic lethal due to liver apoptosis and hyper-sensitivity to TNFα (Li et al., 1999). This phenotype is shared with the *nemo*$^{-/-}$ mouse (Rudolph et al., 2000). Canonical NF-κB signalling is activated through the action of NEMO and IKKβ, with TNF receptor stimulation encouraging the rapid, and transient, degradation of IKKα (Solt and May, 2008). The IKKα kinase mediates the activation of the non-canonical pathway. Whilst some scientists propose that IKKα dimers exist to activate the non-canonical pathway, the most common form of the complex is IKKα, IKKβ and a NEMO dimer. IKKβ directly phosphorylates, and triggers the degradation of the IκBs . Whereas, IKKα directly phosphorylates p100 to activate the process of proteasomal processing (Xiao et al., 2004). The kinase activity is carried out through the helix-loop-helix domains possessed by the enzymes, and dimerisation is mediated by the leucine zipper domains. Both catalytic IKK subunits also contain a NEMO binding domain (Karin, 1999). Only IKKβ contains a conserved ubiquitin-like domain that ensures its catalytic activation (Hinz and Scheidereit, 2014).

NEMO, the regulatory subunit, is a scaffold protein (Hinz and Scheidereit, 2014). The regulatory subunit has domains that mediate dimerisation, oligomerisation and interactions with the IKKs as well as upstream proteins. The subunit serves as a bridge and enables the activation of the catalytic subunits via proximity induced activation. NEMO can specifically bind to linear ubiquitination, which is important for the activation of the signalling pathway. Through this binding, NEMO brings the IKK complex in close proximity to kinases that function to phosphorylate and thus activate, the catalytic IKK subunits (Ea et al., 2006, Zhang et al., 2014). Interestingly, NEMO has been found to mediate the downregulation of

IKK by serving as a platform for the binding of negative regulators, such as deubiquitinases A20 and CYLD (Kovalenko et al., 2003, Zhang et al., 2000).

Non-degradative ubiquitination has been shown to be important in the activation of the IKK complex (Sun and Ley, 2008) Within the IKK complex, it has been established that NEMO is directly ubiquitinated during the activation of IKK. Various lysines are modified in response to different stimulation. T-cell receptor has been linked to K399, and NOD2 to K285, K68-linked polyubiquitination. DNA damage incudes mono ubiquitination on K277 and K309 (Chen, 2005). These events lead to IKK activation as described above. However, ubiquitination of NEMO is not the mechanism for all types of IKK activation, for example stimulation with LPS has been suggested to be independent to NEMO ubiquitination. On the other hand, activation of NF-κB via TLR signalling is reliant upon NEMO ubiquitination to activate proinflammatory gene expression. The first E3 ligase to be identified as a key player was TRAF6, which facilitates K63-linked ubiquitin chains (Chen, 2012). The activity of the ligase has been implicated in the response to various NF-κB inducers, such as DNA damage (Hinz et al., 2010), toll-like receptor action (Lupi et al., 2020)and IL-1 stimulation (Schimmack et al., 2017). TRAF2 is another E3 ligase which responds to TNF receptor signalling (Wang et al., 2017). Both ligases have been found to mediate self-ubiquitination, the poly-ubiquitination of pathway members, as well as free ubiquitin chains that serve as scaffolds during IKK activation.

The activation of the IKK complex is predicted to occur is various ways, such as phosphorylation with IKK kinases or trans-autophosphorylation (Solt and May, 2008). In order to become active, the kinases need to be phosphorylated on the activation loop. On IKKβ serine 117 and serine 181 are required, and serine 176 and 180 and required for IKKα activation (Hacker and Karin, 2006). It is hypothesised that two possible mechanisms are able to co-ordinate the phosphorylation of the IKKs. Firstly, the IKKs could phosphorylate one another via transautophosphorylation (Solt and May, 2008). It is proposed this occurs through conformational changes in the proteins or proximity induced activation via oligomerisation of the complex. Secondly, IKK kinases (IKKK) could directly phosphorylate the activation loops. It is possible that conformational changes in the IKKs could expose the activation loop for phosphorylation events. Equally, it is possible that IKKKs are recruited to the IKK complex via receptor or adaptor proteins. An established ubiquitin-dependent IKKK

is TAK1 (Adhikari et al., 2007). TAK1 is found in a complex with TAB1 and TAB2, the latter possesses a ubiquitin binding domain. NEMO contains the same domain, which allows both proteins to bind ubiquitin chains and any adaptor proteins associated with the chains (Sun and Ley, 2008). For example, TNFα stimulation leads to the linear and K63-linked ubiquitination of RIP1, an adaptor protein. NEMO is recruited to the linear ubiquitination, bringing the IKK complex in close proximity to TAK1, which is recruited to K63-linked ubiquitin chains via TAB2 (Chen, 2005). This allows the activation of IKK through phosphorylation events. However, in response to TLR or IL-1R stimulation, TRAF6 self ubiquitinates to serve as the adaptor protein (Sun and Ley, 2008). This recruits TAK1 and IKK to allow IKK phosphorylation.
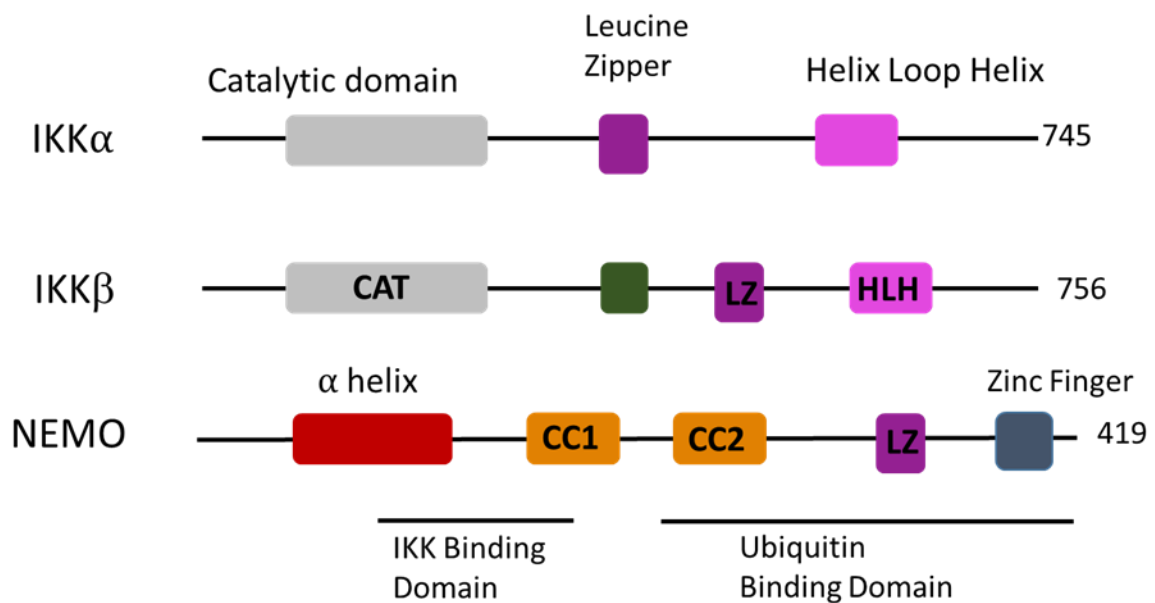
Figure 1.5 The mammalian IKK family. Depiction of the structural domains of the NF-κB activator complex. The two catalytic subunits contain a catalytic domain and have the most similar structures. This domain facilitates kinase activity. They also contain leucine zipper and helix loop helix domains that are involved in dimerisation. The regulatory subunit, NEMO, contains an IKK binding domain and a ubiquitin binding domain to carry out its function during the activation of the signalling pathway.

1.2.6.   Canonical signalling pathway

The canonical signalling pathway results in activation of the RelA/p50 heterodimer (Figure 1.6). This pathway is mostly linked to the upregulation of pro-inflammatory genes in response to inflammatory stresses and the release of inflammatory cytokines (Gilmore, 2006). In unstimulated cells the RelA/p50 heterodimer is kept inactive via IκBα. When a canonical pathway-activating ligand binds to its receptor, IKKβ becomes activated through proximity induced activation, involving the phosphorylation and ubiquitination of the regulatory subunit NEMO (Ea et al., 2006). This targets IKKβ for phosphorylation on the activation loop of the protein. This is achieved via various kinases, such as receptor interacting kinase 1, transforming growth factor beta-activating kinase 1, or TANK binding kinase (Pflug and Sitcheran, 2020). The now active catalytic subunit of the IKK complex is able to phosphorylate IκBα on serine 32 and serine 36. The RelA/p50 dimer is freed through the degradation of IkBα. The now active heterodimer can translocate to the nucleolus of cells to bind to, and regulate the transcription of, specific κB sites on target genes (Perkins and Gilmore, 2006). (Yu et al., 2020). The canonical pathway can be activated by a variety of specific receptor-ligand binding events, such as Toll-like receptors, T-cell receptors, B-cell receptors and proinflammatory cytokine receptors (Gilmore, 2006). One of the major inducers of the canonical pathway is the tumour necrosis factor (TNFα), it has been well documented that activation of the pathway through the TNF receptor is both rapid, within 15 minutes, and transient (Van Antwerp et al., 1996). This is because one of the target genes of the canonical NF-κB pathway is the IκB gene, thus creating a negative feedback loop to avoid constitutive activation (Yu et al., 2020).

Further target genes of the canonical pathway include regulators of apoptosis (e.g. the anti-apoptotic gene Bcl-xL) and cytokines (e.g. BAFF) (Liu et al., 2022b). Interestingly, the BAFF ligand is an inducer of the non-canonical pathway. It has been shown that the canonical signalling cascade can trigger the non-canonical signalling pathway.
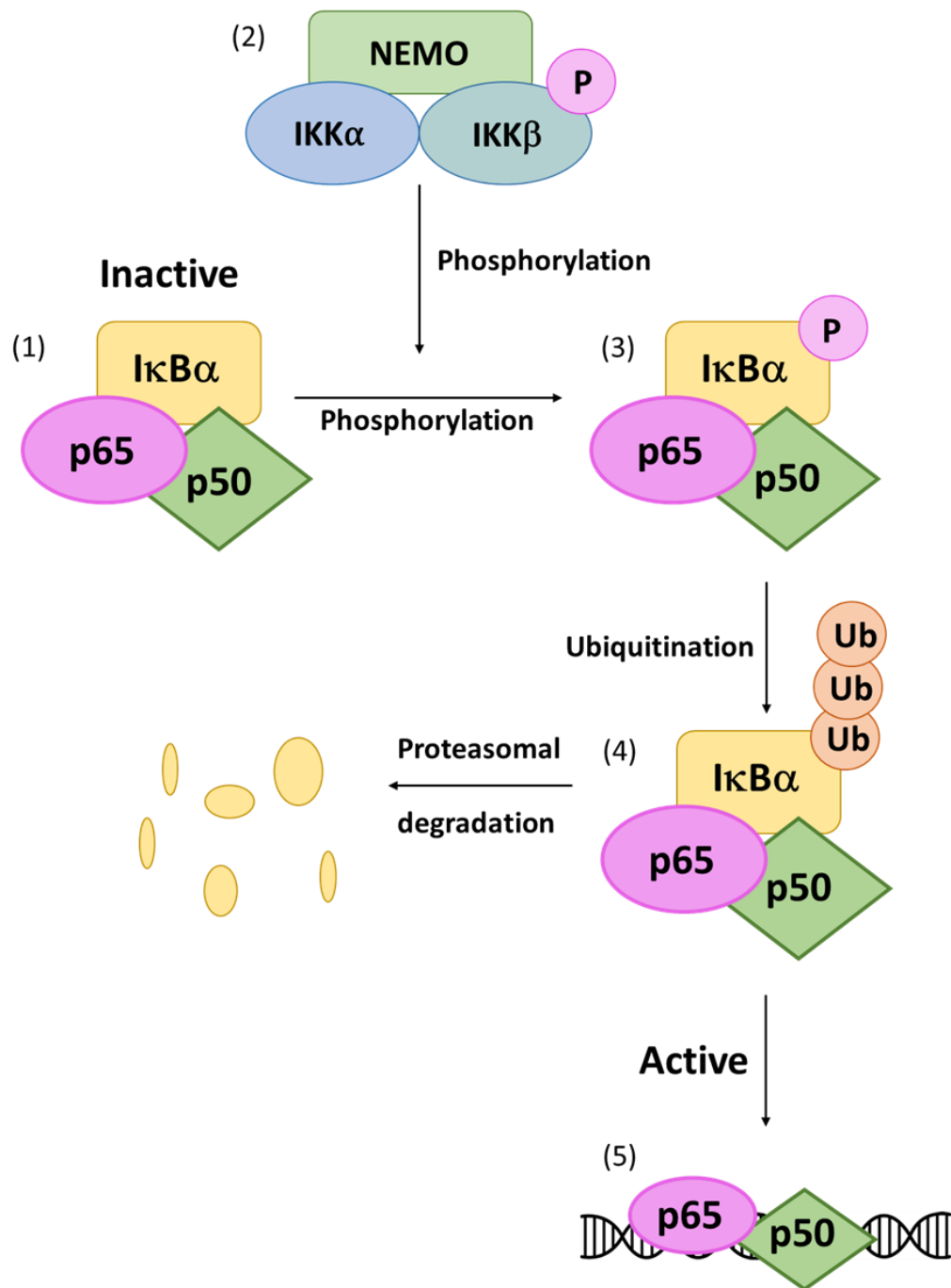
Figure 1.6 The canonical NF-κB signalling pathway. (1) The pathway is regulated and kept inactive through the binding of the IκB repressor protein to the p65/p50 heterodimer. (2)Upon activation of the IKK complex, through post-translational modifications, (3) it can carry out its role by phosphorylating IκB. (4) This serves as a marker for the degradation of the protein. (5) Once the heterodimer is free from the repressor, the active dimer can translocate to the nucleus to regulate target gene expression.

1.2.7. Non-canonical signalling pathway

The non-canonical NF-κB pathway is mostly linked to immune cell development, namely the development of B and T cells during an immune response. The pathway is mostly connected to a RelB/p52 heterodimer and responds to a different subset of stimuli as well as regulating different subsets of target genes (Sun, 2017). Activators of this pathway include the CD40 receptor (Coope et al., 2002) and the B cell activating factor receptor (BAFF-R) (Claudio et al., 2002). The signalling cascade, however, is also activated by specific members of the tumour necrosis factor superfamily of receptors e.g. Tweak receptor as well as lymphotoxin β receptor (Dejardin et al., 2002) and receptor activator of NF-κB (Novack et al., 2003).

It must be noted that the non-canonical signalling pathway is understudied when compared to the canonical. This leaves gaps in the knowledge, from the kinases that induce critical phosphorylations to activate the pathway, to the wider role the pathway plays in disease. Furthermore, it has led to a greater availability of reagents for the laboratory based study of the canonical signalling pathway. For instance, chromatin immunoprecipitation (ChIP) is a useful technique in the study of transcription factors as it is utilised to capture specific protein-DNA interactions. This technique, however, requires antibodies of a very high quality, and sometimes at a high concentration. The limits facing scientists during the study of p52-DNA binding capacities compared to, for example, RelA-DNA interactions, is much greater. This, of course, adds to the lesser knowledge and lesser publications describing the non-canonical NF-κB signalling pathway.

1.2.8. *The role of p100*

Similarly to the IκB family, the p100 subunit contains seven ankyrin repeats in the C terminal end of the protein (Figure 1.7). Therefore, this subunit is able to dimerise with other NF-κB subunits through the Rel Homology Domain whilst simultaneously carrying out a repressor function (Liao and Sun, 2003). These act to sequester the non-canonical NF-κB pathway in the inactive state, providing an important method of regulation. The p100 subunit is encoded by the NFKB2 gene (Schmid et al., 1991). The NFKB2 gene was largely studied in B and T cell lymphomas. In this context, the gene can be subject to a chromosomal

translocation resulting a truncated form of the protein lacking the C-terminal ankyrin repeat region being produced, leading to the constitutive activation of the non-canonical pathway (Chang et al., 1995). This highlights the importance for negative feedback of the pathway through the presence of the repressive C terminus of the p100 protein.
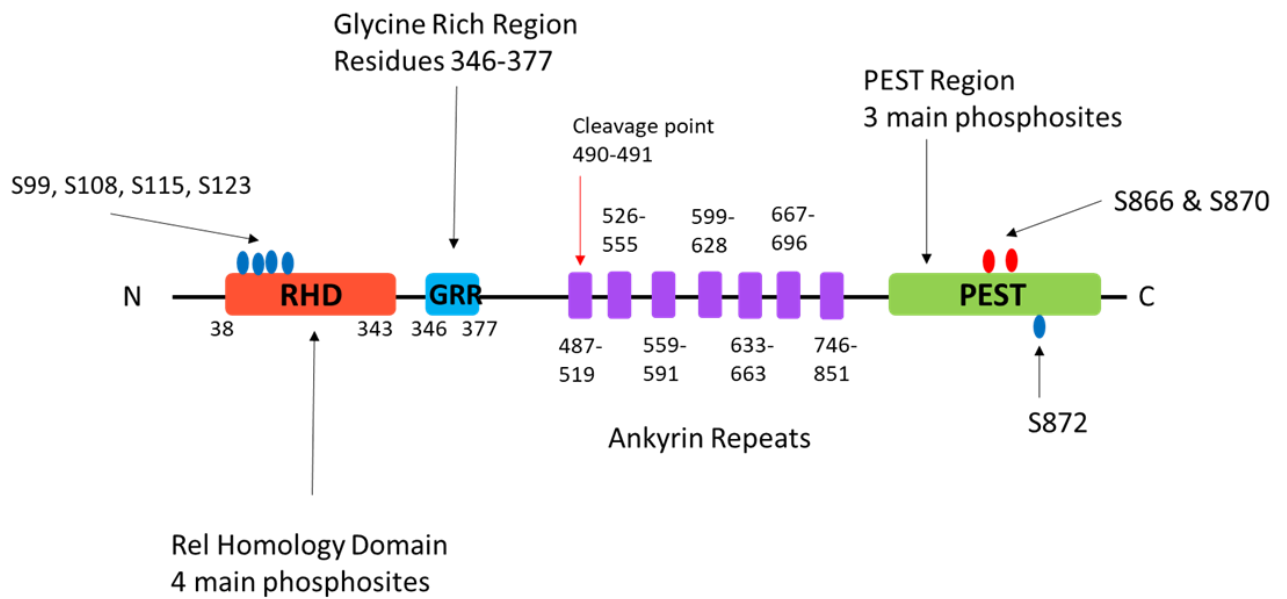
Figure 1.7 A detailed view of the p100/p52 protein. Overall, there are six critical serine residues that serve as phosphosites during the activation of the non-canonical pathway and the induction of p100 processing. These sites are represented by ovals, four in the Rel Homology domain and three in the PEST domain. The cleavage point is depicted by the red arrow.

1.2.9. Activation of the non-canonical pathway

Canonical NF-κB activation occurs in just 15 minutes. However, non-canonical activation is much slower due to the dependency on protein synthesis of NF-κB inducing kinase (NIK) (Sun and Ley, 2008). NIK mRNA is continuously synthesised, however, the protein is constitutively degraded and thus undetectable in unstimulated cells (D'Ignazio et al., 2018). Activation of the pathway requires the stabilisation of newly synthesised NIK protein (Xiao et al., 2001). NIK degradation is achieved through the recruitment of NIK via TNF-receptor associated factor 3 (TRAF3) to a complex with TRAF2 and cellular inhibitors of apoptosis 1 (cIAP1) and cIAP2 (Figure 1.8). TRAF3 associates with newly synthesised NIK to facilitate degradation. The active E3 ligases are the cIAP proteins, cIAP1 and cIAP2, which possess RING domains that are responsible for the ubiquitination of NIK (Yang and Sun, 2015). The binding of NIK and subsequent degradation was found to be dependent on TRAF2, a member of this degradation complex. Furthermore, overexpression of cIAP1 leads to increased degradation of NIK. It has been suggested that the cIAP proteins specifically function to target NIK for degradation. It is clear that the proteins recruited in this regulatory complex depend highly on one another to keep NIK protein low. This is key to regulating the downstream activation of the non-canonical NF-κB pathway (Sun and Ley, 2008). In response to pathway stimulation, NIK is stabilised via the degradation of TRAF2 and TRAF3 by cIAP1 and cIAP2 or direct stabilisation by the receptor. NIK then undergoes a conformational change involving the extension of the N terminus to create the active form of the protein (Liu et al., 2012).

The role of NIK is to bind to trigger a series of phosphorylation events that leads to the generation of p52 via proteasomal processing (Qing et al., 2005). NIK phosphorylates serine 176 and serine 180 in the activation loop of IKKα (Figure 1.7). The catalytic subunit IKKα directly phosphorylates and triggers the generation of p52 (Ling et al., 1998). Unlike the canonical pathway, which relies on the IKK complex in entirety, NEMO and IKKβ are dispensable for non-canonical pathway activation (Perkins, 2003). The critical role of NIK is reflected in the murine phenotype of *Map3k14*^{-/-} mice. The deletion of the *Map3k14* gene led to disruption or even absence of secondary lymphoid organ architecture. These mirror the defects seen in Nfkb2^{-/-} mice, discussed in Section 12.7.5. The knockout of Nik in mice

leads to significantly decreased activation of the non-canonical pathway, hence the crossover in the phenotypes (Yin et al., 2001, Li et al., 2016).

The pathway is also stimulated by a different subset of receptors involved in B cell maturation and lymphoid organogenesis (Sun and Ley, 2008). The lymphotoxin β receptor (LTβR) is a member of the TNF superfamily, controlling processes involving development and organisation of lymphoid tissue. Xiao *et al* documented in 2001 that overexpression of LTβR in HEK 293 cells enhanced NIK-mediated p100 processing (Xiao et al., 2001). Interestingly, the receptor is able to activate the regulation of a different subset of target genes through the activation of the canonical signalling pathway. This highlights the delicate balance in the cellular environment that drives the subsequent activation of the pathways (Dejardin et al., 2002). One of the target genes of LTβR-mediated NF-κB activation is the BAFF receptor.
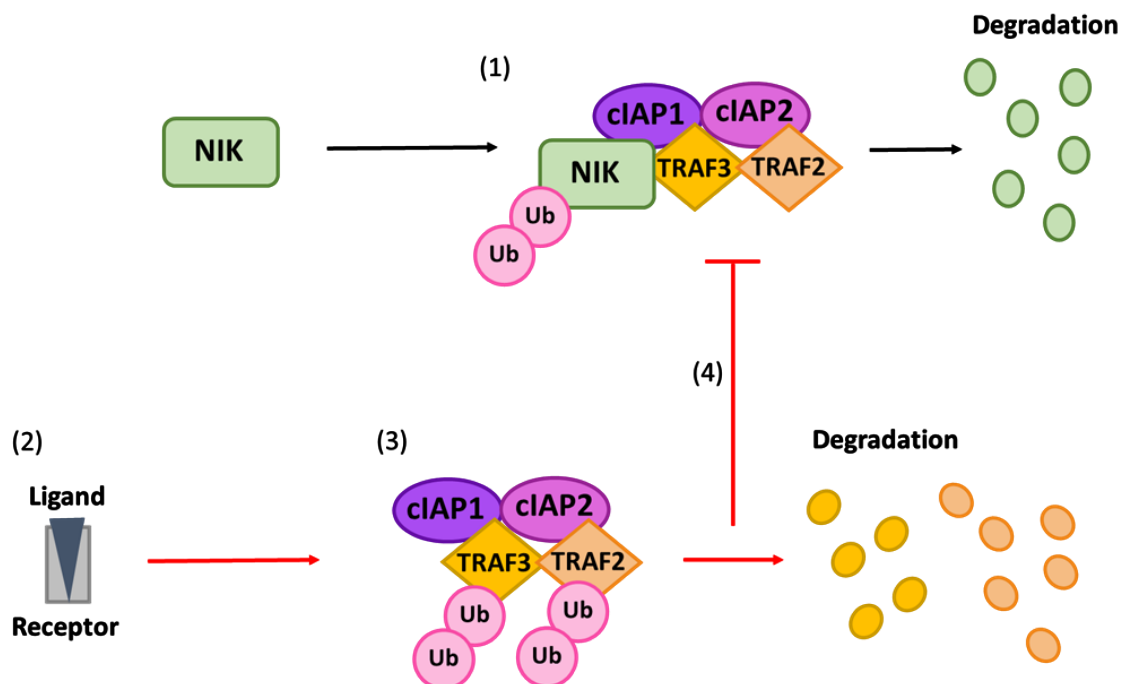
Figure 1.8 Activation of the non-canonical pathway. The regulation of the pathway is shown with black arrows. The active pathway is shown with red arrows. (1) The degradation of NIK is mediated by a complex involving TRAF2/TRAF3/cIAP1/cIAP2. NIK is targeted for ubiquitination leading to its proteasomal degradation. This is the key pathway in the regulation of the non-canonical signalling pathway. (2) When an appropriate ligand binds to its receptor, such as BAFF or CD40, the non-canonical pathway is triggered. (3) The TRAF2 and TRAF3 are targeted for degradation. (4) Therefore, NIK is no longer degraded and can carry out its function in the activation of p100 processing.

1.2.10. Phosphorylation of p100, proteasomal processing and generation of p52

The activation of NIK brings p100 into close proximity with IKKα and leads to the generation of p52 from the precursor, p100 (Figure 1.9). The partial degradation of p100 by the proteasome provides the mechanism to remove repressive C-terminal ankyrin repeat domains. This is referred to as regulated ubiquitin/proteasome-dependent processing (Rape and Jentsch, 2004, Xiao et al., 2001). There are two key regions of p100 that processing is reliant upon: the glycine rich region (residues 346-377) and highly conserved C terminal serine residues in the PEST region (S866 and S870) that are phosphorylated by NIK (Figure 1.7)(Coope et al., 2002, Xiao et al., 2004). The event results in further phosphorylation by IKKα at S99, S108, S115, S123 and S872, highlighted in Figure 1.7, which signal for ubiquitination (Xiao et al., 2004). The E3 ligase β-TrCP facilitates the creation of a K48-linked ubiquitin chain at K856. This serves as the marker for proteasomal processing via the 26S proteasome (Figure 1.9) (Ling et al., 1998, Tegowski and Baldwin, 2018). The importance of S866 and S870 has been demonstrated by the mutation of these residues to alanine, mimicking the loss of phosphorylation. This also leads to the loss of the IKKα docking site which has knock-on effects on ubiquitination and therefore p52 generation. Hence, NIK is the key driver of the processing of p52 and the activation of the non-canonical NF-κB pathway (Liang et al., 2006).

The proteasomal processing of p100 to the shorter form, p52, frees the NF-κB dimer from the repressive ankyrin repeats. The dimer is able to translocate and bind to κB sites in the nucleus, regulating target gene expression (Figure 1.9) (D'Ignazio et al., 2018).
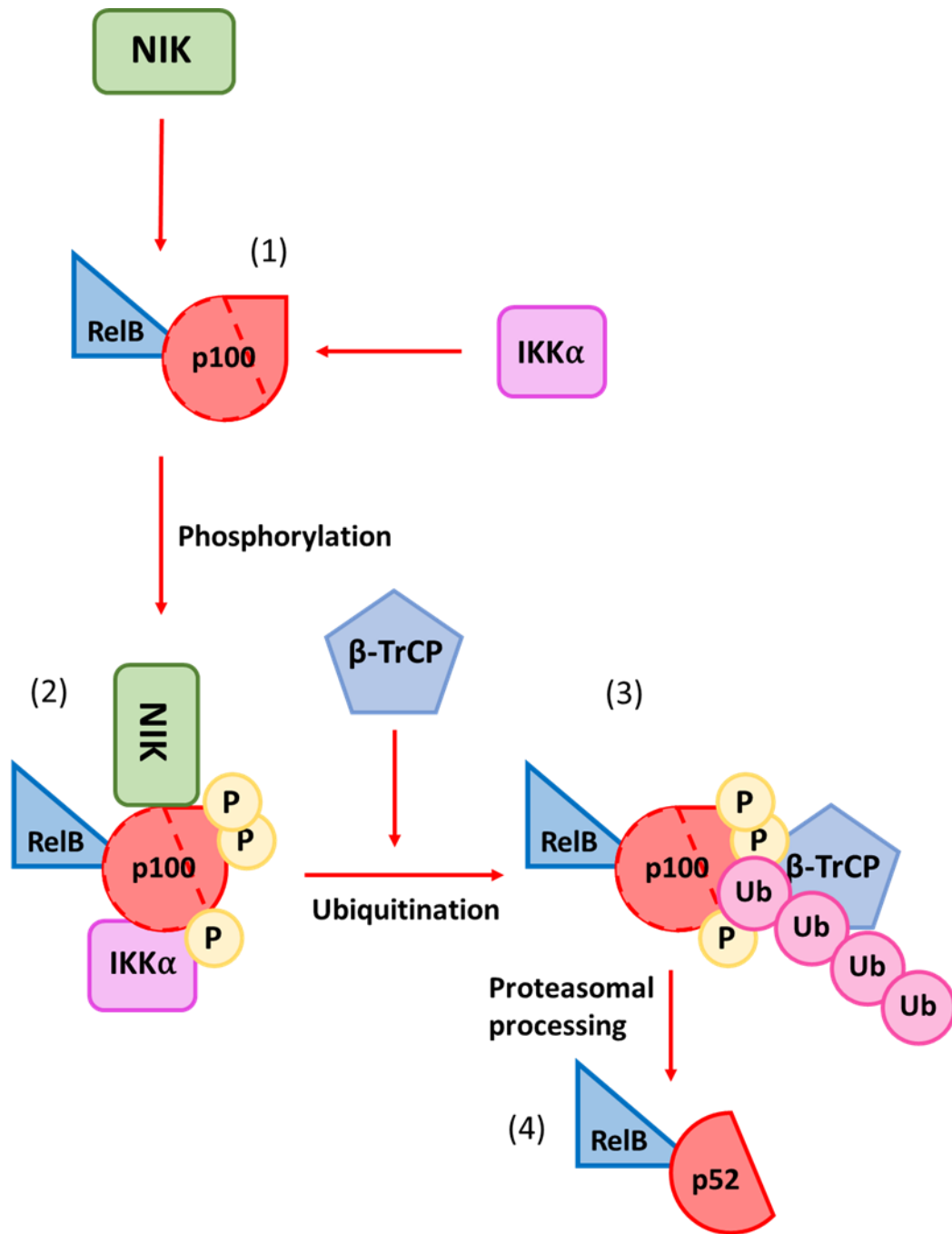
Figure 1.9 The processing of p100 and the generation of p52. (1) Now stabilised NIK and IKKα are recruited to p100. (2) p100 is phosphorylated on key residues which targets the protein for ubiquitination. (3) β-TrCP is recruited to the complex and mediates the ubiquitination of p100, which leads to proteasomal processing. (4) The now active RelB/p52 dimer is able to translocate to the nucleus to regulate target genes.

1.2.11. Insight from Nfkb2 murine phenotypes

The generation of genetically engineered NF-κB modified mouse models has served as a useful tool in the study of the functions that individual subunits play within organisms.

The *Nfkb2*$^{-/-}$ knockout mouse disrupts expression from the entire *Nfkb2* gene and therefore depletes both the p52 and the p100 protein (Caamaño et al., 1998). This causes a rather crude ablation of the non-canonical signalling pathway. The knockout leads to immunological defects such as abnormal spleen and lymph node development, as well as defects in T cell responses. Furthermore, the study found a decreased number of B cells in addition of impaired B cell function (Caamaño et al., 1998). Papoutsopoulou *et al* found significant impacts to gut physiology (Papoutsopoulou et al., 2022). Using a combination of RNA-Seq and proteomics analysis, the study investigated the transcriptional and protein signatures of the *nfkb2*$^{-/-}$ mouse. They determined major defects in B lymphocytes of the small intestine leading to deregulated levels of small intestinal immunoglobulins. Immunoglobulin A was undetectable in the samples. This indicates that p52/p100 plays an important role in the regulation of immunoglobulins in the gut. Finally, the study showed the *nfkb2*$^{-/-}$ mice were resistant to LPS-mediated small intestinal apoptosis.

Removal of the C terminus of the *Nfkb2* gene in mice leads to constitutively active p52 protein. The *NfkbΔ*C murine phenotype involves early post-natal death, enlarged lymph nodes as well as gastric hyperplasia (Ishikawa et al., 1997). This highlights the pivotal role that the regulators of NF-κB plays in the cell and the crucial role the p100 precursor protein plays. Moreover, it reinforces the part that non-canonical NF-κB signalling plays in immunological development as well as the role p52 has as a regulator of cellular proliferation.

Lym1 is a nonsense mutation used by Tucker *et al* to study a form of p100 that is unable to be processed into the active form, p52 (Tucker et al., 2007). The *nfkb2*$^{Lym1/Lym1}$ mouse was genetically engineered to have a heterozygous Lym1 mutation in the *nfkb2* gene. The mice are unable to activate the non-canonical signalling pathway. The mutation caused an accumulation of p100 protein leading to defects in splenic architecture and a significant decrease in circulating mature B cells in the bone marrow and spleen. Furthermore, in the

mutant mice, increased incidences of inflammatory infiltrates were detected in the lung and liver (Tucker et al., 2007). Interestingly, inflammatory infiltrates in the liver have been linked to non-alcoholic liver disease and hepatocellular carcinoma (Llovet et al., 2022). The lym1 mutation highlighted an element of crosstalk between canonical and non-canonical NF-κB signalling. It was found that the inhibitory precursor, p100, was able to bind to RelA containing dimers. Therefore, without the processing of the full length protein, RelA containing dimers became repressed. The repression caused defective lymph node formation and bone homeostasis due to the lack of p50/RelA heterodimers translocating to the nucleus to regulate target genes (Jacob et al., 2019).

1.2.12. p52 target genes

The p52 subunit has a wide range of target genes, of which this section will discuss four subtypes: cell cycle and proliferation, apoptosis, immunity and inflammation, and NF-κB feedback signalling (Sun, 2017). The regulatory transcription factor functions of the p52 subunit are less discussed in the literature in comparison to other NF-κB subunits.

Firstly, it is clear p52/p100 plays a role in cell cycle progression and cellular proliferation through direct gene regulation (Ledoux et al., 2013). Chromatin immunoprecipitation experiments have shown that the oncogene, c-Myc, can be regulated by p52/RelB heterodimers to promote cellular proliferation (Demicco et al., 2005). Another way p52/p100 supports cell growth is through the encouragement of cell cycle progression. A definitive link has been demonstrated between p52 and the G1 Cyclin, Cyclin D1 (Schumm et al., 2006). The p52 subunit works alongside Bcl-3 and RelA to regulate CCND1 gene expression. Furthermore, p52/RelB heterodimers have been shown to bind directly to the promoter of the SKP2 gene (Schneider et al., 2006) The Skp2 protein is an E3 ubiquitin ligase that facilitates the degradation of the Cdk inhibitor, p27. This action of p52 is a further example of the role the protein plays in cellular proliferation. Schumm *et al* implied a link between p52/p100 and cell division (Schumm et al., 2006). The study showed that p52/p100 siRNA knockdown led to G2/M arrest. Further research by the Perkins laboratory published Polo-like kinase 4 as a direct NF-κB target gene (Ledoux et al., 2013). The p52 subunit was shown to bind to several loci on the PLK4 promoter, regulating expression. PLK4 is a critical regulator of centriolar duplication during mitosis. Cells challenged to prolonged p52/p100

depletion showed significant defects in chromosome structure. Thus, the study implicates p52 within the regulation of cell division.

The direct regulation of apoptotic genes by p52 containing NF-κB dimers is further proof of the subunit's cell survival and cellular proliferation role. Bcl-xL is an anti-apoptotic member of the Bcl2 family. RelA/p52 heterodimers were found to bind to the promoter of the gene encoding Bcl-xL regulting in its upregulation (Marinari et al., 2004). Similarly, Vacca *et al* showed via chromatin immunoprecipitation that *BCL2* was a direct p52 target gene (Vacca et al., 2006). The *BCL2* gene encodes the protein Bcl-2, which is also an anti-apoptotic member of the family. The p52 subunit activates the expression of both gene, which in turn suppresses apoptosis, encouraging cell survival and cellular proliferation.

The NF-κB family is known to have a role in the inflammatory and immune responses. The p52/p100 subunit has been shown to regulate genes involved in both cellular processes. One link between p52 and the inflammatory response was through the regulation of Interleukin-7 receptor α(IL-7 Rα) by p52/RelA heterodimers (Vacca et al., 2006). A further example of pro-inflammatory signalling capabilities of p52 is through direct regulation of Interleukin-8 (IL-8) (Marinari et al., 2004). IL-8 is a pro-inflammatory cytokine that enables neutrophils to locate sites of infection. A heterodimer containing p52/RelA has been proven to bind to the promoter region of the gene encoding IL-8 following CD28 stimulation in T cells. CD28 can lead to T cell receptor-independent signalling which regulates a specific subset of target genes. In the same study, it was determined that p52/RelA could activate B-cell activating factor (BAFF) gene expression. BAFF is a cytokine within the TNF superfamily which plays a role in the proliferation and differentiation of B cells.

The critical activator of B cells is also a potent stimulator of the non-canonical NF-κB signalling pathway. The regulation of BAFF expression via p52/RelA is an example of a positive feedback mechanism within non-canonical signalling. Further, the same heterodimer was shown to activate *NFKB2* gene expression (Liptay et al., 1994b, Schmid et al., 1991, Duckett et al., 1993). The positive autoregulation of the *NFKB2* highlights the important feedback loops that the NF-κB pathway participates in. Through expression of *NFKB2* and translation to p52/p100, the cell can reinstate the repressive full length of the protein to avoid constitutive expression of the pathway, which is linked to various diseases.

1.2.13. Crosstalk between p52/p100 and p53 signalling

The tumour suppressor, p53, also known as the guardian of the genome, facilitates apoptosis, senescence and cell cycle arrest in response to DNA damage or oncogene activation (Vousden and Prives, 2009). The Perkins laboratory have previously demonstrated events of crosstalk between the p52 and the p53 transcription factors that results in modulation of p53 target gene expression. Rocha *et al* detailed that induction of p53 through UV radiation repressed cyclin D1 promoter activity leading to decreased cellular levels of cyclin D1 mRNA and protein (Rocha et al., 2003). The study determined that expression of the transcriptional cofactor, Bcl-3, was inhibited through p53 induction. Bcl-3 acts as a transcriptional coactivator with p52 homodimers, due to the p52 protein lacking a transactivation domain, and decreased expression of the cofactor led to increased association between p52 homodimers and histone deacetylase 1 (HDAC1). Therefore, in response to p53 induction, p52 homodimers were proven to switch from associating with a transcriptional activator to a transcriptional repressor, leading to downregulation of cyclin D1 gene expression. This serves as an example of the regulation of NF-κB activity via p53 signalling.

The p52 subunit was later found to be recruited to the promoters of p53 regulated genes (Schumm et al., 2006). For example, it was demonstrated that p52 could directly bind to the promoter of the cyclin D1 gene to modulate expression. However, the role of p52 in cellular proliferation also included the ability to modulate p53 activity through cooperation with p53 leading to the regulation of p53 target genes. Alongside upregulation of cyclin D1 expression, the study found that p52 repressed gene expression of Cdk inhibitor, p21, in a p53-dependent manner, supporting cellular proliferation. Finally, through co-immunoprecipitation experiments, Schumm *et al* showed that p52 could be recruited to the promoters of other p53 target genes. These genes include pro-apoptotic gene, PUMA (encoded by *BBC3)*, and cell cycle regulators Chk1 (*CHEK1*) and GADD45A (*GADD45A*). The study determined that p52 could associate with the promoters of these genes and regulate binding of transcriptional co-activators and co-repressors. The research highlighted the diverse regulatory role p52 plays within p53-dependent cellular proliferation and the cell cycle, both directly and indirectly.

Lastly, the Perkins laboratory defined a link between non-canonical NF-κB signalling at p53 via the EZH2 gene (Iannetti et al., 2014). EZH2 encodes an H3 M27 histone methylase which is known to be indirectly regulated by p53. Heterodimers containing p52/RelB were found to both directly bind to the EZH2 promoter, as well as indirectly modulating expression through the retinoblastoma (Rb) protein. Either way, the p52/RelB dimer upregulated expression of the gene. EZH2 then supressed p53 activity leading to repression of p53-dependent cellular senescence. This is an example of p52 and p53 crosstalk leading to cell survival via downregulation of cellular mechanisms.

1.3. NF-κB in health and disease

1.3.1. NF-κB in inflammatory diseases

Considering the nature of the NF-κB pathway, it is unsurprising that deregulated signalling contributes to a range of diseases. In particular, the canonical signalling pathway is known for regulating inflammatory signalling. In cases where the deregulation of the pathway results in constitutively active NF-κB, incidences of chronic inflammation can develop (Greten et al., 2004). These states of chronic inflammation can therefore be initiated by NF-κB and are linked to diseases such as rheumatoid arthritis and inflammatory bowel disease.

Rheumatoid arthritis (RA) is an autoimmune disorder involving chronic inflammation and damage to cartilage and bone (McInnes and Schett, 2011). Physiologically, the disease is defined by the presence of infiltrating immune cells in the synovium. Early studies into the disease detected high levels of NF-κB activation in synovial tissues of RA patients (Asahara et al., 1995). As NF-κB can upregulate the transcription of pro-inflammatory genes, such as cytokines, inflammation can spread from cell to cell. Sometimes this can be caused by the loss of existing negative feedback loops that eliminate aberrant NF-κB activity (Karin, 2009). Feed forward loops, however, can also been developed in prolonged states of inflammation such as with the NF-κB target gene, TNFα. This ligand also stimulates the canonical pathway. In some instances this can be beneficial, as it causes the recruitment of cytotoxic immune cells. On the other hand, when constitutively active it can form the inflammatory microenvironment (Perkins, 2000). In the context of RA, the NF-κB pathway can activate pro-inflammatory cytokines in monocytes and macrophages, which are cell types known to contribute to the pathophysiology of the disease (Davignon et al., 2013). Through feed

forward loops, this can contribute to disease progression. Further, the NF-κB dependent upregulation of inflammatory cytokines can indirectly encourage the differentiation of Th17 cells, a type of T cell that is important in RA (Liu et al., 2017). The NF-κB pathway has been shown to directly activate the expression of genes encoding transcription factors that aid the differentiation of Th17 cells. Bone loss is another symptom of RA (Deal, 2012). The RANK ligand is an inducer of NF-κB signalling that leads to the differentiation of monocytes and macrophages into osteoclasts (Yao et al., 2009). Deregulation of NF-κB leads to the deregulation of osteoclast differentiation and therefore contributes to the destruction of bones.

Inflammatory bowel disease (IBD) impacts the gastrointestinal tract and is believed to be caused be deregulated responses to intestinal microbes (Xavier and Podolsky, 2007). Colonic tissues of patients suffering from IBD were analysed, which revealed constitutively activated NF-κB activity (Schreiber et al., 1998). The disease has been linked to the p50/p105 subunit as mutations resulting in the inhibition of NFKB1 expression were found in patients (Liu et al., 2017). A murine phenotype was created involving a knock-in mutation within the *Nfkb1* gene (Chang et al., 2009). A stop codon was introduced at the processing site of p105, leading to the synthesis of p50, without the negative regulator precursor protein, p105. The study found that mice carrying the mutation developed IBD-like symptoms. This shows that p50/p105 plays a critical role in mediating and regulating the inflammatory response in the gut. Chronic inflammation and related inflammatory diseases can predispose an individual to developing various types of cancer (Multhoff et al., 2012).

1.3.2. NF-κB in cancer

Constitutive NF-κB activation is linked to various types of cancer. Genetic mutations contribute to the aberrant activation of the pathway, however these are mostly seen in haematological cancers. In some cases, mutations reside in the genes encoding the subunits, this is mostly associated with the REL (encoding c-Rel), NFKB1 (encoding p50/p105) or NFKB2 (encoding p52/p100). Mutations in the REL gene are mostly point mutations that lead to amplification of the gene. These are found in Hodgkins lymphoma and diffuse large B cell lymphomas. Mutations in NFKB1 or NFKB2 usually involve the constitutive removal of the repressive C terminal domains. Upstream activators or

regulators of the pathway are also found to be mutated in cancer contributing to the constitutive activation of the NF-κB pathway. For example, gain of function mutations are found in activators, such as CD79 and MYD88. Conversely, loss of function mutations are found in regulators, such as deubiquitinases, CYLD, A20 and negative regulator, IKB. The loss of IκB activity leads to constitutively nuclear NF-κB dimers. This has been found in DLBCL, Hodgkins lymphoma, glioblastoma and nasopharyngeal cancer.

Once active, constitutive NF-κB has been found to contribute to the hallmarks of cancer (Gilmore, 2021). Inflammation is one of the hallmarks of cancer. It is known that chronic inflammation can lead to cancer through inducing DNA damage or suppression of tumour suppressive genes (Colotta et al., 2009). NF-κB often links incidences of chronic inflammation and cancer, as the pathway is often found to be active in solid tumours. It is thought inflammation can either promote the growth of a tumour or develop as a consequence of cancer progression. Either way, NF-κB has the ability to modify the microenvironment of a tumour by inducing cytokine expression, for example IL-6. The NF-κB-mediated upregulation of cytokinesis found in breast and lung cancers. Feed forwards loops involving increased NF-κB activity induced by the increase in pro-inflammatory cytokines was found to encourage the tumour environment by functioning as cell survival or cellular proliferation factors (Perkins, 2000, Multhoff et al., 2012). Deregulated inflammatory signalling has been linked to enhancing angiogenesis, another hallmark of cancer. Angiogenesis is the process by which cancer cells develop new vasculature to aid the survival of a tumour. Tumour growth is limited unless angiogenesis occurs, allowing the supply of vital nutrients. Genes involved in encouraging angiogenesis, *VEGF*, *IL8* and *MMP9* are NF-κB target genes. Thus, constitutive activation of the pathway leads to the upregulation of these genes, promoting the development of new blood vessels. Furthermore, in high grade prostate adenocarcinoma increased RelA and p50 expression was found and this leads to increased expression of *MMP9* and *VEGF*, genes known for stimulating angiogenesis and cell migration, respectively (Shukla et al., 2004). Angiogenesis is said to function alongside metastasis. Metastasis is the development of secondary tumours at a new site. The process requires cell migration and invasion. Deregulated NF-κB has been linked to metastasis through direct gene regulation. A study investigating metastasis in breast cancer revealed that genes involved in the EMT, such as *TWIST* and

SLUG, are target genes of the NF-κB pathway. Aberrant NF-κB activation, therefore significant upregulation of those genes, is associated with aggressive, metastatic cancers.

Cell survival is a necessity for malignant cancer cells to continually divide and contribute to progression of the disease. Cancerous cells evolve to evade apoptosis, it is thought that aberrant NF-κB activation in tumours contributes to an anti-apoptotic signal (Kaltschmidt et al., 2018). Interestingly, several anti-apoptotic genes are NF-κB target genes, such as Bcl2-like factors, *BCL2L1* (encoding Bcl-cL) and *BCL2* (encoding Bcl-2), *TNFAIP3* (encoding A20) and the cellular inhibitors of apoptosis cIAPs (Perkins, 2000).

Whilst there are certain circumstances in which the NF-κB family acts as a tumour suppressor, this is understudied in comparison to tumour promoting roles. This, however, could be influenced by the fact that researchers have a tendency to study end stage malignant cancer cells. During those circumstances, NF-κB is generally a tumour promoter, as outlined above. When NF-κB was studied in the context of cancer, it was mostly within its role inflammation or mutations that activate the pathway. A fascinating example of the tumour suppressive capacity of NF-κB involves a link between RelA and the DNA damage response (Moles et al., 2016). The residue that bridges these pathways is threonine 505 of RelA. The cell cycle checkpoint kinase, Chk1, phosphorylates T505. This induces the expression of pro-apoptotic target genes and provides a tumour suppressing role. The Perkins laboratory created a knock-in mouse to study this, mutating T505 to alanine 505 which removes the possibility of phosphorylation.

The mouse model proved a useful tool in establishing that the removal of the phosphorylation event caused a reversal of the tumour suppressing role to one of a tumour promoting nature. The molecular switch caused the mice to develop early onset hepatocellular carcinoma.

1.3.3.   p52/p100 in cancer

NFκB2 has been implicated in various cancer types (Kaltschmidt et al., 2018). The subunit can contribute to cancer development either through chromosomal rearrangement of the NFKB2 gene or through the mutation of upstream members of the non-canonical pathway (Perkins, 2012). Gene rearrangement has been documented in lymphomas, such as multiple myelomas, B-cell non-Hodgkin lymphomas, but mostly in cutaneous T-cell lymphomas (Gilmore, 2021). The outcome of the rearranged gene is a truncated form of the p100

protein, removing repressing ankryin repeat domains. The truncated protein can bind to κB sites rendering the non-canonical signalling pathway constitutively active. Rearrangement of this manner correlates to poor survival for patients. Mutations of upstream non-canonical proteins can also lead to the constitutive activation of the pathway having detrimental effects (Schumm et al., 2006). Multiple myeloma is a cancer involving aberrant proliferation of bone marrow plasma cells (Rajkumar, 2011). The non-canonical pathway is known to be critical for the development of B cells and formation of germinal centres (Sun, 2017). Pathway activating mutations have been described in 20% of multiple myelomas, such as gain of function mutations of NIK and CD40 (activating ligand), or loss of function mutations of key regulators, such as the cIAPs (Gilmore, 2021). The most frequent loss of function mutation is within the TRAF3 gene. This type of mutation leads to the stabilisation of NIK, causing aberrant pathway activation. (Keats et al., 2007).

Non-canonical NF-κB signalling has been linked to several of the hallmarks of cancer (Hanahan and Weinberg, 2011). The p52/p100 subunit has been linked to increased cellular proliferation and cell survival of cancer cells (Kaltschmidt et al., 2018). Increased levels of upstream non-canonical NF-κB activating kinase, NIK, is seen in pancreatic cancer samples. It has been documented that NIK is critical for the proliferation of pancreatic cancer cells through regulation of non-canonical NF-κB target genes (Döppler et al., 2013). In order to continue aberrant cell growth and cell division, cancerous cells must maintain the integrity of their telomeres (Bordeira Gaspar et al., 2018). Telomeres are repetitive regions at the end of chromosomes that shorten with every round of division. TERT, telomerase enzyme catalytic subunit, maintains the length of telomeres and mutations in the gene are associated with driving cancer (Dratwa et al., 2020). The activation of the non-canonical signalling pathway has been linked to increased expression of TERT in glioblastoma cells contributing to aberrant cell division and cancer cell survival (Li et al., 2015). Another example of p52/RelB dimers contributing to cancer cell survival is through the link to nucleic acid editing enzymes, known as APOBECs. These enzymes can directly mutate cancer cell DNA which can drive tumorigenesis (Tegowski and Baldwin, 2018). Chromatin immunoprecipitation analysis found that protein kinase C activation induced the binding of RelB/p52 on the promoter of the APOBEC3B gene. This was found in HPV positive cervical head and neck tumour derived cell lines (Leonard et al., 2015). Therefore, p52 is known to

play a tumour promoting role, in a wide range of cancers, through the enhancement of cell survival and cellular proliferation.

There is a definitive link between the p52/p100 protein and the p53 tumour suppressor protein (Rocha et al., 2003, Schumm et al., 2006, Iannetti et al., 2014). Some cancer mechanisms have been found to function by hijacking the transcription factor action of p52/p100 containing dimers. The Perkins laboratory has previously described a link between RelB/p52 heterodimers and increased EZH2 expression in CLL cells (Iannetti et al., 2014). RelB/p52 have the ability to bind to the promoter of EZH2, which is a histone methyltransferase that facilitates gene repression. This binding event can inhibit p53 mediated senescence by repressing the expression of p53 target genes. Interestingly, this mechanism has also been found in melanoma cells. This is an example of tumour promoting activity of p52 via p53 signalling. Further to this, Schumm *et al* detailed a p53-dependent link between p52 and Cdk inhibitor, p21, in cancerous cell lines (Schumm et al., 2006). p52 homodimers can be recruited by p53 to the CDKN1A gene (encoding p21) to repress expression. The downregulation of the cell cycle regulator could contribute to aberrant cell division and cellular proliferation which is characteristic of cancerous cells. Therefore, p52 could contribute to the cell survival of cancer cells through the p53 tumour suppressor protein.

NFκB2 has also been found to play a role in angiogenesis and metastasis (Kaltschmidt et al., 2018). The former being the creation of a new blood supply allowing a tumour to grow larger than 1-2mm^2. The latter involving the invasion of cancerous cells into surrounding tissues. ICAM is known for angiogenesis and is a p52 target gene. Matrix metalloprotease, MMP-9, is also upregulated by p52 dimers (Chaisson et al., 2004). NFκB2 overexpression has been found in breast and colon cancer. Non-canonical NF-κB signalling isknown to regulate the development of mammary glands. High levels of p52/p100 and RelB expression in their tumours are associated with poor patient survival (Rojo et al., 2016). Whilst the mechanisms underlying the contribution of non-canonical NF-κB signalling to breast cancer are unclear, it is thought that it could effect the epithelial mesenchymal transition (EMT), which contributes to metastasis (Tegowski and Baldwin, 2018).

1.4. The nucleolus and cellular stress

The primary function of the nucleolus is ribosome production. Within this organelle, the components of the large and small subunits of the ribosome are synthesised (Boulon et al., 2010). The first three events in the process of ribosome biogenesis occur within the nucleolus prior to export to the cytoplasm for the final assembly step (Sloan et al., 2013a). First, transcription of ribosomal DNA to synthesise the long precursor ribosomal RNA takes place in the fibrillar centre (FC) (Boisvert et al., 2007). Hence, the FC contains required machinery for this that includes RNA polymerase I. The second step, pre-RNA processing, occurs in the dense fibrillar component (DFC). Thus, the DFC houses the required components for this step, such as snoRNAs and snoRNPs. The granular component surrounds the FC and the DFC, and is the site at which the assembly of the pre-ribosomal subunits takes place (Boulon et al., 2010). This is the stage in which the maturing large and small ribosomal subunits are formed through assembling of complex large RNA-protein complexes. The size of the nucleoli within cells is dependent upon cellular activity. For example, the higher the growth rate or metabolic rate, the larger the nucleoli (Yang et al., 2018).

Cellular stress causes a reorganisation to the overall structure of nucleoli. This is described as nucleolar segregation (Boulon et al., 2010). Initially, this involves the condensation of the FC and GC which leads to the separation of these nucleolar structures. Proteins involved in the process of ribosome biogenesis are repurposed to form nucleolar caps (James et al., 2014). This leads to the breakdown of the nucleolar structure. Nucleolar stress, also referred to as ribosomal stress, is the term used to describe this structural breakdown (Sloan et al., 2013a). Nucleolar stress can be caused by DNA damage, including damage by UV radiation, nutrient stress, hypoxia, viral infection and artificially by various drug treatments (Pelava et al., 2016). Ribosomal components contained within the nucleolus, such as ribosomal proteins, are released. Hence, the terms nucleolar stress and ribosomal stress being interchangeable. Proteomic analysis of nucleoli reveals the protein content of the nucleolus redistributes to the nucleoplasm following stress (Boulon et al., 2010). A study performed in HCT116 cells both with and without the presence of p53 revealed the shuttling and redistribution of proteins in response to stress-induced nucleolar breakdown, is dependent on p53 (Boisvert and Lamond, 2010). As well as protein localisation, further studies have

suggested the concentration of the proteins in the nucleolus and nucleoplasm, also change. This suggests a complex reorganisation of the organelle during cellular stress (Yang et al., 2018).

1.5. The Eukaryotic Ribosome

The eukaryotic ribosome is a large ribonucleoprotein complex, consisting of an array of ribosomal proteins and ribosomal RNAs (rRNA) (Doudna and Rath, 2002). rRNAs are the most common type of RNA in the cell. They form the majority of the ribosome and play a critical catalytic role within the organelle. The function of the ribosome is as a catalyst for the translation of messenger RNA (mRNA) into protein (Catez et al., 2019). The mature eukaryotic ribosome is also known as the 80S ribosome and consists of a small subunit (40S) and a large subunit (60S) (Thomson et al., 2013). The 'S' refers to their sedimentation coefficient, which relates to the sedimentation of a particle during centrifugation. The two subunits are mostly connected through RNA-RNA contacts and play a synergistic role in the synthesis of polypeptides from mRNA (Doudna and Rath, 2002). The primary function of the 40S subunit is the decoding of mRNAs through the correct pairing of codons with appropriate transfer RNAs (tRNAs) (Fraser et al., 2007). tRNAs act as a bridge between mRNA and the amino acid sequence of the corresponding protein (Berk et al., 2006). The small subunit contains 32 ribosomal proteins and the 18S rRNA (Sloan et al., 2019). The 60S subunit serves to catalyse peptide bond formation throughout protein synthesis as it contains the peptidyl transferase active site (de la Cruz et al., 2015). The large subunit houses 46 ribosomal proteins and the 28S, 5.8S and the 5S rRNAs. Both of the ribosomal subunits are needed to translocate the mRNA to the following codon to start a fresh translation cycle (Khatter et al., 2015).

Interestingly, the eukaryotic ribosome possesses one additional rRNA and around 20-30 additional proteins in comparison to prokaryotic ribosomes (Doudna and Rath, 2002). There is, however, a large degree of conservation between species, mostly contained within the core of the ribosome. It has been seen upon comparison of yeast and bacterial ribosomes that outside of the conserved rRNA core, there are differences to the structure (Kressler et al., 2010). These are likely to serve a functional purpose, however this still remains unclear.

1.6. Eukaryotic Ribosome Biogenesis

A human cell contains 2-10 million ribosomes. Every time a single cell undergoes mitosis resulting in two identical daughter cells, each ribosome must be accurately replicated (Pelava et al., 2016). The rate of ribosome biogenesis is one of the most energetically costly processes ongoing in the cell. As protein production is dependent on ribosomes, ribosome biogenesis directly impacts cellular growth and proliferation (Sloan et al., 2013a). Therefore, the regulation of this process is critical, with deregulation being associated with disease (Kampen et al., 2019). Eukaryotic ribosome biogenesis requires the organisation and involvement of RNA polymerase I, II and III alongside 200 ribosome assembly factors (Thomson et al., 2013). Due to the energy required to carry out the process, ribosome biogenesis is rapidly inhibited in response to various cellular stresses, such as hypoxia, ultraviolet radiation, and oncogene expression, causing nucleolar stress (Pelava et al., 2016).

The synthesis of a new ribosome begins with the transcription of ribosomal DNA (rDNA). The nascent ribosomal RNA (rRNA) is then processed, modified and joined by newly synthesised ribosomal proteins to form the maturing large and small ribosomal subunits (Pelava et al., 2016). The final step involves the joining of the two subunits to form the mature 80S ribosome. The entire process occurs in three different cellular localisations; the nucleolus, the nucleoplasm and the cytoplasm (Sloan et al., 2014).

1.6.1. rDNA transcription

There are four ribosomal RNAs (rRNA) that need to be transcribed: the 18S, the 5.8S, the 28S and the 5S. Three of the rRNAs (18S, 5,8S and 28S) are transcribed as a single precursor rRNA, the 47S, by RNA polymerase I (Tafforeau et al., 2013). This occurs in the nucleolus. The genes encoding rRNAs are located on the short arms of chromosomes 13, 14, 15, 21 and 22. These genes are uniquely organised in clusters of tandem repeats and are susceptible to recombination (Lindström et al., 2022). When RNA polymerase I is recruited to the promoter regions of rDNA genes, the pre-initiation complex assembles. The complex consists of upstream-binding factor and promoter selectivity factor SL1 complex (Raška et al., 2004). Formation of this complex allows RNA polymerase I to initiate transcription and translocate across the gene. TTF-1 factor binds to the termination sequences of the gene

and serves as a marker for RNA polymerase I to terminate transcription (Jansa and Grummt, 1999).

The 5S rRNA is unique as it is transcribed independently by RNA polymerase III (Ciganda and Willaims, 2014). The gene encoding the 5S rRNA is located on chromosome 1 and transcription of the gene is dependent upon a 5' flanking region in the DNA sequence. Transcription factor IIIA binds to an internal control region in the 5S rDNA gene to control transcription and has also been found to bind to the freshly synthesised 5S rRNA aiding transport and storage (Lee et al., 2006). The 3' end of the transcript is removed via processing which, in humans, is thought to be dependent on the ribosomal protein, RPL5 (Sloan et al., 2013a).

1.6.2. Mammalian rRNA processing

The pre-cursor rRNA transcript, the 47S rRNA, is subject to a sequence of endonucleolytic cleavages and exonucleolytic processing events (Mullineux and Lafontaine, 2012, Sloan et al., 2013b). The end result of this being the three rRNAs required for incorporation into the ribosome: the 18S, the 5.8S and the 28S. There are four spacers that need to be removed, two external transcribed spacers, the 5' and 3' ETS, and two internal transcribed spacers, ITS1 and ITS2 (Nazar, 2004). The detailed mechanism of rRNA processing is not fully undestood in mammals with the process being much better understood in yeast (Sloan et al., 2019).

Within the 5' ETS there are two cleavage sites, the A' and the A0. Cleavage of A' has been found to occur in a co-transcriptional manner and processing of the site requires multiple cofactors, for example snoRNPs and the exonuclease XRN2 (Kass et al., 1987, Sloan et al., 2014). A' processing produces the 45S pre-rRNA intermediate (Mullineux and Lafontaine, 2012). In close succession, the 45S is cleaved within the ITS1 at site 2 by RNAse MRP (Goldfarb and Cech, 2017). This creates the 30S and the 32S pre-rRNA intermediates. ITS1 cleavage is the first step in the separation of the small subunit rRNAs and the large subunit rRNAs (Tomecki et al., 2017).

The cleavage and processing of sites A0 and 1 in the 30S pre-rRNA intermediate generates the 21S pre-rRNA. The exact cofactors performing the cleavage sites in mammals is not known. However, it is suggested that UTP23 cleaves at site A0 and UTP24 at site 1 (Wells et

al., 2016, Wells et al., 2017). The 18SE precursor is formed through the exonucleolytic cleavage of site 2 and 2a by the exosome and RRP6. The final step in the nucleolus involves the further processing of ITS1 of the 18SE rRNA in the nucleolus by the protein, PARN (Sloan et al., 2014, Kobyłecki et al., 2018). The maturing 18S rRNA is then exported and subject to a final cleavage event at site 3 facilitated by NOB1. This produces the mature 18S rRNA (Bai et al., 2016).

Simultaneously, processing of the 32S pre-rRNA occurs. This involves processing of ITS2 leading to separation of the two large ribosomal subunit rRNAs (Sloan et al., 2013b). The initial stage involves a cleavage at site 4 which gives rise to the 12S and the 28S pre-rRNA. Whilst the factor responsible for this cleavage step remains unknown, it is suggested to be LAS1 (Gasse et al., 2015). The 5' and 3' ends of the 5.8S rRNA are cleaved from the 12S pre-RNA via exonucleases alongside a multitude of other factors (Tafforeau et al., 2013). The pre-28S rRNA is processed to form the mature 28S rRNA. All three mature rRNAs are exported into the cytoplasm, however it remains unclear at which stage and by which mechanism this occurs (Wang and Pestov, 2011).

There is an alternative pre-rRNA processing pathway in mammalian cells, termed the minor pathway (Sloan et al., 2013b). This involves the initial cleavage step that forms the 18SE and the 36S pre-rRNA. The 18SE pre-rRNA is processed into the 18S rRNA. The 36S pre-rRNA is processed into the 5.8S and 28S rRNAs (Tomecki et al., 2017, Wells et al., 2016). This pathway is said to more closely resemble the processing events in yeast.

1.6.3. Ribosomal protein production

The genes encoding ribosomal proteins (RPs) exist as single genes that contain specialised elements to aid synchronised transcription and co-regulation of translation (de la Cruz et al., 2015). The latter being facilitated by a genetic sequence encoding a terminal oligopyrimidine (Levy et al., 1991). Transcription of these genes is carried out by RNA polymerase II. Once complete, RP mRNAs are exported to the cytoplasm to be translated (de la Cruz et al., 2015). The mTOR signalling pathway is a critical regulator of cellular metabolism (Iadevaia et al., 2014). It has been shown to play a role in the translation of RP mRNAs. Through enabling the preferential translation of ribosomal proteins, the mTor

signally pathway has a direct influence on ribosome biogenesis, protein synthesis and therefore cellular proliferation.

Following translation, the ribosomal proteins are transported to the nucleolus to carry out their role in ribosome biogenesis. The RPs assemble with pre-rRNA as well as having secondary roles in rRNA processing, maturation and folding (Henras et al., 2015). It is known that RPs are produced in excess and rapidly degraded. This mechanism ensures that RP production does not limit the vital progression of ribosome biogenesis during cell division, with proteasomal degradation ensuring that the nucleolus is not overwhelmed with unused RPs (Lam et al., 2007).

RPs are often accompanied with chaperones that protect the protein from degradation (de la Cruz et al., 2015). A general chaperone network exists, however some RPs are known to interact with a specific chaperone. Chaperones are known for making contact with newly synthesised polypeptides and can play a role in protein folding together with protecting RPs from premature protein-protein interactions (Pillet et al., 2017). The majority of research into RP chaperones has been conducted in yeast, therefore little is known about human RP chaperones. One emerging, and important, human RP chaperone is the protein HEATR3 (Zhang et al., 2013, O'Donohue et al., 2022). It has been shown that cells depleted in HEATR3 have impaired nucleolar import of RPL5 (O'Donohue et al., 2022). This protein is a member of the 5S RNP, an important complex discussed in Section 1.6.4 and Section 1.7. Interestingly, defects in the HEATR3 protein were found in patients with Diamond Blackfan Anemia (DBA) and Chrohn's disease. DBA is known to be caused directly from defects in ribosome biogenesis (discussed further in Section 1.8) (Choesmel et al., 2007).

RPs are best known for their incorporation into the maturing ribosome, however, many have been implicated in having extraribosomal functions (Warner and McIntosh, 2009, Molavi et al., 2019). These include activation of p53 signalling, crosstalk with the NF-κB pathway and association with cell cycle regulators.

1.6.4. 5S RNP production and incorporation into maturing ribosome

The 5S ribonucleoprotein particle (5S RNP) is comprised of the 5S rRNA and ribosomal proteins, RPL5 and RPL11 (Sloan et al., 2013a). The 5S RNP complex assembles prior to incorporation into the large subunit and forms part of the central proturberance of the

ribosome (Madru et al., 2015). This functions as a link between the LSU and SSU (Ciganda and Willaims, 2014). The assembly pathway of the 5S RNP has not been fully described in human cells. It does, however, begin in the cytoplasm with the association of RPL5 and the 5S rRNA. This interaction is critical for the stability of the 5S rRNA allowing the 5S rRNA/RPL5 complex to translocate to the nucleoplasm where RPL11 binds (Pelava et al., 2016). The stability of the 5S RNP complex relies upon the presence of all three components (Bursać et al., 2012). The 5S RNP is therefore unique within ribosome biology, as the three members are the only ribosomal components to join as part of a pre-existing complex (Ciganda and Willaims, 2014).

It is likely that the 5S RNP interacts with a myriad of ribosome assembly factors. Many of these still remain unknown but been shown that incorporation of the 5S RNP into the LSU involves RRS1 and BXDC1 (Sloan et al., 2013a). However, it can be said that the recruitment of the 5S RNP into the LSU is not dependent upon these factors as depletion of RRS1 and BXDC1 did not cause a significant impact on ribosome biogenesis (Kharde et al., 2015). These factors were the first to be investigated in human cells as they are direct homologues of yeast proteins, Rrs1 and Rpf2, that have been shown to be critical to the integration of 5S RNP into the large subunit. On the other hand, PICT1 has been shown to have a distinct role in 5S RNP incorporation in human cells (Sloan et al., 2013a). It was demonstrated that PICT1 was able to bind to all of the components of the 5S RNP, with depletion of the protein causing significant impairment to LSU assembly. It is unlikely that the 5S RNP solely relies upon one protein chaperone. Sloan *et al* demonstrated that depletion of NOP2 and BOP1 proteins also impaired the recruitment of the 5S RNP into the LSU. It is predicted that each ribosomal component that is incorporated into the maturing human ribosome requires a variety of chaperones. These chaperones may exist in transient complexes or are involved in sequential transient interactions. Either way, 5S RNP recruitment relies upon the action of several assembly factors that remain unknown.

1.6.5. Assembly of the 80S ribosome

The assembly of the 80S ribosome is the final step in ribosome biogenesis (Thomson et al., 2013). Each ribosomal subunit matures independently prior to the final assembly step. The exact mechanism of this final step in humans remains unknown. A study found that the

human protein eIF6 is capable of keeping the ribosomal subunits apart *in vitro* (Valenzuela et al., 1982). This was followed up by Ceci *et al*. who found that eIF6 could bind to the 60S ribosomal subunit, however not to the 80S ribosome (Ceci et al., 2003). The study proposed that release of eIF6 is required for the joining of the LSU and SSU in humans. The study of ribosome biogenesis in humans is greatly understudied in comparison to yeast. This is likely due to the complexity of human biology. However, further insight into the biogenesis pathway in humans could aid the understanding of mechanisms by which deregulation of the pathway contributes to disease and therefore the design of specifically targeting therapeutics.

1.7. The Regulatory Role of the 5S RNP

As mentioned previously, ribosomal proteins are known to have functions independently to the ribosome (Molavi et al., 2019). The 5S RNP is a prime example of this. The complex is unique as it can exist stably in the cell independent to the ribosome (Pelava et al., 2016). The stability of the complex is dependent upon the presence of all three members (Bursać et al., 2012). This allows the 5S RNP to carry out regulatory roles and function as a regulatory hub for multiple signalling pathways. In incidences of stress, ribosome biogenesis is rapidly inhibited (Pelava et al., 2016). This state is often referred to as nucleolar stress, or ribosomal stress. Through this inhibition, the 5S RNP can accumulate and carry out functions to respond to the stress (Sloan et al., 2013a).

1.7.1. The 5S RNP/MDM2/p53 pathway

The p53 protein is kept at low cellular concentrations in unstimulated, non-cancer cells through the action of its key regulators, MDM2 and MDMX (Schon et al., 2002). These proteins work together to catalyse E3 ubiquitin ligase functions that lead to degradation of p53 via the 26S proteasome (Hannan et al., 2022). The removal or inactivation of MDM2 is required to stabilise and activate p53 leading to the transcription of p53 target genes. This tumour suppressor is best known for its role in promoting cell cycle arrest and apoptosis following DNA damage or oncogene activation and is referred to as the 'guardian of the genome' (Vousden and Prives, 2009). Different RPs have been implicated in the p53 response to nucleolar stress (Yang et al., 2018, Fumagalli et al., 2012). Originally, it was believed that ribosomal stress and subsequent ribosome biogenesis inhibition led to an increase in ribosomal protein production, which in turn led to activation of p53 signalling.

This was later disproved, due to the rapid degradation and high instability of RPs (Bursać et al., 2012). One example of an RP reported to regulate p53 is RPL26, which was shown to bind to the untranslated region of p53 mRNA and promote its translation (Chen and Kastan, 2010). However this model has been criticised due to the instability of solitary RPs making it unlikely that a single RP would be capable of forming a complex with p53 mRNA and facilitating protein synthesis (Pelava et al., 2016). The 5S RNP, however, is a stable complex.

Fumagali *et al*. performed a stringent analysis of the specific role each ribosomal protein plays in nucleolar stress (Fumagalli et al., 2012). Each RP was depleted in turn and the structure of the nucleolus and the activation of p53, was studied. As mentioned previously, cellular stress and the inhibition of ribosome biogenesis causes the breakdown of the nucleolar structure. Depletion of essential RPs would be sensed by the cell as deregulation of ribosome biogenesis, which would cause inhibition of the process. The majority of RPs were found to not impact the structure of the nucleolus or p53 action. A subset of RPs did not impact nucleolar structure yet activated p53 and, finally, only eight were implicated in both. Depletion of RPL5 and RPL11 caused a major breakdown of nucleolar structure without activating p53 (Bursać et al., 2012, Fumagalli et al., 2012). Further, double depleting RPs known to cause p53 activation alongside RPL11 or RPL5 was sufficient to inhibit p53 activation. Therefore, the study showed that RPL11 and RPL5 are critical to p53 activation following ribosomal stress.

In normal cellular conditions, the majority of the 5S RNP is incorporated into the maturing 60S ribosomal subunit (Pelava et al., 2016). In response to the inhibition of ribosome biogenesis, the 5S RNP accumulates in a ribosome free state (Figure 1.10). The 5S RNP is a key player in the response to nucleolar stress through direct regulation of p53 stabilisation (Sloan et al., 2013a). The role that the 5S RNP plays within this pathway is by promoting the dissociation of MDM2 from p53, allowing p53 to stabilise. RPL11 of the 5S RNP directly binds to MDM2 thus inhibiting its E3 ligase function (Zheng et al., 2015). Interestingly, through the study of the crystal structure of RPL11 bound to MDM2, it can be determined that this association is mutually exclusive to RPL11's incorporation into the ribosome (Zheng et al., 2015, Khatter et al., 2015). Whilst other RPs have been found to activate p53 signalling via this mechanism, it is clear that the 5S RNP is the most critical. Upon depleting RPL11 or RPL5 and challenging cells to nucleolar stress, Hannan *et al* demonstrated a 'blunting' effect upon

p53 stabilisation and activation (Hannan et al., 2022). The study investigated the impact of RPL11 or RPL5 depletion in response to various nucleolar stress activators, including chemotherapeutic drugs, actinomycin D and 5-fluorouracil, UV radiation and ionising radiation. Furthermore, a mutant MDM2 cell line was used. A single point mutation was introduced into the MDM2 gene to prevent the binding of RPL11 to MDM2, thus ablating the 5S RNP/MDM2/p53 pathway. In response to a panel of nucleolar stress inducers, the point mutation resulted in decreased p53 activation and stabilisation. This was an important study, as depleting ribosomal proteins will cause ribosome biogenesis to inhibit through the critical quality control mechanisms. Therefore, depletion alone can cause states of nucleolar stress in the cell. On the other hand, the point mutation within the MDM2 gene leaves ribosome biogenesis pathways intact and allows the specific investigation of the loss of the 5S RNP/MDM2 interaction. Given that the MDM2 mutation was sufficient to negatively impact the stabilisation and activation of p53, it suggests that 5S RNP/MDM2 is critical for the p53-dependent response to nucleolar stress.

Prior to the identification of the 5S RNP complex interacting with p53, it was determined that p53 activity could be induced through overexpression of RPL11 or RPL5 (Horn and Vousden, 2008). Interestingly, co-expression of the two proteins led to increased p53 activity. Furthermore, depletion of RPL11, which in turn depletes RPL5 as they are mutually dependent for stability, was sufficient to disable p53 activation in response to ribosomal stress (Bursać et al., 2012). Although the prevalent model proposes that MDM2 dissociates from p53 following 5S RNP binding, this has recently been challenged through a combination of chromatin immunoprecipitation and co-immunoprecipitation data. Mahata *et al* found that RPL11 is able to bind to the promoter of p53 target gene, *CDKN1A*, in a p53 dependent manner and this association is enhanced through the induction of ribosomal stress (Mahata et al., 2012).Furthermore, unpublished work from the Watkins laboratory demonstrated, via co-immunoprecipitation, the 5S RNP in association with MDM2 and p53 simultaneously. Therefore, it is possible that the 5S RNP can bind to the MDM2/p53 complex. This supercomplex could then translocate to the promoter region of p53 target genes to modulate gene expression. Either way, as ribosome biogenesis is so rapidly inhibited in response to cellular stress, the 5S RNP/MDM2/p53 pathway serves as a critical regulator of cellular fate (Pelava et al., 2016).
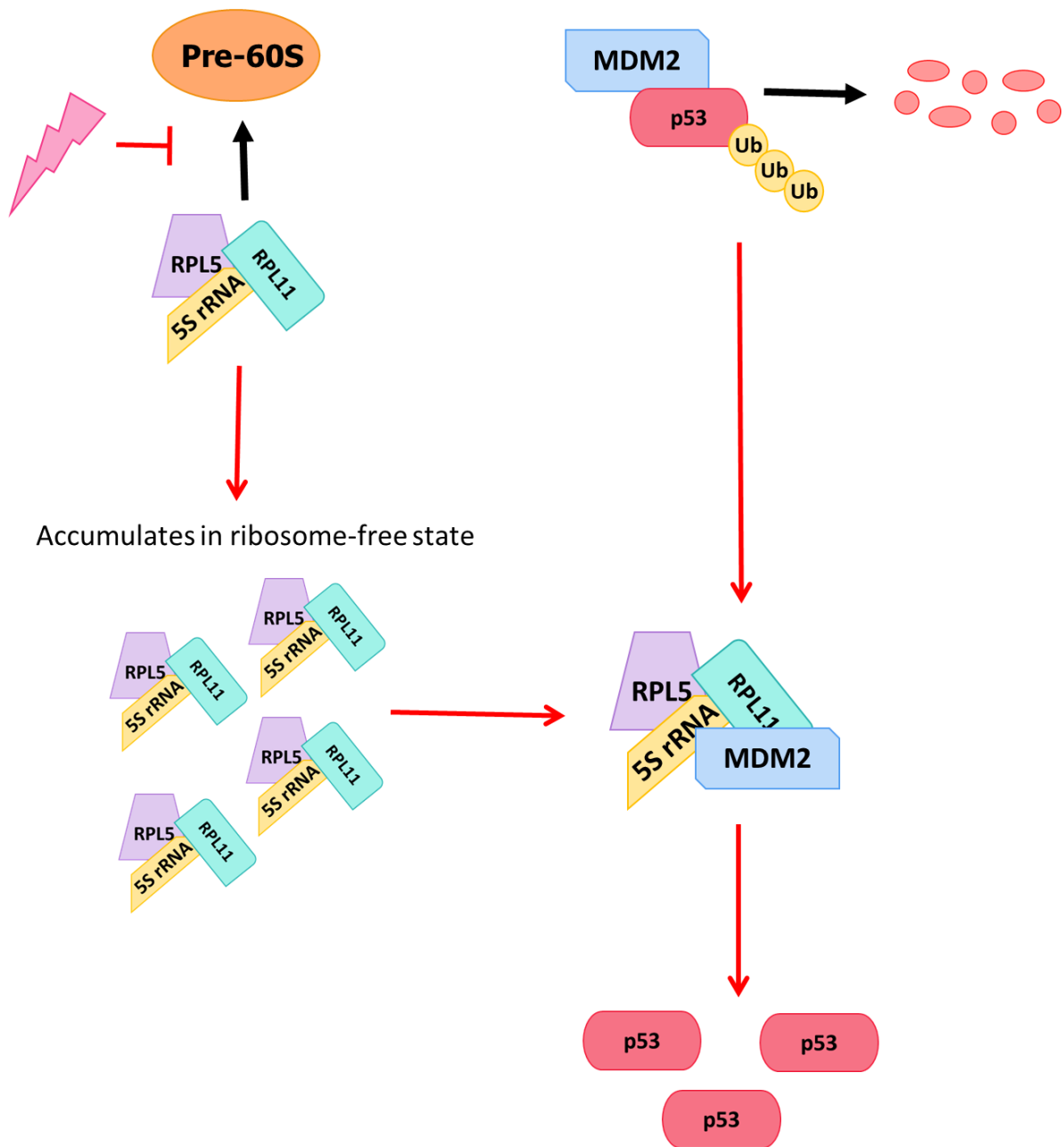
Figure 1.10 The 5S RNP mediated response to nucleolar stress. In normal cellular conditions (signified with black arrows) the 5S RNP is incorporated into the 60S ribosomal subunit during ribosome biogenesis. MDM2 binds to p53 to facilitate proteasomal degradation. However, in response to various cellular stresses, ribosome biogenesis is rapidly inhibited causing a state of nucleolar, also referred to as ribosomal, stress (signified by red arrows). This causes an accumulation of ribosome-free 5S RNP which is able to bind to MDM2 via RPL11, inhibiting the degradation of p53. The p53 tumour suppressor protein stabilises and activates to carry out its role in the cell.

1.7.2. Regulation of the oncogene, c-Myc

The human *MYC* gene encodes the oncogene, c-Myc (van Riggelen et al., 2010). Mutation or amplification of this gene are often linked to cancer due to c-Myc being a master regulator of cellular growth and metabolism. One mechanism through which this is achieved is through upregulation of ribosome biogenesis. c-Myc has been linked to the regulation of ribosomal protein synthesis, exportation of ribosomal subunits and rRNA transcription through the recruitment of cofactors and RNA polymerase I (Macias et al., 2010).

Interestingly, RPL11 of the 5S RNP has been found to interact with c-Myc (Dai et al., 2007b). This interaction decreased histone acetylation at the promoters of c-Myc target genes, thus repressing transcription. Moreover, siRNA mediated knockdown of RPL11 was sufficient to upregulate transcription and translation of the *MYC* gene itself in human U2-OS cells. Conversely, overexpression of RPL11 repressed the activation of MYC target genes (Dai et al., 2007a). Ribosomal stress results in impaired cellular proliferation due to the inhibition of ribosome biogenesis. It is hypothesised that RPL11 and c-Myc exist in a negative feedback loop, and that the constrained proliferation during ribosomal stress occurs through inhibition of c-Myc dependent gene expression.

1.7.3. Regulation of the tumour suppressor protein, p14ARF

The tumour suppressor p14^{ARF} operates in the same cellular signalling pathway as the p53 tumour suppressor, causing cell cycle arrest and apoptosis in response to stresses (Sugimoto et al., 2003). The p14^{ARF} tumour suppressor protein activates p53 to repress aberrant cell proliferation in response to oncogene activation (Cilluffo et al., 2020). Similarly to p53, p14^{ARF} is found to be mutated, deleted or inhibited in around 40% of cancers (Sugimoto et al., 2003). p14^{ARF} is known to bind to, and inhibit the action of, MDM2 allowing p53 activity (Weber et al., 2002).

ARF has also been shown to bind to the C terminus of RPL11, forming a complex of RPL11/ARF/MDM2/p53 (Dai et al., 2012). The use of siRNA mediated knockdown of RPL11 in U2-OS cells was sufficient to lower ARF-dependent p53 activation. On the other hand, overexpression of ARF leads to RPL11 accumulation in a ribosome independent state. The ribosome free state allows RPL11 to bind to MDM2 and carry out its regulatory role of p53 signalling. Sloan *et al* demonstrated that each member of the 5S RNP complex is vital for p53 activation via ARF (Sloan et al., 2013a).

1.8. Ribosome Biogenesis and Disease

Mutations in genes encoding ribosomal proteins, or defects within the ribosome biogenesis pathway, can lead to disease (Zhou et al., 2015). Mutated ribosomal proteins have been implicated in a wide range of diseases, from cardiovascular and neurodegenerative, to various cancers. For example, mutations in the gene encoding RPL10 has been linked to autism (Klauck et al., 2006). Further, increased phosphorylation of RPS15 has been linked to neurodegeneration and sporadic Parkinson's disease, with the introduction of a point mutation at threonine 136 to alanine was able to rescue the degeneration in a *Drosophila* model (Martin et al., 2014).

There is a group of 20 genetic diseases specifically linked to defected ribosome biogenesis. These are referred to as, ribosomopathies (Kampen et al., 2019). The most widely studied of these diseases are Diamond Blackfan anaemia, Treacher Collins syndrome, Schwanchman-Diamond syndrome and 5q syndrome.

Diamond Blackfan anaemia (DBA) involves mutations of ribosomal proteins, causing decreased expression (Choesmel et al., 2007). These include, but are not restricted to: RPL5, RPL11, RPS19, RPS7, RPS17, RPS15, RPS27a and RPL36. RPS19 is the most prevalent RP involved in DBA onset, with 25% of patients possessing a mutation in the gene (Boria et al., 2010). Patients suffer from extreme cases of anaemia caused by the failure of red blood cell production in the bone marrow. The disease has been linked to a predisposition to cancer, in particular acute myeloid leukaemia (McGowan and Mason, 2011). Some researchers believe that DBA results from the disruption of the 5S RNP/MDM2/p53 pathway leading to reduced p53 activity (Pelava et al., 2016). The protein components of the 5S RNP complex, RPL5 and RPL11, are mutated in 11.4% of DBA patients (Narla and Ebert, 2010). DBA leads to developmental issues, such as abnormal thumb formation and cleft palette malformations. Mutations in RPL11 are associated with the former, and RPL5 mutations the latter (McGowan and Mason, 2011, Cmejla et al., 2009). It was recently determined that deletion in a single *Rpl11* allele in adult mice leads to acute anaemia (Franklin et al., 2023). This haploinsufficiency is able to activate p53 in hematopoietic tissues and impacts red blood cell development by disrupting erythroid differentiation. Interestingly, the phenotype was rescued through a single allele p53 deletion, as well as by disrupting the 5S RNP/MDM2

interaction . This indicates that the murine phenotype is driven by the 5S RNP-induced activation of p53, highlighting the link between defective 5S RNP and DBA.

Haploinsufficiency of the TCOF1 gene is linked to Treacher-Collins disease. The TCOF1 gene is involved in pre-ribosomal complexes and is vital for the assembly of ribosomes (Jones et al., 2008). Patients with Treacher-Collins develop craniofacial defects (Kadakia et al., 2014). Crossing the *Tcof1* heterozygous knockout mice with p53-null mice rescued facial defects developed by the tcof1 mutant mice (Jones et al., 2008). This suggests that the disease arises from inappropriate activation of p53 and supports the link between p53 signalling and ribosome biogenesis. Finally, the study highlights the role of p53 in the apoptotic pathways of bone cells (Pelava et al., 2016).

1.8.1. Ribosome biogenesis in cancer

The link between ribosome biogenesis and cancer has been widely reported (Pelletier et al., 2017). For instance, cancer cells display a large increase in nucleolar size and number accompanied by increased ribosome biogenesis. In 2002, it was proposed that ribosomes could house a degree of heterogeneity, arising from variability in the many components of the ribosome (Mauro and Edelman, 2002). It is said to function in the regulation of translation through the varying ribosomes having preference for different subsets of mRNA (Li and Wang 2020 JCB). This is predicted to aid the cell to respond to the need to adjust protein levels during cellular processes. It has been more recently suggested that ribosome heterogeneity could directly play a role in tumorigenesis through the development of 'onco-ribosomes' that preferentially synthesise proteins that aid cancer progression (Elhamamsy et al., 2022). Cancerous cells go through reprogramming of cellular signalling pathways and metabolic processes (Hanahan and Weinberg, 2011). The reprogramming can lead to abnormal RNA polymerase I activity, contributing to hyperactivity of ribosome biogenesis mechanisms (Ferreira et al., 2020). One of the earliest steps in ribosome biogenesis, the formation of the pre-RNA transcripts, has been directly linked to cancer. Overexpression of the pre-RNA was associated with poor survival of alveolar rhabdomyosarcoma, suggesting deregulation of this step would lead to more advanced cancer progression (Elhamamsy et al., 2022).

One of the main drivers of ribosome-associated cancer are mutant ribosomal proteins. Low level mutations will inhibit the process of ribosome biogenesis (Zhou et al., 2015). This will

lead to the activation of p53, enabling downstream processes, such as cell cycle arrest or apoptosis which will aim to prevent onset of disease. Significant mutations, however, have the ability to escape the quality control mechanisms in place (Zhou et al., 2015, Pelletier et al., 2017). Such mutations are heterozygous mutations in genes encoding ribosomal proteins, often found in patients with genetically inherited ribosomopathies (Pelletier et al., 2017). linked to acute myeloid leukaemia, colon carcinoma and osteogenic sarcoma (Ajore et al., 2017). During circumstances in which the cancer cell evades regulatory mechanisms, such as tumour suppressor activation, DNA damage response or programmed cell death, aberrant ribosome biogenesis and protein translation is able to occur (Pelletier et al., 2017). Moreover, as the 5S RNP is linked to both oncogenes and tumour suppressors that are often mutated in cancer, this could lead to the loss of those important cellular stress responses. For example, the oncogene c-Myc is known for increasing translation events through regulating genes involved in ribosome biogenesis (Elhamamsy et al., 2022).

A murine mouse model was created to eliminate the RPL11/MDM2 interaction (Macias et al., 2010). Cysteine 305 of the MDM2 gene was mutated to phenylalanine, which has been shown to prevent the binding of RPL11 to MDM2 in response to ribosomal stress (Liu et al., 2014). Macias *et al* studied this model in the context of B cell lymphoma to determine the influence the 5S RNP/MDM2/p53 pathway had upon disease progression (Macias et al., 2010). The MDM2-C305F mutants possessed less p53 protein than the wild-type due to the prevention of the MDM2/RPL11 interaction. Therefore, MDM2 is able to mediate the ubiquitination and subsequent degradation of p53 (Macias et al., 2010). Murine embryonic fibroblasts were cultured from the mutant mice and in response to ActD induced ribosomal stress, decreased cell cycle arrest and increased cellular proliferation was observed. This study demonstrated the important tumour suppressive role the 5S RNP/MDM2/p53 pathway plays. B cell lymphoma is often c-Myc driven. To study this *in vivo,* scientists have developed a mouse model called the Eμ-myc mouse. These mice constitutively express c-Myc in their B cells (Adams et al., 1985). Crossing the C305F homozygous mouse with the Eμ-myc mouse enabled the study of the 5S RNP/MDM2 interaction within the context of B cell lymphoma (Macias et al., 2010). The eradication of the interaction led to early onset of B cell lymphoma and decreased survival rates. It has therefore been suggested that the 5S

RNP/MDM2/p53 pathway could be a good target for chemotherapeutic agents (Catez et al., 2019).

It has been hypothesised that mutation of the RPL5 gene is a driver of cancer (Zhang et al., 2022). The gene is included within the COSMIC (Catalogue of Somatic Mutations in Cancer) database as a tier 1 cancer driver. RPL5 frameshift, nonsense and missense mutations are present in 34% of breast cancers, 11% of glioblastomas and 28% of melanoma patients. Patients with multiple myeloma and glioblastoma have a worse overall survival if they express low levels of RPL5 mRNA (Fancello et al., 2017).

Because of the definitive link between ribosome biogenesis, tumour suppressors and oncogenes, it is not surprising that scientists are looking to target the pathway therapeutically (Catez et al., 2019). For example, the chemotherapies ActD, 5FU and olaparib, a PARP inhibitor, which all induce p53 activity through 5S RNP-mediated mechanisms (Iapalucci-Espinoza and Franze-Fernández, 1979, Sun et al., 2007, Han et al., 2022). Ribosome biogenesis inhibition through direct inhibition of RNA polymerase I, such as through the use of ActD, tends to lead to cell cycle arrest rather than apoptosis (Lindström et al., 2022). Therefore, the use of such drugs in the treatment of cancer is not as favourable as those that directly induce cell death. Through *in silico* design a small molecule RPL11 mimetic was designed and synthesised to disrupt the RPL11/MDM2 interaction (Wang et al., 2022). Whilst further research is needed to support the claims, the publication demonstrated the disruption of the interaction inhibited tumour cell growth through apoptotic mechanisms. The compound studied, named S9, was demonstrated to bind directly to MDM2. Treatment of U2-OS and HCT116 cells with the S9 mimetic led to G2/M arrest and apoptosis. It is suggested the cellular effects are due to the S9 induced stabilisation and activation of p53. The study included an *in vivo* model involving the use of HCT116 cell derived xenograft models in mice. Despite an insignificant impact on the weight of the mice, the use of S9 was able to significantly decreased tumour volumes. Thus, the small molecular mimetic functions to bind to MDM2, inhibiting its E3 ligase activity, and allowing p53 to activate in cancerous cells, which leads to an inhibition of cellular proliferation.

1.9. Experimental Aims and Objectives

This thesis aimed to elucidate the role of p52 in the ribosomal stress response. A previous collaboration between the Perkins and Watkins laboratory demonstrated an association between p52 and RPL11 of the 5S RNP. This association was enhanced through ultraviolet radiation, a known inducer of ribosomal stress. The link between p52 and p53 signalling, and the regulation of p53 signalling via the 5S RNP, has been widely discussed. I further investigated the p52/RPL11 interaction and its role in cross-talk between non-canonical NF-κB activity and the 5S RNP/MDM2/p53 pathway.

Chapter 2   Materials and Methods

2.1. Mammalian cell culture

All cell lines were grown at 37°C and 5% CO_2 in an incubator. Upon reaching 70% confluency, cells were passaged using 1X Trypsin-EDTA in sterile phosphate buffered saline. All cell lines were cultured in Dulbecco's Modified Eagles Medium (DMEM) supplemented with 1% L-glutamine and 10% foetal bovine serum. Various cell lines were utilised, including those with stably transfected plasmids. The cell lines, transfected plasmids, selection and tag inducing reagents are detailed in Table 2.1. Selection reagents were added to cell culture media at every other passage. Tag inducing reagents were added at least 24 hours prior to further treatment or harvest to ensure adequate expression of plasmid encoded proteins. Drugs utilised, drug targets and concentrations are indicated in Table 2.2.

2.1.1.   Cell freezing and cell storage

Cell pellets were resuspended in freezing media consisting of FBS supplemented with 1% DMSO. Aliquots of the suspension were transferred to cryovials before being insulated and placed in a -80°C freezer. Once frozen the vials were moved to liquid nitrogen storage or stored in a -152°C freezer.

Cell line	Description	Transfected plasmid	Selection reagents	Tag inducing reagent
U2-OS	Osteosarcoma cell line; wild-type p53			
HCT116	Colorectal cancer cell line; wild-type p53			
GFP U2-OS	Osteosarcoma cell line expressing GFP; wild-type p53	pEGFP-C2	G418 Sulphate 200µg/ml	
GFP-p52 U2-OS	Osteosarcoma cell line expressing GFP-tagged p52; wild-type p53	pEGFP-C2-p52	G418 Sulphate 200µg/ml	
H1299	Human non-small-cell lung carcinoma cell line			
FLAG	U2-OS cells stably expressing a Flp-IN T-Rex tetracyclin includible plasmid	pcDNA5/FRT/TO	100µg/mL hygromycin B 10µg/mL blastacidin S	1µg/mL Tetracyclin
FLAG-MDM2	U2-OS cells stably expressing a Flp-IN T-Rex tetracyclin includible plasmid	PcDNA5/FRT/TO-MDM2	100µg/mL hygromycin B 10µg/mL blastacidin S	1µg/mL Tetracyclin

Table 2.1 Details of human cancer cell lines used

Drug name	Target	Concentration
Actinomycin D	RNA polymerase II	5nM
UV radiation	RNA polymerase I	40J/m^2
5-flurouracil	thymidylate synthase	50µM
Doxorubicin	Topoisomerase II	1µM
Z-VAD FMK	Caspase 1, Caspase 3 - 10	50µM

Table 2.2 Details of drug treatments

2.1.2. Transfections

Prior to transfections, culturing media was changed from DMEM to Opti-MEM Reduced Serum Media (Gibco, Life Technologies) due to a correlation with increased transfection efficiency. Transfections were carried out as detailed below. Cells were left to grow in the Opti-MEM containing the transfection mixture overnight before being replaced with DMEM to allow cells to recover prior to drug treatment.

2.1.3. Transient transfection

Cells were seeded to a confluence of 50% the day before the intended transfection. Per 2mL of Opti-MEM used, the following transfection mixture was used: 2µL Lipofectamine 2000 (Life Technologies), 1µg plasmid DNA and 100µL Opti-MEM. The preparation of the transfection mixture was carried out by incubating Lipofectamine 2000 with Opti-MEM for 5 minutes followed by the addition of plasmid DNA. The mixture was further incubated for 10 minutes prior to being added to cell cultures in a drop-wise manner.

2.1.4. RNAi transfection

Cells were seeded to a confluence of 30% the day before transfection. The transfection mixture contained siRNA (final concentration 5nM), InterferIN (Polyplus) and Opti-MEM. The InterferIN transfection reagent and Opti-MEM were used at a ratio of 1:100 with volumes varying in relation to the size of culture dish used. InterferIN was added to Opti-MEM and incubated for 5 minutes. siRNA was added gently and incubated for 10 minutes. The transfection mixture was added to cells in a drop-wise manner.

2.2. Cell Harvest

To harvest solely the adherent population of cells, media was poured off prior to scraping the cells in 1 X PBS. The total population of cells were harvested by scraping cells in growth media. This allows the harvest of both adherent and floating cells in the dish. Cell pellets were collected by spinning cell suspensions at 300 x g at 4°C for 5 minutes. Pellets were washed once with 1 X PBS and supernatants were removed prior to protein or RNA extractions.

2.3. Glycerol Gradient Centrifugation

The 10-40% glycerol gradient was produced using a BioComp Gradient master (model 107ip) by adding 2ml of 10% glycerol (10% glycerol (v/v), 0.2% Triton-X-100 (v/v), 1.5mM $MgCl_2$, 20mM HEPES, 150mM KCl, 0.5mM EDTA, 1mM DTT) solution to an Ultra-Clear™ Centrifuge tube (Beckman) followed by 2ml of 40% glycerol solution (40% glycerol (v/v), 0.2% Triton-X-100 (v/v), 1.5mM $MgCl_2$ 20mM HEPES, 150mM KCl, 0.5mM EDTA, 1mM DTT). Cell pellets, previously snap frozen, were resuspended in 1x gradient buffer E (20 mM HEPES pH 8.0, 150 mM KCl, 0.5 mM EDTA, 0.1 mM DTT, 5% glycerol) and sonicated for two 15 second intervals separated by a 30 second break. Triton X-100 was added to a final concentration of 0.2% and the sample was spun at 4°C at 18,000xg for 10 minutes. 400µl was loaded onto the gradient. The gradients were centrifuged in a swTi60 rotor (Beckman L7-80) at 4°C at 52,000rpm for 90 minutes. Fractions of 200 µl were removed sequentially from the supernatant until fraction 21. Fractions were snap frozen in liquid nitrogen and stored at -80°C. The proteins in the fractions were analysed via western blotting (Section 1.5.6).

2.4. Flow Cytometry

To analyse the cell cycle profiles of whole U2-OS cells, the cells were harvested in PBS and fixed in 1mL of 70% ethanol whilst continuously vortexing to avoid the formation of clumps. Cells were stored at -80°C. To stain the cells, the cell suspension was spun at 6000xg for 5 minutes prior to washing in PBS. To collect cells, an additional spin was performed. The cell pellets were resuspended in 200uL of staining solution (20ug/mL RNase A, 50ug/mL propidium iodide) and incubated in the dark for 20 minutes. Samples were analysed on a Canto Flow Cytometer. Subsequent data analysis was performed using FlowJo.

2.5. In Vitro Techniques and Cloning

2.5.1.   Bacterial transformation

Appropriate strains of bacteria were selected for use depending on whether DNA (XL1-blue or DH5α) or protein (pLysS) were being isolated. Between 0.5-1μg of plasmid DNA was incubated with 25μL of competent bacteria for 30 minutes on ice. The mixture was subject to heat shock at 42°C for 30 seconds and placed back on ice for 5 minutes. The mixture was spread evenly on an LB-ampicillin plate and incubated at 37°C overnight to allow the formation of colonies. Plasmids used throughout the project are detailed in Table 2.3.

For plasmids exhibiting a low transformation efficiency, an extra recovery step was performed prior to spreading bacteria on the plate. 900μL of SOC media was added to the competent bacteria/plasmid DNA mixture and incubated at 37°C whilst being constantly agitated.

Plasmid name	Vector backbone	Bacterial selection agent
GST control	pGEX-61-P	Ampicillin
GST-p52	pGEX-61-P-p52	Ampicillin
GST-RPL11	pGEX-61-P-RPL11	Ampicillin
GFP control	pEGFP-C2	Ampicillin
GFP-p52	pEGFP-C2-p52	Ampicillin
RSV control		Ampicillin
RSV-RelB		Ampicillin
pJET-p52E86A	pJET1.2	Ampicillin
pJET-p52E86Q	pJET1.2	Ampicillin
pJET-p52E86V	pJET1.2	Ampicillin

Table 2.3 Details of plasmids and selection agents required.

2.5.2. Recombinant protein expression and purification

Following bacterial transformation of the desired plasmid containing the gene encoding a recombinant protein, a single colony was grown in 20mL LB-ampicillin (100µg/mL) overnight in a shaking incubator set at 37°C and 200RPM. The 20mL starter culture was added to 400mL LB-ampicillin and grown in the same conditions. Each hour 1mL of culture was taken to measure the optical density. Once the optical density indicated the exponential growth phase of the culture, IPTG (1mM) was added. After four hours of IPTG induction, the bacteria were pelleted by centrifugation at 3000xg for 30 minutes. Protein was extracted using BugBuster (Merck Millipore) according to manufacturer's specifications. GST and GST tagged proteins were isolated from crude extracts by incubation with glutathione-agarose beads for 1 hour.

2.5.3. Cleavage of GST Tag from GST-tagged proteins

Crude extracts of GST-tagged proteins were diluted with 1 X phosphate buffered saline and incubated with 50µL glutathione agarose bead slurry, being turned end over end, for 1 hour at 4°C. The protein/bead complexes were incubated in 500µL cleavage buffer (50mM Tris pH 7, 150mM NaCl, 1mM EDTA) and 2 units of PreScission Protease for a further 2 hours at 4°C. The GST/bead complexes were pelleted and supernatant containing untagged recombinant proteins harvested. The solution containing recombinant proteins were subject to two further incubations with 30µL glutathione agarose bead slurry to ensure successful removal of PreScission Protease, GST and GST-tagged proteins.

20µL of supernatant was supplemented with 1X SDS loading buffer and the size of the protein checked via coommassie staining of SDS PAGE gels before use in pulldown assays.

2.5.4. Isolation of plasmid DNA

In order to isolate plasmid DNA from transformed colonies of XL-1 blue or DH5α E. Coli, single colonies were grown in LB-ampicillin media overnight. Depending upon the desired DNA yield either a 10mL culture or 50mL culture was created. For the former, DNA was purified using the GeneJet Plasmid Miniprep kit (ThermoFisher) and for the latter a MidiPrep Plasmid Kit (Qiagen). Both extraction protocols were performed according to manufacturer's specifications. The miniprep or midiprep kits yielded varying concentrations of DNA in 30-50µL or 100-200µL total volume, respectively.

2.5.5. Restriction endonuclease digest of DNA

All DNA digests were performed to manufacturer specifications. One Weiss unit of enzyme was used per 1μg of lambda DNA and incubated at the appropriate temperature for an hour. Specific restriction endonucleases used are specified in figure legends.

2.5.6. Design of gBlock sequences

Short sequences of double stranded DNA were designed at a specific locus of the p52 gene using SnapGene. Any mutations were encoded in the sequences before ordering the DNA in the form of a gBlock (Integrated Data Technologies). The double stranded DNA was resuspended in nuclease free water and incubated at 50°C for 15 minutes.

2.5.7. Ligation of gBlock into pJET1.2

The designed gBlocks were cloned into pJET1.2 plasmid backbones using the CloneJet PCR cloning kit (ThermoFisher Scientific) according to manufacturer's specifications.

2.5.8. Ligation

Vector backbone and insert DNA that was previously digested with restriction endonucleases and gel extracted was quantified through comparison to known concentrations of DNA on a 1% agarose gel. A molar ratio of either 1:3 or 1:5 (vector:insert) was incubated in a total volume of 20μL with 1 X T4 DNA ligase buffer (ThermoFisher) and one Weiss unit of T4 DNA ligase (Thermo Fisher) at 16°C overnight. 5μL of ligated DNA was used in a DNA transformation as described above (Section 1.4.1).

2.6. Protein Techniques

2.6.1. Protein extraction – mammalian whole cell lysates

Harvested cell pellets were resuspended in PhosphoSafe (Merck Millipore) extraction buffer to harvest cytosolic proteins. The samples were left to lyse for 5 minutes at room temperature. Lysates were spun at 20,000xg at 4°C for 10 minutes to remove nuclear and chromatin associated proteins. Prior to spinning at 20,000xg at 4°C for 10 minutes. The supernatant was used for future analysis.

2.6.2. BCA assay

Quantification of protein concentrations was carried out using the microplate Pierce™ BCA Assay (ThermoFisher Scientific; ref: 23225). Bovine serum albumin (BSA) standards were made according to manufacturer's specification. 2µL of standard concentrations of BSA were added to corresponding wells to create a standard curve. The same volume of each sample was loaded into designated wells. A 1:50 dilution of reagent B:reagent A was made and 100µL added to each well on a microplate. The plate was incubated at 37°C for 30 minutes and a spectrophotometer was used to measure the absorbance (562nm). The protein concentrations were quantified relative to the standard curve.

2.6.3. Coommassie blue staining

To visualise the size, presence or abundance of proteins, SDS PAGE gels, detailed in Table 2.4, were run at 140V for 45 minutes prior to being incubated in fixing solution (50% water (v/v), 40% ethanol (v/v), 10% acetic acid (v/v)) for 30 minutes. The fixed gels were washed with distilled water twice for 5 minutes. The coommassie blue stock solution (80% water (v/v), 10% phosphoric acid (v/v) 10% ammonium sulfate (v/v), 0.1% Coomassie G250 (w/v)) was supplemented with 20% methanol and used to stain the gel overnight, being constantly shaken. Images of stained gels were taken using a digital camera.

Gel:	Water (ml)	40% Acrylamide (ml)	1.5M Tris pH8.8 (ml)	1.5M Tris pH6.8 (ml)	10X SDS (µl)	10X Aps (µl)	TEMED (µl)
10%	2.4	1.25	1.25		50	50	1
12%	2.1	1.5	1.25		50	50	2
15%	1.75	1.9	1.25		50	50	2
Stacking	1.46	0.25		0.25	20	20	2

Table 2.4 SDS PAGE Gel components

2.6.4. GST pulldown assay

GST or GST-tagged RPL11 were purified using glutathione-agarose beads and subject to 5 washes with 1 X PBS supplemented with 0.1% Tween-20. The GST/bead or GST-RPL11/bead complexes with incubated end over end with 1μg of untagged recombinant p52 protein for 2 hours at 4°C in cleavage buffer (50mM Tris pH 7, 150mM NaCl, 1mM EDTA). The beads were thoroughly washed with cleavage buffer supplemented with 0.1% Nonidet P-40 prior to eluting potential protein complexes from the beads with the addition of 1 x SDS loading buffer and heating samples at 95°C for 10 minutes. Visualisation of presence of GST, GST-tagged RPL11 or p52 within samples was achieved using western blotting analysis.

2.6.5. Co-immunoprecipitation

The Chromotek GFP-Trap system allows rapid purification of GFP-tagged proteins. GFP and p52-GFP expressing U20S cells were grown to 70% confluency. Half of the dishes were treated with actinomycin D for 5 hours and cell pellets left in 250μL NP-40 lysis buffer (10mM Tris pH 7.6, 150mM NaCl, 0.5mM EDTA, 0.75% (v/v) NP-40) on ice for 30 minutes with extensive pipetting every 10 minutes. Samples were spun for 10 minutes at 20,000g (4°C). The protein concentration was determined using a BCA assay and equal amounts of protein were added per IP followed by dilution using a 1:1 ratio of lysis buffer:dilution buffer (10mM Tris, 150mM NaCl, 0.5mM EDTA) to a final volume of 350-500μL depending on protein concentration. Samples were left to rotate at 4°C overnight with 10μL of equilibrated GFP-Trap agarose beads or 5μL of equilibrated GFP-Trap magnetic beads per IP reaction. The following day, the beads were washed with dilution buffer and eluted in 20-40μL 2X SDS buffer (120mM Tris pH 7.6, 20% (v/v) glycerol, 4% (w/v) SDS, 0.04% (w/v) bromophenol blue, 10% (v/v) β-mercaptoethanol) depending on the amount of protein loaded per IP. Proteins present in complexes isolated by the beads were visualised via western blotting.

2.6.6. Western blotting

Each SDS page gel was prepared according to Table 2.4. Following Co-IPs a third of the eluted sample volume was loaded per well with corresponding input samples. Specific percentage of input loaded per experiment indicated in figures and calculated in relation to total volume. Following protein lysis 10 μg of sample diluted in 5X SDS loading dye (0.25M Tris pH6.8, 1% SDS (w/v), 40% Glycercol (v/v), 8% β-mercaptoethanol (v/v), 0.05 bromophenol blue) were boiled for 10 minutes and loaded into each well. Following glycerol

gradient centrifugation, 20µl of sample was diluted in 5X SDS loading buffer to reach a final concentration of 1X, boiled and loaded in each well. Gels were run at 90mV for 10 minutes followed by 140mV for 45-60 minutes. PVDF membranes (Merck Millipore) were submerged in methanol for 15 seconds, 2 minutes in water and 5 minutes in 1X semi-dry transfer buffer (4.8mM Tris, 3.9mM Glycine, 0.01% SDS, 20% MtOH (v/v)). Proteins were transferred from gel to membrane at 20mV for 30 minutes using the Trans-Blot® Turbo^{TM} Transfer System (Biorad). Membranes then underwent the blocking step in 5% (w/v) milk-Tris buffered saline-Tween (TBS-T; 20mM Tris, 0.5M NaCL, 0.1% Tween-20, pH 7.6) for one hour. Membranes were incubated in primary antibody overnight at 4°C (Table 2.5). The following day the primary antibody was washed off using TBS-T and the membranes incubated in secondary antibody (Table 2.6) diluted in 5% milk TBS-T for 120 minutes. Secondary antibodies were washed off the membranes before developing using chemiluminescence (Pierce^{TM} ECL Western Blotting Substrate; Thermo Scientific ref:32106) according to manufacturer's specification. The blots were visualised either using film in a dark room, a Li-Cor Odessey or a BioRad ChemiDoc. Following the use of film, images were scanned onto a computer. Following the use of a digitised imaging protocol, images were exported and analysed using the following software: Image J (Li-Cor images) or ImageLab (BioRad ChemiDoc image. Image J or ImageLab were used to quantify western blots. The data was exported to Microsoft Excel. If three independent repeats were carried out, either a fold change calculation or normalisation by sum was performed (Degasperi et al., 2014). The latter involves calculating the total number of pixels in the protein of interest using the loading control. Following that, data point X was divided by the sum of all data points across the replicate. This was performed to eliminate the experimental variations that arise between each repeat of a western blot to allow direct comparison of the biological repeats. Three independent repeats were plotted using Prism 6 and a two-way ANOVA performed. Due to the normalisation by sum leading to increased false positives rates of statistical significance, the significant p value was altered to 0.025.

Antibody name	Species raised in	Dilution	Diluent	Supplier	Reference
RPL11	Rabbit	1/1000	5% Milk TBS-T or 2% BSA supp. 0.1% NaN_3	Abcam, St John's (50/50 mix)	Ab79532, STJ28490
p52/p100	Mouse	1/1000	5% Milk TBS-T or 2% BSA supp. 0.1% NaN_3	Merck Millipore	05-361
RelB	Rabbit	1/1000	5% Milk TBS-T	Cell Signaling Technologies	4954
GFP	Rabbit	1/1000	5% Milk TSB-T	New England Biolabs	2956S
p53	Mouse	1/1000	2% BSA supp. 0.1% NaN_3	Santa Cruz	Sc-126
PARP	Rabbit	1/1000	2% BSA supp. 0.1% NaN_3	Cell Signaling Technologies	9542
p21$^{WAF1/CIP1}$	Rabbit	1/1000	2% BSA supp. 0.1% NaN_3	Cell Signaling Technologies	2947
MDM2	Mouse	1/1000	5% Milk TBS-T	Calbiochem	OP46
RPL5	Rabbit	1/1000	2% BSA supp. 0.1% NaN_3	Cell Signaling Technologies	14568
Phospho-cdc2 Tyr15	Rabbit	1/1000	5% Milk TBS-T	Cell Signaling Technologies	9111
cdc2	Rabbit	1/1000	5% Milk TBS-T	Cell Signaling Technologies	77055
Wee1	Rabbit	1/1000	5% Milk TBS-T	Cell Signaling Technologies	4936
Cyclin D1	Rabbit	1/1000	5% Milk TBS-T	Cell Signaling Technologies	29RRS

Table 2.5 Primary Antibodies

Antibody name	Dilution	Supplier	Reference
Anti-rabbit IgG	1/3000 - 1/5000	Cell signalling	7074
Anti-mouse IgG	1/3000 - 1/5000	Sigma	7076
Anti-mouse 800CW	1/10000	LiCor	926-32212
LiCor Rabbit 680RD	1/10000	LiCor	926-68073
Anti-rabbit 800CW	1/10000	LiCor	926-32211

Table 2.6 Secondary Antibodies

2.7. RNA Techniques

2.7.1. RNA extraction for polymerase chain reaction

RNA was extracted using PeqGold RNA Kit (VWR). Cell pellets were resuspended in 350µL
TRK Lysis buffer. RNA was homogenized and isolated using columns provided and according
to manufacturer's protocol before being eluted using 40µL RNAse-free water.

2.7.2. RNA quantification

Concentrations of RNA in a sample were quantified using a NanoDrop. Prior to reverse
transcription, 500ng of each RNA sample was prepared to a final volume of 12µL.

2.7.3. Reverse transcription

RNA samples were reversed transcribed using the QuantiTect® Reverse Transcription Kit
(Qiagen; 205313) to generate copy DNA (cDNA). Genomic DNA was removed during
incubation with gDNA Wipeout reagent (Qiagen) at 42°C (2 minutes) and 1 µg of cDNA was
prepared according to the manufacturer's Quick-StartProtocol. cDNA was diluted 1:10 in
RNase-free water upon completion of the reaction.

2.7.4. Quantitative real-time polymerase chain reaction

Quantiative real-time PCR (qRT-PCR) was carried out using 20ng of cDNA, in duplicate, and
master mix which included primers with a total reaction volume of 20µL (Table 2.7). Samples
were run and analysed on a Rotor-gene Q system (Qiagen). A housekeeping gene, selected
due to stability of gene expression levels, was always run alongside genes of interest. Details
of genes studied and primers used are listed below (Table 2.8). Cycling conditions and primer
sequences indicated in Table 2.8. All cycling threshold (CT) values were normalised to
housekeeping gene levels using the Pfaffl method.

Reagent	Manufacturer	Concentration (v/v) %
5x PCR buffer	Promega	26.7
dNTPs	Life technologies	20
MgCl$_2$	Promega	16.7
SYBR (1/200 DMSO)	Life technologies	1.3
Taq Polymerase	Promega	1.3
Primer mix	Eurogentec custom oligos	3.3

Table 2.7 PCR Master Mix

Gene Name	Sequence	Cycling conditions
Housekeeping - ACTB		40 cycles 30 seconds 95°C 30 seconds 60°C 30 seconds 72°C
CCNB1	F= ATA-AGG-CGA-AGA-TCA-ACA-TGG-C R= TTT-GTT-ACC-AAT-GTC-CCC-AAG-AG	40 cycles 30 seconds 95°C 30 seconds 60°C 30 seconds 72°C
CDKN1A	F= ACT-CTC-AGG-GTC-GAA-AAC-GG R= GGG-CTT-CCT-CTT-GGA-GGA-GAT	40 cycles 30 seconds 95°C 30 seconds 60°C 30 seconds 72°C
BCL2-Like 1	F= GGT-CGC-ATT-GTG-GCC-TTT-TTC R= TGC-TGC-ATT-GTT-CCC-ATA-GAG	40 cycles 30 seconds 95°C 30 seconds 60°C 30 seconds 72°C
BCL2	F= GAA-CTG-GGG-GAG-GAT-TGT-GG R= CCG-GTT-CAG-GTA-CTC-AGT-CA	40 cycles 30 seconds 95°C 30 seconds 60°C 30 seconds 72°C

Table 2.8 Primers used for quantitative RT-PCR

2.7.5. RNA extraction for Northern blotting

Cell pellets were harvested as previously described before resuspension in 500μL of TRI-reagent (Invitrogen). Samples were left to incubate at room temperature for 5 minutes. 100μL of chloroform was added to the mixture and vortexed for 15 seconds. Samples were incubated at room temperature for 2 minutes and the aqueous phase separated by centrifugation at 13,000 rpm for 15 minutes. The upper, aqueous, phase was harvested and 250μL isopropanol was added and the mixture incubated for 15 minutes. RNA was pelleted via centrifugation at maximum speed for 10 minutes. Following the removal of the supernatant, RNA was washed with 75 % ethanol. The pellets were dried for one minute in a SpeedVac Vacuum Concentrator and stored at -80°C to be analysed via Northern Blotting.

2.7.6. Northern blotting

For detection of the 5S rRNA, extracted RNA pellets were resuspended in 1x RNA loading dye (40 % formamide, 0.5 mM EDTA, 50 μg/ml bromophenol blue, 50 μg/ml xylene cyanol), and boiled for 2 minutes. Samples were placed on ice for 2 minutes before being loaded onto an 8 % acrylamide/7 M urea gel in 1xTBE solution. After being separated by size, RNA was transferred from the gel to a Hybond N membrane in 0.5x TBE solution at 65 V for 90 minutes. A Stratalinker UV Crosslinker was utilised to crosslink the RNA to the membranes followed by a pre-hybridisation step. This involved incubation of the membrane for 1 hour in SES1 (0.5 M sodium phosphate pH 7.2, 7 % SDS (w/v), 1 mM EDTA) at 37°C. After which the membranes were incubated overnight at 37°C with a ^{32}P-labelled 5S rRNA and 5.8S rRNA probe (provided by Watkins laboratory) diluted in SES1 (Table 2.9). The membranes were subject to two 15 minute washes with 1x SSC/0.1 % SDS solution at 37°C. Finally, a phosphoimager screen was exposed to the membrane in order to visualise the 5S rRNA presence using a Typhoon Phosphoimager (GE Healthcare).

Name of probe	Sequence
5S rRNA	CCGAGATCAGACGAGATCGGGCGCGTTCAGGGTGGTATGG
5.8S rRNA	CAATGTGTCCTGCAATTCAC

Table 2.9 Northern blot radioactive probe sequences

2.8. Computer Modelling Methods

2.8.1. Acquisition of files

Relevant files were obtained using online databases. Protein structure files, in PDB format, were downloaded from the Protein Data Bank webserver (https://www.rcsb.org/). FASTA sequences of proteins were downloaded from Uniprot (https://www.uniprot.org/ - UniProt IDs: p52 - Q00653, RPL11 – P62913).

2.8.2. Protein-protein interface prediction

A panel of software were utilised to highlight the residues in NF- κB p52 and RPL11 that were predicted to contribute to protein-protein interfaces. This provided a map of the regions within each protein that are most likely to participate to general protein-protein interactions. It must be stressed the sofware is unable to predict residues actively contributing to specific protein-protein interactions. The interface can be predicted by analysing the FASTA sequence (PSIVER and PredictProtein) or the structure of a protein using the PDB file (PredUS, CPORT,WHISCY, and Promate). Files of p52 or RPL11 were uploaded to the webservers in the relevant format. The FASTA sequence for PSIVER and PredictProtein and a PDB file for PresUS, CPORT, WHISCY and Promate (Table 2.10). The residues returned as "active" relate to the predicted presence or contribution of that residue to a protein-protein interaction. The identification of a particular residue as active by a singular software was given a score of one. The cumulative scores of the predicted interface given by the panel of software were calculated using Microsoft Excel and plotted as a line graph. Regions of the proteins that were predicted to have the highest interactivity corresponded to the highest peaks on the line graph. The data was used to generate a heat map-style image of the structure of the proteins using Chimera (Table 2.10). Residues with scores of one were coloured yellow, two were coloured orange and finally three and above coloured red.

2.8.3. In-silico molecular docking

The PDB file for each protein to be docked was loaded onto the relevant webserver. GRAMM-X was used for larger complexes and HADDOCK 2.2 for docking a single protein to a single partner protein (Table 2.10). Standard docking parameters as set by the webservers were used. Data generated from interface prediction was used in the docking run to ensure more robust prediction. The most feasible complex returned, justified by the lowest GRAMM-X or HADDOCK score, was downloaded in PDB format for further analysis of the interaction.

2.8.4. Protein structure manipulation and analysis

Chimera was used to manipulate, visualise and analyse protein structures of the complexes returned by the docking software (Table 2.10).

2.8.5. *Creating truncations*

The p52 protein structure was truncated using Chimera. The relevant regions were selected using the command [select:x.A,y.A,z.A] where x,y and z are residues and A refers to the chain. The selected residues were deleted using the following: [Actions --> Atoms/Bonds --> delete].

2.8.6. *Mutagenesis*

Specific point mutations were introduced onto the p52 protein using Chimera. Relevant residues were selected using the "select" command followed by the code [swapaa X: Y.Z]. Where X the desired and new amino acid, Y is the amino acid number and Z is the chain letter.

2.8.7. *Predicting contacts/clashes*

[Tools --> Structure Analysis --> Find Clashes/Contacts]

The contact/clash tool was used to highlight any steric clashes and residue-residue contacts between the docked proteins.

2.8.8. *Predicting hydrogen bonds*

[Tools --> Structure Analysis --> FindHbond]

The H-bond tool was used to highlight predicted hydrogen bonds between the docked proteins.

2.8.9. *Alignment and superimposition*

In instances of manipulation of the p52 protein structure prior to docking, the complex returned by the docking software was compared to the wild-type conformation. Both the modified and the wild-type complex structures were opened on Chimera. Following this the MatchMaker tool was used [Tools --> Structure Comparison --> MatchMaker]. The modified and wild-type structures were differently coloured.

2.8.10. Determining integrity of protein complexes

A combination of the HADDOCK scores and the protein complex's ΔG value were studied. The HADDOCK scores were returned at the end of every docking run and noted. The ΔG value was calculated using the PRODIGY webserver. PDB files of the complex were uploaded to the software and the ΔG value returned and noted.

Name of software	Use	Link
UCSF Chimera	Protein structure visualisation, modification and analysis	https://www.cgl.ucsf.edu/chimera/
HADDOCK 2.2	Molecular docking	https://alcazar.science.uu.nl/enmr/services/HADDOCK2.2/haddockserver-easy.html
Vasker Lab GRAMM-X	Molecular docking	http://vakser.compbio.ku.edu/resources/gramm/grammx/
Prodigy	ΔG calculation	https://wenmr.science.uu.nl/prodigy/
PSIVER	Sequence based interface prediction	https://mizuguchilab.org/PSIVER/
PredictProtein	Sequence based interface prediction	https://predictprotein.org/
PredUS	Structure based interface prediction	https://honiglab.c2b2.columbia.edu/PredUs/index.html
CPORT	Structure based interface prediction	http://milou.science.uu.nl/services/CPORT/
WHISCY	Structure based interface prediction	https://bianca.science.uu.nl/whiscy/
Promate	Structure based interface prediction	Webserver since removed

Table 2. 10 Software used in the *in silico* protein-protein interaction prediction

2.9 Statistical analysis

Statistical analysis was performed using the Prism 6 software. Due to two or more independent variables being tested in the quantitative data performed throughout this thesis, two-way ANOVAS with multiple comparisons were performed. Statistical significance was indicated using the symbol "*" and determined by a P value of <0.05. On the Prism 6 software a P value of less than, or equal to, 0.01 was denoted by "**", and of less than, or equal to, 0.001 as "***". Discussion of the adjustment made to the P value in relation to the western blotting data specifically can be found in Section 2.6.6.

Chapter 3   Elucidating the Role of p52/p100 in the Response to Ribosomal Stress

3.1. Introduction

3.1.1.   Nucleolar stress versus ribotoxic stress

Nucleolar stress, also referred to as ribosomal stress, does not have a strict definition, nor is any single definition widely accepted. The definition is evolving with the field (Yang et al., 2018). Nucleolar stress is an umbrella term for events involving the breakdown of the nucleolus resulting from stress-induced inhibition of ribosome biogenesis. The end result of the stress response is p53 activation (Sloan et al., 2013a). Historically, the terms ribotoxic stress and nucleolar stress were used interchangeably. The exact definitions of ribotoxic stress as described by Iordanov et al in 1997 describes a slightly different cellular event. Here ribotoxic stress is defined as the disruption of the interaction of the 3'-terminal of the 28S ribosomal RNA with the large subunit (Iordanov et al., 1998b). Disruption of this would impact protein synthesis but also result in inhibition of ribosomal RNA synthesis. This in turn would lead to a state of nucleolar stress. Thus, it is understandable why the two terms are used to describe the same responses. Both states of stress lead to 5S RNP mediated p53 activation, involving the same mechanism. However, it is important to note the slight differences in the true definitions of the stresses.

3.1.2.   Using drugs to stimulate the 5S RNP-mediated response to nucleolar stress

The 5S RNP/MDM2/p53 pathway has been a therapeutic target used in a range of chemotherapies. There are several ways to disrupt ribosome biogenesis, causing the accumulation of the 5S RNP and leading to the subsequent activation of p53. The pathway is a useful target for chemotherapy as activation can cause p53-mediated apoptosis within the cancerous cells. One way of therapeutically targeting this pathway is through the inhibition of RNA polymerase I. This is achieved with low concentrations of Actinomycin D. Inhibiting RNA polymerase I prevents the transcription of the long precursor ribosomal RNA leading to the rapid inhibition of ribosome biogenesis through the lack of ribosomal RNA (Deisenroth and Zhang, 2010). It must be noted that ActD at higher concentrations can cause generation of free radicals (Flitter and Mason, 1988). ActD is known under the clinical name, Cosmegen

Lyovac (Choong et al., 2009). It was the first drug developed to target ribosome biogenesis in cancer cells. The drug, however, is not widely used in the clinic due to low specificity and toxicity issues which has led to the development of alternative RNA polymerase I inhibitors, such as BMH-21 (Catez et al., 2019). This drug functions by binding to GC-rich regions of DNA. As such regions are abundant in ribosomal DNA, BMH-21 has more specificity for cancerous cells, leaving healthy cells intact (Peltonen et al., 2014). Nonetheless, ActD is still experimentally used to study the process of nucleolar stress in the laboratory.

Another method to induce the 5S RNP dependent activation of p53 is through the depletion of nucleotides required for ribosomal RNA synthesis (Cho et al., 2020). For example, the drug 5-FU, works by forcing the cellular transcription machinery to misuse fluoro-uracil in place of uracil. This damages RNA. As the synthesis of ribosomes is such a highly regulated procedure, damaged ribosomal RNA causes the inhibition to the synthesis leading to p53 action (Sun et al., 2007). 5-fluorouracil is the main treatment for patients with colorectal cancer (Cho et al., 2020). It is, however, debated whether the main action of the drug is through the 5S RNP as it can also cause DNA damage as well as RNA damage. Furthermore, ribosomal RNA is not the only RNA present in cells (Deisenroth and Zhang, 2010). Therefore, the presence of fluoro-uracil could interfere with transcription of other types of RNAs causing damage, and cell death, through other cellular mechanisms.

3.1.3. Tumour suppressor p53

TP53, encoding the p53 tumour suppressor, is one of the most widely studied genes. Despite this, there is still new and emerging questions surrounding p53 regulation, activation, and function. Referred to as the 'guardian of the genome', p53 is the most frequently mutated gene in cancer (Pflaum et al., 2014).

The tumour suppressor protein, p53, is expressed from the *TP53* gene of chromosome 17 and is best known for roles in cell-cycle arrest and apoptosis. The transcription factor is kept at low concentrations in healthy cells by its negative regulator, the E3 ubiquitin ligase MDM2, which targets p53 for proteasomal degradation (Vousden and Prives, 2009). In response to a variety of cellular stresses p53 is stabilised and is able to translocate to target genes to regulate their expression. Covering a length of 19,200 base pairs, the gene has three known promoters and a multitude of known isoforms (Pflaum et al., 2014). Not all isoforms harness the same activity as the full-length protein, with some have opposing effects. For example, the amino-terminally truncated isoform, Δ133p53, favours G2/M cell-

cycle arrest and inhibits p53-dependent apoptosis (Aoubala et al., 2011). There are 4 domains present in human p53: the central DNA-binding domain (DBD), N-terminal transcription-activation domain (TAD), C-terminal oligomerisation domain (CTD), and the proline-rich domain (PR). The DBD is the most conserved region of p53 across isoforms and is the site that the protein binds target genes (Okorokov et al., 2006). This is the domain that most mutations are present within. The TA provides a binding site for positive and negative regulators of p53, for example p300 and MDM2, respectively (Mavinahalli et al., 2010). The CTD is subject to post-translational modifications and alternative splicing events. This domain has been shown to have a role in DNA binding and activity of p53 (Sauer et al., 2008).

3.1.4. p53 and MDM2

p53 is kept inactive by MDM2 through an autoregulatory feedback loop. MDM2 is a target gene of p53 and binds to the transactivation domain of the p53 protein. This is one component of MDM2-dependent p53 inhibition. MDM2 also drives the nuclear export of p53 through a nuclear export signal within the MDM2 protein sequence, rendering p53 unable to carry out transcription factor activities which occur in the nucleus. Lastly, MDM2 is an E3 ubiquitin ligase and promotes p53 polyubiquitination, leading to its degradation by the 26S proteasome. In normal cellular conditions, p53 is continuously degraded leading to the low levels of cellular abundance (Schon et al., 2002).

The MDM2/p53 interaction is critical to responding to cellular stress or damage. Many signalling pathways lead to p53 activation through the control of the MDM2/p53 interaction. This can occur through post-translational modification of p53, through phosphorylation, which interferes with MDM2 binding (e.g. through DNA damage pathways) (Hafner et al., 2019). Alternatively, proteins can bind to and inhibit MDM2 (e.g. through nucleolar stress and ARF expression) (Sloan et al., 2013a). MDM2 is found to be overexpressed in some cancers, mostly soft-tissue tumours. The overexpression of MDM2 inhibits p53-mediated apoptosis, senescence and cell cycle arrest contributing to cancer growth and tumour burden (Schon et al., 2002). The study of MDM2 knockout mice showed the phenotype to be embryonic lethal. This phenotype was able to be rescued by introducing a *Tp53* knockout, preventing constitutively active p53 activity (Jones et al., 1995).

3.1.5. p53 function

p53 is widely known for tumour suppressive properties within the cell. In response to cellular stress, p53 is activated and can carry out its role as a transcription factor by regulating target genes. This pathway is mostly associated with the upregulation of pro-apoptotic genes, such as PUMA, or cell cycle regulators, including CDKN1A (Vousden and Prives, 2009). The activation of CDKN1A, leading to the expression of the p21$^{WAF1/CIF1}$ protein, is the main route of p53-mediated senescence (Brown et al., 1997). It is, however, becoming increasingly clear that the functions of p53 span many fields of research. Interestingly, there is also a link between p53 activity and metabolism. In response to challenging metabolic environments, such as starvation, p53 can negatively regulate the mTOR pathway via the upregulation of AMP-activated kinase. mTOR exists as a central regulator for cellular processes, such as protein synthesis. This mode of control allows p53 to regulate cellular proliferation and growth, especially in cancerous cells (Jones and Thompson, 2009). p53 can also promote to cell survival. Although this is counterintuitive, the consequences of inducing cell death in response to all acute cellular stresses sensed would be too much. Hence, in certain environments, cell cycle arrest is favoured, allowing cells time to repair any damage. This is further facilitated through the activation of cell survival pathways, such as the AKT pathway (Vousden and Prives, 2009).

There has been increased interest in studying whether p53 dynamics plays a role in deciding cell fate (Hafner et al., 2019). Purvis *et al.* determined that pulsed waves of p53 activity, induced by ionising radiation, encouraged temporary cell cycle arrest (Purvis et al., 2012). When the pulsed waves were converted to sustained p53 activity, the cell entered permanent cell cycle arrest, leading to senescence. As the field progresses, it is becoming clearer that relative abundance of target gene expression also influences the cellular outcome, alongside p53 dynamics (Fischer, 2017). For example, the decision between cell cycle arrest and apoptosis is steered by the ratio of PUMA to CDKN1A gene expression (Hafner et al., 2019). Therefore, whilst p53 dynamics determines which subset of target genes are expressed to which extent, it is suggested that the relative abundance of target gene expression is also coordinated to decide cell fate.

3.1.6. The mammalian cell cycle

The cell cycle is the mechanism by which cells divide to produce two genetically identical daughter cells. The mammalian cell cycle consists of five phases. Each phase is responsible for a particular role within the journey towards cell division (Nurse, 2000). Of the three gap phases, G_0 is the resting state. The stage at which cells are quiescent. Progression of the cell cycle begins with G_1 during which synthesis of RNA and protein occurs (Hume et al., 2020). This allows the synthesis of replication machinery, quality control machinery and other factors required for the following phase to be produced. S phase involves the replication of DNA (Takeda and Dutta, 2005). In order for the cell to divide to create two daughter cells, DNA for the new daughter cell needs to be synthesised. Upon completion, cells enter G_2, the final gap phase (Nurse, 2000). This phase serves as a quality control to ensure no mistakes within DNA replication occurred, including scanning for strand breaks, thus ensuring no mistakes are carried through to the new cell (Satyanarayana and Kaldis, 2009). The cell can then progress to M phase. This phase involves the processes of mitosis and cytokinesis. This is the final stage in which two identical daughter cells are produced (Riabowol et al., 1989, Lindqvist et al., 2009). At this point the cell will either re-enter G0, or if significant levels of growth factors are still present, the cell will undergo further rounds of division (Nurse, 2000).

Among the factors contributing to a successful round of the cell cycle are Cyclins (Ding et al., 2020). Cyclins are produced and degraded at specific points throughout the cell cycle to encourage progression through a particular phase (Satyanarayana and Kaldis, 2009). Whilst there is an entire family of Cyclins, only five: Cyclin A, B, C, D and E are known to play a critical role within the mammalian cell cycle. Cyclins complex with cyclin-dependent serine/threonine kinases (cdk) to drive the progression of the cell cycle (Satyanarayana and Kaldis, 2009). The activity of the cdks peaks alongside the presence of the associated cyclin. At the early stages of the G1 phase, Cyclin D complexes with Cdk6 or Cdk4. The kinase phosphorylates p130, p107 and Rb, members of the retinoblastoma protein family (Sherr and Roberts, 2004). Downstream, this leads to the activation of E2F target gene expression, which includes Cyclin E and Cyclin A (Sherr and Roberts, 1999). The latter stages of G1 involves a complex of Cdk2/Cyclin E. This causes further phosphorylation of Rb and the transition to S phase (Satyanarayana and Kaldis, 2009). At this point, Cdk2/Cyclin A complexes phosphorylate proteins involved in DNA replication. During the G2/M transition,

Cdk2/Cyclin A activity increases encouraging the initiation of mitosis, which is then driven by Cdk1/Cyclin B (Lindqvist et al., 2009).

3.1.7. Cell cycle regulation

Rounds of the mammalian cell cycle must be executed faultlessly to ensure genomic integrity. To facilitate that, stages of the cell cycle and associated cell cycle factors must be regulated (Nurse, 2000). Cdks are regulated by the INK4 family and the Cip/kip family (Satyanarayana and Kaldis, 2009). The former can bind Cdk4 and Cdk6 and inhibits the action of Cyclin D. The latter inhibits Cdk2/Cyclin E, Cdk2/Cyclin A, Cdk1/Cyclin A and Cdk1/Cyclin B. Therefore, these families function across the different stages of the cell cycle.

Cell cycle checkpoints are an important mechanism in the maintenance of accurate and successful rounds of cell division (Panagopoulos and Altmeyer, 2021). Several checkpoints exist within the cycle and ensure genomic integrity is upheld, with the major checkpoints being the G1/S, G2/M and spindle checkpoints. The activation of the checkpoints and the introduction of cell cycle arrest involves a web of cellular signalling that is co-ordinated to sense stress and faults in DNA and facilitate repair (Lukas et al., 2004). Whilst it was originally believed that the cell cycle was paused, repair pathways activated, and the cycle restarted, an emerging hypothesis proposes more of a deceleration (Lemmens and Lindqvist, 2019). Recent data proposes the cell cycle reserves halting the cell cycle in entirety for more severe cases of stress (Panagopoulos and Altmeyer, 2021). Low level DNA damage and endogenous replication stress, on the other hand, could be dealt with by slowing certain cellular processes while maintaining others to bring balance between genomic surveillance and cell cycle progression. Either way, the DNA damage response (DDR) is critical to cell cycle regulation (Ciccia and Elledge, 2010). This entails a web of cellular signalling that recognises specific types of DNA damage to mediate an appropriate response. Activation of the DDR is linked to cell cycle checkpoints to allow repair mechanisms to be activated prior to the termination of the DDR for the cell cycle to progress (Panagopoulos and Altmeyer, 2021).

The first is the G1/S checkpoint (Bartek and Lukas, 2007). When cells enter S phase they become committed to DNA replication and cell division unless DNA damage is sensed. It is critical that the cell ensures no damage is present within the DNA prior to replication. Damage that is copied into the daughter strand of DNA can incorporate mutations which have the potential to lead to disease, such as cancer (Willers et al., 2000). DNA damage will

cause G1/S cell cycle arrest. This typically occurs through the action of the checkpoint kinases, ATM (ataxia telangiectasia mutant) and ATR (ATM-and Rad3-related), which activate Chk1 and Chk2 (Awasthi et al., 2015). ATM responds to double stand DNA breaks whereas ATR responds to single stand breaks (Hunter et al., 2022a). ATR is the primary kinase in S phase during the response to problems with DNA replication (Hunter et al., 2022b). The kinases lead to the stabilisation of p53 (Kastan and Bartek, 2004). Once stabilised and active the transcription factor can upregulate target gene expression, such as the CDK2 inhibitor, p21[WAF1/CIP1]. CDK2 forms complexes with both E type Cyclins and A type Cyclins, thus its action will arrest cells in the G1 and G2 phase of the cell cycle. Cyclin dependent kinase inhibitors, such as p21, can bind and inhibit Cyclin/CDK complexes directly (Sherr, 1994).

Progression through the G2/M cell cycle checkpoint is driven by CDK1, also referred to as CDC2. CDK1 forms complexes with Cyclin B1 (Riabowol et al., 1989). This checkpoint checks the accuracy of the DNA replication undertaken in S phase of the cycle. The cell cycle is inhibited at this point through post-translational modifications on CDK1. The WEE1 kinase phosphorylates CDK1 on tyrosine 15, pausing the cell cycle at the checkpoint (Parker et al., 1992). If no DNA damage is detected and DNA replication completed, phosphatase enzymes remove the inhibitory marker. The phosphotase family responsible for the dephosphorylation of Cdk1 at G2/M is the cell division cycle 25 (CDC25) family (Nilsson and Hoffmann, 2000). These enzymes are key regulators of the eukaryotic cell cycle. They facilitate the activation of Cdks through the removal of phosphorylation markers (Boutros et al., 2007). As targets of the DDR, the proteins are inactivated and degraded during cell cycle checkpoint activation . At G2/M, CDC25B is responsible for the initial activation of Cdk1/Cyclin B complexes at the cetrosome, however all CDC25 family members (CDC25A, CDC25B, and CDC25C) are able to remove Cdk1 phosphorylation to allow mitotic entry. This allows the cell to progress into mitosis, the final cell division step (Hernansaiz-Ballesteros et al., 2021). Similarly to G1/S, the G2/M checkpoint can be activated via the p53 dependent DNA damage response. Target genes p21 and GADD45α can directly cause cell cycle arrest. The p21 protein can inhibit CDK1/Cyclin B1 complexes whilst GADD45 binds to the complex sequestering it in the cytoplasm (Dash and El-Deiry, 2005). Finally, p53 can directly inhibit CDC25C keeping inhibitory phosphorylations of CDK1 in place (Giono and Manfredi, 2006).

3.1.7.1.   NF-κB and the cell cycle

The link between NF-κB signalling and the cell cycle has been well documented since its initial discovery in 1991 (Ledoux and Perkins, 2014). Multiple studies in varying cell types have shown increased binding of NF-κB to DNA during the cellular transition between G0 and G1 (Sée et al., 2004, Hinz et al., 1999, Westerheide et al., 2001). Further research has found both the canonical and non-canonical pathway, along with their respective NF-κB dimers, to have a potential role in cell cycle progression. Overexpression or depletion of various NF-κB subunits have been shown to have marked impact on the mammalian cell cycle in various cell types (Ledoux and Perkins, 2014). Overexpression of the c-Rel subunit has been linked to G1/S cell cycle arrest in HeLa cells (Bash et al., 1997). More recently, it has been shown that depletion of c-Rel through CRISPR/Cas9 gene editing in HeLa cells leads to significant disruption to mitosis (Slotta et al., 2017). The findings showed delays in the mitotic stage involving the separation of the nuclear membrane which coincided with resistance to two chemotherapeutic treatments. Overexpression of RelA has been shown to cause cell cycle arrest in some cell types but this is predicted to be due to a link with p21 induction (Sheehy and Schlissel, 1999). Similarly, p50, RelB and c-Rel overexpression has been shown to induce p21 in epithelial cells, U937 lymphoma cells and HeLa cells, respectively (Seitz et al., 2000, Bren et al., 2001). It is likely that altering the amount of NF-κB in the cell can impact the cell cycle via transcriptional regulation.

A subsection of NF-κB target genes are associated with cell growth and the cell cycle. The best documented being the gene encoding Cyclin D1, CCND1. The gene contains three short sequences with the potential to be κB sites within the promotor region (Ledoux and Perkins, 2014). All of the NF-κB subunits, dependent on dimeric partner, have the capability to regulate Cyclin D1 expression. The mechanism by which they regulate expression is dependent upon the dimer involved. In epithelial cells, repression of CCND1 can be achieved by binding of p50 (Zhang et al., 2007). The response to TNFα stimulation replaces the repressive p50 dimer with p52/RelB, leading to upregulated gene expression. Furthermore, Cyclin D2 and Cyclin D3 also possess κB elements in their promoters (Huang et al., 2004, Wang et al., 1996). Increased expression of the mitotic Cyclin, Cyclin B1, has also been linked to increased NF-κB activity. It is hypothesised this occurs through the κB site located in the genetic sequence of the CCNB1 gene (Ahmed and Li, 2008). As mentioned in Section 1.2.7.4 there is a strong link between p52 and regulation of the cell cycle. Schumm *et al* published

that p52 can bind directly to promoter regions of the Cyclin D1 gene and be recruited to the promoter of the p21 gene (Schumm et al., 2006). Moreover, induction of p53 can alter the association of p52 homodimers with co-activator, Bcl-3 being replaced by the co-repressor, HDAC1, leading to repression of CCND1 gene expression (Rocha et al., 2003). Finally, flow cytometry analysis was performed following propidium iodide staining in cells depleted with the p52/p100 subunit (Schumm, 2006). Interestingly, a decrease in the number of cells seen in S phase was captured as well as an increase in the number of cells in G1 and G2. Schumm *et al* repeated this assay in H1299 cells which naturally lack the p53 protein and the cell cycle phenotype was no longer captured suggesting the effects were p53 dependent (Schumm, 2006). This further proves a link between NF-κB, but more specifically, non-canonical NF-κB signalling and the cell cycle which potentially occurs through the well-established relationship between NF-κB and p53.

3.2. Results - Investigating the role of p52 in the nucleolar stress response through siRNA mediated knockdown

Previous data from the Perkins laboratory had suggested a link between p52, p53 and ribotoxic stress. The influence of UV radiation upon the transcriptional regulation of p52 target genes was outlined by Rocha et al as decribed above (Rocha et al., 2003). Furthermore, the binding of p52 to the promoters of p53 target genes to modulate expression is responsive to UV radiation (Schumm et al., 2006). It has been widely documented that UV radiation is an inducer of ribosomal stress (Iordanov et al., 1998b, Hannan et al., 2022). Therefore, to learn more about the potential role of p52 during ribotoxic stress, I investigated its role in response to treatment with Actinomycin D (Act D).

U2-OS cells or HCT116 cells were transfected, or co-transfected, with small interfering RNAs (siRNAs) targeting proteins of interest. Both cell lines are cancerous cell lines possessing wild-type p53. U2-OS is an osteosarcoma cell line and HCT116 is a colorectal cancer cell line. Following siRNA mediated knockdown, cells were challenged to drug treatment for durations indicated in the figures presented. ActD and 5-FU were used to stimulate the ribosomal stress response. ActD functions by inhibiting RNA polymerase I action and 5-FU leads to nucleotide depletion via incorporation of fluoro-uracil (Hannan et al., 2022). Both drugs cause rapid ribosome biogenesis inhibition and the activation of the 5S RNP/MDM2/p53 pathway. Either, images were taken under 10X magnification, or protein and RNA was

extracted from the cells. Protein extraction was followed by western blot analysis. RNA was reverse transcribed to make copy DNA (cDNA), which was analysed via quantitative RT-PCR.

3.2.1. *Depletion of p52/p100 impacts cell number both basally and in response to Actinomycin D treatment*

As described above, the p52/p100 subunit of the NF-kB family has been shown to regulate cellular proliferation. It has been previously shown in the Perkins laboratory that depletion of p52 within U2-OS cells display a lower cell number and impacted morphology (Schumm, 2006). To view the impact that ActD treatment made on this observed phenotype, siRNA transfected cells were treated to 0 or 24 hours of the drug. Images were taken of the cells under 10X magnification to observe effects.

The images taken of the control siRNA cells appeared similar in shape, size and number in both the untreated and ActD treated culture plates (Figure 3.1). There was, however, a larger number of floating cells seen. The cells treated with ActD appeared to have a higher number of floating cells in the image. This suggests that using the drug alone is able to cause the U2-OS cell line to lose its adherence. This could indicate that the cells are either dying or arrested during mitosis.

In comparison, the p52/100-targeting siRNA caused U2-OS cells to adopt a different shape in comparison to the control cells (Figure 3.1). The cells were less densely packed, indicating impaired cellular growth and proliferation caused by the p52/p100 siRNA knockdown. The lesser number of cells in the dish could have caused the change in morphology seen, rather than being a direct result of the siRNA knockdown. The shape of the p100 siRNA U2-OS cells after 24 hours of ActD appeared relatively similar to that of the untreated, however more floating cells were visualised. This shows that cells that have undergone siRNA mediated knockdown of the p52/p100 subunit change morphology, have impacted cellular growth and are more susceptible to losing adherence in response to ActD treatment. Together this suggests impacted proliferation and changes to cellular fate.

10x magnification   **Enlarged**

NS siRNA untreated U2OS

NS siRNA 24h ActD U2OS

siRNA p100 untreated U2OS

siRNA p100 24h ActD U2OS
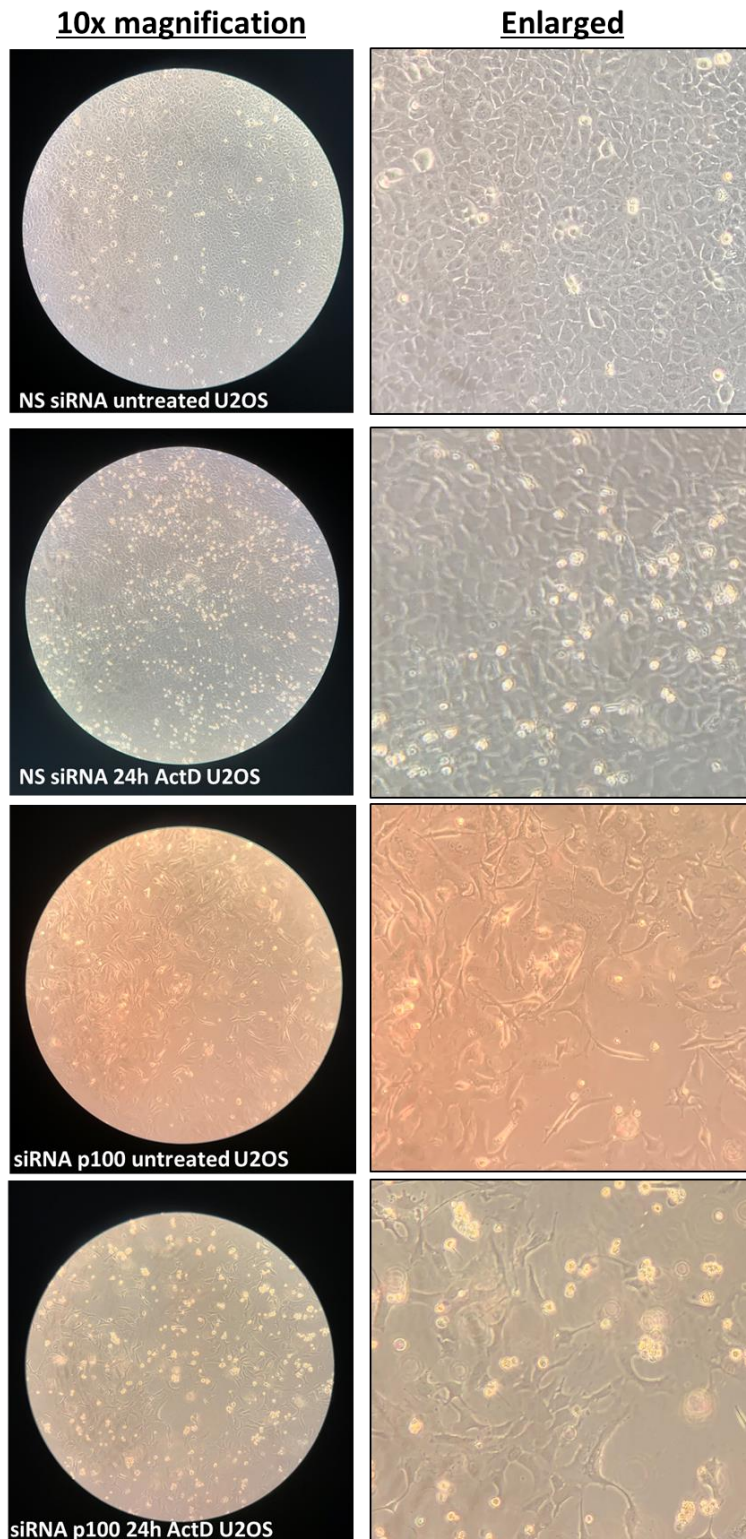
Figure 3.1 siRNA mediated knockdown of the p52/p100 subunit causes a change in morphology and cell number in U2-OS cells. Cells were transfected with a non-specific siRNA or one targeting the p52/p100 protein. After recovery, cells were left untreated or treated with 5nM actinomycin D. After 24 hours, an image of the cells were taken through a light microscope at 10X magnification using an iPhone XR.

3.2.2. Depleted cellular p52 leads to insignificant changes to nucleolar stress induced p53 stability

To investigate the cellular mechanisms behind the phenotype observed in Figure 3.1, western blot analysis was performed on cells depleted in p52/p100 compared to control siRNA cells. The stability of the p53 protein in response to nucleolar stress induction was measured.

An ActD time course, measuring both short and long time points of treatment, in U2-OS cells was performed to compare p52/p100 depleted cells with matched controls (Figure 3.2A). The quantification of three repeats was plotted to visualise any impact upon p53 stabilisation in response to ribosomal stress (Figure 3.2B). The NS control samples show an increase in p53 protein level from 0 to 8 hours of ActD treatment. After 8 hours the protein levels decreased. The p52 knockdown cells showed an increase of p53 up to 16 hours post treatment. Only a slight decrease in protein presence was detected between 16 and 24 hours. Statistical analysis of the data concluded that these differences were insignificant. Incidences of PARP cleavage (Figure 3.2C) as well as abundance of yH2AX (Figure 3.2D) were simultaneously measured and discussed below in Section 1.2.4. Alongside U2-OS cells, the assay was repeated in HCT116 cells utilising the chemotherapeutic drug, 5-fluorouracil (Figure 3.3). As this experiment was performed as a single repeat, quantification was not performed. As expected, p53 was found to stabilise across the 24 hour time course. This stabilisation was unchanged when a p52/p100 targeting siRNA was used in place of the NS control.

It was predicted that the insignificant differences were due to cells with the highest levels of p53 stabilisation undergoing cell death. Therefore, the caspase inhibitor Z-VAD was added to the U2-OS cells prior to ActD treatment (Figure 3.4A). In the non-specific (NS) siRNA treated cells, the p53 protein increased between 0 and 16 hours, however remained unchanged by 24 hours. Whilst in the western blot image the p53 protein appears to decrease at 24 hours in the NS siRNA samples, the actin control is lower for that sample which accounts for the decrease in p53. The p53 protein levels in the p100 siRNA treated cells was seen to increase largely between 0 and 16 hours however only minimal increase is seen between 16 and 24 hours. Finally, in the p100 knockdown cells that were exposed to the Z-VAD caspase inhibitor before ActD treatment, the stabilisation of p53 is slightly higher in those samples compared to both the non-specific siRNA and the p100 siRNA samples. The quantification of three

independent repeats prove insignificant differences between the conditions (Figure 3.4B, top graph). Again, this was repeated in HCT116 cells treated with 5FU (Figure 3.4C). A very similar pattern was observed. The stabilisation of p53 protein increased over time in the NS control samples. Cells transfected with the p52/p100 siRNA saw an increased stabilisation between 0 and 16 hours and a slight decrease after 24 hours of treatment. Finally, p52/p100 depleted cells with the addition of Z-VAD treatment had a higher stabilisation of p53 compared to both p52/p100 siRNA alone and the control samples. Whilst this increase appears larger than that observed in the U2-OS cell experiment, statistical analysis revealed this to be insignificant (Figure 3.4D, top graph).

3.2.3. p52/p100 mediates caspase dependent PARP cleavage in response to nucleolar stress in U2-OS and HCT116 cells

As the increase in 'floating' cells in response to nucleolar stress in p52/p100 depleted cells was not due to changes to p53 levels, it was important to look for other potential explanations. Poly-ADP ribose polymerase (PARP) becomes cleaved during the initiation of apoptosis. Cleaved PARP is known as a marker of cellular death and can be assessed through western blotting (Chaitanya et al., 2010).

It was found that U2-OS cells transfected with a p52/p100 siRNA and treated with ActD had higher rates of PARP cleavage when compared with NS controls (Figure 3.2A). Cleaved PARP can be seen as the lower band of the western blot. In the p52/p100 knockdown cells, quantification demonstrated significantly higher levels of PARP cleavage after 16 hours of ActD treatment (Figure 3.2C). At prolonged periods of ActD treatment in p52/p100 depleted cells, the large induction of PARP cleavage was accompanied by less full length PARP protein, indicating cell death.

The significant rise in PARP cleavage following nucleolar stress in p52/p100 depleted cells indicates the potential mechanism behind the increased floating cells found in Figure 3.1 is cellular death. PARP cleavage could be a result of significant DNA damage. Therefore, alongside the detection of cleaved PARP via western blot, yH2AX were also investigated. The phosphorylation of variant histone H2AX on serine 139 is a marker of double strand breaks in DNA and is referred to as yH2AX (Podhorecka et al., 2010). In the control U2-OS cells that were treated with ActD, yH2AX was detected via western blotting after 6 hours of treatment and increased for the duration of the time course (Figure 3.2A). The p52/p100 depleted cells showed higher incidences of DNA damage. Not only was the marker detected from as early

at 2 hours post treatment, the increase detected rose to be much higher than the control. At 16 and 24 hour time points, yH2AX levels were significantly higher in the p52/p100 depleted cells compared to the non-specific control (Figure 3.2D). ActD treatments appear to cause DNA damage after prolonged use. This phenotype is exaggerated through the knockdown of p52/p100. Therefore, p52 may play a role in the response to nucleolar stress induced DNA damage in U2-OS cells.

The high incidences of PARP cleavage was also captured in p52/p100 depleted HCT116 cells treated with 5FU (Figure 3.3). The level of PARP cleavage was found to be less dramatic in the colorectal cell line compared to the U2-OS. This could be due to a lower cellular levels of the p52 protein naturally in the HCT116 cell line. Therefore, less of an impact is found when the protein is depleted.

The addition of the caspase inhibitor, Z-VAD to p52/p100 depleted U2-OS cells responding to nucleolar stress revealed PARP cleavage to be caspase dependent (Figure 3.4A). The quantification of the western blots revealed the increase in PARP cleavage in the 16 and 24 hour samples between NS siRNA and p100 siRNA cells was statistically significant (Figure 3.4B, bottom graph). Furthermore, the huge reduction of cleaved PARP with the addition of the Z-VAD caspase inhibitor was also statistically significant for those time points. This suggests that the p52/p100 subunit plays an important role in caspase-mediated PARP cleavage in U2-OS cells, which is described as a marker of cell death. The western blot quantification of cleaved PARP in the HCT116 cell line showed p52/p100 depletion caused a significant increase at 16 hours (Figure 3.4C and 3.4D, bottom graph). Interestingly, at 24 hours after 5FU treatment the difference between control and knockdown was insignificant. Similarly to the U2-OS cell line, the addition of Z-VAD to the p52/p100-depleted response to 5FU led to the blocked of PARP cleavage events.

A) DNA damage and cell death markers

B) p53 protein quantification
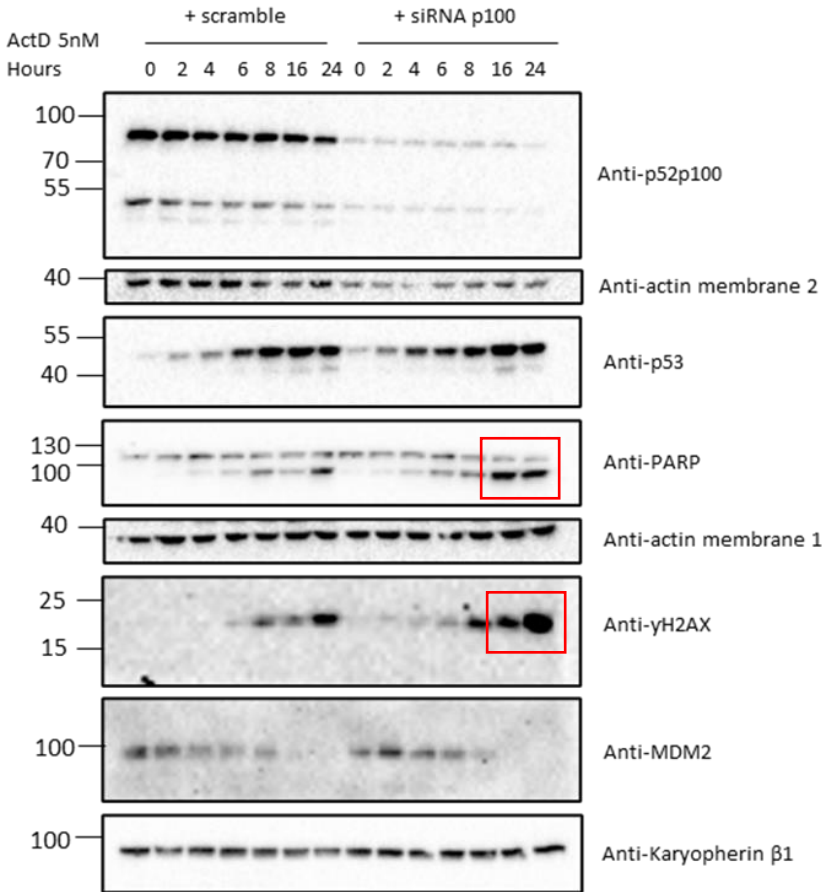
C) Cleaved PARP protein quantification
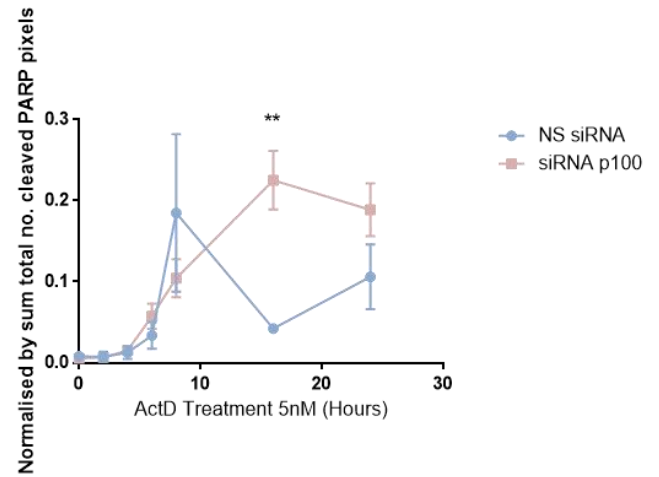
Caspase mediated PARP cleavage:
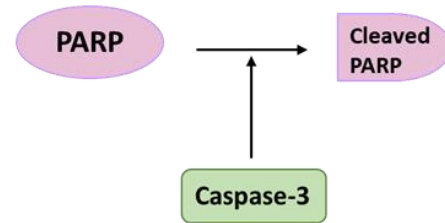
D) γH2AX protein quantification

p53 activation during ribosomal stress:

Phosphorylation of H2AX:

86
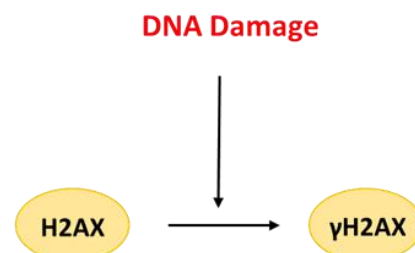
Figure 3.2 Analysis of DNA damage and cellular death markers in p52/p100 depleted cells during the ribosomal stress response –page 86. U2-OS cells were transfected with p52p100 targeting siRNA alongside a non-specific control. Following recovery, cells were harvested and analysed via western blotting. A) Western blot image representative of three independent repeats. Significant changes in protein abundance indicated by red box. B) Quantification p53 protein using ImageLab. Three independent repeats plotted using Prism 6. Two-way ANOVA was performed to test statistical significance. Image represents a simplified schematic of p53 stabilisation during ribosomal stress. C) Quantification of cleaved PARP protein using ImageLab. Three independent repeats were plotted using Prism 6 and a two-way ANOVA performed. Significant results represented with * or **. Image presents a schematic depicting the caspase mediated cleavage of PARP. D) Quantification of yH2AX protein across three independent repeats. Graph plotted using Prism 6. A two-way ANOVA was performed to test statistical significance. Significant results represented with * or **. Schematic depicts the DNA damage induced phosphorylation of H2AX.
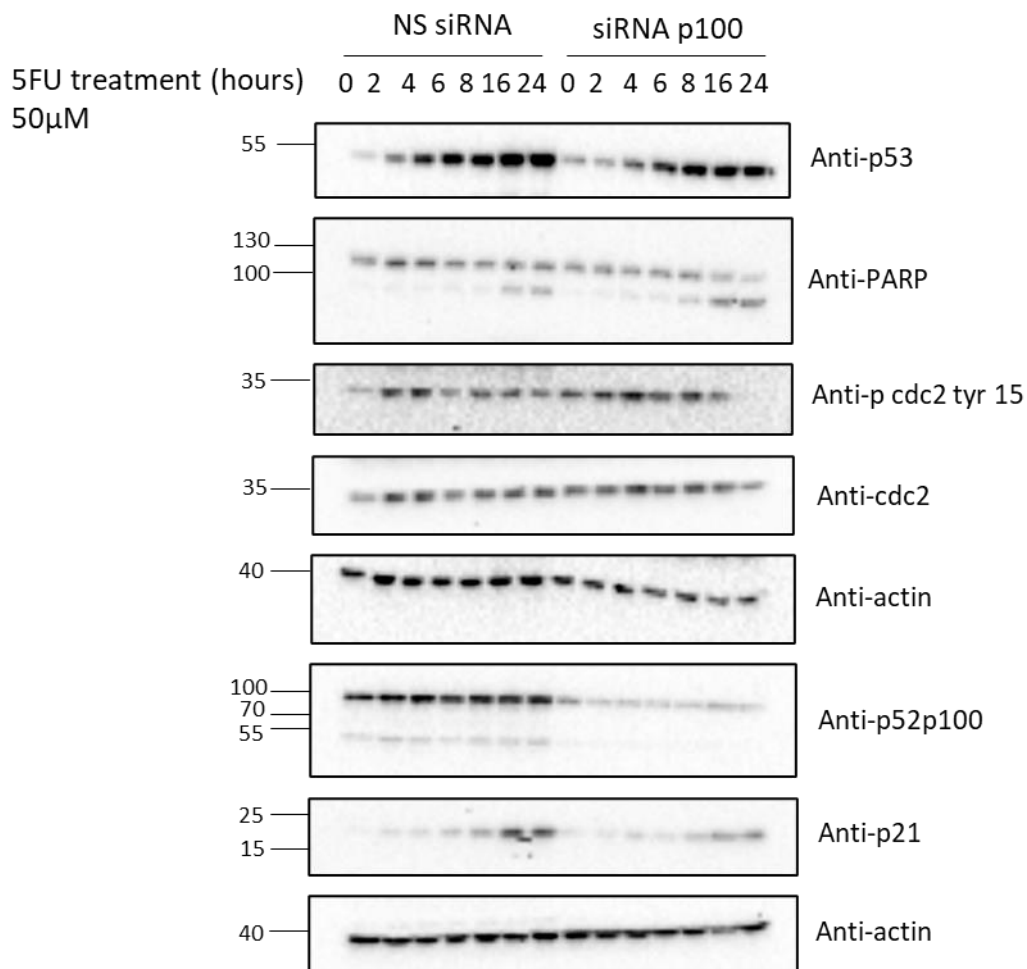
Figure 3.3 p52/p100 depletion causes increased PARP cleavage in HCT116 cells responding to nucleolar stress. HCT116 cells were transfected with non-specific of p52/p100 targeting siRNAs. Cells were challenged to 5-flurouracil treatment prior to protein harvest. Protein was analysed via western blotting in which a BioRad ChemiDoc was utilised to visualise bands.

A) U2OS cells – cell death markers

α p52p100

α actin

α PARP

α p53

α actin

ActD 5nM   0 16 24   0 16 24   0 16 24

+ NS siRNA   + siRNA p100   + siRNA p100 + Z-VAD
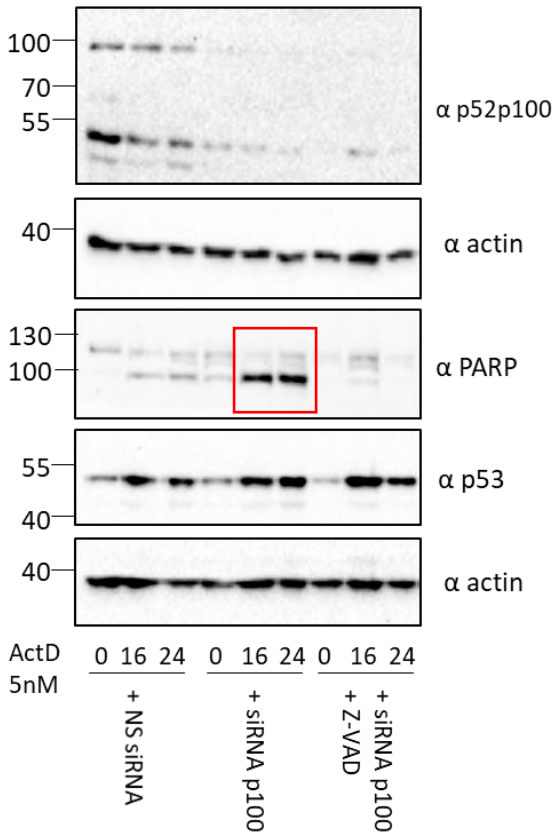
B) Quantification - U2OS cells – p53 (upper) and cleaved PARP (lower)
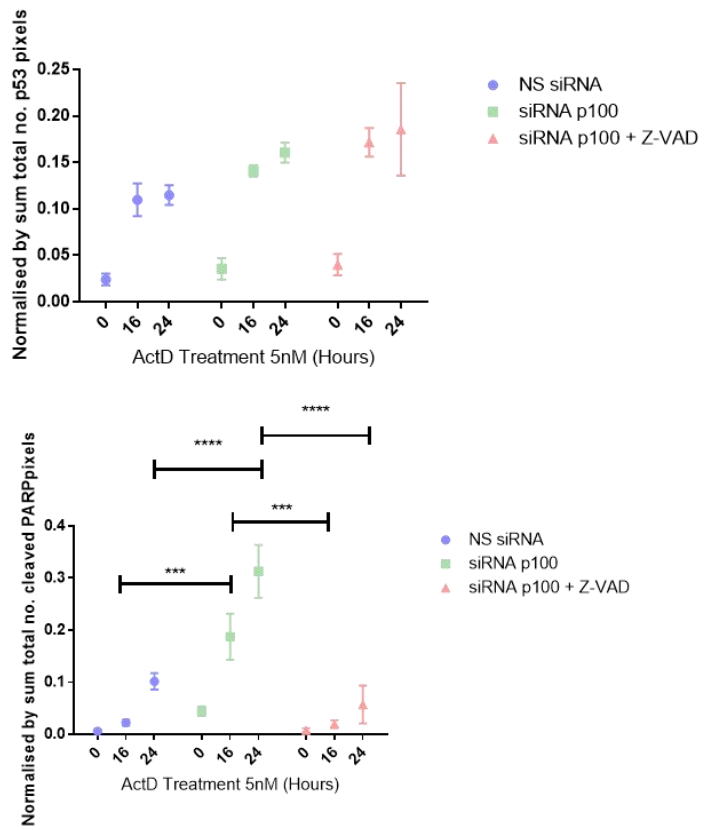
C) HCT116 cells – cell death markers

α p52p100

α actin

α PARP

α p53

α actin

5FU 50μM   0 16 24   0 16 24   0 16 24

+ scr   + siRNA p100   + siRNA p100 + Z-VAD
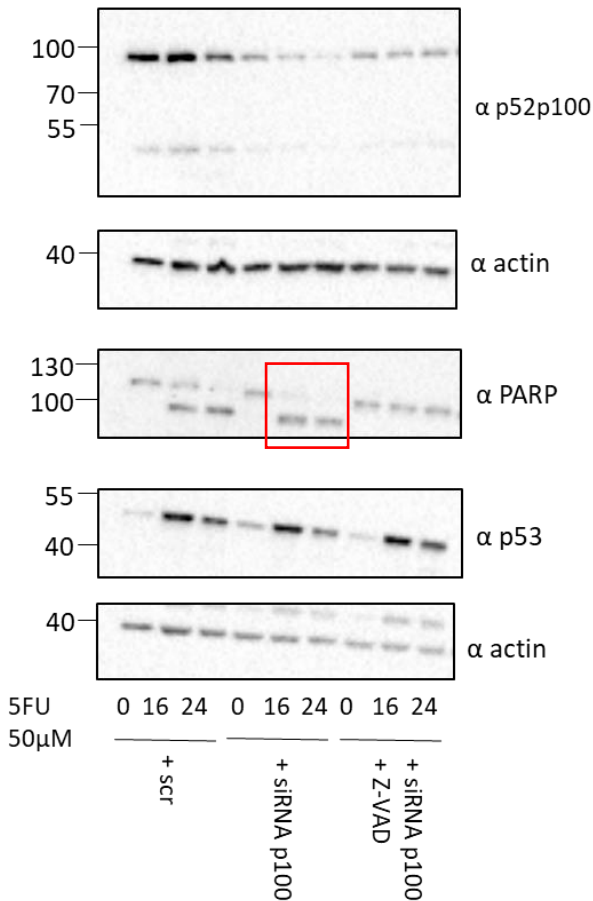
D) Quantification – HCT116 cells – p53 (upper) and cleaved PARP (lower)

88
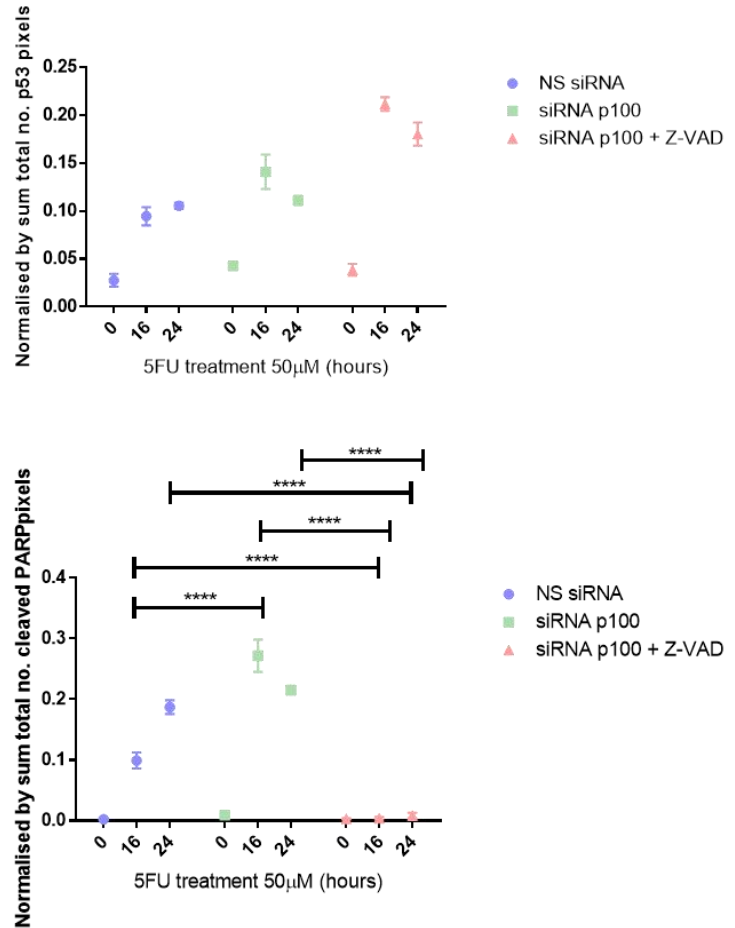
Figure 3.4 p52/p100 depletion causes caspase-mediated PARP cleavage in response to nucleolar stress – page 88. Cells were subject to siRNA knockdown of p52/p100 prior to drug treatment. In a subset of cells, the caspase inhibitor Z-VAD was added 15 minutes prior to the drug. Protein was harvested for western blotting analysis and developed using a BioRad ChemiDoc. Three independent repeats were quantified, normalised by sum and statistical analysis performed. In this case a two-way ANOVA was used to test statistical significance. A) U2-OS cell line with actinomycin D drug treatment. Significant increase in protein indicated by red box. B) Quantification of p53 and cleaved PARP protein levels. C) HCT116 cell line with 5-flurouracil. Significant increase in protein indicated by red box. D) Quantification of p53 and cleaved PARP protein levels. Three independent repeats were plotted on Prism 6 and a two-way ANOVA was performed to test statistical significance.

3.2.4. Is the p52-mediated response to nucleolar stress associated with the cell cycle?

When DNA damage is detected within a cell, cellular mechanisms are activated. Either, the cell cycle will be arrested in order to repair the damage, or, the cell will undergo apoptosis (Hafner et al., 2019). Given the link between p52 and DNA damage following nucleolar stress identified above, cell cycle markers were investigated as depicted in Figure 3.5A. Firstly, G1/S associated proteins the CDK inhibitor p21 (inhibitory) and Cyclin D1 (promoting). Secondly, the G2/M associated proteins WEE1 and CDK1 were investigated. WEE1 inhibits CDK1 by phosphorylating it on Tyr 15 (Hernansaiz-Ballesteros et al., 2021).

When the control siRNA treated cells were analysed, p21 protein levels were relatively low across all time points and were not hugely affected by ActD treatment (Figure 3.5B). After the three repeats were quantified and statistics analysed, it was shown that p52/p100 depletion causes a significant increase to basal p21 protein levels. The drug time points at 2, 4, 6, and 16 hours also showed a significantly higher level of p21 (Figure 3.3C). Interestingly, at 24 hours the p21 protein level rapidly decreased to become comparable with the control 24 hour treated lysate. This suggests that p21 is upregulated to cause cell cycle arrest but degraded after prolonged periods of nucleolar stress (between 16 and 24 hours) when the cells are undergoing significant cell death. Cyclin D1 protein levels were also measured (Figure 3.5A). Cyclin D1 can be seen to be lost over time in NS control transfected cells. Cells with depleted p52/p100 also showed a lag in the decrease in protein levels. Interestingly, the Cyclin appeared to be stabilised from 0 to 6 hours of ActD treatment before protein levels decreased. However, upon quantification of three independent repeats, it was found that differences in Cyclin D1 protein between control and depleted samples were not statistically significant (Figure 3.5D). The analysis indicates that cells with depleted p52/p100 could be undergoing arrest at the G1/S checkpoint due to significantly increased p21 protein levels.

An antibody recognising phosphorylated CDK1 was used to measure this marker of cell cycle arrest over 24 hours of treatment (Figure 3.5B). In the control cells, phospho-CDK1 only slightly decreased across the time course. In the western blot image used, the phospho-CDK1 levels were higher in the p52/p100 knockdown cells before rapidly decreasing at 16 and 24 hours of treatment. When all three repeats were quantified on ImageLab and plotted on Prism, it became clear that the differences between control and p52/p100 depleted cells were mostly insignificant (Figure 3.5E). Interestingly, at 4 hours of ActD treatment the level of phospho-CDK1 was significantly higher in the p52/p100 depleted cells versus control. The most interesting change occurs at hours 16 and 24 hours after ActD treatment. The figure shows the phosphorylation in the p100 siRNA cells decreases to be slightly below the control level, and dramatically decreased compared to the upregulation seen at 4 hours. This indicates the inhibitory marker is being removed and the cells are moving through the G2/M phase of the cell cycle after prolonged exposure to the drug. This mirrors the decrease in p21 protein levels, suggesting cells are restarting the cell cycle and then undergoing cell death. An anti-WEE1 antibody was also used (Figure 3.5B). In the control cells, WEE1 protein is seen to be degraded over time and the protein is undetectable at 24 hours. The p52/p100 depleted cells appeared to stabilise WEE1 when compared to the NS control until a slight decrease at 8 hours and the subsequent degradation at 16 and 24 hours. Interestingly, this is in line with the decreased phospho-CDK1 levels captured, however differences between control and p52/p100 depleted cells were found to be insignificant upon quantification of WEE1 protein (Figure 3.5F). This figure indicates cell cycle arrest due to increased phospho-CDK1 presence after ActD treatment and sustained WEE1 protein abundance. ActD treated cells, however, could see a removal of the inhibitory phosphorylation on CDK1 and the degradation of WEE1 after prolonged periods of treatment. This suggests cells are allowed to pass through the G2/M checkpoint.

A) Roles of the cell cycle arrest markers
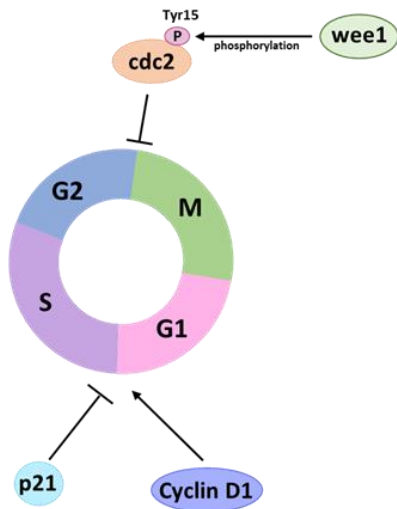
B) Cell cycle arrest markers
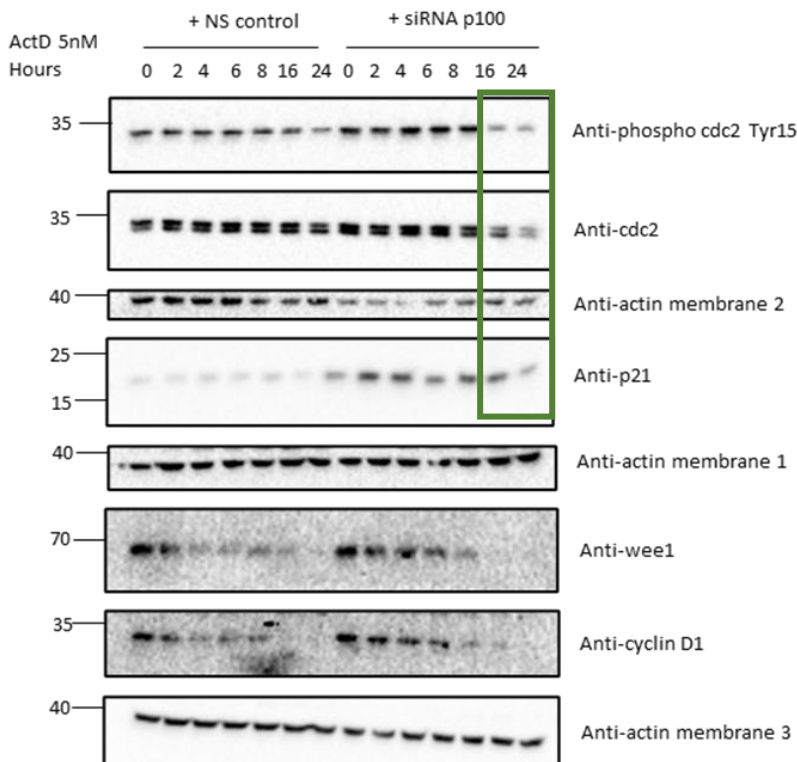
C) p21$^{WAF1/CIP1}$ quantification
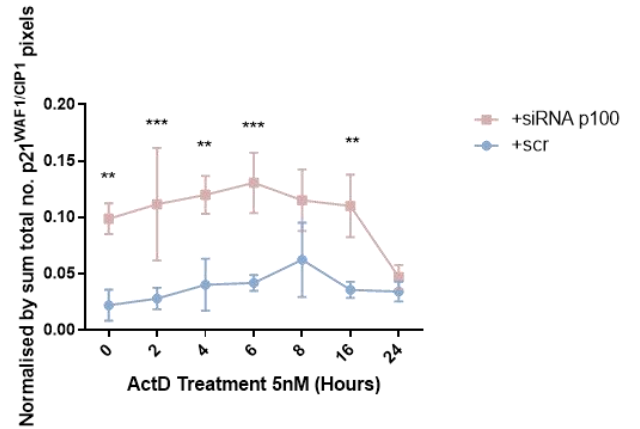
D) Cyclin D1 quantification
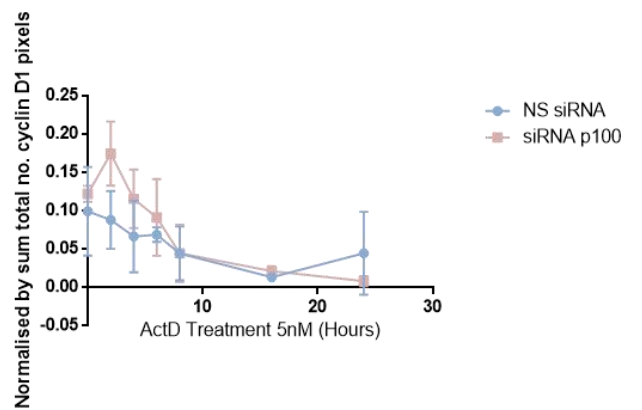
E) Phospho-cdc2 quantification
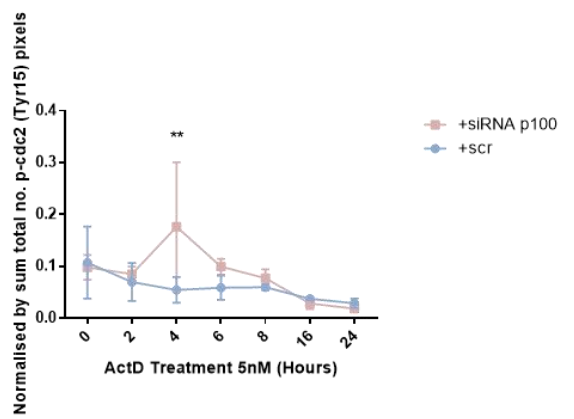
F) Wee1 quantification

91
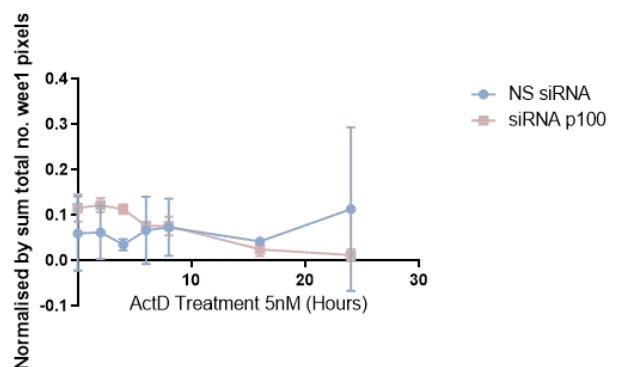
Figure 3.5 Analysis of cell cycle arrest markers in p52 depleted cells responding to nucleolar stress – page 91. U2-OS cells were transfected with a siRNA targeting p52/p100 alongside the non-specific control. Cells were treated with varying lengths of actinomycin D before harvest and protein extraction. Protein was analysed via western blotting. A) A representative western blot of three independent repeats. B) A schematic depicting the roles that cell cycle arrest markers (probed for via western blotting) have during the mammalian cell cycle. Green box to highlight large decrease in protein discussed in text. C-F) Quantification of three independent repeats plotted using Prism 6. Proteins are indicated in the figure. Two-way ANOVAs were performed to using Prism 6 to test statistical significance.

The response in HCT116 cells to 5FU and p52/p100 depletion showed differences to U2-OS cells at the G1/S checkpoint, but similarities at the G2/M checkpoint (Figure 3.3). The presence of p21 protein in the cells were found to increase across the 24 time course in the NS siRNA cells. Interestingly, and oppositely to the U2-OS cell line, the induction of p21 protein appeared to be dampened after depletion of p52/p100. The NS siRNA cells displayed relatively consistent phospho-CDK1 Tyr15 levels in response to 5FU treatment over 24 hours. In the p52/p100 depleted cells, the p-CDK1 levels appeared higher compared to the NS cells between 0 – 16 hours. Considering the lower amount of protein loaded in the p52/p100 depleted cells, the increased phospho-CDK1 levels could be more pronounced than captured on the western blot image. At 24 hours of 5FU treatment in the p52/p100 depleted cells, the phosphor-CDK1 level was undetected where in the NS control the phosphorylation was still captured. This follows the pattern displayed in U2OS cells whereby the inhibitory phosphorylation is removed after prolonged nucleolar stress.

3.2.5. *Flow cytometry analysis of U2-OS cell cycle following control depletion or p52/p100 depletion in response to actinomycin D*

To further evaluate the impact of p52/p100 depletion and subsequent ActD treatment had upon U2-OS cells, flow cytometry was performed. Cells were transfected with siRNAs as previously described and treated with the drug for times indicated in the Figure 3.6. Cells were harvested, fixed and stained using propidium iodide to analyse cell cycle profiles.

The comparison of basal cell cycle profiles in non-specific transfected U2-OS cells and p52/p100 depleted U2-OS cells suggests that the knockdown increases the percentage of cells in the G2/M phase (Figure 3.6). After 8 hours of ActD treatment the profiles are mostly comparable between the two conditions. The major difference is a slight decrease detected in p52/p100 depleted cells in S phase. This decline continues and is most pronounced at 16 hours ActD treatment. At the 16 hour time point, the control cells showed a slight decrease

in the percentage of G2/M cells compared to 0 hours. Cells depleted in p52/p100, however, displayed a more dramatic decline in G2/M cells, accompanied by an increase in cells in the G1/S phase. The combination of more cells in G1/S transition and less cells in S phase suggests the cells have been arrested at the G1/S checkpoint. Interestingly, these changes are reversed by 24 hours of ActD treatment. This could be due to cells rendering the cell cycle after prolonged ActD treatment, as discussed previously. On the other hand, the profile of p52/p100 knockdown cells after 24 hours of ActD treatment could reflect solely the surviving population if many cells underwent apoptosis after 16 hours. Whilst only a singular repeat was performed of this experiment, the figure suggests a role of p52 within the G2/M checkpoint of the cell cycle, both basally and in response to ActD treatment.
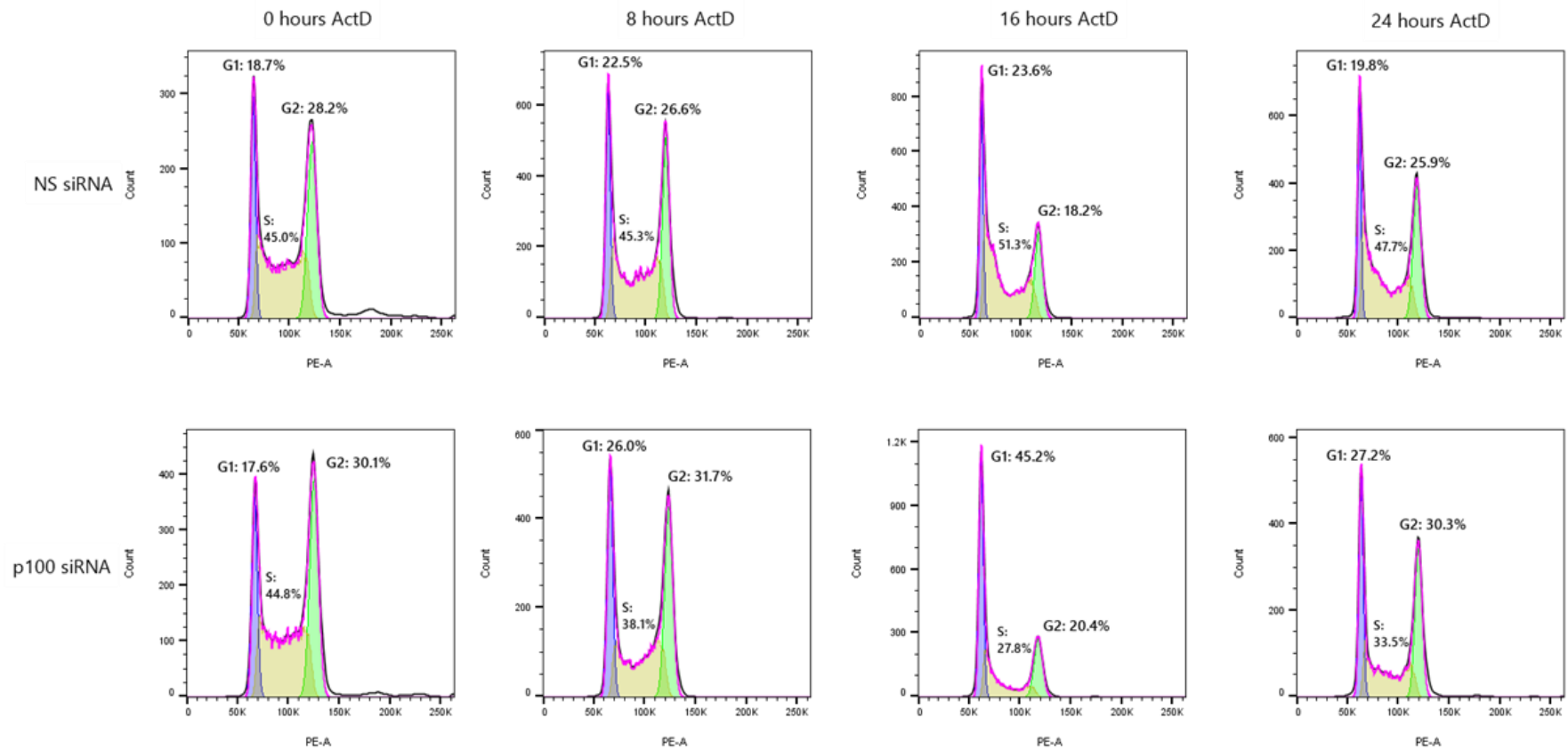
Figure 3.6 p52 depletion impacts the cell cycle profile of U2-OS cells both basally and in response to ActD treatment. Cells were transfected with either a non-specific siRNA or siRNA targeting p52/p100 and treated with 5nM ActD. Cells were harvested, fixed in ethanol and stained with propidium iodide. Flow cytometry analysis was performed to create the cell cycle profiles. Analysis *was performed using FlowJo.*

3.2.6. Analaysis of gene expression changes following p52/p100 depletion and ActD treatment in U2-OS cells

Regulation of the stabilisation or degradation of proteins can be achieved at the gene expression level. In order to investigate whether p52/p100 depletion of U2-OS cells affected gene expression in response to ActD treatment, mRNA was extracted. RNA was reverse transcribed to make cDNA and finally analysed via quantitative RT-PCR.

The CDKN1A gene encodes the p21 cell cycle regulator (Radhakrishnan et al., 2006). This protein primarily inhibits progression through the G1/S phase of the cell cycle. Basally, cells with depleted p100 contained slightly higher CDKN1A gene expression compared to the NS control (Figure 3.7A). Following treatment, the gene expression profiles follow the same pattern however the p100 siRNA cells consistently showed higher levels of CDKN1A transcript. However, although this higher level of CDKN1A mRNA was consistent with the higher levels of p21 protein discussed above, analysis of 3 independent repeats and revealed these differences to be statistically insignificant (Figure 3.7A).

CCNB1 is a gene encoding Cyclin B1. This Cyclin is upregulated in the G2 phase and plays a role in the progression through G2/M phase of the cell cycle (Dash and El-Deiry, 2005). At 0 hours of ActD treatment, the expression levels of CCNB1 are comparable between the NS control and p100 targeting siRNA (Figure 3.7B). In response to ActD, CCNB1 expression is downregulated. This either suggests cell cycle arrest is occurring, or that cells are passing through the G2/M checkpoint thus targeting Cyclin B1 for degradation. The gene expression between the conditions remains similar throughout the time course. Insignificant changes to the CCNB1 gene were found upon the depletion of p52/p100.

The BAX gene encodes the pro-apoptotic protein, Bax (Fischer, 2017). The mRNA levels of this gene were found to be very low in the U2-OS cells. This remained unchanged after drug treatment, regardless of the depletion of p52/p100 (Figure 3.7C).

The BCL2L1 gene encodes Bcl-xL, an anti-apoptotic gene. In the NS siRNA cells, the gene was downregulated at 8 hours of treatment, then remained low through to 24 hours. This is consistent with induction of the cell death mechanisms at around 8 hours of treatment (Figure 3.7D). The p100 siRNA cells had the same basal BCL2L1 expression, however less of a decrease was found at 8 hours and a slower downregulation of the gene was captured. This suggests that the cells with depleted p52/p100 had a lag in the induction of the apoptotic

pathway. However, as the data was not significant, further analysis with other apoptotic markers is required.

Overall, a strong link between the role of p52 in nucleolar stress and gene expression changes within the cells was not identified. This therefore suggests that other genes are the primary p52 targets after ActD treatment of that any role that p52 is playing in the stress response occurs at the protein level.

A) CDKN1A (cdk inhibitor)
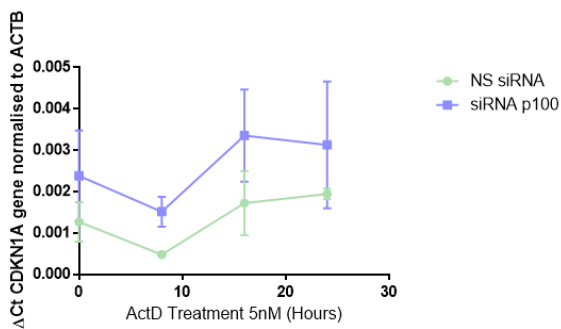
B) CCNB1 (G2/M progression)
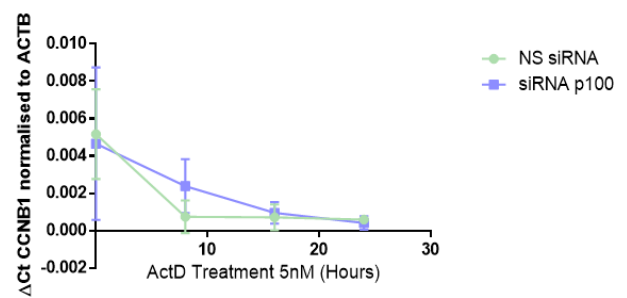
C) BAX (pro-apoptosis)
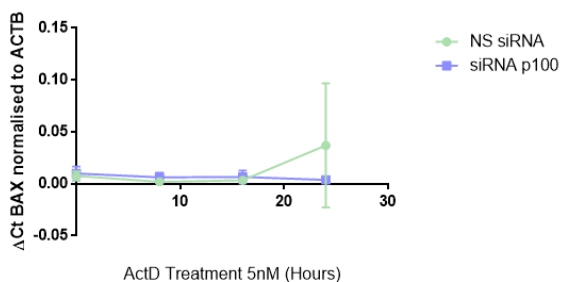
D) BCL2L1 (anti-apoptosis)
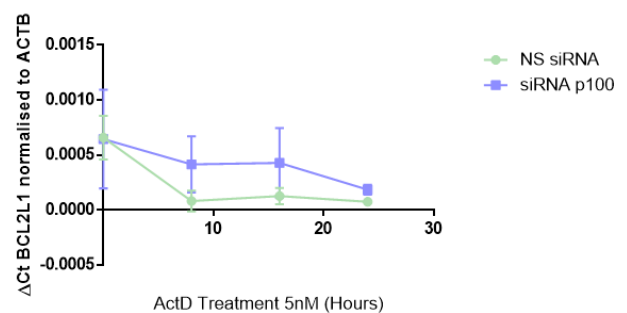
Figure 3.7 p52/p100 knockdown causes insignificant impact on gene expression of target genes. Protein was harvested from cells subject to p52/p100 siRNA knockdown and treated to varying lengths of actinomycin D treatment. RNA was harvested and converted to copy DNA prior to performing quantitative RT-PCR. A and B) Cell cycle genes, indicated in y axis, investigated. Three independent repeats plotted using Prism 6. One-way ANOVAs were performed to test statistical significance. C and D) Apoptotic genes measures, indicated in y axis. Three independent repe*ats were plotted using Prism 6.* Two-way ANOVAs were performed to test statistical significance.

3.3. Results - Is there a link between p52 and the 5S RNP/MDM2/p53 pathway?

The 5S RNP is the critical regulator of p53 stabilisation and activity in response to ribosomal stress. Furthermore, the 5S RNP is known to have a role in the stabilisation and activation of p53 in response to nucleolar stress. The 5S RNP accumulates in stressed conditions allowing the complex to bind to MDM2 thereby stabilising p53 (Sloan et al., 2013a). My data suggested that there is a link between p52 activity, caspase-dependent PARP cleavage and the cell cycle in response to nucleolar stress. Given that p52 depletion led to increased cell death in response to ribosomal stress, it was important to address whether the death was mediated by p53 signalling via the 5S RNP. In order to investigate if p52 signalling in linked to the 5S RNP/MDM2/p53 pathway, U2-OS cells were co-transfected with combinations of siRNAs. This allowed the determination of whether proteins were having an additive or an opposite impact on the stress response. To study this, single siRNA knockdowns were run parallel to double knockdowns and compared to a NS control.

3.3.1. Investigating the role of p53 within the p52-dependent ribosomal stress response

Initially, the impact of a double depletion of p52 and p53 was studied. PARP cleavage and p53 stabilisation was measured via western blotting which was later quantified (Figure 3.8A). As expected p52/p100 depletion did not significantly affect p53 stabilisation (Figure 3.8B). Interestingly, and unexpectedly, after the depletion of tumour suppressor p53, the levels of PARP cleavage increased compared to NS control and p52/p100 siRNA samples (Figure 3.8C). The quantification of cleaved PARP showed that cells depleted of p53 showed a greater increase in PARP cleavage up to 8 hours of treatment. At prolonged time points (16 and 24 hours) the level of cleaved PARP detected decreased compared to basal levels. The double knockdown samples displayed the highest degree of PARP cleavage up to 8 hours of ActD treatment. The detected protein levels of cleaved PARP decreased after 8 hours of treatment. As full length PARP protein also decreased at later time points, it suggested that cells double depleted in p52/p100 and p53 suffered significant cell death as a result of prolonged treatment. This suggests the double depletion of p52/p100 and p53 worsens the cell death phenotype in response to ActD treatment, raising the question of whether p52 and p53 are working together in the cellular response to nucleolar stress.

A) p52/p100 and p53 double knockdown ActD time course
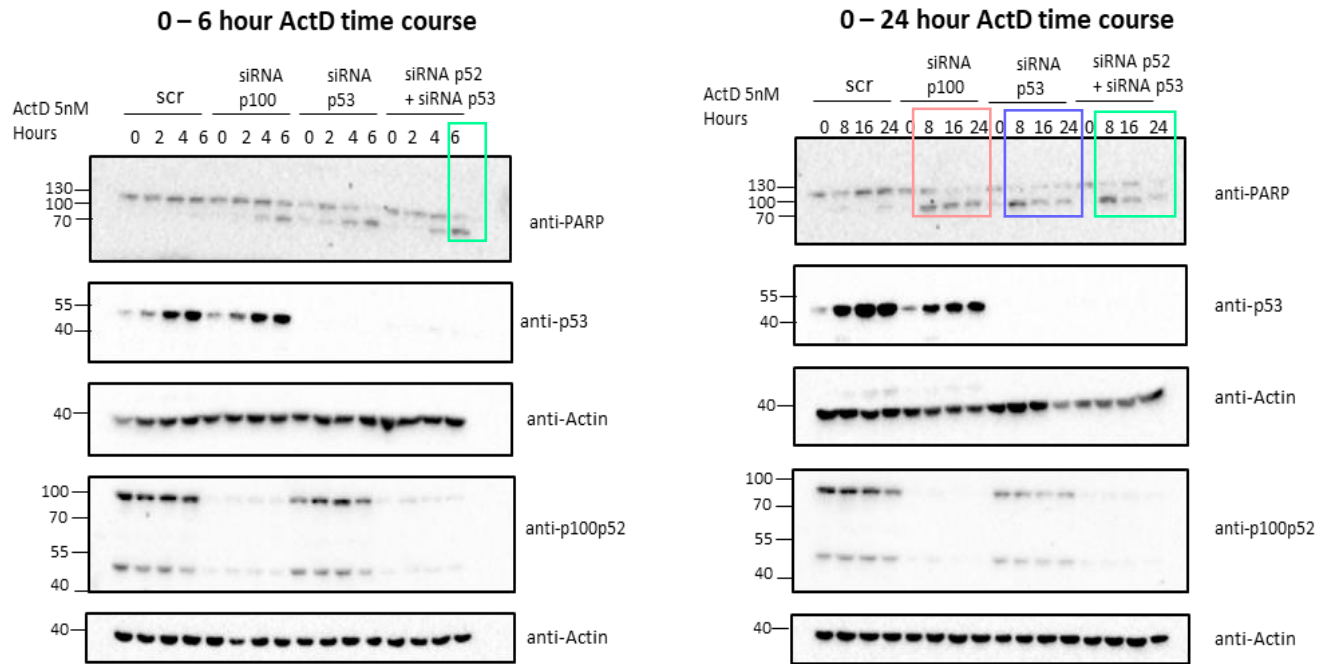
B) p53 quantification
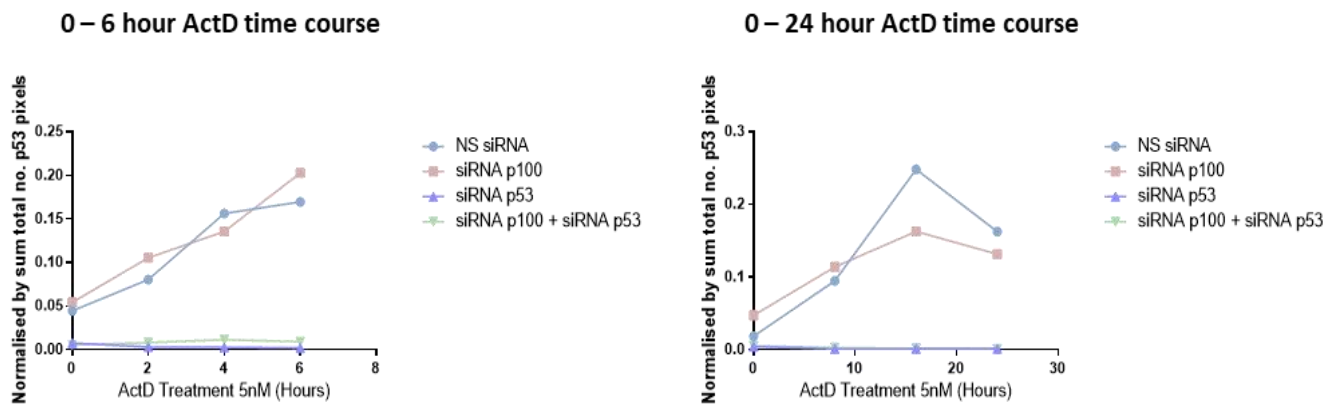
C) Cleaved PARP quantification
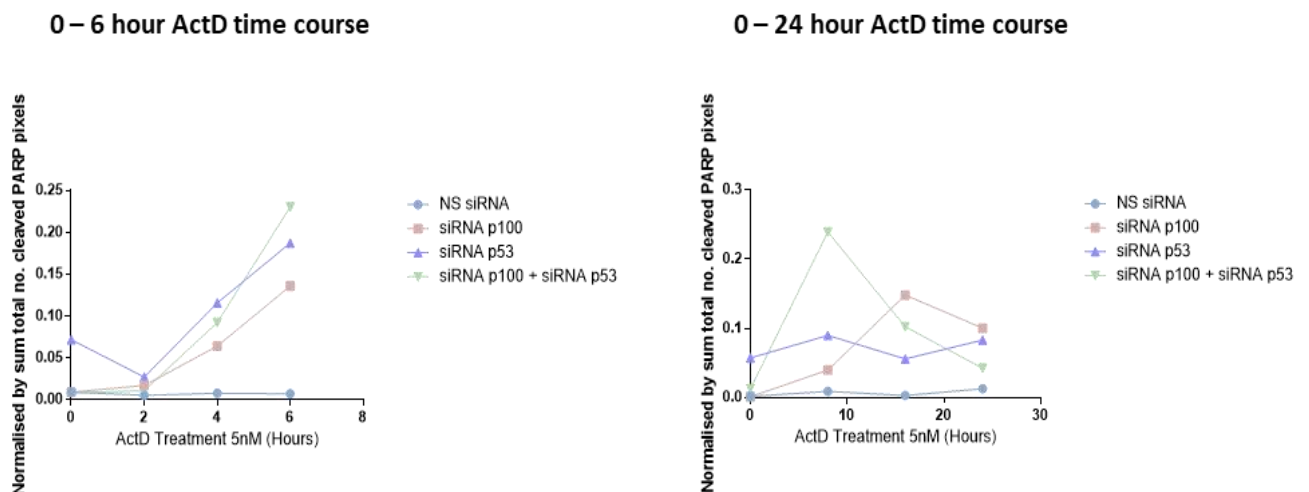
Figure 3.8 A double knockdown of p52/p100 and p53 leads to increased PARP cleavage following actinomycin D treatment – page 99. U2-OS cells were treated with a non-specific siRNA, p52/p100 targeting, p53 targeting or a combination of p52p100 and p53 targeting siRNAs. Cells were treated with ActD for both short and longer time courses before protein was extracted. Analysis was achieved via western blotting and developed using a BioRad ChemiDoc. A) Western blot image showing the single repeat of this experiment. Coloured boxes to highlight key areas on quantification graphs. B) Quantification of the p53 pixels. C) Quantification of the cleaved PARP pixels, performed on ImageLab.

To visualise the role p53 plays in the p52-dependent ribosomal stress response in an alternate way, the lung carcinoma cell line, H1299 was utilised. This was chosen as the model system as these cells are naturally p53 null. H1299 cells were treated with a NS siRNA or an siRNA targeting p52/p100. Cells were then treated to varying time points of ActD at 5nM prior to harvest. Protein was extracted and analysed via western blot.

The NS siRNA lysates contained negligible cleaved PARP levels (Figure 3.9). Little full length PARP was detected across the time course. The cells treated with siRNA p100 also contained very little cleaved PARP in response to drug treatment. The cleaved PARP in the 16 and 24 hour samples were insignificantly increased compared to the NS control. A slight increase in full length PARP in the 16 and 24 hour siRNA p100 lysates was also detected. Comparing these to the actin loading control revealed higher protein levels overall. Therefore, it suggests insignificant differences in PARP cleavage in the control versus p52/p100 depleted cells.

The assay also showed very little phospho-CDK1 detected in all of the samples at all time points (Figure 3.9). The NS siRNA and p100 siRNA results were comparable. Whilst little phospho-CDK1 was detected, the level of total CDK1 remained stable. This suggests little G2/M cell cycle arrest across all samples. The G2/M checkpoint was predicted to be unaffected by p52/p100 depletion in H1299 cells.

Finally, p21 protein was studied (Figure 3.9). In NS cells, p21 slightly increases at 6 and 16 hours of treatment, however this increase is insignificant. In the siRNA p100 cells, p21 also increases at 6 and 16 hours. It is important to note that the 16 hour siRNA p100 sample was overloaded, as seen in the actin control blot. Thus, the image shows insignificant differences in p21 protein levels over time in response to ActD either with basal p52/p100 levels or depleted.

Therefore the nucleolar stress response in H1299 cells does not appear to be affected by the depletion of p52/p100. It is possible that the lack of p53 in the cells reverses the phenotype

shown in U2-OS and HCT116 cells following a p52/p100 knockdown, as those cells naturally

posses p53. Therefore, their intrinsic signalling pathways are reliant upon using that protein,

whereas H1299 cells do not require p53 for survival. In summary, this figure displays that

cells naturally lacking p53, and following depletion of p52/p100, do not show the same

phenotype in response to ribosomal stress. Therefore, the figure suggests the p52

dependent ribosomal stress response requires p53.
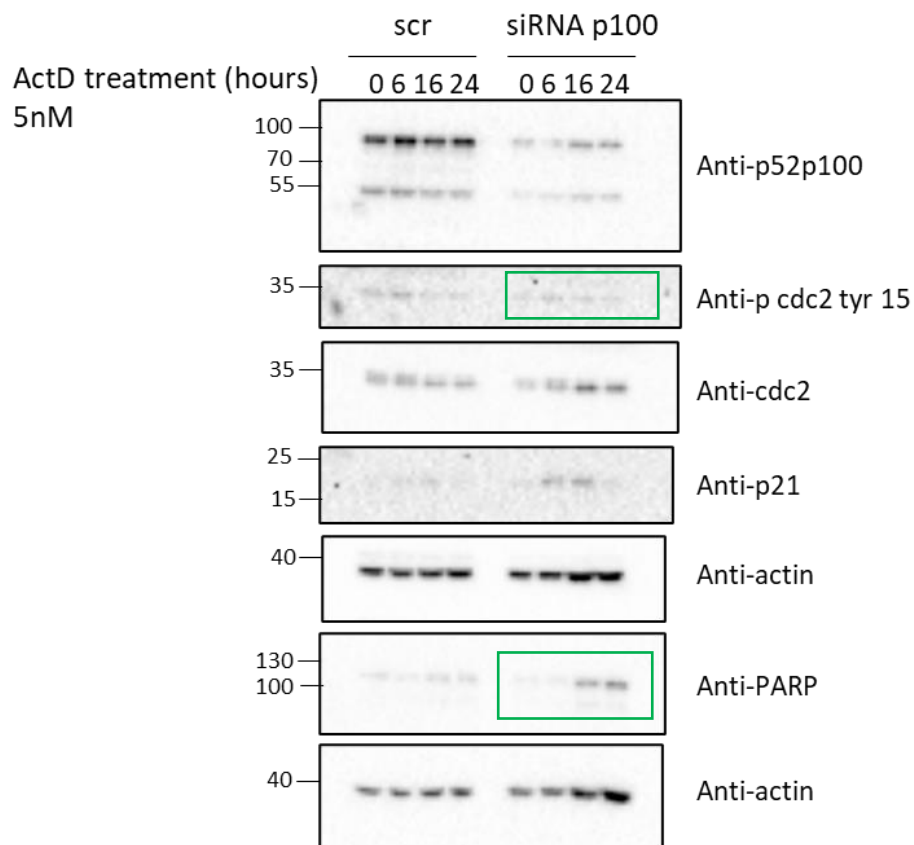
Figure 3.9 The p53-null cell lines, H1299, does not show impacted response to actinomycin D following p52/p100 depletion. H1299 cells were treated with a p52/p100 siRNA and treated with ActD. Protein was anlaysed via western blotting and developed using a BioRad ChemiDoc. Green boxes highlight the lack of phenotype induction following siRNA knockdown and ActD treatment.

3.3.2. Double depletion of p52 and RPL11

Taken together this data indicated that p52 plays a role in the response to nucleolar stress. However, whether the 5S RNP was involved in this process had not been addressed. The 5S RNP is responsible for p53 activation following nucleolar stress by binding to, and inhibiting the action of, negative regulator MDM2 (Sloan et al., 2013a). To investigate whether the 5S RNP might also regulate p52, the response of U2-OS cells to RPL11 siRNA or a double knockdown of p52/p100 and RPL11 were measured (Figure 3.10).

The cell cycle arrest markers, CDK1 phosphorylated at tyrosine 15 and p21, were probed for via western blotting (Figure 3.10A). Western blotting analysis revealed insignificant differences between p52/p100 knockdown, RPL11 knockdown and p52/RPL11 double knockdown samples. The p52/p100, RPL11 and p52/RPL11 knockdown, however, displayed lower phospho-CDK1 in their 24 hour samples in comparison to the non-specific control. As three repeats were not performed, statistical analysis was not carried out. The different knockdowns had differing impacts on p21 protein levels. Non-specific control samples saw a rise in p21 protein across the ActD time course. The p52/p100 depleted cells saw high basal levels of p21 that were degraded over time. Interestingly, RPL11 depletion caused a basal increase of p21 protein levels which was similar to the p52/p100 knockdown. However, p21 protein remained relatively similar across the 24 hours of ActD treatment. Finally, the double knockdown caused a basal increase of p21 protein. This was then slightly degraded across the time course. The degradation seen was not as dramatic as that captured in the p52/p100 knockdown alone, suggesting the additional RPL11 knockdown could be dampening the effects seen after solely depleting p52/p100. It is important to state that the two repeats revealed variation in cell cycle markers. Therefore, at present, the results are speculative, quantification was not performed and further repeats are required.

The presence of cleaved PARP, however, was measured (Figure 3.10B). Two repeats were plotted together and therefore statistical analysis was not available. RPL11 depletion was sufficient to cause an increase in PARP cleavage at 24 hours. Strikingly, the double depletion of p52/p100 and RPL11 caused the largest increase of PARP cleavage, mirroring the results of the p52/p100 and p53 double depletion. The error bars in the 24 hour sample following the RPL11 or the double knockdown were large. This is indicative of instability within the cells. Figure 3.10B suggests the double knockdown had a higher activation of cellular death mechanisms.

Overall, the p52/p100 depletion caused an upregulation of cell cycle arrest markers basally in the cells compared to the control. The addition of the RPL11 siRNA alongside the p52/p100 siRNA leads to lesser effects on the cell cycle of U2-OS cells by slightly dampening the effects seen upon p21 protein abundance. The double knockdown, however, made a profound impact upon PARP cleavage in response to ActD. Thus, Figure 3.10 suggests that p52 could be co-operating with the 5S RNP/MDM2/p53 pathway, or, that RPL11 regulates p52 activity.

A) p52/p100 and RPL11 double knockdown ActD time course
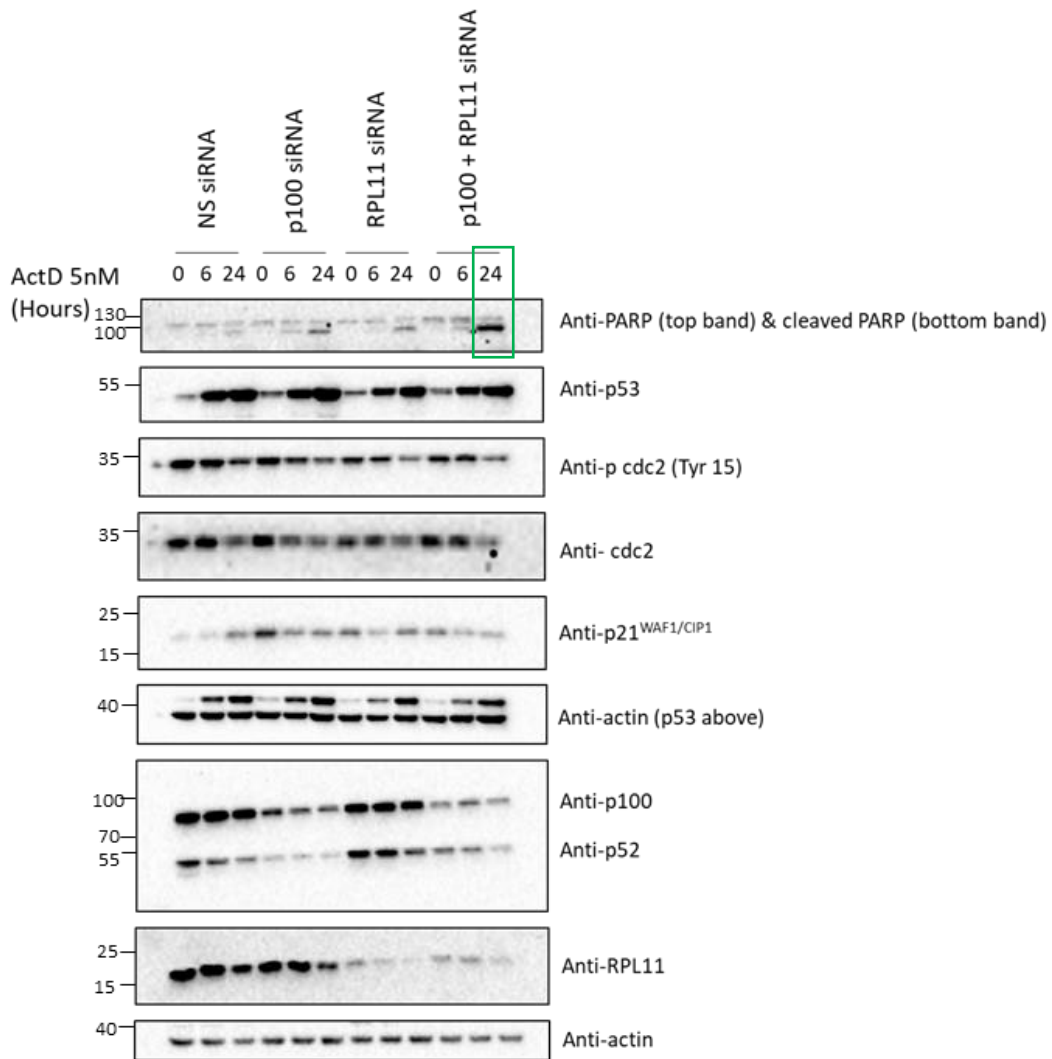
B) Cleaved PARP protein quantification
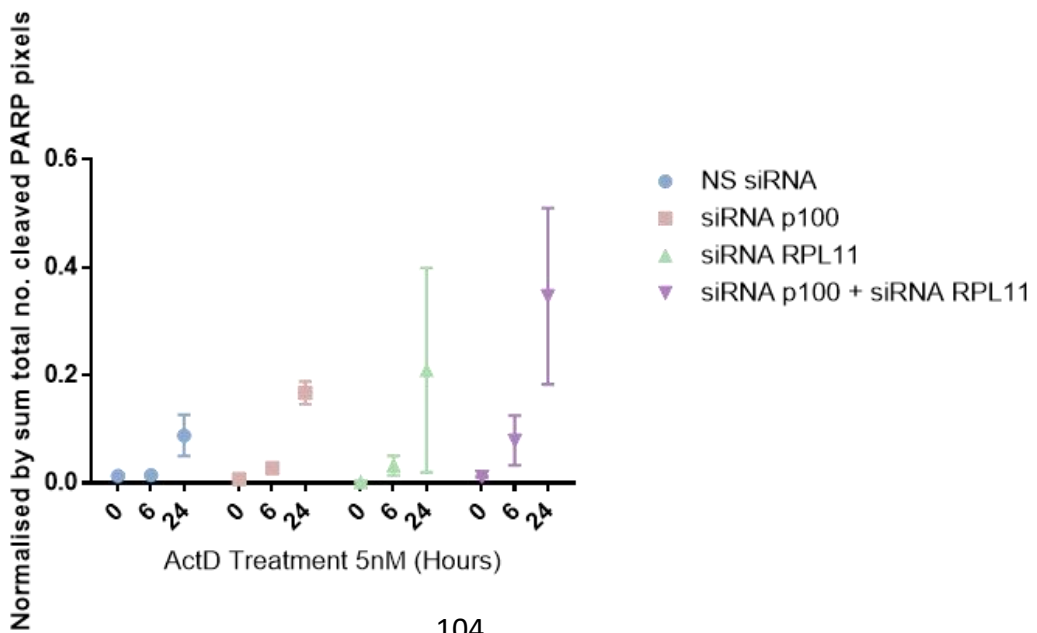
Figure 3.10 A double knockdown of p52/p100 and RPL11 leads to higher incidences of PARP cleavage following actinomycin D treatment – page 104. *U2-OS cells were treated with siRNAs as indicated in figure. Cells were then treated with ActD and protein was harvested for western blotting. A BioRad ChemiDoc was used for visualisation of the bands. A) The image represents one of two independent repeats. B) Quantification of cleaved PARP protein presence.*

3.4. Results - Is the role of NF-κB in the context of nucleolar stress specific to non-canonical signalling?

3.4.1. Comparing the roles of p52 and RelB in response to Actinomycin D

The p100/p52 subunit of the NF-κB family exists in homo- or heterodimers. The preferential dimer of the non-canonical pathway is the p52/RelB heterodimer (Perkins, 2012). It had not been established whether RelB was having an effect within the nucleolar stress response, and if the effect would indicate p52 was participating in a p52/RelB heterodimer during the response. To review whether RelB plays a role in the response to ActD treatment, cells were transfected with a RelB specific siRNA alongside a NS control siRNA and a p100 targeting siRNA.

The experimental repeats of Figure 3.11A were performed by students Kirsten Ramsay and Aleksandra Sukova under my direct supervision. The data revealed insignificant changes in p53 stabilisation in response to drug treatment. The stabilisation of p53 was unaffected by the depletion of both RelB and p52/p100. Interestingly, in the RelB knockdown cells, PARP cleavage was substantially effected. The basal levels of cleaved PARP were increased and after 4 hours of ActD exposure the level of cleaved PARP detected in the samples had already increased to a higher degree than in the 24-hour control sample. Furthermore, full length PARP was found to decrease which indicates a high level of cell death. Lastly, cleaved PARP levels continued to increase at 24 hours of treatment leaving little full length PARP intact. The p52/p100 knockdown showed less dramatic induction of the PARP cleavage pathway. Therefore, while p52/p100 depletion caused a marked effect on the induction caspase-mediated PARP cleavage compared to NS control, RelB depletion was found to have the most profound effect on the stability of the cells.

Given the indication that the p52-mediated response to nucleolar stress could involve cell cycle arrest, it was important to compare cell cycle arrest markers; phosphorylated CDK1 and p21. In the phospho-CDK1 and p21 western blots the RelB depleted samples and the control samples contained comparable changes in protein abundance across the time course

(Figure 3.11A). The p52/p100 depleted samples were unique in showing decreased presence of phospho-CDK1 at 6 and 24 hours of ActD treatment. Further, the p21 protein levels appeared higher both basally and at 6 hours of treatment prior to degradation in p52/p100 but not in RelB depleted samples. Therefore, it is sappears that in the response to ActD, p52 causes a more noticeable impact on cell cycle arrest proteins in comparison to RelB. On the other hand, RelB depletion caused a much greater impact on PARP cleavage following nucleolar stress.

3.4.2. *Investigating the role of canonical NF-κB signalling in the nucleolar stress response*

NF-κB signalling can function through two distinct pathways: the canonical and the non-canonical (Gilmore, 2006). Previously, the major players within the non-canonical pathway, p52 and RelB, were studied in the ribosomal stress response. Canonical signalling is more prevalent and more widely studied in the context of cellular stress. Therefore, it was important to determine whether the proposed role of NF-κB as a regulator of nucleolar stress is specific to non-canonical signalling or a family-wide role. To test this, the p50 and RelA NF-κB subunits were depleted using siRNAs. This was followed by treatment with Actinomycin D and analysis of the protein abundance through western blotting.

The non-specific control siRNA showed the expected increase of p53 stabilisation over time (Figure 3.11B). The level of PARP cleavage insignificantly increased after 6 hours of treatment followed by a larger increase at 24 hours. The level of full length PARP, however, remained unchanged. Following the p50 knockdown, the stabilisation of p53 was comparable to the control in response to the induction of nucleolar stress. PARP cleavage was undetectable at 0 hours, a small increase was seen after 6 hours of drug exposure. This was slightly higher when compared to the 6 hour time point in the control experiment. Finally at 24 hours after ActD treatment, cells with depleted p50 saw an increased level of cleaved PARP, similar to control. Finally, RelA was targeted with an siRNA. The depletion had no impact on the p53 response following drug treatment when compared to NS control and p50 siRNA samples. Equally, no differences were seen in PARP cleavage in response to nucleolar stress. This suggest that the NF-κB family members involved in canonical signalling do not play a significant role in the response to nucleolar stress.
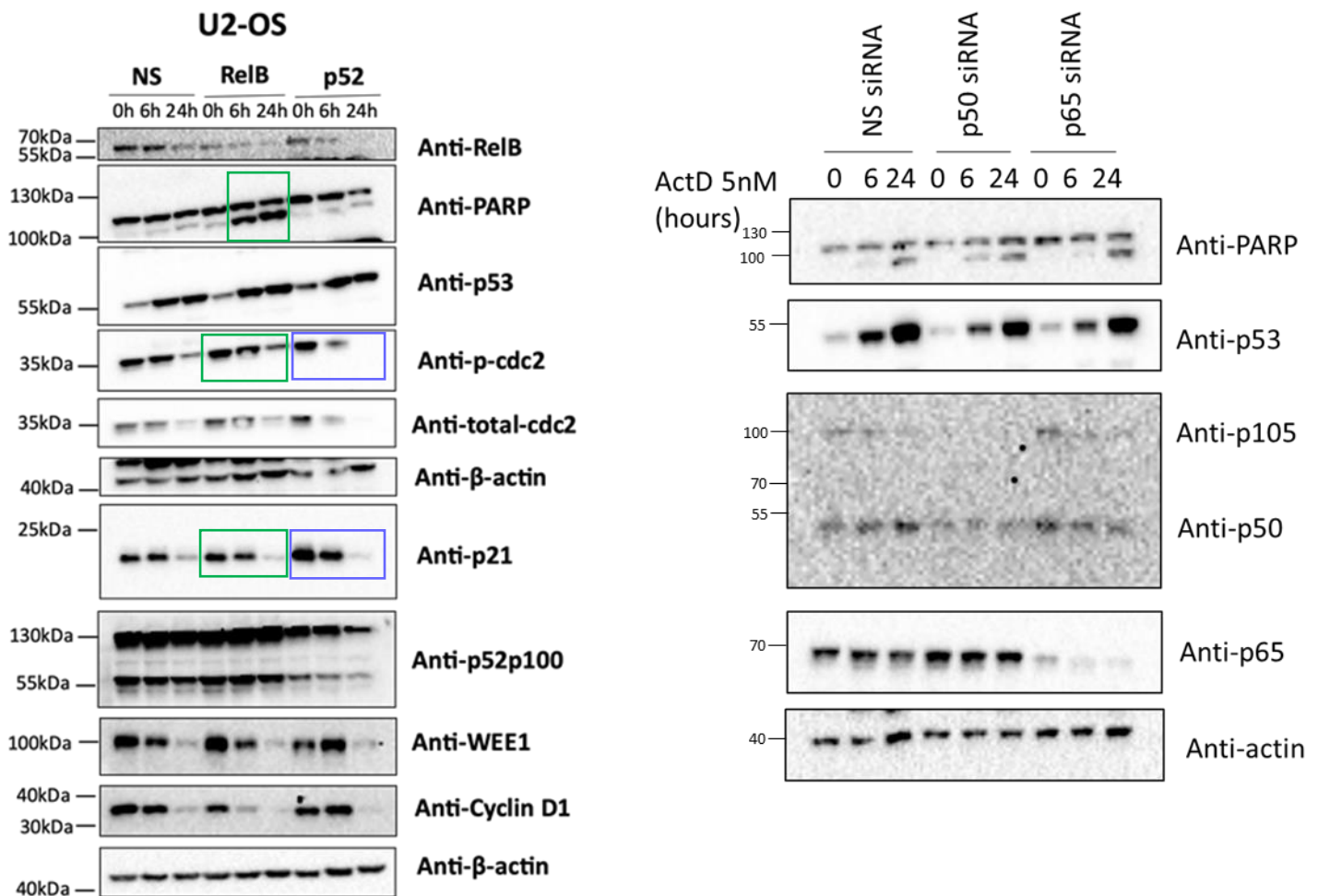
Figure 3.11 The role of NF-κB in the nucleolar stress response is specific to the non-canonical signalling pathway. U2-OS cells were treated with siRNAs as indicated in the figure. Recovered cells were treated with ActD for the times indicated and protein analysed via western blotting. A) Non-canonical NF-κB members were knocked down. Figure provided by Kirsten Ramsay, a Masters of Research student under direct supervision. Two independent repeats were performed by Ms Ramsay and an additional repeat performed by Aleksandra Sukova, an undergraduate student. Both students were under my direct supervision. B) Canonical members of the NF-κB family were knocked down. The image represents one of three independent repeats. One repeat was performed by Aleksandra Sukova.

3.5. Discussion

3.5.1. The response to nucleolar stress is specific to the non-canonical pathway

A striking finding from this chapter is that depletion of the canonical NF-κB subunits, p50/p105 and RelA, did not affect the response to nucleolar stress (Figure 3.11B). On the other hand, members of the non-canonical pathway, p52/p100 and RelB, did. It is uncommon for the non-canonical signalling pathway to function independently from the canonical. Usually, reports find that the pathways are intertwined and non-canonical pathway activity is often accompanied by the canonical (Shih et al., 2011). For example, the *RELB* and *NFKB2* genes contain κB sites in their promoters, meaning that they are subject to RelA dependent transcriptional regulation (Bren et al., 2001, Liptay et al., 1994a). Other evidence of crosstalk stems from the study of knockout mice. For example, the R*ela*^{-/-} mouse is embryonic lethal through liver apoptosis and a sensitivity to TNF (Beg et al., 1995). However, the mice also showed an absence of splenic architecture and lymph nodes, resembling the phenotype of a non-canonical subunit deficient mice. Furthermore, it has been shown that in *Nfkb2*^{-/-} murine cells, the lack of p52/p100 able to form dimers with RelB actually pushes RelB into heterodimers with the p50 subunit. Similarly, in N*fkb1*^{-/-} murine cells, p100 protein levels were found to be depleted as more p52 was being generated in order to form a heterodimer with RelA. The RelA/p52 dimer was found to regulate RelA target genes (Basak et al., 2008, Shih et al., 2011). An example of non-canonical activity independent of the canonical was reported to be linked to hypoxia inducible factor 2α. Prior to this study, the link between hypoxia and NF-κB had only been shown via canonical signalling through a RelA/p50 heterodimer (D'Ignazio et al., 2018). The Rocha laboratory, however, found that treating cells with TNFSF14/LIGHT – an inducer of the non-canonical NF-κB pathway – led to HIF-2α induction in a p52 dependent manner. Therefore, an incidence of non-canonical activity occurring independently to canonical activity is an exciting discovery in NF-κB biology. In particular, unique cellular responses that occur following the depletion of the non-canonical subunits is of interest in the field, as NF-κB subunits are known to reshuffle in order to restore a sense of balance.

3.5.2. RelB and p52 potentially function through different mechanisms following nucleolar stress induction

The data in Figure 3.11A indicates a different role for p52 and RelB in the ribosomal stress response. Firstly, RelB depletion leads to a much more dramatic onset of PARP cleavage, a

marker of cell death. Whilst the effects seen after p52 depletion are not as strong in the context of PARP cleavage, there the data to suggests that p52 plays a more important role than RelB as a regulator of the cell cycle. The potential role of p52 in nucleolar stress is discussed below.

RelB is known for promoting cell survival in cancer cells (Kaltschmidt et al., 2018). Kuhn *et al* created a murine phenotype to investigate the role of RelB in CD40-driven B cell lymphomas (Kuhn et al., 2022). Mice expressing constitutively active CD40 receptor were crossed with the RelB knockout mouse. This resulted in impaired survival and activation of B cells. Whilst this did not remove the onset of lymphoma, the progression of the cancer was slow and the latency period increased (Kuhn et al., 2022). Thus, the study indicates RelB plays a role in cancer cell survival. Further, in prostate cancer cell lines, increasing cellular RelB levels were found to increase tumorigenicity (Josson et al., 2005). Interestingly, increasing RelA protein levels did not achieve the same result. Therefore, a role for RelB in the survival of U2-OS cells facing nucleolar stress is unsurprising. Through the study of 67 chronic lymphocytic leukemia bone marrow samples, it was determined that RelB activity was found in all of the samples. Furthermore, lower RelB activity was linked to better patient prognosis (Xu et al., 2014). This indicates that RelB contributes to cancer survival, presumably through encouraging cell survival.

3.5.3. Actinomycin D functions through the stabilisation of p53 which is unaffected by depleting members of the NF-κB family

The abundance of the p53 protein and the rate of stabilisation was unaffected by any NF-κB targeting siRNA used (Figure 3.2, Figure 3.11). Actinomycin D is a widely studied inducer of nucleolar stress. It has been shown that low levels of ActD can contribute to cell cycle arrest, where higher concentrations are linked to cell death (Merkel et al., 2012). Choong *et al* discovered that low doses of ActD specifically induce cell cycle arrest via p53 signalling (Choong et al., 2009). The study demonstrated via flow cytometry an increase of HCT116 cells in the gap phases of the cell cycle in response to ActD treatment. This corresponded to a decrease in cells found in S phase of the cell cycle. This profile is indicative of cell cycle arrest. Interestingly, the arrest was found to be reversible. Whilst low percentages of apoptotic cells were detected, this was negligible in comparison to cells undergoing arrest (Choong et al., 2009). Overall, the results presented in Chapter 3 display that ActD-induced p53 stabilisation is a robust mechanism that functions through the 5S RNP. The depletion of

NF-κB subunits at the basal level were unable to alter this particular response in both U2-OS and HCT116 cell lines.

3.5.4. p52 plays a protective role in the response to nucleolar stress - U2-OS cells display a strong link between p52/p100 and the cell cycle in response to nucleolar stress

The link between p52 and the cell cycle has been previously described. For example, it has been previously shown that p52 depletion in U2-OS cells reduces cell number (Schumm, 2006). Furthermore, p52 has been found to bind to the promoter regions of several p53 target genes that serve roles in the regulation of the cell cycle (Schumm, 2006). It was determined that UV radiation, a potent inducer of ribosomal stress (Iordanov et al., 1998b), changes the nature by which p52 regulates those target genes.

Interestingly, Schumm *et al.* found that siRNA mediated knockdown of p52/p100 resulted in increased p21 mRNA and protein levels (Schumm et al., 2006). This result was also seen in Figure 3.5, indicating that p52 could function to repress p21 transcription and translation. In the p52 depleted cells, p21 protein levels are significantly increased at basal levels and during actinomycin D treatment until prolonged treatment times (16 hours and longer). At that point, p21 protein decreases, presumably by being degraded. Further, Schumm *et al.* performed flow cytometry on U2-OS cells following p52/p100 knockdown, alongside control samples. The cells were stained with propidium iodide to visualise the stage of the cell cycle that the cells were in upon harvest. It was seen that p52/p100 depletion caused a decrease of cells in the S phase and an increase of cells in G1/S and G2/M phases, indicative that p52 plays a role during several stages of the cell cycle (Schumm, 2006). This is in line with both the increased p21 protein levels, a known mediator of cell cycle arrest, and the increased number of cells appearing to lose adherence in Figure 3.1. Adherent cell populations have been shown to detach following cell death, or, during significant cell cycle arrest. Hence, the data presented, alongside Dr Schumm's findings, show that p52 plays a role in p21 synthesis in U2-OS cells. It appears that p52 may repress p21 gene expression and subsequent translation due to the increased protein abundance after siRNA knockdown of p52/p100 (Figure 3.5B). Further, the depletion of the protein causes cells to undergo cell cycle arrest both basally and up to 16 hours of ActD treatment. However, it could also be an example of dependency on p52 for the regulation of the cell cycle. Perhaps, lacking this vital cell cycle regulator causes the cells to sense an instability surrounding the cell cycle, forcing them to

arrest. It is interesting that the cell cycle inhibitor, p21, is degraded after 16 hours of treatment, this is discussed later.

Whilst it is not known which dimer p52 is forming during the response to ActD, it has been shown that p52 homodimers can switch association with its cofactors to either repress or activate gene expression. Rocha *et al* showed that p52 homodimers become repressive of the Cyclin D1 gene in response to UV radiation (Rocha et al., 2003). The homodimers change from an association with Bcl-3, a co-activator, to HDAC1, a transcriptional corepressor protein. Cyclin D1 upregulation is necessary for the successful progression through the G1/S phase of the cell cycle (Rocha et al., 2003). Therefore, this indicates a role for p52 homodimers in cell cycle arrest through repressing protein expression in response to UV radiation, an inducer of ribosomal stress. It must be noted, insignificant differences in Cyclin D1 protein abundance were captured in p52 knockdown cells versus control in my experiments, however the protein was seen to be degraded at later time points (Figure 3.5). Future experiments could investigate the presence of HDAC1 and Bcl-3 throughout the time course to determine whether p52 homodimers are associating or re-associating throughout the response. Whilst the different cellular responses in cells with p52 depletion versus RelB depletion seen in Figure 3.11A suggest the response is unlikely to be governed by a p52/RelB heterodimer, further experimentation would be useful to determine p52's dimeric partner.

A G2/M cell cycle arrest marker was also investigated. Phosphorylation of CDK1 at Tyr 15 by the kinase WEE1 causes the inhibition of the cell cycle at the G2/M checkpoint (Parker et al., 1992). Cells depleted in p52 displayed a significant initial increase in CDK1 phosphorylation, however insignificant differences were found for the remainder of the time course (Figure 3.5C). The more interesting finding, however, was that across the ActD time course, CDK1 phosphorylation was being lost. The decrease in phosphorylation occurs at the same time that the WEE1 protein appears to be degraded. This indicates cells are starting to progress through mitosis. This is echoed by the flow cytometry data shown in Figure 3.6.

3.5.5. HCT116 cells show a link to the cell cycle during response to nucleolar stress
The link between p52/p100 and the cell cycle in U2-OS cells had been previously studied, however HCT116 cells had yet to be investigated. HCT116 cells are a colorectal cancer cell line possessing wild-type p53 (Kaeser et al., 2004). The usual treatment for colorectal cancer

in the clinic includes the chemotherapeutic drug 5FU. 5FU has been shown to activate p53 through the 5S RNP and is therefore used to study nucleolar stress (Sun et al., 2007). By contrast to the results seen in U2-OS cells, p52/p100 depleted HCT116 cells displayed a decreased protein presence of the cell cycle inhibitor p21 basally and in response to drug treatment (Figure 3.3). Unfortunately, this result was performed as a single repeat so statistical significance was not able to be determined. Even so, this suggests p52 could be involved in the activation of p21 transcription and translation in HCT116 cells. Perhaps, p52 is involved in a different dimer during the response in these cells or, if a p52 homodimer, it is associated with Bcl-3. This speaks to the difference and variety of NF-κB activity in different cellular environments and different cell types. One theory as to why the cell cycle responses are so different in HCT116 cells compared to U2-OS cells, is that there is much less p52 naturally in the cell. It can be seen in Figure 3.3 that HCT116 cells possess much higher amounts of p100 in comparison to p52, and that basal p52 levels are relatively low – almost undetectable by western blot. Therefore, the cells must have other natural mechanisms of cell cycle regulation that does not involve the little p52 protein they possess. On the other hand, p52 is more abundant in U2-OS cells and much work of the NF-κB field is performed in these cells due to the cell's reliance on the NF-κB pathway. Thus, HCT116 cells serve as an important control. Despite the result only being a single repeated experiment, it is still striking to see some similarities between the responses to nucleolar stress following the depletion of p52/p100. The data presented in this chapter suggests that the effects in HCT116 cells could be due to a loss of p100, rather than p52, given the higher basal levels of the full length repressive protein.

One similarity between the U2-OS and HCT116 cells is the presence of the phosphorylation of CDK1 at tyrosine 15. In the control samples, phospho-CDK1 stays present throughout the duration of the 24 hours of drug treatment. In the p52/p100 depleted cells, however, phospho-CDK1 decreases at 16 hours and is lost by 24 hours of treatment. This is indicative of p52/p100 depleted HCT116 cells being allowed to progress through mitosis at prolonged treatments with 5FU.

3.5.6. Cancerous cell lines depleted in p52/p100 could undergo mitotic catastrophe during prolonged periods of ribosomal stress

In cases of overwhelming DNA damage, cells undergo programmed cell death (Paek et al., 2016). The 16 hour time point following ActD treatment induced significant incidences of

PARP cleavage (Figure 3.2A, Figure 3.3 and Figure 3.4). The caspase-mediated cleavage of PARP is a well-known marker of cell death. Whilst some argue this is a marker of apoptosis, it is becoming clearer that PARP cleavage events can occur during various types of cellular death (Chaitanya et al., 2010). As preliminary quantitative RT-PCR analysis revealed insignificant changes in genes involved in apoptosis (Figure 3.7), it can be predicted the cells are dying through alternative mechanisms. Whilst apoptosis is the most widely studied form of cell death, other mechanisms of cell death, such as autophagy, have been previously linked to NF-κB signalling. Recent studies have shown that NF-κB family members can modulate autophagy as well as the process itself impacting NF-κB signalling. This indicates that NF-κB activity is not limited to crosstalk with apoptotic signalling pathways and the transcription factor family could be involved in multiple mechanisms of cell death.

At 16 hours of ActD treatment it was found that the p21 protein was rapidly degraded following on from being significantly increased. Additionally, the inhibitory phosphorylation marker on CDK1 was removed (Figure 3.5). Comparing the western blot analysis with the cell cycle profile of control and p52/p100 knockdown cells revealed the cell cycle-dependent role p52 plays in the nucleolar stress response in U2-OS cells. At the 16 hour time point, flow cytometry revealed that p52/p100 depleted cells showed a large decrease in cells within the G2/M phase of the cell cycle (Figure 3.6). This suggests cells are progressing through this cell cycle checkpoint. In summary, from 16 hours of ActD treatment, significant PARP cleavage is induced, p21 is degraded, CDK1 is dephosphorylated and significant DNA damage is detected (Figure 3.12). The phosphorylation of H2AX at serine 139 is a marker of DNA damage, specifically double stranded DNA breaks. This marker is produced rapidly following DNA damage, thus serving as an important cellular indicator (Podhorecka et al., 2010). U2-OS cells depleted in p52/p100 show increased γH2AX protein levels from 16 hours of treatment (Figure 3.2). DNA damage is sensed through increased levels of γH2AX. This triggers the activation of repair pathways such as homologous recombination and non-homologous end joining. The latter being more error prone and less favourable (Zhou and Elledge, 2000).

This combination of DNA damage and the removal of cell cycle arrest markers in the context of cell death leads to the hypothesis that the U2-OS cells are undergoing mitotic catastrophe. The true definition of mitotic catastrophe is widely debated as it is unsure whether cells die due to defective mitosis or whether cells die following mitotic entry (Castedo et al., 2004, Sazonova et al., 2021). Either way, mitotic catastrophe is a result of a

defective G2/M cell cycle checkpoint. This checkpoint normally ensures cells have accurately and completely replicated cellular contents prior to the final division step. This stage is irreversible (Swift and Golsteyn, 2016). Therefore, if the G2/M checkpoint is not functioning adequately, any faults or damage within the DNA sequence will be replicated alongside the aberrant cell division. The large increase in yH2AX at the 16 hour time point could be a result of the cells rushing through mitotic cell division, therefore replicating DNA damage present in the cells leading to an increase in cell death (Figure 3.2). If cells lacking p52 causes a higher onset of double stranded DNA breaks, it suggests that p52 could play a role in the adequate DNA repair pathway during nucleolar stress. Potentially, its role in the cell cycle is to ensure the integrity of the process, allowing cells to cope with the stress and continue to survive.

It has been determined that p52/p100 can regulate the transcription of RAD51, a recombinase enzyme that promotes homologous recombination (Budke et al., 2022). Homologous recombination results in the accurate repair of damage DNA, allowing cells to continue with the cell cycle. When p52/p100-dependent signalling was inhibited, cancer cell lines became sensitised to DNA-damage inducing chemotherapies as there was a significant decrease in homologous recombination activity. Interestingly, RelB depletion did not cause the same outcome, meaning the link between homologous recombination and non-canonical NF-κB signalling is specific to p52. Further, p52 depletion did not impact non-homologous end joining, which is more likely to introduce errors into the DNA sequence (Pointer et al., 2020). This is a great example of p52 playing a role in cancer cell survival through the promotion of DNA damage repair via homologous recombination.

The research presented in this chapter was performed in cancer cell lines, and this, of course, would be advantageous to these cancer cells. Thus, it is proposed that p52 plays a cell survival role in cancer cells through direct regulation of the cell cycle. In future experiments, it would be interesting to examine changes to the DNA damage response and DNA repair pathways in p52 depleted U2-OS cells following nucleolar stress.
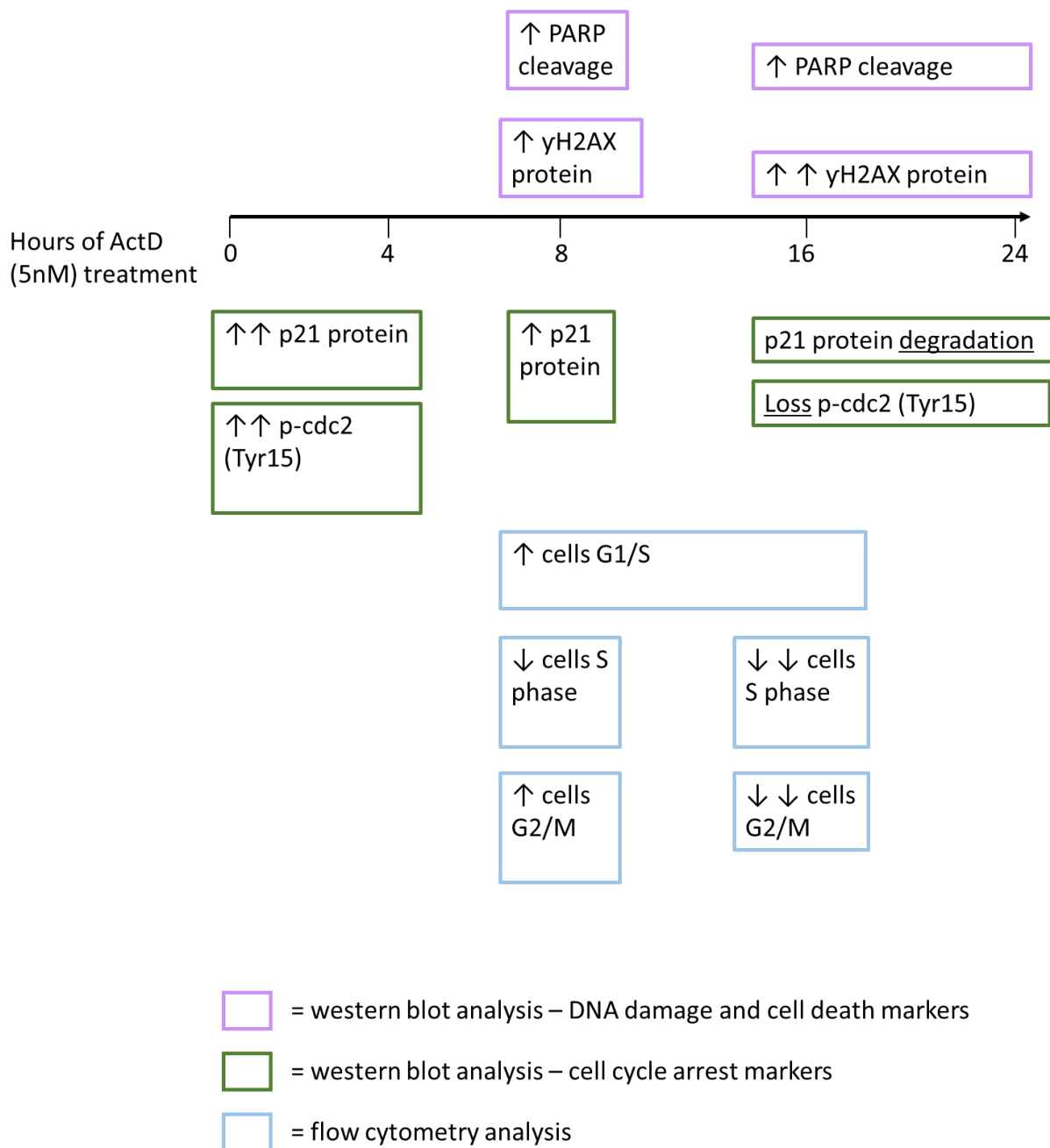
Figure 3.12 Summarising the cellular effects captured following p52/p100 depletion in U2-OS cells challenged to Actinomycin D treatment. Between 0 and 4 hours of treatment, there is increased abundance of cell cycle arrest markers, indicated by green boxes. From 8 hours, DNA damage markers and cell death markers begin to increase. This occurs at the same time as a an increase of cells in G1/S, and G2/M and a decrease of cells in S phase of the cell cycle. Finally, at prolonged exposure to the drug, from 16 hours onwards, there is a large increase in cell death and DNA damage markers accompanied by a decrease in cell cycle arrest markers and cells in the S and G2/M phases of the cell cycle.

3.5.7. Could p52 and the 5S RNP be influencing cellular fate?

The relationship between p52 and members of the 5S RNP/MDM2/p53 pathway were explored through siRNA-mediated knockdown. The depletion of p53 alone gave rise to an increased response to ActD treatment (Figure 3.8). This was rather unexpected considering ActD functions by disrupting ribosome biogenesis leading to the breakdown of the nucleolus and allowing ribosomal proteins to translocate. The 5S RNP is then able to bind to MDM2 which subsequently stabilises p53. It was thus predicted that the removal of p53 would reverse cell death phenotypes observed under the microscope and through the detection of cleaved PARP in response to prolonged ActD treatment. The p53 knockdown, however, resulted in increased detection of cleaved PARP. Simply, the p53 tumour suppressor aids the decision of a cell to undergo cell cycle arrest or the more definitive, apoptosis (Vousden and Prives, 2009). It is possible the removal of p53 from the cells in response to ActD treatment bypassed the ability to induce cell cycle arrest (Figure 3.8). Thus, cells underwent cell death. Whilst p53 is an important driver of apoptosis, many p53 independent cell death mechanisms exist in the cell (Galluzzi et al., 2018).

The double depletion of p53 and p52 led to earlier incidences, and higher abundance of, PARP cleavage in comparison with the single depletion of p52 (Figure 3.8C). This was particularly interesting as it could be predicted that depleting p53 alongside p52 would rescue the cell death phenotype. This assumption is based on p53 being known as the 'guardian of the genome' and regulating cellular death pathways. However, following the single p53 knockdown, the p53-depleted U2OS cells were still undergoing cellular death following ActD treatment, suggesting p53-independent cell death mechanisms. The double p52-p53 depletion demonstrated that the proteins do not oppose one another as the lack of both proteins enhances the cell death phenotype in response to drug treatment. Whilst it is entirely possible that these proteins are acting independently, the proteins could be working within the same pathway to co-ordinate cell survival in the context of ribosomal stress. It is known that p52 binds to the promoter regions of p53 target genes to regulate expression. This includes genes involved in the cell cycle; CDKN1A (encoding p21), PUMA, and GADD45α (Schumm et al., 2006). The dimer recruits different cofactors that either lead to the repression or activation of a gene (Rocha et al., 2003). This is evidence that p52 has been linked to the influence of the cell cycle in a p53 dependent manner. Perhaps, the loss of the two proteins causes cells to have impacted induction of cell cycle arrest pathways. Without

the ability to pause cellular proliferation and repair damage induced from cellular stress, cells would face increased events of DNA damage which ultimately leads to cell death.

When a double depletion of p52 and the ribosomal protein, RPL11 was performed, similar results were seen. Depleting the 5S RNP member simultaneously with p52 caused a more dramatic induction of PARP cleavage. Both the single p52 knockdown and the single RPL11 knockdown were sufficient in inducing an increase in PARP cleavage, however the double knockdown had an additive effect (Figure 3.9). The similarities in the p52/p53 double knockdown and the p52/RPL11 double knockdown are intriguing. Perhaps, knocking down p52 and RPL11 impair p53 activation following nucleolar stress. Thus, instead of a cell cycle arrest based response to the drug, the cells undergo cell death as they are unable to cope with the levels of cellular stress. Without p52 and RPL11 present to induce repair responses, cells undergo cell death, potentially through mitotic catastrophe, due to rising levels of DNA damage that is not able to be resolved prior to cellular division.

Chapter 4   Investigating the Interaction between RPL11 of the 5S RNP and the p52 NF-κB subunit

4.1. Introduction

4.1.1. Protein-protein interactions

Protein-protein interactions (PPIs) are a critical part of cellular biology. PPIs are required for many biological processes and when these interactions are disrupted they can contribute to disease progression. The knowledge base of the protein interactome is growing rapidly, thanks to a multitude of online databases, such as STRING and UniProt (Szklarczyk et al., 2020, Consortium, 2020). Proteins are highly concentrated in specific cellular domains facilitating these interactions. However, not all proteins that come into close proximity will interact since such interactions require these proteins to possess the appropriate PPI motifs. The nature of PPIs varies depending upon the purpose of the interaction. Some need to be transient, as the next stage in the pathway relies upon the disassembly of the oligomer; others are permanent, typically because the stability of each protein member relies upon the interaction (Nooren and Thornton, 2003a). Most cellular signalling pathways rely heavily upon transient and sequential interactions. A substantial example of PPIs that ultimately form a large protein complex, is ribosome biogenesis. The synthesis of ribosomes requires the assembly of a multitude of proteins with the synergistic action of many chaperones and accessory proteins (Thomson et al., 2013). The process utilises both transient and permanent PPIs. In both cases, the PPI interface is often hydrophobic and highly specific (Nooren and Thornton, 2003b).

A protein may only have one binding partner, or several possible binding partners, however the way in which they bind to these partners will occur through specific amino acid residues. Ultimately, whether a protein can contribute to a PPI or not will depend upon the unique amino acid sequence which folds to create the 3D structure (Valdar and Thornton, 2001). Numerous protein domains that mediate PPIs have been described. For example, the RING domain can, in addition to facilitating a protein's ubiquitin ligase function, also be responsible for PPIs. The domain allows E3 ligases to bind simultaneously to the substrate and enzyme (Chasapis and Spyroulias, 2009). Proteins that have the capability of binding to multiple proteins often involve a degree of competition within the overlapping binding sites.

This competition can be influenced by protein concentration, localisation or even post-translational modifications. Equally, proteins may have a higher affinity for one interactor in comparison with another. The higher affinity will be favoured as it will form a more stringent interaction (Nooren and Thornton, 2003b).

The affinity by which a protein binds to another is determined by the type and number of interactive forces made. It is rare that proteins form covalent bonds within PPI interfaces. Covalent bond formation would involve the creation of disulphide bonds which are very hard to break (Cao and Wang, 2022). Most PPIs form non-covalent bonds, such as hydrogen bonds, ionic bonds and van de Waals forces (Nooren and Thornton, 2003a). Therefore, each PPI will have a unique interface. Each participating residue from the proteins will contribute a different chemical property to the interaction. The binding affinity depends upon the different forces in the interaction, with some requiring more energy to reverse than others. Moreover, each PPI will be effected to a varying degree by different pH, ion concentration and chemical environment (Nooren and Thornton, 2003b). This is crucial to understanding a PPI and assessing the overall stringency.

The methodology to study and identify protein-protein interactions in the laboratory has evolved over time. From simpler techniques, such as yeast-two hybrid (Brückner et al., 2009), to novel and more complex, such as cryogenic electron microscopy (cryo-EM – discussed further in Chapter 5) (Shen, 2018). Two-hybrid screening involves the use of yeast to orchestrate a colour-changing interaction if a PPI occurs through the use of a reporter gene. This technique can be used in a high-throughput way to screen libraries of potential interactors (Brückner et al., 2009). High-throughput screening can also be performed using proteomic methods. Tandem mass purification, using a tag to isolate a protein of interest, followed by mass spectrometry, is a powerful tool to identify proteins interacting with the tagged target protein (Bouwmeester et al., 2004). The technique relies upon a co-immunoprecipitation (co-IP) experiment (Berggård et al., 2007). Co-IPs are used to capture protein-protein interactions in cell lysates. A tagged protein, for example with GFP, is captured using antibody-coated beads. This will also capture any proteins that are bound to the protein of interest. This is usually followed by western blotting analysis to visualise the interactions of interest. A co-IP alone is not a high-throughput way of determining a proteins interactome, but serves as a useful tool for confirming interactions, especially following a more high throughput proteomics approach (Campbell et al., 2021).

4.1.2. The importance of protein-protein interactions in cellular signalling pathways

Cellular signalling pathways are dependent on PPIs. These interactions are usually transient associations. Often, a signalling cascade depends on the disassociation of a complex. This can occur through degradation, or competition (Westermarck et al., 2013). For example, large protein complexes can form as part of a signalling pathway that disassemble once their role is carried out. The BRCA-1 associated genome surveillance complex consists of approximately a dozen different proteins. This complex functions to locate and signal the repair of damaged DNA. The complex assembles and disassembles in response to stimulus (Wang et al., 2000). An example of how this can be regulated for transient PPIs is by the addition of post translational modifications (PTMs). PTMs can affect protein folding, facilitating the removal of a binding site, and are known for modifying chemical properties. The use of certain PTMs can act as chemical markers to trigger subsequent cellular processes (Westermarck et al., 2013). For example, transient interactions occur between NF-κB inducing kinase (NIK) and p100 at the activation of the non-canonical NF-κB signalling pathway. NIK then phosphorylates p100. The phosphorylation serves as a marker for further modification by the kinase IKKα (Ling et al., 1998). Similarly, when ubiquitination occurs, cumulative effort from a group of proteins is required to form the ubiquitin chains (Liang et al., 2006). This involves the transient assembly of a protein complex. The very basis of enzymatic reactions is within the PPI. Without the specific fit, the reaction is unable to occur.

PPIs have been implicated in many diseases. When a pathogen infects a host cell, this can be facilitated by a PPI. In the case of COVID-19, the virus contacts the human angiotensin-converting enzyme 2, a membrane bound enzymatic receptor (Zhang et al., 2021). The COVID-19 spike protein interacts with the receptor, allowing the intake of the virus, infecting the host (Chang et al., 2021). The study of PPIs, therefore, is a useful tool in drug discovery. PPI-targeting drugs can function by blocking the binding interface, or causing a conformational change which disrupts the binding site. As PPIs are so specific, a small change in the conformation, or a single base change within the interface, can be sufficient to disrupt an interaction.

The protein interactome has been found to change in cancer cells. As cancer cells are evolving to evade apoptosis and continually proliferate, the cell requires the disruption of certain PPIs and the promotion of others (Gulfidan et al., 2020). In certain types of cancer, p53 activity is found to be suppressed even though the protein is still wild-type. This can be

due to the over expression of the E3 ubiquitin ligase, MDM2 (Azer, 2018). A small molecular inhibitor family, called nutlins, were synthesised in 2004 to inhibit the MDM2/p53 interaction. Nutlins allow wild type p53 to be stabilised and activated, promoting the onset of disrupted cellular processes, such as cell cycle arrest and apoptosis (Ghassemifar and Mendrysa, 2012). This has been shown to be the case in human medulloblastoma cells, which saw an increase in cell death following treatment with nutlin-3.

In summary, PPIs are the backbone of cellular signalling and crosstalk between cellular signalling pathways. It is critical to continue the research and gain understanding into these complex cellular signalling webs.

4.2. Results

4.2.1. Investigating the dependency of actinomycin D and 5-fluorouracil upon the 5S RNP

As discussed previously, chemotherapeutic drugs, 5-flurouracil (5FU) and actinomycin D (ActD) can stabilise p53 by causing nucleolar stress (Deisenroth and Zhang, 2010). It is known, however, that both drugs are capable of inducing other cellular effects and may not act in one specific manner. Therefore, it was important to determine whether 5FU and ActD function in a 5S RNP dependent manner in U2-OS cells.

To test this, cells were transfected with RPL5 targeting or RPL11 targeting siRNAs alongside a non-specific control (NS control). Following the knockdown, cells were treated with ActD or 5FU and harvested for protein analysis. Specifically, the stabilisation of p53 following drug treatment was monitored via western blotting.

It has been documented that the stabilisation of the protein components of the 5S RNP, RPL11 and RPL5, rely upon one another. This can be visualised in Figure 4.1A through the sustained decrease in protein abundance of both proteins when treated with either an RPL5 siRNA or an RPL11 siRNA compared to the NS control.

The multiple western blots were quantified to visualise the changes in p53 protein abundance in response to both drugs and siRNA treatment. ActD showed a marked decrease in p53 stabilisation following both RPL5 and RPL11 siRNA knockdown (Figure 4.1A). β-actin was used as the loading control. In the RPL knockdown lanes, the actin control was higher than in the control siRNA samples. Therefore, it is suggested more protein was loaded overall, contributing to the p53 levels appearing higher in the RPL lanes. Therefore, quantification was performed. The quantification demonstrated that cells depleted with

either of the ribosomal proteins show very little p53 stabilisation overall (Figure 4.1B). Thus, the mechanism by which ActD functions to activate p53 in U2-OS cells is heavily reliant upon the 5S RNP. On the other hand, 5FU treatment did not cause as significant of a defect in p53 stabilisation (Figure 4.1C). The control siRNA cells had an initial increase of p53 stabilisation after 6 hours of treatment, which decreased at 24 hours (Figure 4.1D). Following siRNA knockdown of either RPL11 or RPL5, the p53 stabilisation was limited following the use of 5FU. It must be noted that the siRNA knockdowns were not very efficient in the samples challenged with 5FU, perhaps leaving enough 5S RNP intact to carry out its role. Alternatively, the figure suggests that the 5S RNP has different roles in the response to 5FU, in comparison to ActD. Overall, it can be determined that ActD has a higher dependency upon the 5S RNP than 5FU across 24 hours, however further repeats are required to make the data conclusive.
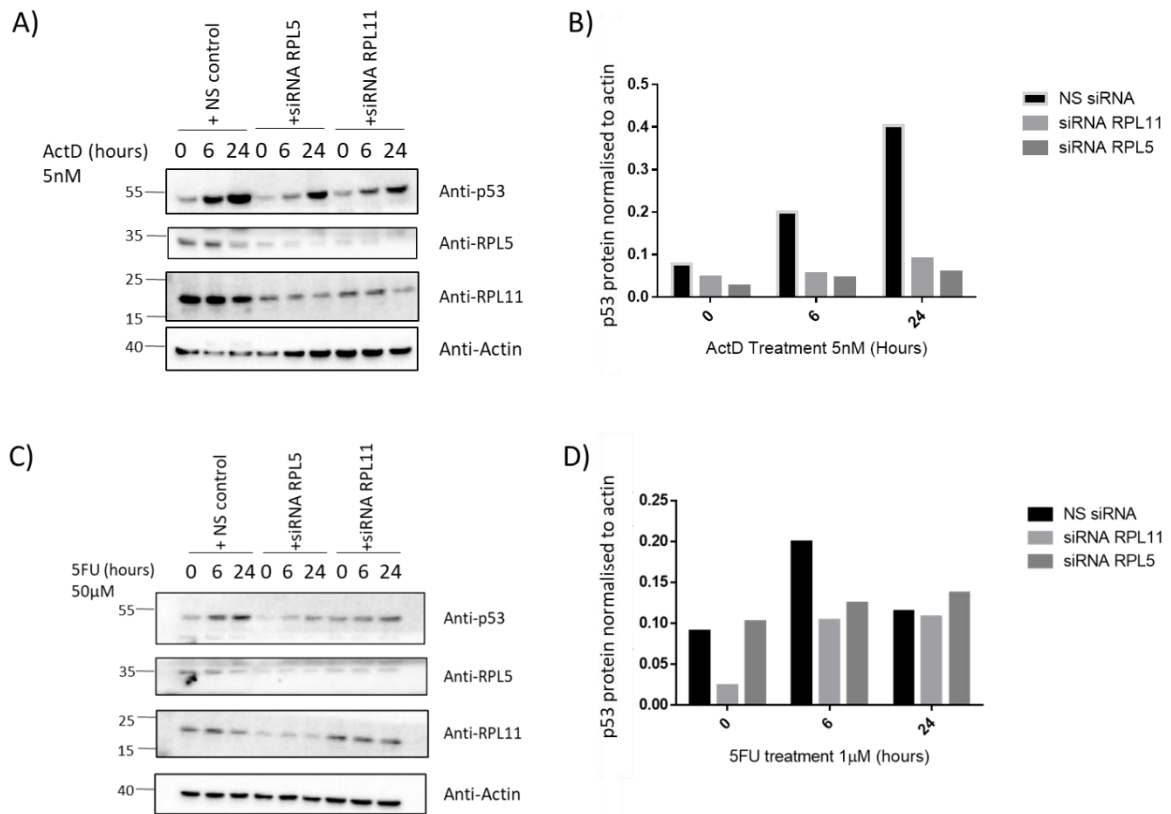
Figure 4.1 Actinomycin D functions in a 5S RNP dependent manner. The ribosomal proteins of the 5S RNP, RPL11 and RPL5, were depleting using siRNA mediated knockdown. A) Cells were treated with ActD for the times indicated in the figure and visualised via western blot. A BioRad ChemiDoc was used to develop the blots. The image represents a single repeat. B) The total number of p53 pixels was quantified using ImageLab. The graph was created using Prism 6. C) Cells were treated with 5-flurouracil (5FU) for the times indicated in the figure. The protein was visualised via western blot and developed using a BioRad ChemiDoc. The image represents a single repeat. D) The total number of p53 pixels across the 5FU time course was quantified using ImageLab. The graph was generated using Prism 6.

4.2.2. RPL11 and p52 are present in ribosome-free fractions basally and in response to actinomycin D treatment

Glycerol gradient centrifugation is a technique that is used to separate protein complexes based on their size and conformation. It can be used to determine whether proteins are present in fractions associated with the ribosome or fractions that are 'ribosome free' (Sloan et al., 2019). This technique can be used to investigate the localisation and possible re-localisation of proteins to protein complexes in response to drugs, such as ActD (Gibson, 2016).

U2-OS cells were harvested for glycerol gradient centrifugation to investigate which fractions RPL11 and p52/p100 were present in, both with and without ActD treatment. Fractions 1-8 are considered free from the ribosome and fractions 9-21 contain ribosomes (Gibson, 2016). Following a high-speed centrifugation step, fractions were separated and protein analysed via western blotting.

ActD is known to cause nucleolar stress, which in turn allows certain ribosomal proteins to be released from the nucleolus. In the case of RPL11, the protein translocates as part of the 5S RNP complex to bind to MDM2 and induce p53 activity. It can be seen that RPL11 was largely present in the ribosomal fractions regardless of drug treatment (Figure 4.2). In the untreated samples, a very small percentage of RPL11 was present in the free fractions (Figure 4.2A). This is unsurprising as a small amount of RPL11, as part of the 5S RNP, functions independently to the ribosome in cells in a 'normal' state. Following 16 hours of ActD treatment, RPL11 was found to accumulate in the free fractions (Figure 4.2B). In particular, high levels of RPL11 were found in fractions 1-3. Presumably, this build-up of RPL11 in the free fractions occurs to carry out the essential role in regulating the p53 response to nucleolar stress.

In untreated cells, the p52/p100 protein was found in the free fractions (Figure 4.2A). The NF-κB subunit was mainly located in fractions 2 and 3. In response to ActD treatment, p52/p100 seemed to shift fractions, becoming located in fractions 1-3 (Figure 4.2B). Following 16 hours of ActD exposure, the RPL11 content in fraction 1 was comparable to that of the 10% total (lane 'T'). This was a particularly intriguing observation as it appeared as if p52/p100 was shifting to accumulate in the same fractions as RPL11. Both proteins were present at high levels in the first three fractions, indicating they could be forming a complex following nucleolar stress.
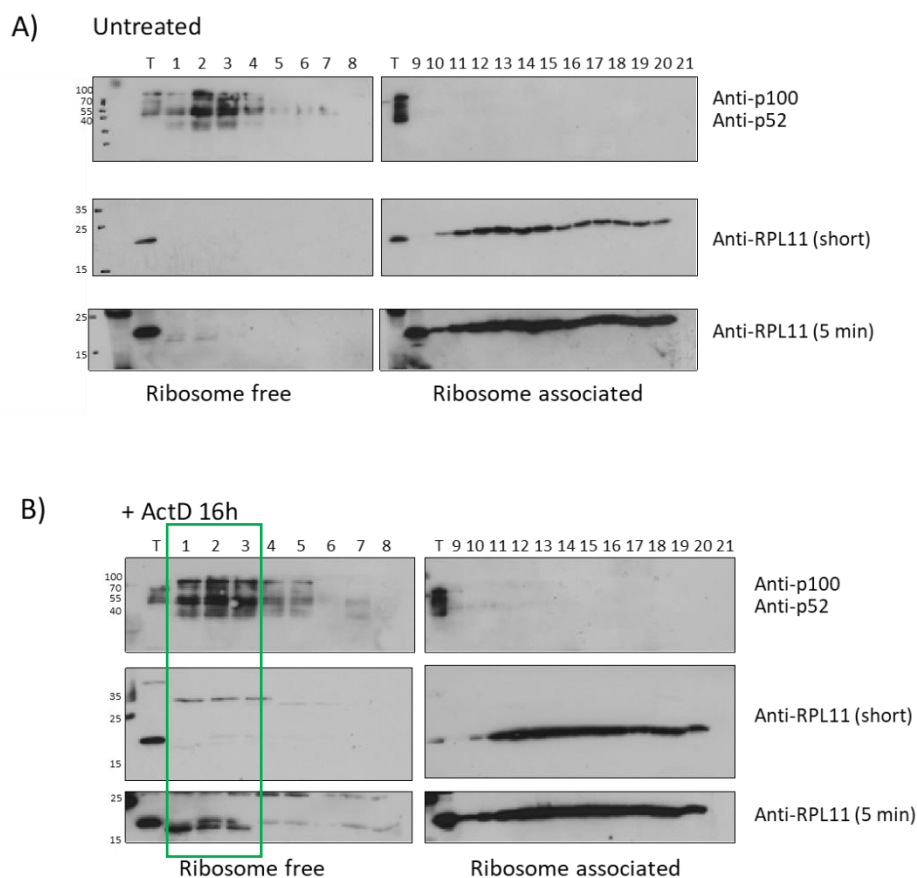
Figure 4.2 Glycerol gradient analysis of U2-OS cells both with and without ActD treatment. Following the treatment of U2-OS cells were harvested and centrifuged at a high speed through a glycerol gradient. The fractions were separated, with fractions 1-8 being 'ribosome free' and fractions 9-21 'ribosome associated'. T represents a 10% total taken from the whole cell lysate. Each set of samples was analysed via western blotting alongside a 10% input. Chemiluminiscence and film were used during developing. The image is representative of two independent repeats. 'Short' refers to a 30 second exposure onto film during developing. '5 min' refers to a 5 minute exposure during developing.

4.2.3. p52 and RPL11 directly interact

While Dr Iannetti had previously shown that p52 and RPL11 could associate in a pull down from cell extracts, it was not known if this interaction was direct. To address this question, recombinant p52 and RPL11 proteins were expressed as glutathione S transferase (GST) fusions in *Escherichia Coli.* The proteins were isolated using the GST tag, which was then removed from the GST-p52 protein using PreScission Protease. GST-RPL11 and recombinant p52 were then incubated together in the presence of glutathione beads to isolate any potential complexes.

To recombinantly express the GST-RPL11 protein, transformed bacteria were grown and induced using IPTG. Samples were taken for a total of 4 hours to measure the expression, which was visualised on a coommassie stained SDS PAGE gel (Figure 4.3A). It was clearly seen that the addition of IPTG led to the sufficient expression of GST-RPL11. It was necessary to remove the tag from the GST-p52 protein (provided by Dr Niall Kenneth) since the ability of GST to interact with itself would cause a false positive for the interaction. GST-p52 was incubated with PreScission Protease to cleave the GST tag from the recombinant p52 protein. Following this, the PreScission Protease, containing a GST tag, and the free GST was removed with glutathione-agarose beads. To confirm the successful removal of the tag was performed, the p52 protein was visualised through coommassie staining. The clean band at 52kDa, and the lack of band at around 25kDa confirms the removal of GST from the solution (Figure 4.3B).

To test the direct interaction between p52 and GST-RPL11, a pulldown assay was performed. Glutathione agarose beads were used to isolate potential GST-RPL11 and p52 complexes. The presence of the p52 protein alongside GST-RPL11 was visualised via western blotting in comparison to an input sample. It was attempted to capture the interaction between GST-RPL5 and p52. However, due to issues with the expression of GST-RPL5 from *E. Coli*, this was not possible.

The pulldown assay confirmed that p52 and RPL11 were able to interact (Figure 4.3C and 4.3D). Furthermore, GST-L11/p52 complexes were present even at high stringency, 500mM NaCl concentrations. Increasing salt concentrations are used to test the stringency of an interaction. Therefore, the interaction has a high enough affinity to withstand a high salt

concentration. It must be noted that bands were detected in the GST control lanes. This could be due to unspecific binding, which was able to be removed through increasing the salt concentration of the buffer.
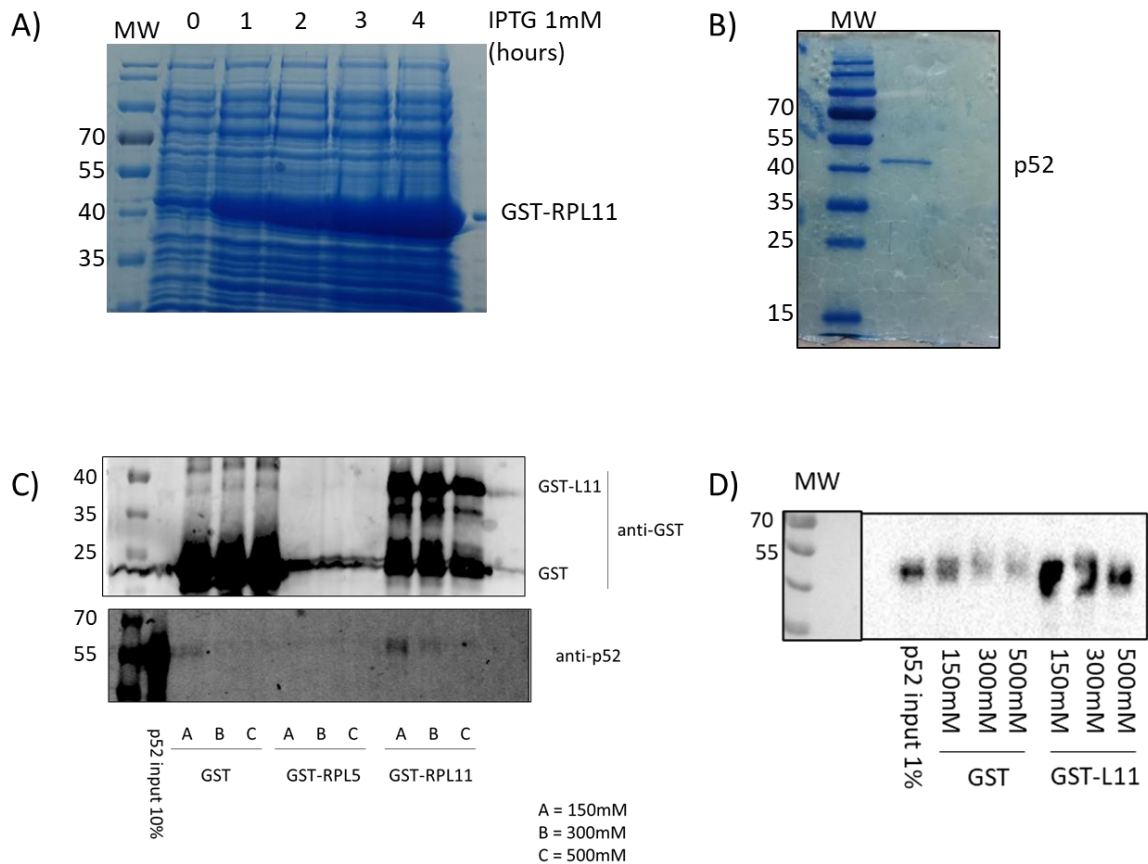
Figure 4.3 p52 and RPL11 directly interact. A) GST-RPL11 was recombinantly expressed using E. coli and IPTG induction. Samples were taken from the bacterial culture at various time points during the induction to monitor plasmid expression. The bacterial cells were pelleted and boiled in 5 X SDS loading buffer prior to performing coommassie staining on an SDS PAGE gel. B) GST-p52, supplied by Dr Niall Kenneth, was cleaved using PreScission Protease to remove the GST tag. Following the procedure, a coommassie stain was performed to ensure all GST was removed. C) A GST pulldown assay was performed to capture the association between GST-RPL11 and p52. Increasing concentrations of NaCl in the pulldown buffers were used to test the stringency of the interaction. A 10% input was taken during the assay. The final figure was produced through western blotting developed on a LiCor Oddessy. D) A GST pulldown assay was performed as described previously. A 1% input was taken. Varying concentrations of NaCl was used in the pulldown buffers. Western blotting analysis was developed using a BioRad ImageDoc.

4.2.4. GFP-p52 associates with members of the 5S RNP/MDM2/p53 pathway

The RPL11 protein is a member of the 5S RNP, which is known to bind to MDM2 in response to certain cellular stress to allow p53 activation (Sloan et al., 2013a). Dr Alessio Iannetti identified that GFP-p52 and RPL11 were capable of interacting via GFP-Trap co-immunoprecipitation (co-IP). The previous figure demonstrated that p52 and RPL11 can directly interact *in vitro*. The involvement of other members of the 5S RNP/MDM2/p53 pathway had not been investigated. U2-OS cells with stably transfected GFP-p52, or GFP control, were treated with various nucleolar stress-inducing agents and protein harvested. Following GFP-Trap pull down, potential complexes were analysed via western blotting, for proteins, and Northern blotting, for RNA.

The RPL11/ GFP-p52 interaction was seen in extracts from unstimulated cells and was found to be enhanced in response to all treatments tested (ActD, UV radiation, and 5FU) (Figure 4.4A and 4.4B). In theory, the stability of the RPL11 protein is dependent on the other members of the 5S RNP – RPL5 and the 5S rRNA (Bursać et al., 2012). However, while the interaction between RPL5 and GFP-p52 was seen in unstimulated cell extracts it appeared to decrease after treatment with ActD and UV radiation (Figure 4.4A). The association of RPL5/GFP-p52 was not consistently captured in repeat experiments and so only this example exists meaning it was not possible to confirm this observation. Other members of the 5S RNP/MDM2/p53 pathway were also analysed in these experiments. Interestingly, both MDM2 and p53 were found to interact with GFP-p52. However, unlike RPL11, these interactions were unaffected by the various treatments used (Figure 4.4A & B).

Northern blotting analysis is used to visualise RNA abundance in a sample and was used to investigate if the 5S rRNA was also associated with p52 (Figure 4.4C). GFP or GFP-p52 U2-OS cells were grown, treated and harvested before isolating potential p52-GFP/RNA complexes using the GFP-Trap system. Potential complexes were visualised using Northern blotting. When a GFP Trap pull down was performed using a whole cell lysate, GFP-p52 was seen to associate with the 5S rRNA. Since the radioactive RNA probe used was able to detect both the 5S rRNA and the 5.8S rRNA, this experiment also revealed that p52 also bound to the 5.8S rRNA. The 5.8S rRNA is part of the large ribosomal subunit and is not documented to accumulate in a ribosome-free state during ribosomal stress. Therefore, this suggests that p52 could be in association with the ribosome. This rRNA is always ribosome associated,

indicating a potential role for p52 in the ribosome. Next, a co-immunoprecipitation was performed following a glycerol gradient centrifugation. Here, the ribosome associated fractions were removed and the 'free' fractions were pooled together. When a GFP Trap pull down was performed using this protein extract the GFP-p52/5S rRNA association was again seen both basally and in response to ActD treatment (Figure 4.4C). This suggesting that the interaction takes place independently of the ribosome.

To summarise, the figure indicates the involvement of p52 in the ribosomal stress response in U2-OS cells through protein-protein and protein-RNA interactions. The figure implies p52 could have a role within ribosome biology due to the association between GFP-p52 and the 5.8S rRNA. However, the GFP-p52/5S rRNA association was captured both in the whole cell lysate, and in the ribosome-free fractions only. In the context of ribosomal stress, the figure shows that GFP-p52 can associate with most members of the 5S RNP/MDM2/p53 pathway. The association with RPL5 was inconsistent, therefore implying that the proteins do not directly associate. It can be speculated that as RPL11 and RPL5 are members of the same complex, the proteins remain in close proximity to one another during the ribosomal stress response. Thus, any association captured between GFP-p52 and RPL5 could be indirect via the strong association between p52 and RPL11. Overall, the figure demonstrates that p52 associates with the 5S RNP through direct interaction with RPL11 to play a role in the 5S RNP-mediated ribosomal stress response.
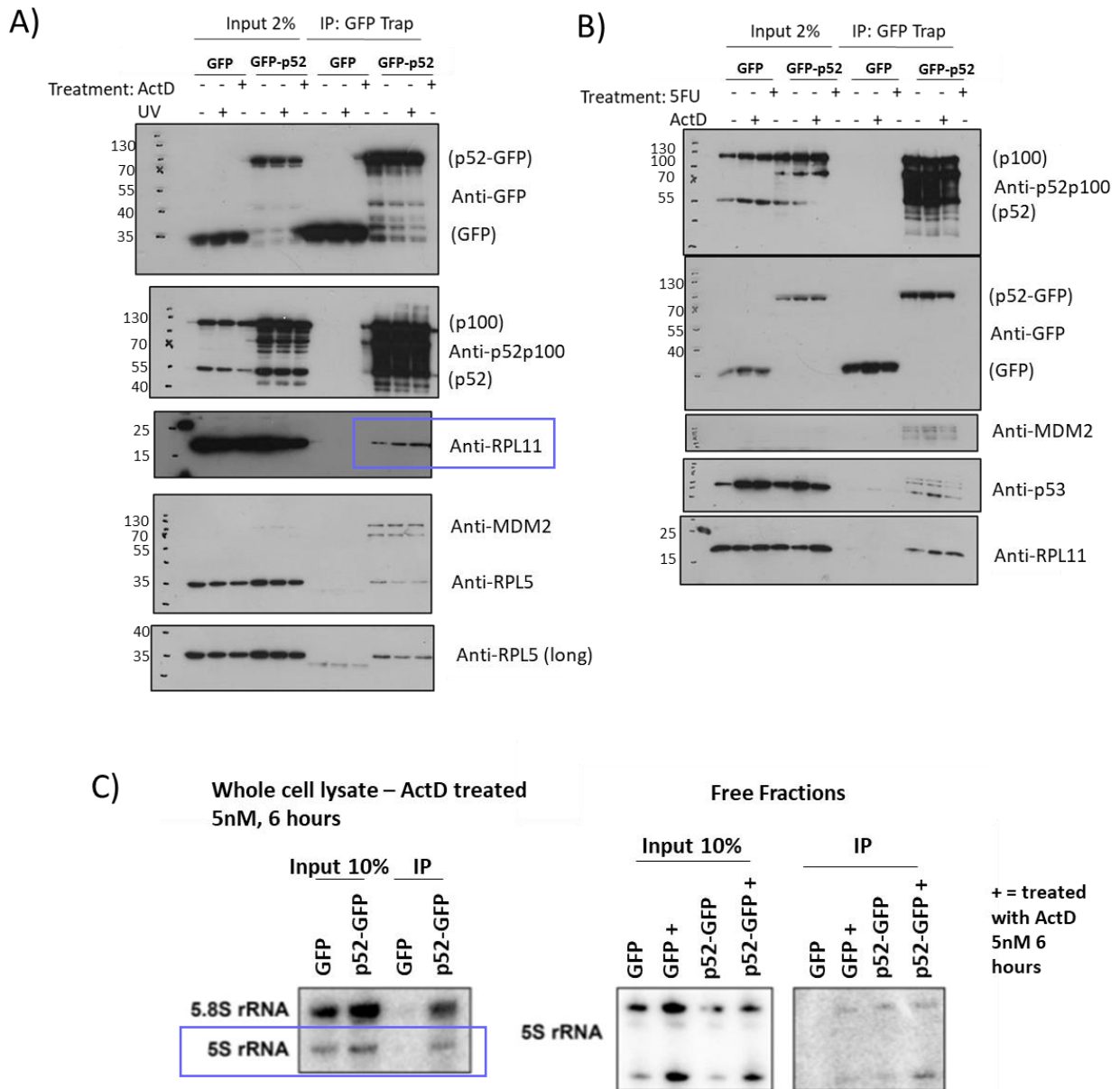
Figure 4.4 p52-GFP interacts with members of the 5S RNP/MDM2/p53 pathway with and without nucleolar stress induction. U2-OS cells stably expressing a GFP control plasmid or p52-GFP were challenged to nucleolar stress for 5 hours prior to cellular harvest. The cells were lysed prior to performing a GFP-Trap co-immunoprecipitation to monitor p52-GFP binding partners. A) Cells were treated with ActD (5nM) or UV 40KJmol^{-1}. Samples were analysed via western blotting developed using film. B) Cells were treated with ActD (5nM) or 5-flurouracil (50μM). Complexes were analysed via western blotting developed using film. The western blot images are representative of three independent repeats. C) Samples were treated with ActD and analysed via Northern blotting. Whole cell lysates are samples taken from whole harvested cells. Analysis of the free fractions was performed following a glycerol gradient and the subsequent removal of the ribosome-associated fractions. The Northern blotting images show the single repeat performed for the experiments. The lower band in the free fraction Northern blot is due to degradation of the RNA during the experiment.

130

4.2.5. Overexpression of p52 results in a lag in p53 stabilisation in response to nucleolar stress

Figure 4.4 proposed that p52 might interact with, potentially to regulate or be regulated by, the 5S RNP/MDM2/p53 pathway. It is predicted that if p52 can interact with RPL11, the interaction could impact the known interaction between RPL11 and MDM2 in response to stress. If that occurs, it could potentially impact the stabilisation of p53. Therefore, p53 stabilisation in cells possessing increased cellular p52 protein levels were studied. GFP and GFP-p52 stable U2-OS cell lines were grown, treated with ActD and harvested to create whole cell lysates. The protein content was studied via western blotting. Three independent repeats were quantified.

GFP-p52 over expression caused a delay in p53 stabilisation following ActD treatment (Figure 4.5A). This was seen more clearly in the shorter time course across 5 hours (Figure 4.5A) than when just 16 and 24 hour time points were investigated (Figure 4.5B). This indicates that any lag present at 5 hours begins to resolve past 16 hours of ActD and that the presence of GFP-p52 does not prevent p53 stabilisation overall, but rather delays the process.

Doxorubicin is a DNA damaging agent that works through inhibiting Topoisomerase II (Ghelli Luserna Di Rorà et al., 2021). The drug also activates p53 signalling but functions through the ATM dependent DNA damage response, rather than the nucleolar stress response. Using this stimulus, the presence of GFP-p52 in the U2-OS cells did not significantly impact the stabilisation of p53 in response to doxorubicin (Figure 4.5C). Therefore, the lag in p53 stabilisation observed in the GFP-p52 cell line could be specific to nucleolar stress.

A) 5 hour ActD time course
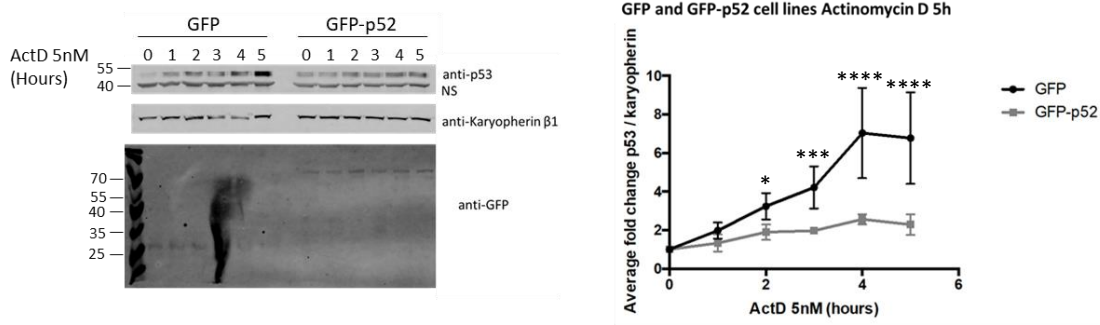
B) 24 hour ActD time course
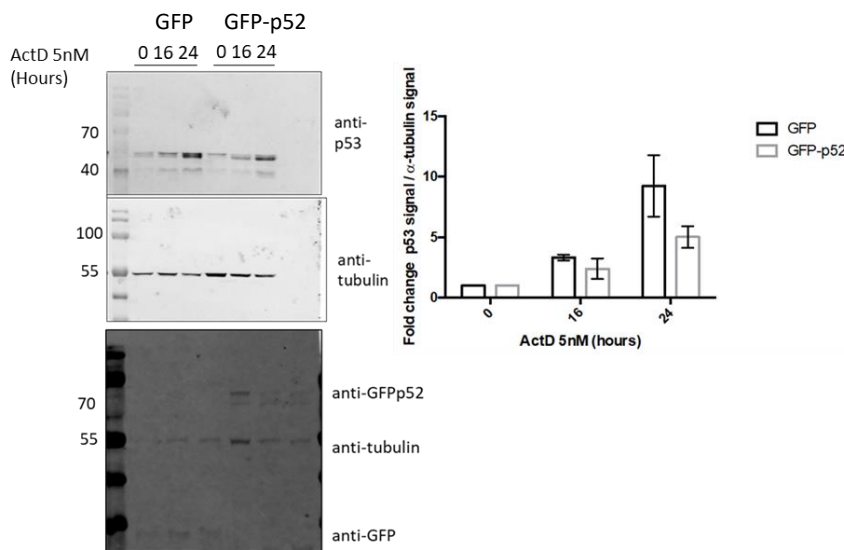
C) 5 hour doxorubicin time course
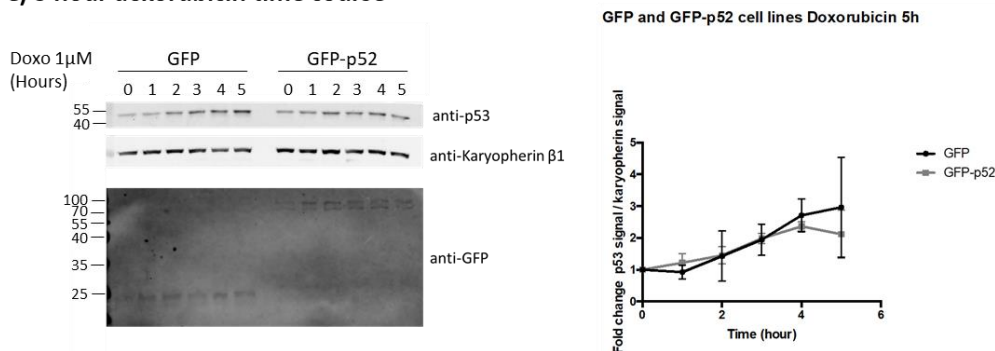
Figure 4.5 GFP-p52 expressing U2-OS cells show a lag in p53 stabilisation in response to actinomycin D but not doxorubicin. Cells were treated with either actinomycin D (ActD) or doxorubicin for times indicated prior to cell harvest. The p53 protein abundance was measured via western blotting. Independent repeats were quantified and the fold change plotted using Prism 6. The software was used to calculate statistical significance using a two-way ANOVA. A) 5 hour ActD time course. Image represents three independent repeats. B) 5 hour doxorubicin time course. Image represents three independent repeats. C) 24 hour ActD time course. Image represents three independent repeats.

4.2.6. Investigating the influence of MDM2 on the GFP-p52/RPL11 interaction

The data above indicated that increased levels of cellular p52 result in a delay in p53 stabilisation following ribosomal stress. A potential explanation for this would be if p52 was competing for binding to RPL11 with MDM2, thus preventing the disruption of the MDM2/RPL11 complex required for p53 activation. Therefore, the relationship between MDM2 and p52 in the context of RPL11 binding, was investigated further.

Initially, an ActD time course was performed in stably transfected GFP or GFP-p52 U2OS cells. The cells were transiently transfected with an inducible overexpression vector encoding a control FLAG tag, or FLAG-tagged MDM2. Following transient transfection, the tags were induced with tetracyclin 24 hours prior to harvest. An ActD time course was performed and whole cell lysates prepared. Any changes in the response to ActD treatment were monitored via western blotting.

The GFP U2-OS cells displayed comparable p53 stabilisation regardless of the presence of overexpressed MDM2 (Figure 4.6A). There were, however, impacts on downstream events. When MDM2 was overexpressed, an increase in PARP cleavage, indicative of an increase in apoptosis, was seen in response to ActD treatment. At the same time, a decrease in p21 protein levels was observed in the MDM2 expressing cells. This indicates the removal of a cell cycle arrest protein simultaneously to the increase of a cellular death marker. A similar result was seen in the GFP-p52 expressing cells, although here the increase in PARP cleavage and loss of p21 appeared to occur earlier. Therefore both results suggested that MDM2 overexpression resulted in an increase in cell death and the removal of a cell cycle arrest protein in cells responding to nucleolar stress.

No effect upon p53 protein was detected with MDM2 overexpression. Therefore, the increased cellular MDM2 presence is not capable of interfering with p53 stabilisation. MDM2, however, could be interfering with the interaction between p52 and RPL11. As p52 can regulate p53 dependent gene expression, interference from MDM2 could impact p53 target gene regulation. Alternatively, MDM2 interference could impact the ability of p52 to regulate its own target genes, such as anti-apoptotic genes, which could lead to the increased cell death suggested by Figure 4.6A. Therefore, it was important to assess the impact of MDM2 upon the p52/RPL11 interaction. (Figure 4.6B). GFP and GFP-p52 U2-OS cells were transiently transfected with inducible FLAG and FLAG-MDM2 plasmids. The tags were induced and an ActD time course performed. Whole cell lysates were prepared and

potential GFP or GFP-p52 protein complexes isolated by GFP-Trap co-IP. Protein complexes were visualised using western blotting. Interestingly, when MDM2 was overexpressed, there was a decrease in the level of the GFP/RPL11 interaction observed both with and without treatment. The result indicated that MDM2 was capable of outcompeting p52 for the binding of RPL11.
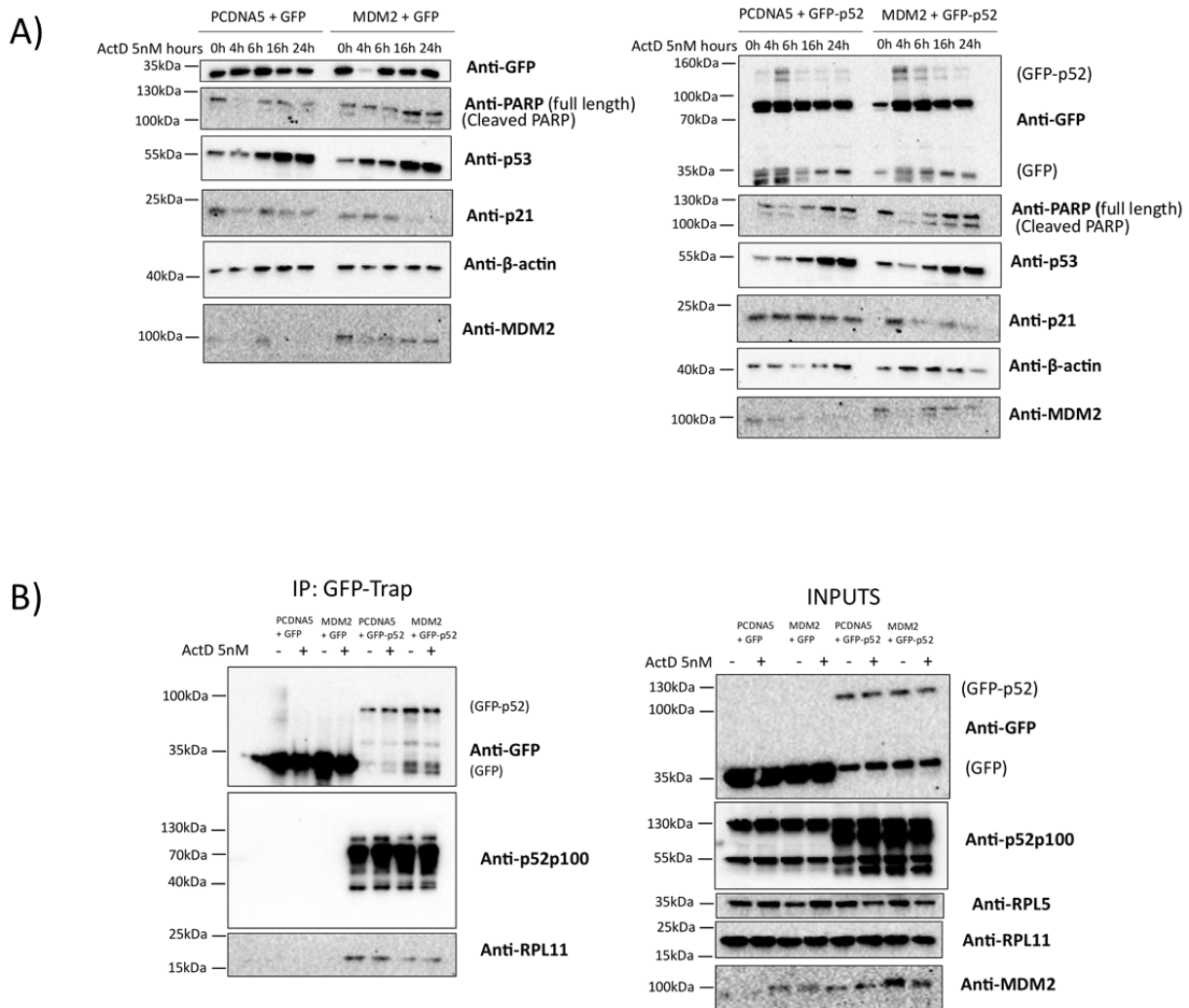
Figure 4.6 The influence of MDM2 on the p52-GFP/RPL11 interaction. These figures were provided by Kirsten Ramsay, a Masters of Research student under my direct supervision. A) GFP or p52-GFP expressing U2-OS cells were transfected with an inducible pcDNA5 control or pcDNA5-MDM2 expressing plasmid. Cells were treated to an ActD time course prior to protein harvest. Analysis was performed via western blotting and developed using a BioRad ImageDoc. The image represents two independent repeats. B) A co-immunoprecipitation performed in GFP or p52-GFP cells transfected with pcDNA5 or pcDNA5-MDM2. Cells were treated with ActD for 5 hours prior to harvest. Potential complexes were visualised via western blotting and developed using a BioRad ImageDoc. The image represents two independent repeats.

4.3. Discussion

4.3.1. p52 directly interacts with RPL11 and the interaction enhances in response to nucleolar stress

The work performed throughout this chapter followed on from work undertaken by Dr Alessio Iannetti. The co-immunoprecipitation data showing the enhancement of the RPL11/ GFP-p52 interaction following UV treatment confirms the result found by Dr Iannetti in a proteomics screen and co-IP. This study expanded the range of nucleolar stress treatment to drug treatments, ActD and 5FU (Figure 4.4). Furthermore, the proteins were found to directly interact *in vitro*. The most obvious hypothesis is that p52 interacts with the 5S RNP during the ribosomal stress response which also mediates the activation of p53. This NF-κB subunit is known for its ability to crosstalk with p53 and to modulate the p53 response in response to UV, a ribosomal stress inducer (Iordanov et al., 1998b, Rocha et al., 2003, Schumm et al., 2006). An association between p52 and the 5S rRNA was observed, it is suggested that this can occur free from the ribosome. It is known that the 5S RNP's role as a regulator of p53 signalling is mutually exclusive with its role in the ribosome.

The association of RPL5 and GFP-p52 was also observed and this appeared to decrease after the induction of nucleolar stress, in contrast to the result seen with RPL11 (Figure 4.4A). This interaction, however, was not consistently seen, suggesting this could be a transient, weak or indirect association. Interestingly, when Dr Iannetti performed the proteomics screen for GFP-p52 binding partners in U2-OS cells, RPL5 was not captured. Moreover, a screen involving tandem affinity purification followed by mass spectrometry confirmed RPL11 as a p52/p100 binding partner, but not RPL5 (Bouwmeester et al., 2004). Ribosomal proteins are known to be synthesised in a large excess and rapidly degraded, with the stability of the 5S RNP members dependent upon the formation of the complex. (Lam et al., 2007). So, in theory, any RPL5 observed should be in a complex with RPL11, especially during the response to stress. Despite this, the laboratory data produced in this chapter cannot confirm an association between RPL5 and p52 but can confirm an association between RPL11 and p52 which is enhanced by ribosomal stress. It is possible that a fraction of RPL11 might be stabilised in the absence of RPL5 through its interaction with p52.

Through co-IP analysis it was shown that GFP-p52 also associated with MDM2 and p53 (Figure 4.4A and 4.4B). This suggests that the interaction between p52 and RPL11 could be playing a role in the ribosomal stress response to regulate the p53 response. Chromatin immunoprecipitation analysis has shown RPL11 to bind to the promoter regions of p53 target genes, and that this presence is increased following nucleolar stress induction (Mahata et al., 2012). This suggests that RPL11 could be part of a 'super-complex' with MDM2 and p53. One hypothesis for the role behind the p52/RPL11 interaction is as a part of this super-complex which functions to regulate p53 stability and transcriptional activity following ribosomal stress.

4.3.2. Increased presence of cellular p52 causes a lag in nucleolar stress dependent p53 stabilisation

The data presented in Figure 4.5 demonstrates the relationship between p52 and p53 stabilisation during the response to nucleolar stress. The U2-OS cell line expressing stably transfected GFP-p52 displayed a lagged increase to cellular p53 levels at earlier time points (Figure 4.5A). This is indicative of a defective stabilisation process following nucleolar stress. It is intriguing that at longer time-points, 16 or 24 hours after treatment, the p53 protein abundance in the GFP-p52 cells and GFP control cell line are increasingly comparable (Figure 4.5B). Therefore, it is suggested that there is a 'catch up' element to this cellular process. Initially, the cells with increased cellular p52 levels have a slow p53 stabilisation but at some point between 5 and 16 hours after treatment, the presence of p53 protein increases. It would be interesting in future experiments to monitor the stabilisation between those time points to determine when this occurs. The relationship between the speed at which p53 is stabilised and the downstream signalling processes has been previously discussed. It has been shown that a slow p53 stabilisation will lead to cell cycle arrest whilst a faster increase in p53 protein is followed by apoptosis (Hafner et al., 2019). Thus, it can be suggested that p52 is contributing to, or facilitating the favouring of, cell cycle arrest in this context. p52 could potentially play a cell survival role in response to ActD-induced nucleolar stress. This could be occurring in Figure 4.5 through increasing the levels of cellular p52 which forces more p52/RPL11 interactions to occur, slowing the p53 response. However, at prolonged periods of drug treatment, p53 protein levels start increase to normal levels.

The use of the drug, doxorubicin, did not show the safe effect on p53 stabilisation in the GFP-p52 cells. Doxorubicin is a chemotherapeutic drug that induces DNA damage (Müller et

al., 1997). The DNA damage response (DDR) leads to p53 stabilisation through specific pathways dependent upon the type of damage sensed (Lindström et al., 2022). Doxorubicin intercalates with DNA causing breakages. Furthermore, the drug inhibits topoisomerase II, the enzyme responsible for unwinding DNA during transcription (Müller et al., 1997). Thus, DNA and RNA synthesis is impaired. Breakages in DNA are located and p53 activated in order to arrest the cell cycle and repair the damage, or in extreme cases initiate apoptosis. For example, it has been shown that ALL cells respond to doxorubicin through the ATR/Chk1 pathway leading to G2/M cell cycle arrest (Ghelli Luserna Di Rorà et al., 2021). However, doxorubicin is known to function primarily through ATM in response to double stranded DNA breaks. ATM then phosphorylates p53, activating transcription factor functions (Kurz et al., 2004). In this experiment, it can be seen that between 0 and 5 hours of Doxorubicin treatment there were insignificant differences between the p53 response in the GFP-p52 and GFP control cell lines (Figure 4.5C). Presumably, this is due to the mechanism by which p53 is activated in response to doxorubicin versus actinomycin D, with the former not requiring the 5S RNP complex. Whilst more drugs need to be tested to prove this hypothesis, it is suggested that the lag in p53 stabilisation brought on by increased cellular p52, is specific to the 5S RNP mediated ribosomal stress response.

4.3.3. Are MDM2 and p52 competing for RPL11 binding?

The co-IP experiment performed in Figure 4.6B was aimed to test the impact MDM2 expression could have upon GFP-p52/RPL11 complexes. The tetracycline induced MDM2 overexpression was able to decrease the abundance of the GFP-p52/RPL11 complex. Interestingly, in the ActD time course performed in the GFP and GFP-p52 cells, the overexpression of MDM2 caused increased levels of PARP cleavage and a decrease in the cell cycle arrest marker, p21 (Figure 4.6A). Not only does this suggest MDM2 could outcompete p52 for RPL11 binding, but also that this competition could contribute to cellular death. The increase in PARP cleavage, a marker of cell death, was not accompanied by an increase to p53 stability. As discussed in the above section, faster p53 stabilisation is associated with an apoptotic outcome.

RPL11 appears to favour its interaction with MDM2 when both GFP-p52 and FLAG-MDM2 are expressed (Figure 4.6B). The introduction of overexpressed MDM2 induced a shift of RPL11 from GFP-p52/RPL11 complexes to MDM2/RPL11 complexes. An MDM2 mutant has been created to study the impact of the loss of MDM2/RPL11 interaction. The MDM2-C305F

mutates the critical binding site between the proteins. Interestingly, it has been shown that mice expressing this mutant MDM2 protein suffered to a greater extent from c-Myc driven lymphomas (Macias et al., 2010). This is likely due to the loss of 5S RNP-mediated p53 stabilisation. The time course data presented in Figure 4.6A suggests stabilisation of p53 that is driven by MDM2/RPL11 leads to a form of cell death in U2-OS cells. Thus the loss of this interaction would contribute to cell survival, allowing cancer cells to divide and spread, as seen in the MDM2-C305F murine phenotype. Furthermore, the C305F mutant has been shown to lead to fat accumulation in murine livers (Liu et al., 2014). The 5S RNP is known to mediate liver homeostasis and fat accumulation is linked to fatty liver disease and hepatocellular carcinoma (Pelava et al., 2016). It would be interesting to investigate whether the p52/RPL11 interaction is present at higher levels in cells expressing MDM2-C305F. This would further confirm that p52 and MDM2 binding are mutually exclusive. Another important follow up experiment would involve performing a co-immunoprecipitation in a non-cancerous cell line. It could be hypothesised that cancer cells have developed the p52/RPL11 interaction in order to evade apoptosis and encourage cell cycle arrest or cellular survival following ribosomal stress. As only cancer cell lines have been used in these experiments, a non-cancerous cell line, such as primary human fibroblasts, would serve as a useful control cell line to determine whether the p52/RPL11 interaction is specifically seen in cancer models. If it was not possible to capture the interaction in the non-cancerous cell line, it would suggest that the cancer cells had developed the crosstalk between p52 and the 5S RNP to aid cancer progression.

Chapter 5   Mapping the RPL11 and p52 Interaction Using *In Silico* Modelling

5.1. Introduction

5.1.1.   In silico in the context of protein-protein interactions

The study of protein-protein interactions (PPIs) has become increasingly important, particularly in the field of drug discovery (Macalino et al., 2018). Historically, biochemists have studied PPIs of interest using recombinantly expressed proteins and molecular cloning (Perkins et al., 1994). For example, to map regions of partner proteins that are critical to a PPI, scientists can create a series of truncated forms of their protein. Once the critical region has been removed, the PPI will not be able to be captured (Murray and Gellman, 2007). This can be furthered by looking into the critical region to locate single residues that can be mutated to disrupt the interaction (Kam-Morgan et al., 1993). This is useful to researchers to allow the study of the loss of that PPI and the impact on downstream processes. Given the rapidly increasing knowledge that the loss or aberrant PPIs significantly contribute to disease, this is an increasingly important field (Macalino et al., 2018). There are, however, limitations to this style of wet-lab experimentation. Recombinant protein studies can be time consuming and require optimisation. In order to perform these techniques, the proteins expressed in bacteria or yeast need to be soluble and non-toxic to the host (Walls and Loughran, 2011). Whilst the full-length protein may be soluble and tolerable, the truncated or mutated forms may not.

The focus within the study of PPIs has shifted to X-ray crystallography, NMR and cryogenic-electron microscopy (cryo-EM) (Siebenmorgen and Zacharias, 2020). X-ray crystallography relies on the development and study of crystallised proteins. Therefore, is unable to account for protein dynamics. On the other hand, NMR is capable of capturing dynamics to a high resolution in smaller proteins but is not suitable for larger proteins. In 2017, the Nobel prize for Chemistry was awarded to scientists that contributed to the development of cryo-EM (Shen, 2018). This powerful type of microscopy allows scientists to see the structure of biomolecules, such as proteins and therefore their interactions. This technique, however, is currently difficult, expensive and therefore inaccessible to many researchers (Fernandez-Leiro and Scheres, 2016).

In recent years, computational power, database availability and deep-learning algorithms have aided the *in silico* study of PPIs (Macalino et al., 2018). These techniques combine

statistics, physics and biochemistry to predict protein structure, residues within a structure that contribute to PPIs and even the prediction of protein complexes. Furthermore, supercomputers hold the ability to simulate protein dynamics (Childers and Daggett, 2017).

Due to the COVID-19 pandemic, and the nationally imposed lockdown, a lot of researchers were forced to take a more bioinformatical approach. In the context of this project, it was not possible to map the critical binding regions of RPL11 and p52 in the wet-laboratory. Therefore, *in silico* modelling was employed.

5.1.2. The basis of interface prediction

The interfaces of protein-protein interactions involve large regions of contact between each contributing protein. These are often hydrophobic (Bogan and Thorn, 1998). Experimental analysis involving the mutagenesis of single residues to alanine has allowed the study of an individual side chain's contribution to the binding free energy of an interface (Wells, 1991, Clackson and Wells, 1995). These clusters of structurally conserved regions of amino acids mostly involve tryptophan, isoleucine, arginine, and tyrosine. These clusters are referred to as 'hot spots'(de Vries and Bonvin, 2011). Hot spots are usually in proximity to one another; however, they can be distanced whilst continuing to work together. They are believed to be major contributors to stability and affinity of protein-protein interactions (Macalino et al., 2018). It is important to note that hot spots are not always specific with some employed for stability and others for specificity (DeLano, 2002). The growing nature of this field has enabled the creation of databases that hold information regarding the contribution of amino acids, and specific sequences of amino acids, to interfaces (Macalino et al., 2018). Furthermore, the information stored has been used in large-scale statistical analysis contributing to the development of computer models. These algorithms combine the aforementioned databases with rapidly growing data from 3D structures and sequences of proteins. Together, these serve to predict the residue-specific location of likely PPI hot spots within a given protein (Murakami and Mizuguchi, 2010, Zhang et al., 2011, de Vries and Bonvin, 2011). These software enable researchers to input solved crystal structures (de Vries and Bonvin, 2011) or the amino acid sequence (Murakami and Mizuguchi, 2010) to predict the location of interface-contributing, or 'active', residues in their protein of interest. The software takes into consideration specific properties of each residue that generally combine biophysics e.g. the hydrophobicity of the residue, biochemistry e.g. secondary structure elements and surface accessibility, with the evolutionary conservation of the residue

(Macalino et al., 2018). The growth of this field, and of computational power, has given rise to many interface prediction software that can be used to strengthen further studies, such as site directed mutagenesis or molecular docking.

5.1.3. The basis of molecular docking

Scientists have relied upon X-ray crystallography and nuclear magnetic resonance (NMR) experiments to study the molecular basis of biomolecular complexes (Sunny and Jayaraj, 2022). In more recent years, cryogenic electron microscopy (cryo-EM) has become increasingly popular allowing larger and more complex protein complexes to be studied to an extraordinary degree of accuracy (Bai et al., 2015). Whilst these approaches have provided vital information within the research of PPIs, this style of experimentation is susceptible to problems when studying protein complexes. For example, ensuring the environment that the protein complex is stored in maintains the structural integrity of the complex as a whole. Furthermore, the structures of complexes solved as a result of these techniques often have missing elements or utilise shorter forms of the proteins (Zheng et al., 2015). This could be due to the reliance on PPIs to form in a specific environment. Hence, experimentation of this nature has the potential to result in misleading data.

Molecular docking software allow researchers to predict the structure of protein complexes by inputting structural co-ordinates of individual proteins via protein data bank (PDB) files (Sunny and Jayaraj, 2022). These files contain the 3D co-ordinates that encode the crystal structures of proteins (Sussman et al., 1998). Typically, the larger protein submitted will be assigned as the receptor protein, and the smaller assigned as the ligand (Macalino et al., 2018). The algorithms have evolved from being bulky, download-only software to being user-friendly webservers. Some software is even powerful enough to allow for some conformational changes that occur during PPIs, for example amino acid rotations (Zacharias, 2010). The software predicts complexes by trialling all possible conformations before arriving at the most energetically favourable. To ensure the growth of this field, the Critical Assessment of Predicted Interactions (CAPRI) experiment occurs and in recent years the High Ambiguity Driven biomolecular Docking (HADDOCK) software has often been identified as a leader in the field (Lensink and Wodak, 2013, de Vries et al., 2010). CAPRI was started in 2000 and makes a head-to-head comparison of the protein docking software during a blind prediction of the structure of a protein complex. Whilst a lot of software provide an *ab initio* approach, meaning the prediction relies on structural coordinates alone followed by using

experimental information to filter results, HADDOCK utilises data-driven docking (de Vries et al., 2010, van Zundert et al., 2016). This involves experimental information being used to drive the docking run as well as filtering the predicted conformations. Many of the readily available docking software are rigid-body techniques (Macalino et al., 2018). These work under the assumption that the protein co-ordinates are unchanged through the formation of the protein complex. Hence, the major limitation that molecular docking software still faces, is the dynamic nature of proteins, especially upon the formation of a protein complex (Harmalkar and Gray, 2021). The software is unable to account for conformational changes that occur when a protein is in a bound state. For example, transcription factors are known to undergo a conformational change when bound to DNA (Sauer et al., 2008). In order to model this, an N8 supercompter would need to be utilised (Childers and Daggett, 2017).

5.1.4. ΔG in the context of protein-protein interactions

The binding free energy change (ΔG) of a PPI offers a numerical value relating to the stringency of an interaction. The more negative a ΔG value, the more stringent and stable the interaction. The calculation of this constant is related to structure-based parameters, such as buried surface area (the size of the interface), number of hotspots and number of hydrogen bonds (Vangone and Bonvin, 2017).

Techniques such as surface plasmon resonance, isothermal titration calorimetry and fluorescence spectroscopy are used to study thermodynamics and kinetics of PPIs (McDonnell, 2001, Di Trani et al., 2018, Eftink, 2000). Comparatively, computational algorithms have been developed to predict the binding affinity, ΔG, of protein complexes which utilise the three-dimensional structure (Vangone and Bonvin, 2017). Like interface prediction and molecular docking software, the prediction of the ΔG of a PPI relies on the vast array of data generated via wet-lab experimentation organised into databases. The prediction algorithm is capable of pooling together the known information and use statistical analysis to predict the ΔG of a given PPI.

5.1.5. Limitations

One of the most widely discussed limitations regarding *in silico* protein-protein modelling surrounds the difficulty for molecular docking software to account for the significant conformational changes that can occur when proteins bind to partners (Kowalsman and Eisenstein, 2006, Zacharias, 2010, Harmalkar and Gray, 2021). For example, at the initiation of apoptosis, pro-apoptotic members of the Bcl2 family of proteins bind their anti-apoptotic

partners (Hinds et al., 2007). One of these pro-apoptotic proteins, Bim, has been found to be highly unstructured in the unbound state. The initiation of apoptosis, and the subsequent binding to a pro-survival partner protein, causes a localised conformational change to Bim. It was found through NMR analysis that the unstructured Bim forms an α-helical structure that contacts the hydrophobic groove of Bcl-xL (Hinds et al., 2007). If this study had been performed using molecular docking, it would not have been possible to account for such dramatic molecular dynamics. Another example involves the RelA/p50 heterodimer in the context of DNA binding as well as upon binding of the NF-κB inhibitory protein, IκBα (Ramsey et al., 2017). Distinct conformational changes occur through this process termed, molecular stripping. IκBα can bind to NF-κB heterodimer, RelA/p50, in the DNA-bound state (Jacobs and Harrison, 1998). When NF-κB dimers bind to DNA, the two dimers 'clamp' around the DNA via DNA binding domain regions that surround the target gene (Chen et al., 1998). When bound to IκB, however, a 'twist' occurs in the N terminus of the protein associated with an opening of the DNA binding region of the dimer (Ramsey et al., 2017). Therefore, in this conformation NF-κB is unable to bind to DNA and the dimer releases from the target gene. Interestingly, IκBα undergoes a conformational change upon binding to NF-κB dimers (Truhlar et al., 2008). The protein consists of ankyrin repeat domains. It has been documented that the 5th and 6th domains fold when bound to a dimer. These cases of conformational change demonstrate the importance of allowing for structural changes in the study of protein-protein interactions (Zacharias, 2010).

5.1.6. Current uses, advancement and potential

In silico modelling is becoming an increasingly important technique in the study of protein biology. With the rapidly developing nature of computational approaches, this type of research could provide vital insight into health, disease and drug discovery. Computer modelling of this nature is used in a wide range of scientific research, from nutrition to bacteriology (Basu et al., 2022, Rivera del Rio et al., 2022). A recent publication details the use of *in silico* modelling in the advancement of COVID-19 research (Tragni et al., 2022). The viral infection relies upon binding between the spike protein from the virus and the ACE2 receptor on the host cell. As the pandemic continued to spread, the virus mutated to form variants of the spike protein (Zhang et al., 2021). The study performed by Tragni et al predicted the impact these variants would have upon ACE2 binding (Tragni et al., 2022). The

use of computation analysis in this context could help to speed wet-laboratory research up preventing lost time, resources and much fewer financial implications.

A major addition to the field of computational structural biology, was the development of DeepMind's programme, AlphaFold (Jumper et al., 2021). The software uses a powerful deep learning algorithm that can predict the 3D structure of proteins to the highest degree of accuracy to date. This is particularly useful in the prediction of protein structure where little to no information of the given protein is available. Upon blind comparison to other protein folding prediction software during the CAPRI experiment, AlphaFold predicted an unknown protein structure to a significantly higher degree of accuracy (Yin et al., 2022). Since development, AlphaFold has been used to predict the structure of at least 100,000 proteins which have been released for public use (Jumper et al., 2021). This provides a useful tool to many biologists in need of studying proteins where the structure has not yet been solved. Additionally, this aids the study of proteins for which the structure is only partly solved.

Overall, *in silico* modelling has the potential to save researchers valuable time, costs and labor which could be channelled elsewhere.

5.1.7. Analysing the solved p52 structure

Since the structure of a p52 homodimer bound to DNA was solved at a 2.1Å resolution in 1997, further structures of the homodimer in the DNA bound form have been solved (Cramer et al., 1997). For example, the homodimer bound to variations of the P-Selectin κB fragments (PDB ID: 7VUP, 7VUQ, 7W7L, 7CLI). The solved structure of p52 is lacking 36 amino acids from the N terminus and 127 amino acids from the C terminus (Cramer et al., 1997). Using information published by Cramer *et al*, the structure of a solved p52 monomer was colour coded to highlight important domains within the protein (Figure 5.1). The p52 subunit is unique as the Rel Homology Domain is split into two sections joined by a flexible linker region, something not seen with the other NF- κB subunits (Cramer et al., 1997, Ghosh et al., 1995). The C-terminal domain, coloured in green, is responsible for dimerisation (Figure 5.1). The N-terminal domain of the p52 monomer, coloured in pink, is predicted to influence DNA binding capacities of the protein (Cramer et al., 1997). Finally, the helix-loop-helix, coloured in light blue, is the insert region. There is little sequence similarity between

insert regions of p50 and p52, however the alpha-helical structure is conserved (Cramer et al., 1997, Ghosh et al., 1995). It is hypothesised that the insert region is an easily accessible surface for protein-protein interactions with other DNA binding proteins.
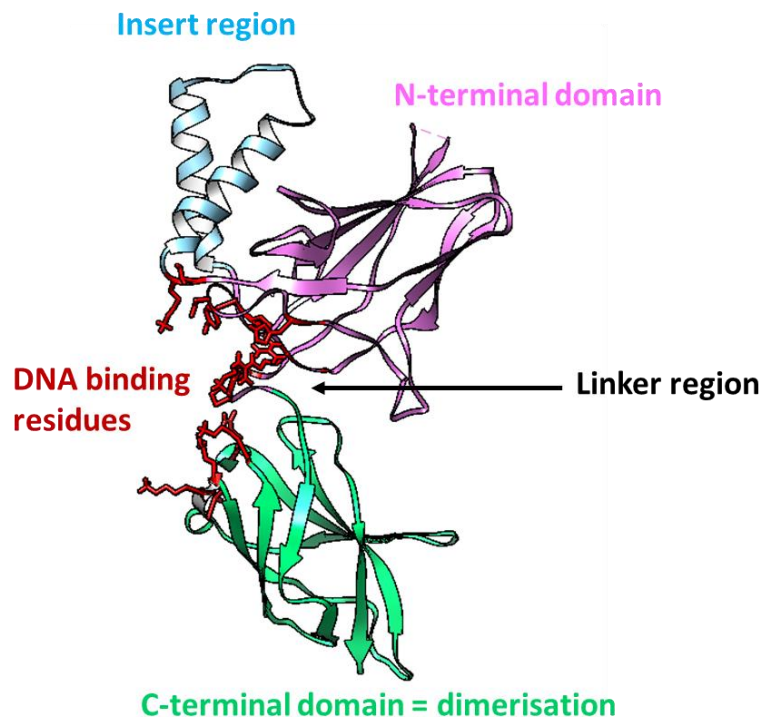
Figure 5.1 The annotated crystal structure of p52. Domains, DNA binding residues and regions of the protein were colour coded according to Cramer *et al*, published in 1997.

5.2. Results

5.2.1. Prediction of regions within RPL11 and p52 actively contributing to protein-protein interactions

The initial stage of this investigation was to predict residues within RPL11 and p52 that are likely to contribute to protein-protein interactions (PPIs). This was achieved by mapping the putative interaction interfaces using interface prediction software. To improve the stringency of the prediction, a panel of software (detailed in Figure 5.2) was used to return 'active' residues, also known as hotspots. It is important to note that residues returned by the software are relative to a protein's entire interactome and not just to the PPI of interest.

Depending on whether the software is a structure-based or sequence-based predictor, the PDB structure or FASTA sequence was uploaded to the software. Residues predicted to contribute to a PPI through the program were given a score of one. Cumulative scores from the panel of software were plotted against the residue number to demonstrate regions of high likelihood of involvement in PPIs. The scores were colour coded onto the crystal structures of the proteins to visualise which secondary structure elements were predicted to be the most interactive.

The analysis of p52 is represented in Figure 5.2A and 5.2B. From the scores alone, the highest peak, relating to the most likely active residue involved in PPIs, can be seen in the region surrounding residue 247. This residue was returned as a hit by five separate software. When the score is translated across to the crystal structure, it can be seen that this residue is within the dimerisation domain in the C-terminal region of the protein. This corresponds to the section coloured green in Figure 5.2A. There are two peaks of hotspots within the dimerisation domain (c, purple arrows, Figure 5.2A). This is unsurprising as NF-κB is always part of a dimer thus the region needs to be very interactive. There are two other distinct areas of interactivity: at the centre of the protein structure (b, blue arrows, Figure 5.2A) and on what will be referred to as the 'shoulder' of the protein (a, green arrows, Figure 5.2A). Both of these regions correspond to the N-terminal domain of the protein, coloured pink in Figure 5.1. Region b identified by the interface prediction, and signified by the blue box in the figure, is within the region that contacts DNA represented by the red residues in Figure 5.1.

147

RPL11 also shows 3 distinct areas that show a high probability for interface inclusion (Figure 5.2C and 5.2D). These are present at either side of the β-pleated sheet that forms a cleft (a, green arrows, and b, blue arrow). Interestingly, the cleft is the area of RPL11 that binds to the ribosome and to MDM2. The third is present on the long loop at the top of the structure (c, purple arrow). This loop is the region of RPL11 that embeds itself into the 5S RNP. All of the peaks are at the same height having received a score of three. This suggests that all three regions of the protein are equally interactive.
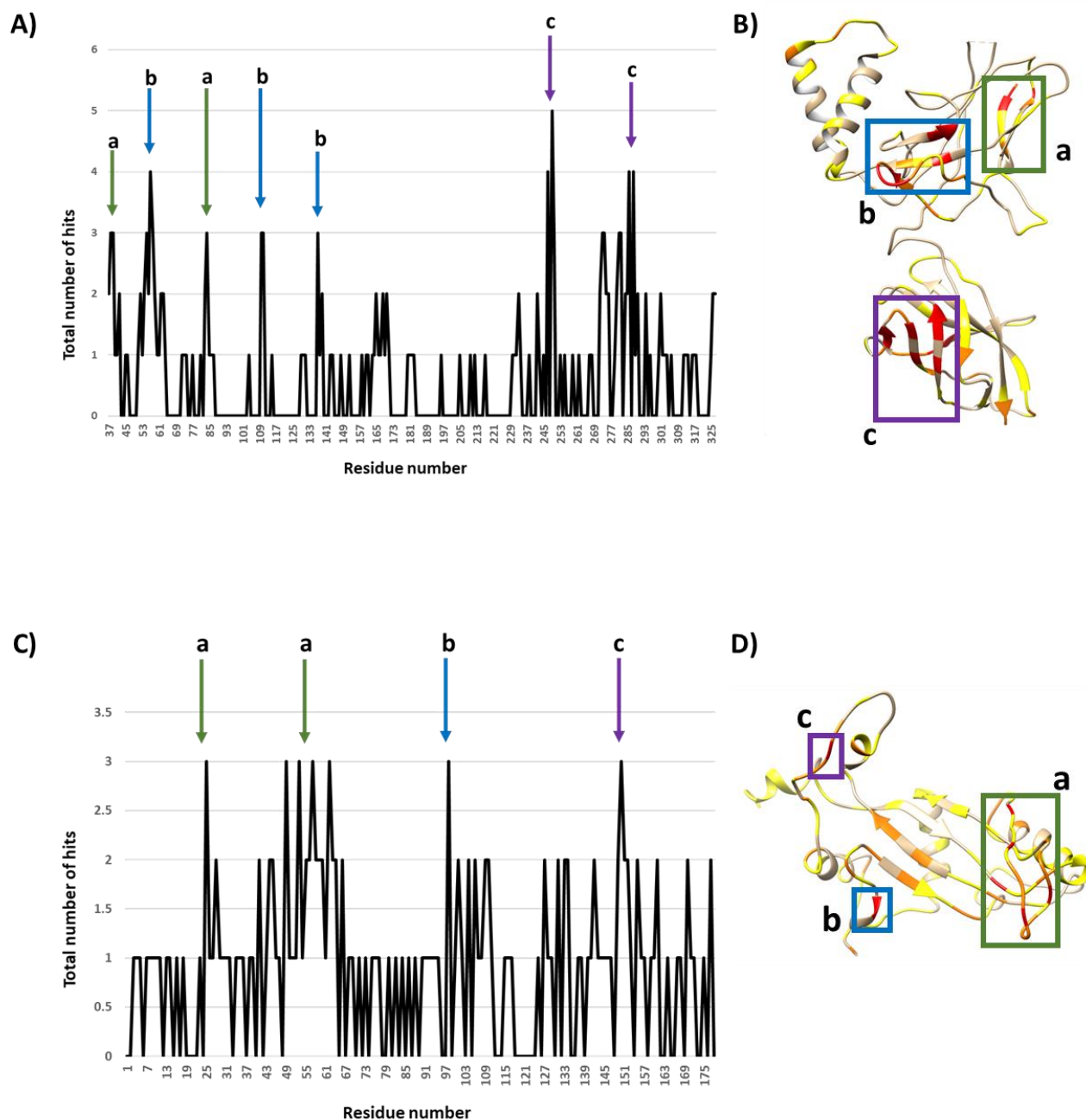
Figure 5.2 The predicted binding interfaces of p52 and RPL11. The FASTA sequence or protein structure coordinates (in PDB format) were uploaded to sequence and structural protein-protein interface prediction software to generate a map of interface hotspots. Residues were given a score based on results returned from the combination of software used and cumulative scores plotted on a graph using Microsoft Excel. The number of hits were mapped onto the crystal structures (1 hit = yellow, 2 hits = orange, 3+ hits = red). A) The graph representative of the number of hits per residue of p52. B) The structure of p52 with hotspots highlighted. C) The graph represnetative of the number of hits per residue of RPL11. D) The structure of RPL11 with hotspots highlighted.

5.2.2. Predicting and assessing the 5S RNP/p52 complex

The initial attempt to map the interaction between RPL11 and p52 utilised the entire 5S RNP complex and a p52 homodimer. This was due to this complex being the most theoretically feasible, given current literature. Thus, in order to predict the confirmation of the complex, the GRAMM-X docking software was utilised. GRAMM-X was developed by the Vasker Lab and employs an *ab initio* style of search. This involves using the PDB co-ordinates alone.

The crystal structure of the 5S RNP, provided by Dr Nick Watkins, was uploaded alongside the solved crystal structure of a p52 homodimer bound to DNA (PDB ID: 1A3Q). The structure returned from GRAMM-X was visualised, colour coded and analysis run using UCSF Chimera.

The complex returned by GRAMM-X showed the 'shoulder' of the N-terminal domain of p52 forming an interface with the cleft of RPL11 (Figure 5.3A, left). This complex reveals regions predicted to have a high probability of being involved in PPI interfaces to be contributing to the formation of the complex. The right side of Figure 5.3A depicts the structure returned by GRAMM-X superimposed onto the structure of the whole 5S RNP. This allows the inclusion of the 5S rRNA, which is unable to be loaded onto the docking software. By eye, it can be seen that the 5S rRNA begins to clash with the p52 homodimer structure. However, due to the nature of superimposing the structures, this may not be true in nature as the dynamic quality of proteins may have been able to avoid a steric clash in this context.

The predicted structure was analysed for steric clashes using Chimera in Figure 5.3B. Two clashes were found between p52 and RPL11. Serine 161 of p52 was found to clash with phenylalanine 50 of RPL11 as well as serine 206 of p52 clashing with lysine 50 of RPL11.

As GRAMM-X uses an *ab initio* algorithm for prediction, it was important to cross-reference the predicted interface hotspots to the predicted GRAMM-X structure. To achieve this, the residues revealed in Figure 5.2 were plotted onto the predicted structure using Chimera (Figure 5.3C). It can be seen that the majority of the coloured residues are within the interface between RPL11 and p52. The residues that are not near or within the interface were mapped to the region of p52 contributing to the homodimer. Therefore, it can be concluded that the *ab initio* methodology utilised by GRAMM-X utilised residues from the proteins that are predicted to have a high interactivity.

Finally, the PRODIGY software was used to predict the ΔG value of the predicted complex. After loading the PDB file returned by the GRAMM-X molecular docking software, PRODIGY returned the binding free energy calculation as -16.8 kcalmol^{-1}. When the specific p52/RPL11 interaction was isolated in the ΔG prediction, the value was returned as -7.8 kcalmol^{-1}.
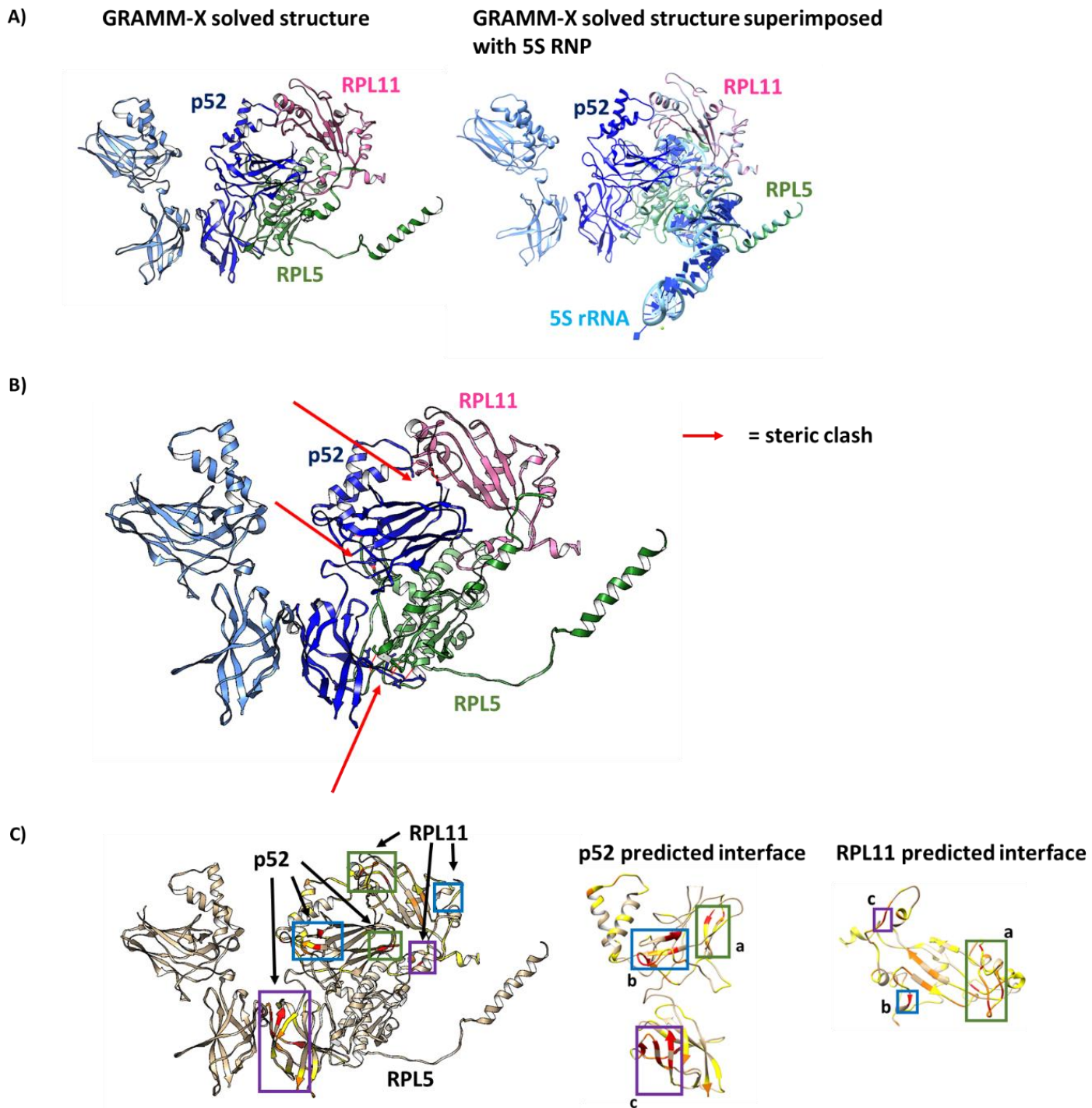
Figure 5.3 Analysis of the GRAMM-X predicted structure of the 5S RNP/p52 homodimer complex.
A) The structure returned from GRAMM-X software predicting the conformation of the protein complex (left). The structure returned from GRAMM-X superimposed onto the structure of the complete 5S RNP (right). B) Analysis of the clashes between RPL11 and p52 using UCSF Chimera. C) Hotspot residues identified using interface prediction were colour coded onto the predicted 5S RNP/p52 homodimer complex. Red = > 3 hits. Orange = 2 hits. Yellow = 1 hit.

5.2.3. A 5S RNP/MDM2/p52 complex is predicted to be less energetically feasible than a 5S RNP/p52 complex

The 5S RNP binds directly to MDM2 via RPL11. The structure of the MDM2/RPL11 complex was solved in 2015 (Zheng et al., 2015). There is also data to suggest that MDM2 remains bound to the 5S RNP upon p53 activation (Pelava et al., 2016). Therefore, it was important to investigate whether MDM2 could be a contributing component of a p52/5S RNP/MDM2 complex.

The structure of the 5S RNP/MDM2 complex, provided by Dr Nick Watkins, was docked to the structure of a p52 homodimer. The GRAMM-X software was used. This software was chosen as the complex involved multiple different proteins.

Firstly, to check the similarity of the 5S RNP/MDM2 structure created and provided by the Watkins lab, the structure was superimposed with the solved crystal structure of RPL11/MDM2 (Figure 5.4A). This precautionary step was taken as the Watkins lab structure was artificially extracted from the solved structure of the 80S ribosome. Following that MDM2 was added in silico. It was important to ensure no major differences between the structures were seen prior to docking the 5S RNP/MDM2/p52 homodimer complex. The superimposition revealed no major changes in the position of MDM2 in relation to the 5S RNP.

Given that the 5S RNP/MDM2 structure and the solved RPL11/MDM2 structure were compatible, a docking run alongside a p52 homodimer was set up. The returned RPL11/RPL5/MDM2/p52 complex was analysed on Chimera and superimposed onto the structure of the 5S RNP.

On initial examination, the structures of the complexes with and without MDM2 appear very similar (Figure 5.4B). RPL11 contacts MDM2 within the beta-sheet cleft. However, in this structure, RPL11 does not directly contact p52 through the cleft as seen in the structure without MDM2 (Figure X). Instead, MDM2 makes the contact with the N-terminal domain shoulder of p52. RPL11, however, may still make contact with p52 either side of the cleft. Therefore, the presence of MDM2 may not eliminate the interaction between RPL11 and p52 but changes the nature of it. The ΔG value of the entire 5S RNP/MDM2/p52 complex was calculated to be -17.1kcalmol^{-1}. This is comparable to the ΔG value of the 5S RNP/p52 complex which was predicted to be –16.8kcalmol^{-1} (Table 5.1). The binding energy of the

direct p52/RPL11 interaction within the complexes was also analysed. Looking more specifically at this, it can be seen that the ΔG increases by 1.4kcalmol^{-1} from -7.8 kcalmol^{-1} to -6.4 kcalmol^{-1}.

Further to this, the steric clashes were analysed on Chimera (Figure 5.4C). This showed that the number of clashes in the 5S RNP/MDM2/p52 complex to be higher, further indicating that it could be less feasible for MDM2 to be involved in this complex. The number of clashes within the complex increased with the presence of MDM2, furthermore clashes between RPL11 and p52 increased from two (without MDM2) to six (with MDM2). Several steric clashes between p52 and MDM2 were also captured by the software. Overall, this begins to suggest that the complex is more energetically feasible without MDM2 present. The number of contacts were counted with both the p52 homodimer and with the removal of a single p52 monomer. This removes the contacts between the p52 subunits. The MDM2 containing structure has more contacts overall compared to the 5S RNP/p52 complex. This is due to the additional protein in the MDM2 containing complex contributing to more contacts, rather than the quality of the conformation. When only regarding contacts between RPL11 and p52, the structure without MDM2 contained more specific contacts. There were 28 contacts counted in the complex with MDM2, versus 36 without. Taken together, the data proposes the structure is less feasible when MDM2 was included in the docking run.
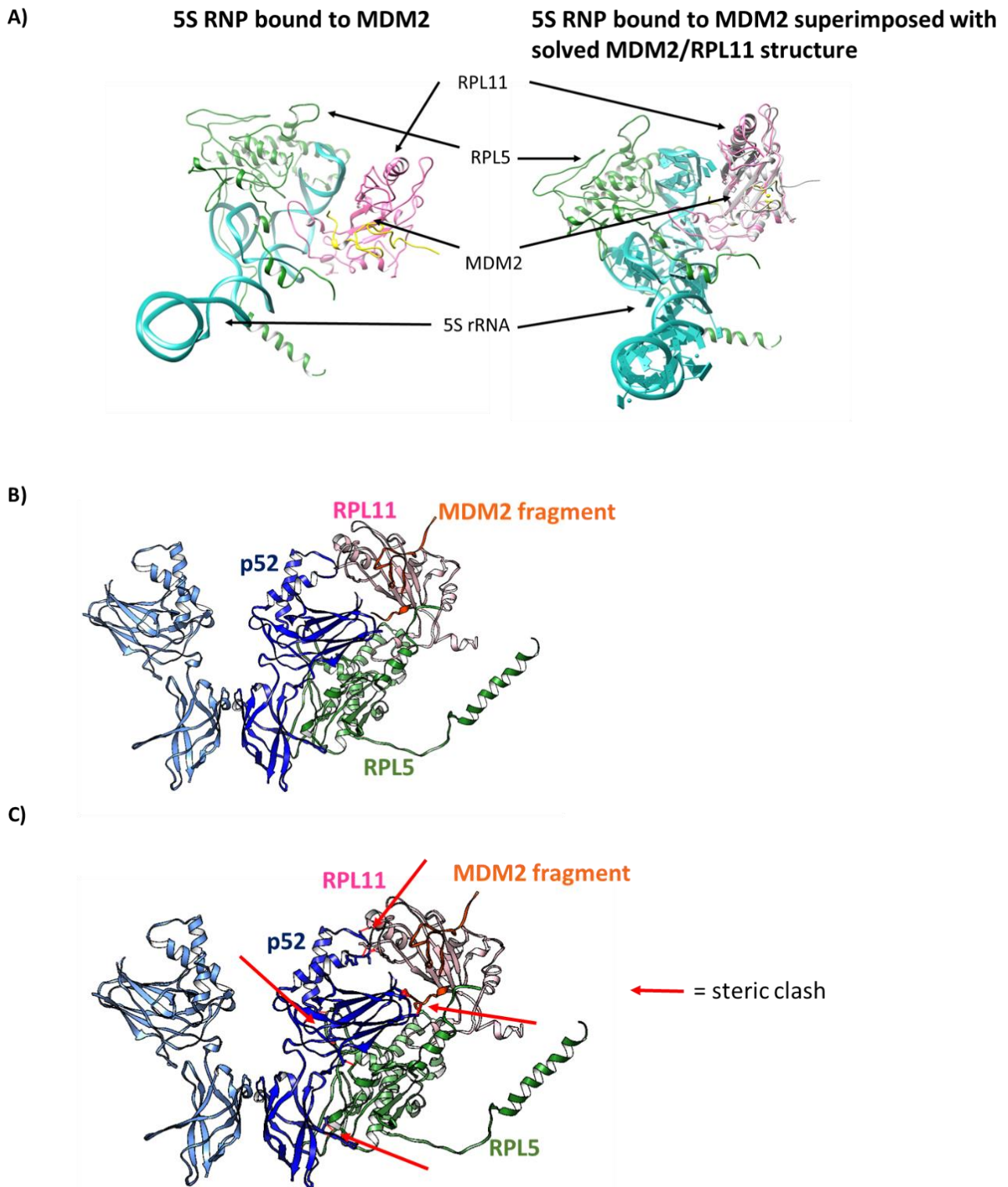
Figure 5.4 Analysis of the predicted structure of the 5S RNP/MDM2/p52 homodimer complex. A) The structure of the 5S RNP/MDM2 provided by the Watkins lab was superimposed onto the solved MDM2/RPL11 complex. B) The predicted p52-p52/5S RNP/MDM2 from GRAMM-X (left) was superimposed onto the structure of the 5S RNP on Chimera (right). C) Analysis of steric clashes between RPL11 and p52, as well as MDM2 and p52. The distance between two selected points in RPL11 and p52 measured in angstroms.

Structure	5S RNP/p52 homodimer	5S RNP/MDM2/p52 homodimer
ΔG whole complex (kcalmol^{-1})	-16.8	-17.1
ΔG RPL11/p52 (kcalmol^{-1})	- 7.8	- 6.4
Contacts	238 overall 154 without second p52 molecule 36 RPL11/p52	255 overall 171 without second p52 molecule 28 RPL11/p52
Steric clashes	13 overall 2 RPL11/p52	25 overall 6 RPL11/p52

Table 5.1 Comparison of binding free energy prediction, residue contacts and steric clashes of GRAMM-X predicted complex with and without MDM2

5.2.4. GRAMM-X software prioritises the interaction between p52 and RPL1 in the 5S RNP complex

With the purpose of designing point mutations capable of disrupting the p52/RPL11 interaction, it was important to determine the regions of each protein that are critical for the interaction. Following the identification of the region, the search could be further narrowed to single amino acids to determine key residues in this protein-protein interaction. RPL11 plays a key role in ribosome biogenesis, a tightly regulated and energetically costly cellular process (Sloan et al., 2013a). Disruption of RPL11 would lead to the rapid inhibition of ribosome biogenesis and subsequent downstream processes. Hence, it was decided that only p52 would be modified.

Firstly, a p52 truncation series was simulated. Truncations were created relevant to the structural domains of p52. To simulate that *in silico*, the protein structure was edited to create truncations on Chimera. The truncations were made in line with the known structural domains of p52. Firstly, the protein was truncated to leave the N-terminal domain of the Rel Homology Domain (RHD) and the insert region intact (Figure 5.5B). Next, the protein was subject to further deletions including the partial removal of the DNA binding associated region (Figure 5.5C) and the helix-loop-helix group encoded by residues 184-227 both of which leaves the shoulder of p52 intact (Figure 5.5D). Lastly, amino acids 37-100 were removed from the structure, keeping the remainder of the RHD and the glycine rich region intact (Figure 5.5E). These p52 truncations were then docked with RPL5 and RPL11 using the 5S RNP complex structure. Structures returned were analysed on Chimera.

The truncations made changed the manner in which p52 interacted with the 5S RNP proteins (Figure 5.6). The deletion of the helix-loop helix, the insert region, within the p52-C-140 truncation showed the biggest impact on the predicted structure (Figure 5.6C). Studying the movement of the 5S RNP complex in relation to the p52 homodimer throughout the truncation series revealed GRAMM-X was prioritising RPL5 rather than RPL11. The 5S RNP was predicted to shift binding site as portions of the p52 protein was removed. The images, however, show that RPL5 stays in contact with the p52 homodimer, whilst RPL11 is at times not part of the interface at all. As molecular docking software will always force an interaction, it suggests that GRAMM-X prefers to use RPL5 within the predicted interfaces. This is likely due to the software only taking into account the static structure of the 5S RNP coupled with the *ab initio* search style. As no data is inputted into GRAMM-X the user is unable to influence the formation of the complex with known data. For example, the data generated from the interface prediction. Furthermore, previous data suggests p52 is directly contacting RPL11 with little data showing an association with RPL5. It must be assumed that RPL11 is the driving force within the 5S RNP during the interaction with p52 due to the laboratory generated data. It remains unclear whether GRAMM-X has prioritised RPL5 in the wild-type 5S RNP/p52 predicted structure. As GRAMM-X may not represent an RPL11-mediated association between the 5S RNP and p52, it is unsuitable for this type of investigation. Finally, as the 5S RNP complex stays static, which likely causes significant steric clashes, docking the complex in entirety is not suitable.
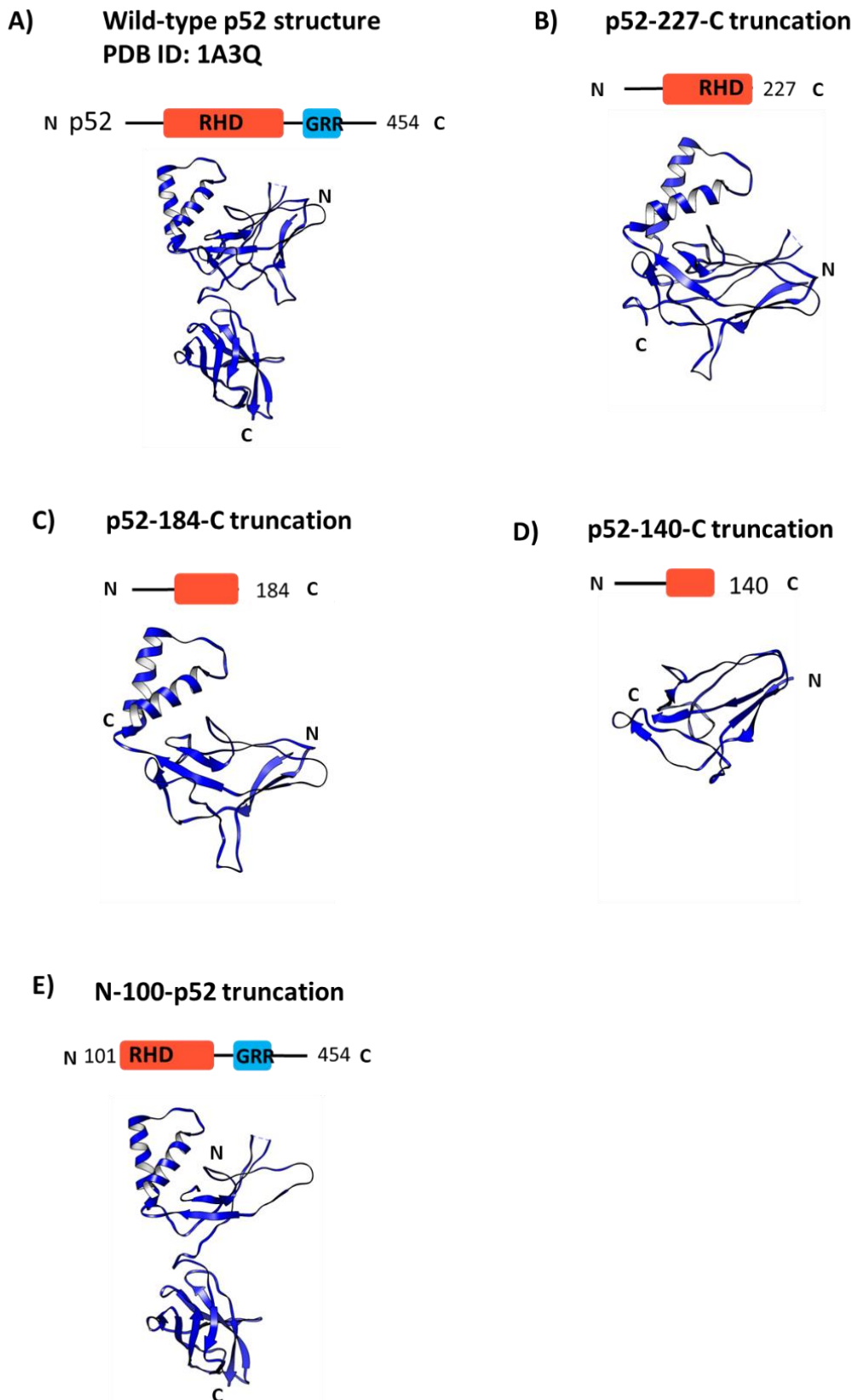
Figure 5.5 In silico truncation series of p52 created using Chimera. The structure of the p52 protein was truncated to remove specific regions of the p52 protein as represented in the schematic drawing of the structural domains as well as the image of the protein structure. Structure a) depicts the wild-type and b) to e) are truncated.
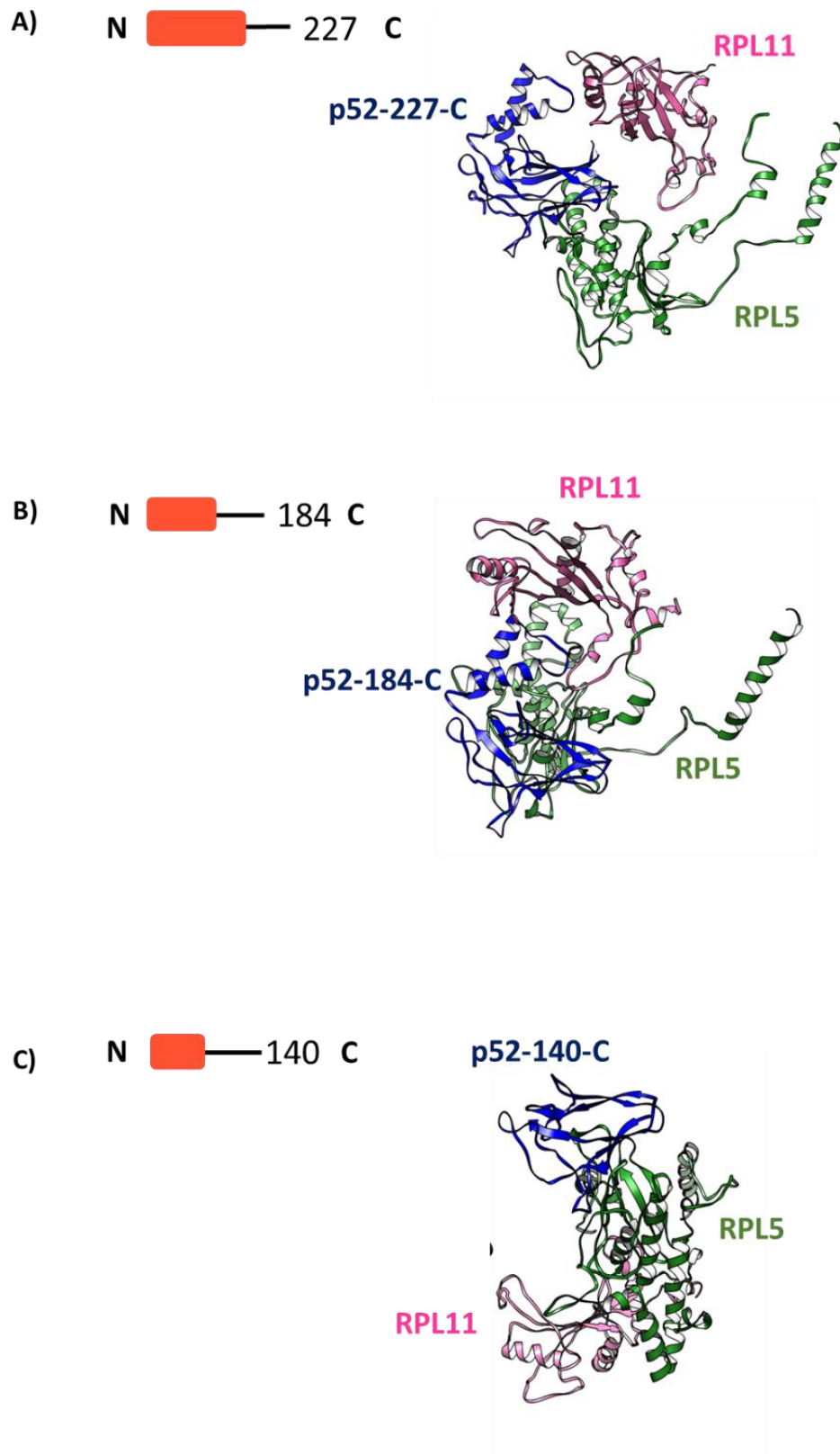
Figure 5.6 GRAMM-X prioritises RPL5 over RPL11 in the orientation of the predicted complex. Truncated forms of p52 were created using Chimera and docked using GRAMM-X to the 5S RNP proteins. Predicted complexes were visualised using Chimera.

5.2.5. HADDOCK software predicts the conformation of the direct p52/RPL11 interaction

The HADDOCK molecular docking software, developed by the Bovin Laboratory, utilises data driven docking algorithms. This means that the interface prediction presented in Figure 5.2 served as a guide for the subsequent molecular docking of p52 to RPL11. The active residues were submitted to the HADDOCK docking software along with the PDB files of the proteins. HADDOCK investigates all possible conformations and scores them according to feasibility (de Vries et al., 2010). HADDOCK combines data inputted with PDB co-ordinates, where GRAMM-X solely relies on PDB structures.

The PDB file of the optimum configuration of the complex both sterically and energetically was analysed on Chimera. Firstly, the proteins were coloured to visualise the complex (Figure 5.7A). Secondly, the predicted contacts, clashes and hydrogen bonds were mapped tools on the Chimera software detailed in the methodology chapter. A contact refers to residues from each protein that are in a close enough proximity to interact. There were many contacting amino acid residues between p52 and RPL11, 22 hydrogen bonds (Table 5.2) and zero steric clashes.

Upon inputting the data generated in Figure 5.2 and colouring specific residues according to the probability of interactivity, it became clear that regions a and b of p52 along with section b and c of RPL11 were forming the interface (Figure 5.7B).

The docking software predicted the cleft of RPL11 slotting onto the shoulder of p52. Interestingly, the cleft of RPL11 that contacts p52 in this predicted conformation is the same region of the ribosomal protein that binds to the ribosome when the 5S RNP is incorporated into the maturing 60S subunit. Given that the association of RPL11 and p52 is predicted to strengthen during stress, it suggests that the RPL11/p52 and RPL11/ribosome interactions are mutually exclusive events. Furthermore, the cleft bound in Figure 5.7A by p52, is the region of RPL11 that binds to MDM2, indicating these events could also be mutually exclusive.

A)

HADDOCK predicted RPL11/p52 complex

HADDOCK complex showing contacts (yellow) and hydrogen bonds (red)

Insert region

p52

RPL11

Residues mediating DNA binding

Dimerisation domain

p52

RPL11

B)

RPL11

p52

p52 predicted interface   RPL11 predicted interface
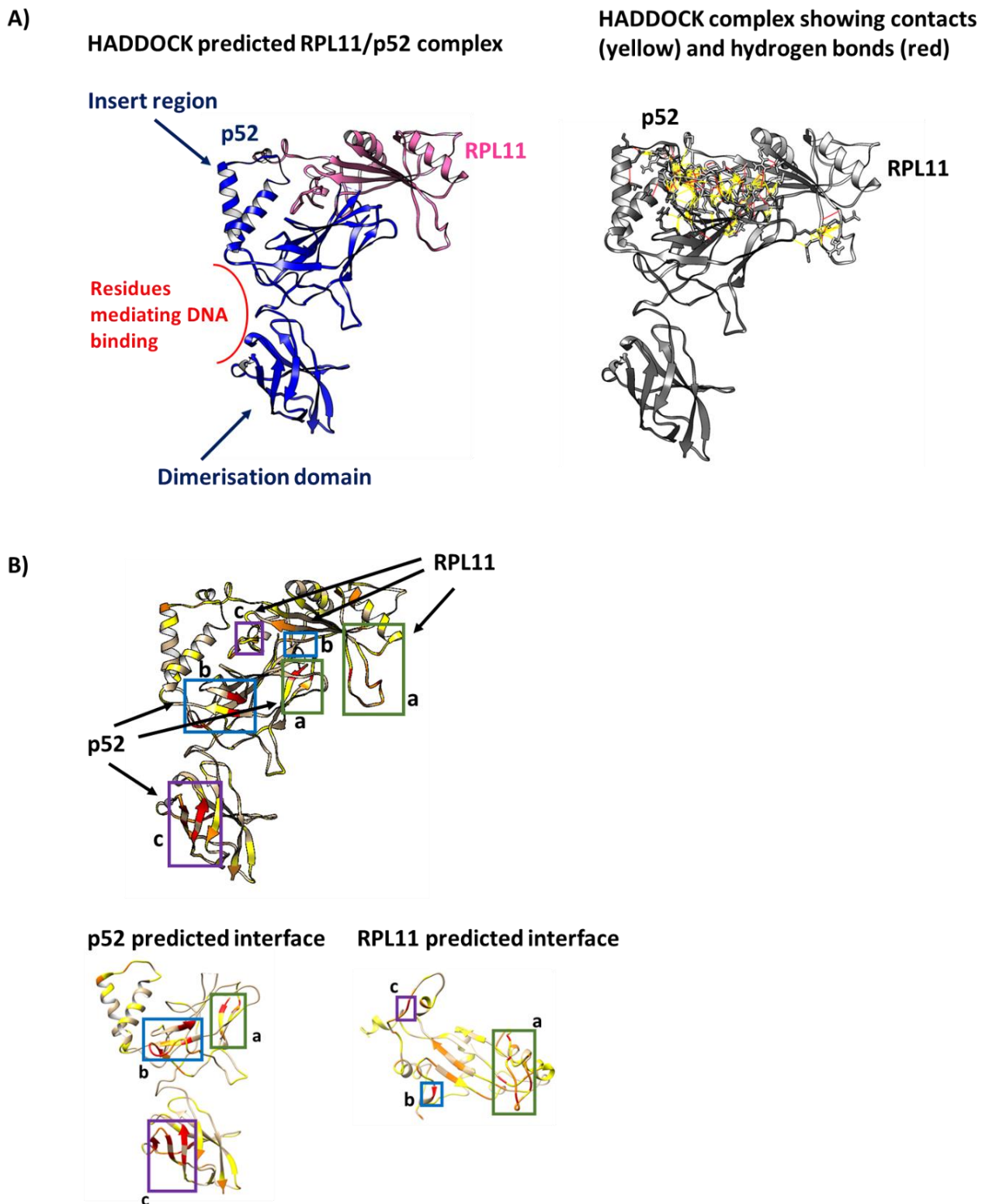
Figure 5.7 The predicted conformation of the RPL11/p52 interaction. A) Active interface residues identified previously were used in a molecular docking run between RPL11 (pink) and p52 (blue) via the HADDOCK software. B) Contact (yellow) and hydrogen bond (red) analysis carried out using Chimera. Lines are drawn between respective points of p52 and RPL11 predicted to be contributing to the interaction.

RPL11 contributing residue	p52 contributing residue
Lys 8	Glu 170
Lys 8	Arg 162
Glu 9	Arg 162
Arg 18	Ser 206
Lys 19	Glu 86
Ala 53	Lys 127
Arg 54	Lys 127
Asn 65	Lys 127
Arg 75	Arg 199
Asp 101	Lys 210
Asn 104	Pro 208
Gly 138	Ser 161
Ala 142	Lys 90
Asp 143	Lys 90
Asp 143	Ser 206
Arg 147	Glu 116
Arg 147	Arg 156
Thr 148	Arg 156
Gly 149	Arg 160
Cys 150	Asp 94
His 155	Ser 161
His 155	Arg 162

Table 5.2 Hydrogen bonds predicted to be formed between RPL11 and p52

5.2.6. The prediction of a direct RPL11/p52 interaction shows a more promising interface

In order to determine whether the HADDOCK p52/RPL11 complex prediction was a better representation of the interaction than the GRAMM-X 5S RNP/p52 complex prediction, the structures were compared using Chimera.

Firstly, the structures were superimposed using the p52 structure as the guide. This allowed any differences in the position of RPL11 to be examined. After the superimposition, RPL5 was removed to clearly view the p52/RPL11 interactions. The HADDOCK complex was kept coloured, and the RPL11 from the GRAMM-X structure was coloured grey. Secondly, the number of clashes, contacts, hydrogen bonds and binding free energy were compared.

Upon initial observation, it can be seen that RPL11 from the GRAMM-X prediction (grey) is further away and less tightly bound to p52 than in the HADDOCK prediction, coloured in pink (Figure 5.8A). To quantify this, the distance between glutamate 86 from p52 and lysine 19 from RPL11, shown to form a hydrogen bond in the HADDOCK structure, was measured. In the HADDOCK structure the distance between the first carbon of each amino acid side chain was measured as 10.073Å. Looking at the structure it can be seen that the residues (orange and yellow) are making contact. By contrast, the distance between E86 and K19 in the GRAMM-X prediction was measured at 16.899Å and do not appear to be contacting.

As visualising changes within the superimposed image is made difficult by similar secondary structure elements overlapping within the RPL11 structure, the interface prediction data generated in Figure 5.2 was used (Figure 5.8B). The location of the three regions of predicted high interactivity within the RPL11 protein were compared. This gave a clearer picture of the vast difference in RPL11 orientation given in the HADDOCK generated structure compared to the GRAMM-X. The purple box in the HADDOCK structure can be seen to slot between the insert region (helix-loop-helix) and the N-terminal domain of the p52 protein. In the GRAMM-X structure, however, it is the green box that is seen in a similar position. The purple box is contacting the opposite side of the N-terminal region as well as making contacts with RPL5. It can be predicted that RPL11 could not be docked to p52 in the same orientation with GRAMM-X as it was using HADDOCK due to the fixed position of RPL11 and RPL5 in the 5S RNP structure. Overall, the two software have predicted RPL11 to be docked

at two different conformations. This could explain why the location of the measured residues (lysine 19 of RPL11 and glutamate 86 of p52) were reasonably unchanged.

Further analysis of the predicted structures favoured the prediction generated by HADDOCK over GRAMM-X (Table 5.3). The two steric clashes between p52 and RPL11 in the GRAMM-X predicted complex were eliminated in the conformation predicted by HADDOCK, utilising solely p52 and RPL11. The GRAMM-X and HADDOCK predictions had a comparable number of contacts overall. However, upon closer inspection, 84 of those were through the dimerization of the p52 proteins. This was determined through the deletion of one of the p52 monomers, thus removing the contacts. Considering RPL11/p52 specific contacts, the GRAMM-X complex consisted of 36 whereas the HADDOCK complex contained 248. The GRAMM-X complex was predicted to have one hydrogen bond between RPL11 and p52, on the other hand the HADDOCK prediction showed 22 hydrogen bonds between the proteins. Finally, comparing the binding free energy of the RPL11/p52 conformations revealed that the HADDOCK complex is almost twice as negative as the GRAMM-X prediction. The value of the p52/RPL11 interaction when RPL11 is within the 5S RNP/p52 complex is -7.8kcalmol^{-1} whereas it is -16kcalmol^{-1} in the HADDOCK direct interaction. The data presented indicates that the predicted HADDOCK interaction is more energetically feasible and therefore more stable.

A)

GRAMM-X RPL11

HADDOCK RPL11

= Lysine 19 of RPL11 from the 5S RNP/p52 predicted complex → = 10.073Å
= Lysine 19 of RPL11 from the L11/p52 predicted complex → = 16.899Å
= Glutamic acid 86 of p52
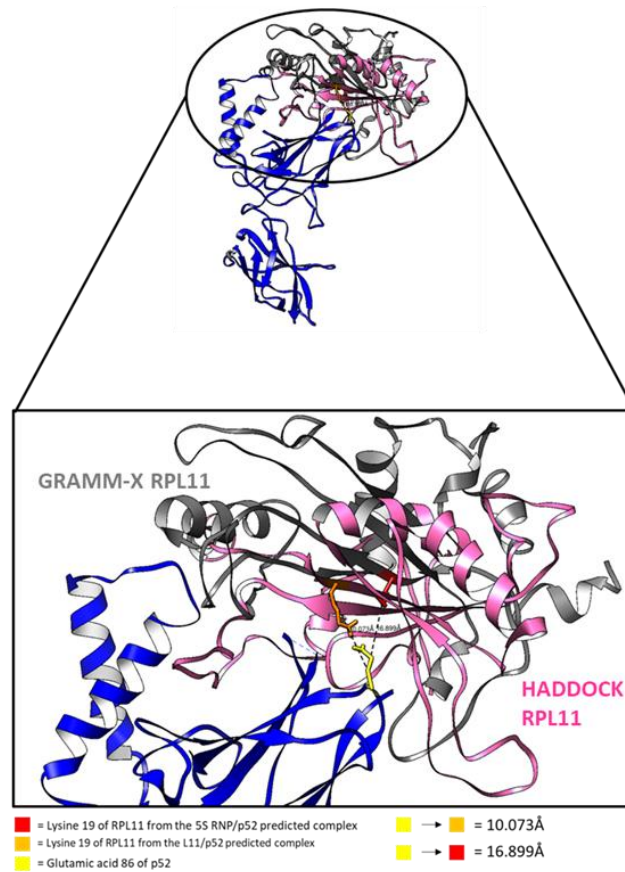
B)

GRAMM-X predicted complex

p52
RPL11
RPL5

HADDOCK predicted complex

p52
RPL11
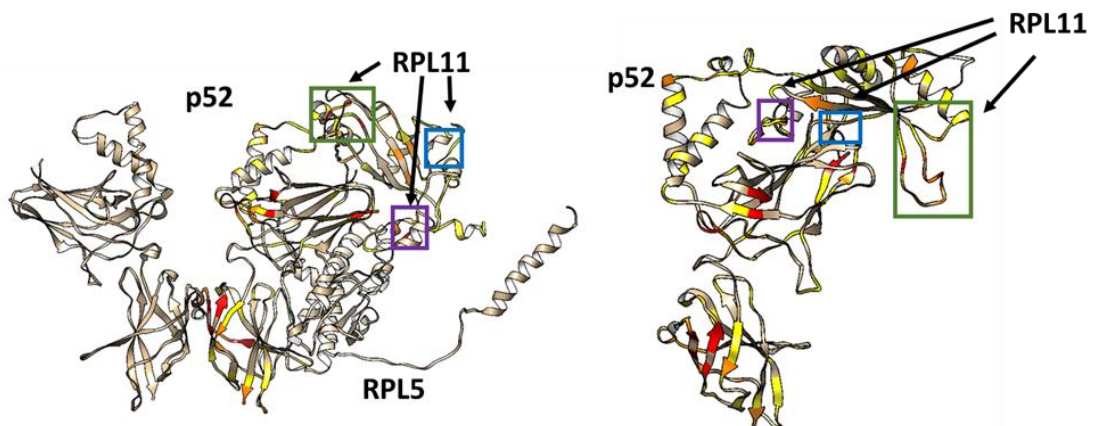
Figure 5.8 Comparing the p52-RPL11 interaction predicted by GRAMM-X and HADDOCK. *A) Blue structure = p52. Pink structure = RPL11 from HADDOCK prediction. Grey structure = RPL11 from GRAMM-X prediction. The p52 protein from the HADDOCK p52/RPL11 complex was superimposed onto the p52 structure from the GRAMM-X 5S RNP/RPL11 complex using the Match Maker tool on Chimera. The p52 and RPL5 from the GRAMM-X structure was removed to isolate the p52/RPL11 interactions. The distances between glutamic acid 86 and lysine 19 were measured within each predicted complex. B) Side-by-side comparison of the interface prediction heat maps coloured onto the GRAMM-X and the HADDOCK predicted structures to view the orientation of RPL11.*

	GRAMM-X **5S RNP/p52 homodimer**	**HADDOCK** **p52/RPL11**
Contacts	• 238 overall • 154 minus p52 monomer • 36 RPL11/p52 specific	• 248 RPL11/p52
Clashes	• 13 overall • 2 RPL11/p52 specific	• 0 RPL11/p52
Hydrogen bonds	• 1 RPL11/p52 • 4 RPL5/p52	• 22 RPL11/p52

Table 5.3 Comparison of contacts, clashes and hydrogen bonds within the GRAMM-X and HADDOCK predicted structures.

5.2.7. Creating an in silico truncation series to locate important regions in the RPL11/p52 protein-protein interaction

Following the confirmation that the HADDOCK software generated complex was more energetically feasible, the same truncation series in Figure 5.5 was used to determine the driving regions of the interaction. As HADDOCK is data driven, the same docking parameters and the same active residues were inputted. Predicted complexes returned were analysed on Chimera. To highlight any visible shifts in the location of RPL11, the wild-type and truncated structures were superimposed relative to p52. The truncated structure was kept coloured in blue (p52) and pink (RPL11), whereas the full wild-type structure was coloured in light blue.

Initially the protein was truncated to leave the N terminal domain Rel Homology Domain (RHD) intact (Figure 5.9A). The p52-227-C truncation revealed little effect on the interaction between RPL11 and p52. This can be seen by the wild-type and truncated structures lining up in the superimposition. This suggested the critical region was within the RHD. Subsequent deletions, p52-184-C and p52-140-C, left the RPL11/p52 interface intact (Figure 5.9B and

5.9C). Slight variation in the p52 structure is likely due to the large number of deleted residues, leaving a small portion of the protein intact. Finally, it was decided to remove residues from the N terminus of the protein. This caused a dramatic change in conformation, shifting RPL11 to bind to a different region of the p52 protein altogether (Figure 5.9D). This indicates that residues 37-100 of p52 are predicted to be critical for binding to RPL11.

To numerically assess the impact of the truncations, the ΔG value was calculated using PRODIGY (Table 5.4). The ΔG value of wild-type RPL11 and p52 is -16kcalmol^{-1}. The p52-454 and p52-227-C structures casued insignificant changes to the binding affinity, which is in line with the structural analysis of the predicted complexes. Interestingly, the p52-184-C and p52-140-C structures resulted in the highest ΔG value which would imply they were the least stable complexes and that these truncations had the most profound effect on the complex. However, the visualisation of the complexes shows no disruption to the conformation of the interaction seen with the full length proteins. This value could be influenced by the instability of the p52 protein with only 184 or 140 amino acids, rather than representing the impact of the truncation upon the binding. Finally, the N-100-p52 truncation had the biggest structural effect increased the ΔG by 2.9kcalmol^{-1} confirming that this is less energetically feasible than the wild-type. This further suggests that the most likely region of p52 mediating the interaction with RPL11 resides in the first 100 amino acids. At a ΔG value of -13.1kcalmol^{-1} the N-100-p52 truncation was still predicted to be more energetically feasible than the solved structure of RPL11 complexed with MDM2, which has a ΔG value of -8.6 kcalmol^{-1}. Therefore, this suggests that the truncation creates a second binding site for RPL11 on the p52 protein. This second site could become available should a conformational change occur in p52 to reveal it.
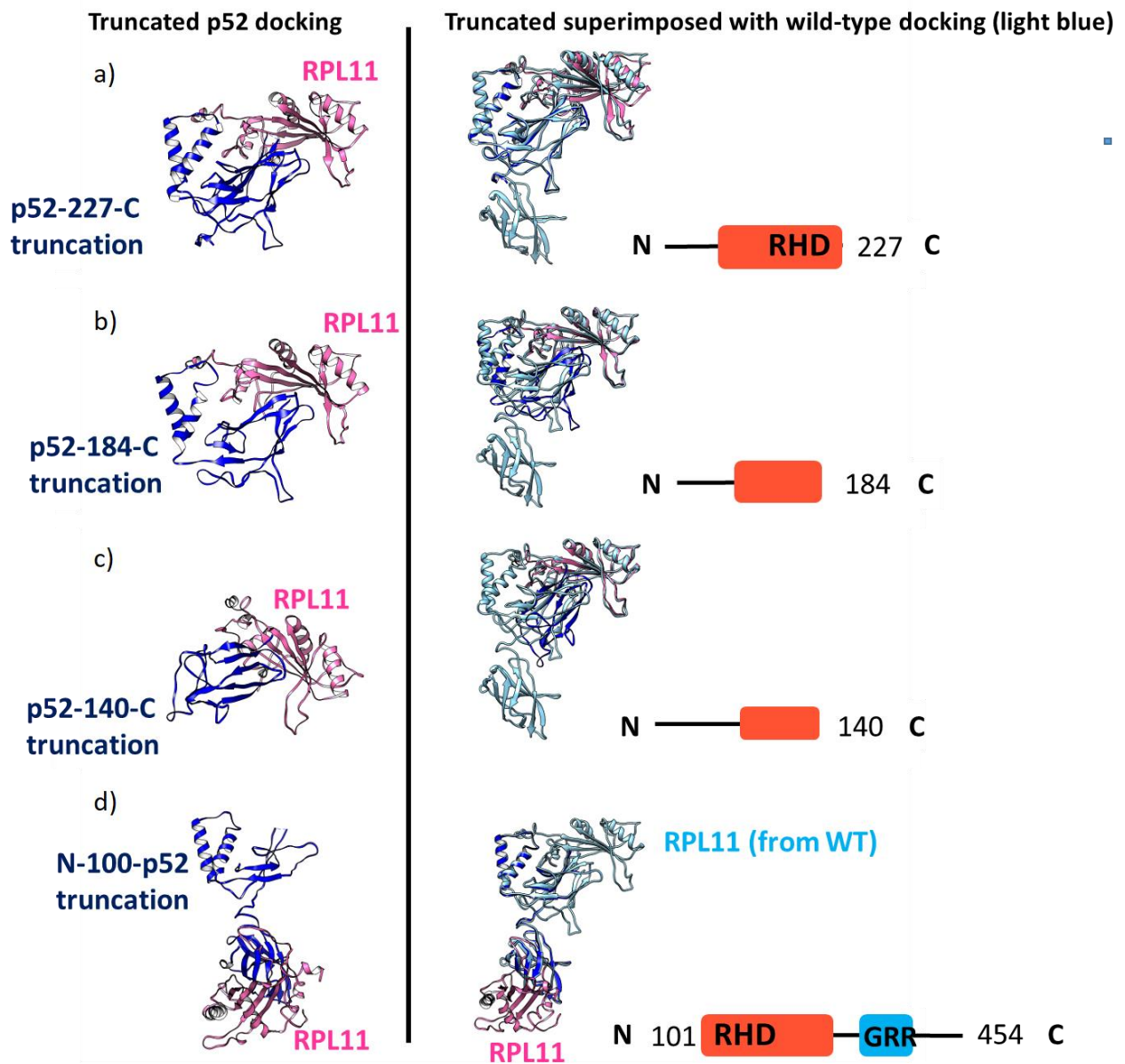
Figure 5. 9 The first 100 amino acids of p52 are critical for the interaction of p52 and RPL11. A – D) Truncated forms of p52 were created using Chimera and docked to wild-type RPL11. The predicted complexes (dark blue and pink) were superimposed onto the wild-type p52/RPL11 complex (light blue).

Structure	ΔG value kcalmol^{-1}
Wild-type p52/RPL11	-16
p52-227-C truncation/RPL11	-15
p52-184-C truncation/RPL11	-12.7
p52-140-C truncation/RPL11	-12.7
N-101-p52 truncation/RPL11	-13.1
Solved RPL11/MDM2	-8.6

Table 5.4 Calculated ΔG values of the truncations, using PRODIGY, compared to the wild-type p52/RPL11 and the solved structure of RPL11/MDM2

5.2.8. Assessing the effect of amino acid changes at residues within the first 100 amino acids of p52 predicted to contribute to hydrogen bonds within the RPL11/p52 interface

Following the prediction that the first 100 amino acids of p52 are critical in the p52/L11 interaction, point mutations were simulated and the impact upon the interaction assessed. The goal of this strategy was to identify key residues through *in silico* modelling that could be introduced into the p52 protein in the wet laboratory.

Residues within the first 100 amino acids of p52, that were also found to be contributing to hydrogen bonds, were investigated. Single amino acid changes were coded into the crystal structure using Chimera and the PDB file for mutated p52 was used in a HADDOCK docking run alongside wild-type RPL11. The docked mutant p52 structure was analysed and superimposed with the wild-type complex to visualise any changes in the interface between RPL11 and p52. It is important to note that the docking software will always force an interaction to occur, even if the interaction is not biologically stable. This reinforces the need to validate the changes in the wet laboratory. Finally, the predicted complexes were uploaded to PRODIGY to compare the binding free energy to the wild-type structure.

Glutamic acid 86 of p52 was predicted to form a hydrogen bond with lysine 19 of RPL11 and is highlighted with a red circle in Figure 5.10. This appears, by eye, to be the point at which p52 sits in the cleft of RPL11 which is in the middle of the predicted interface. When mutated *in silico* to either alanine (Figure 5.10A) or glutamine (Figure 5.10B), RPL11 binding shifts from contacting the 'shoulder' of the N-terminal domain of p52 to the insert region (helix-loop-helix). The amino acid changes created an entirely new binding site for RPL11. The E86A mutant increased the ΔG value from -16kcalmol^{-1} to -11kcalmol^{-1} whereas the E86Q mutant increased the value to -12.1kcalmol^{-1} (Table 5.5). As both of the mutations increased the ΔG value, it is predicted that both mutant complexes are less stable than the wild-type. Interestingly, both of the mutant conformations are still predicted to be more energetically feasible than the solved complex for RPL11/MDM2. This revealed a potential new binding site for RPL11 which is different to the binding site identified in Figure 5.9D.

Lysine 90 was predicted to form hydrogen bonds with alanine 142 and asparagine 143 of RPL11 (Table 5.1). Mutating the residue to either glutamic acid or asparagine causes RPL11

to shift its position in the complex and contact the 'back' side of the shoulder. This causes a rotational change in the conformation of the p52/RPL11 structure compared to the wild-type (Figure 5.10C and 5.10 D). However, in this case, the new binding interface shares large regions with the wild-type binding interface. This conformational change increases the ΔG to -12.3kcal^{-1} in the K90N mutant and to -13.0kcal^{-1} in the K90E mutant (Table 5.5). The data indicates a mutation at K90 would also impact binding affinity.

Aspartic acid 94 of p52 was predicted to contribute to a hydrogen bond with cysteine 150 of RPL11 (Table 5.1). This residue is predicted to contact RPL11 at an edge of the interface. Mutating this residue to alanine was also predicted to cause a rotational conformational change (Figure 5.10E). RPL11 is still binding to a similar region of the mutant p52 protein. Visually, mutating this residue appears to have similar effects as the K90 residue. The ΔG value increases from -16kcal^{-1} to -12.5kcal^{-1} indicating a D94 mutant could also function as a possible mutant to effect binding affinity (Table 5.5).

Both Lysine 90 and aspartic acid 94 derived mutants did not create an entirely new binding site for RPL11, whereas glutamate 86 mutants did. Therefore, the results suggest that glutamate 86 is a critical region within the p52/RPL11 interface.
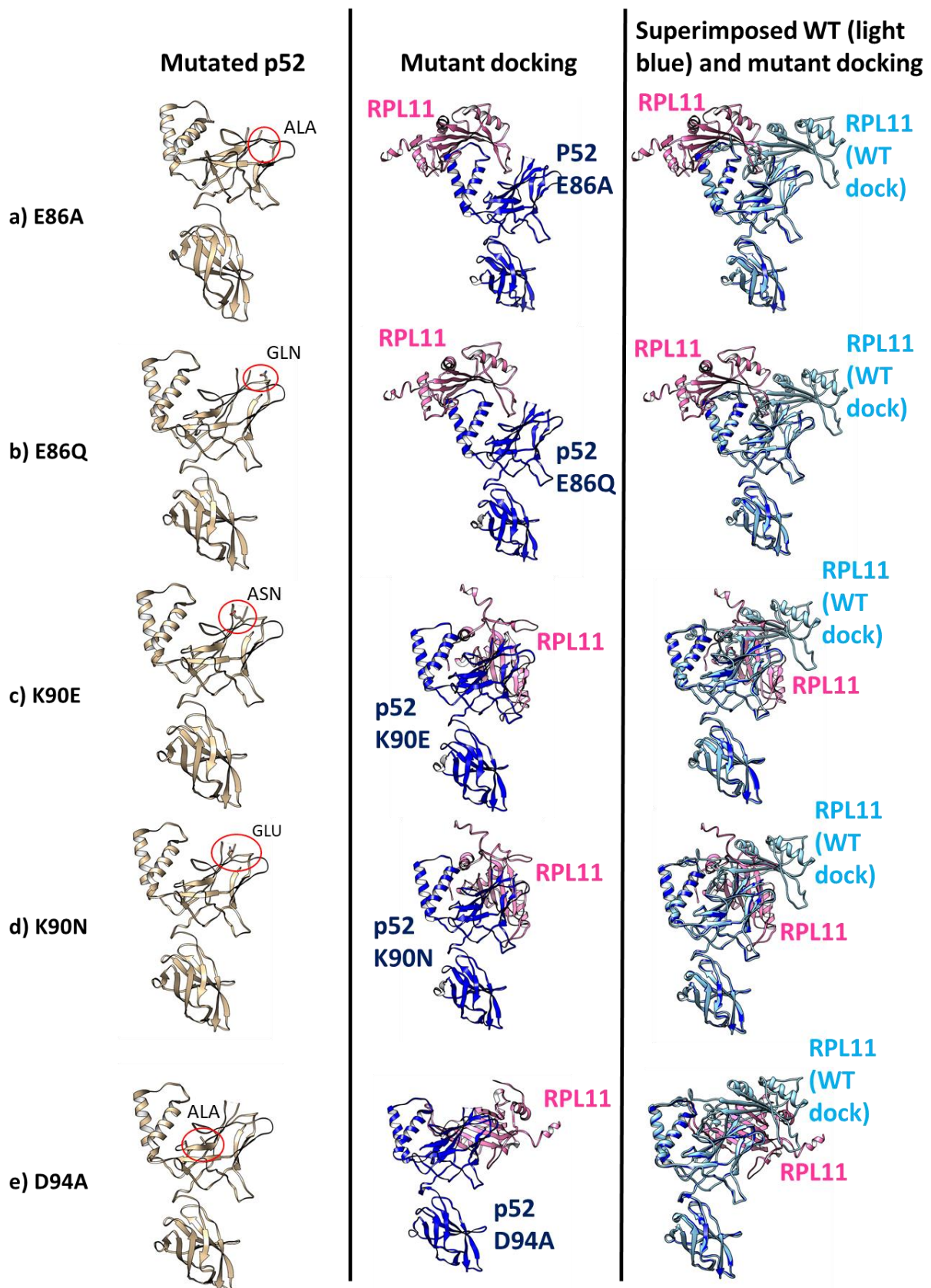
Figure 5.10 Mutating residues in the first 100 amino acids shows disruption to the p52/RPL11 complex. A-E) Individual residues that were predicted to contribute to hydrogen bonds in the protein-protein interface were mutated using Chimera. The mutant p52 was docked to RPL11 using HADDOCK and the predicted complex structure was superimposed onto the wild-type to track changes.

Mutation	ΔG value kcalmol^{-1}
Wild type	-16
E86A	-11.0
E86Q	-12.1
K90N	-12.3
K90E	-13.0
D94A	-12.5
Solved RPL11/MDM2	-8.6

Table 5.5 The predicted binding free energy calculations of the predicted mutant p52 and RPL11 interactions

5.2.9. Assessing the full length predicted p52 structure from AlphaFold and subsequent docking with RPL11

After the release of predicted full length structures of various proteins using AlphaFold, the PDB file for the p52 protein was downloaded. The p52 structure used in the previous docking runs was solved in 1997 by Cramer *et al* (Cramer et al., 1997). Due to the limitations faced by scientists when solving the crystal structure of proteins, the full length of the protein is not always included in the structures solved by NMR or X-ray crystallography. This is the case for the solved structure of p52 utilised during the docking runs (PDB ID: 1A3Q). This structure lacked 36 amino acids at the N terminus of the protein and 129 residues at the C terminus. It must be noted that the portion of the protein folded utilising the DeepMind algorithm has been predicted at a very low confidence. This is likely due to little comparable database information being available.

To decipher whether the additional amino acids were impacting the p52/RPL11 interface, the AlphaFold predicted structure was docked to RPL11. The returned structure was analysed on Chimera and superimposed to the solved p52/RPL11 structure. Parameters and inputs were kept the same to allow fair comparison of the complexes. The AlphaFold

structure was largely based on the available structural data of the p52 protein. As only DNA bound structures are present, these formed the template for the software.

The initial observation of the full length structure shows the first 36 amino acids be an unstructured chain. This are is highlighted in light blue, located at the top of the structure in Figure 5.11A. This suggests it could possibly be a flexible region of the protein. The N terminal region of the protein contains long chains leading into alpha helical regions (Figure 5.11A). The docking prediction of the AlphaFold p52/RPL11 complex reveals RPL11 binds to the same area of the p52 protein (Figure 5.11B). Further analysis revealed a minor shift in the binding of RPL11 to p52. The interface rotates around the 'shoulder' of the protein (Figure 5.11C and Figure 5.11D). Analysis of the hydrogen bonds reveals the majority to reside in the first 100 amino acids (Table 5.6). Namely, residue glutamate 86 that was predicted to be critical for the interaction, was shown to form a hydrogen bond with arginine 18 of RPL11 (Table 5.6). Finally, the predicted structure of the AlphaFold p52/RPL11 complex was 2.9kcalmol^{-1} greater than the solved p52/RPL11 structure. Hence, it is predicted that the complex utilising the solved p52 structure is more energetically feasible. This could be due to the regions of low confidence in the structure predicted by AlphaFold.
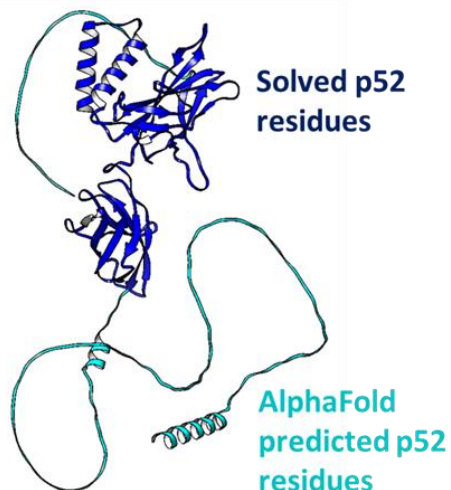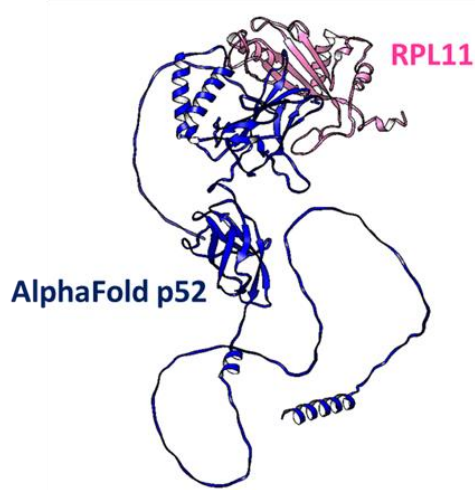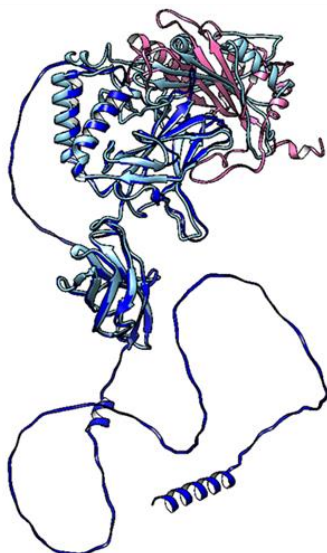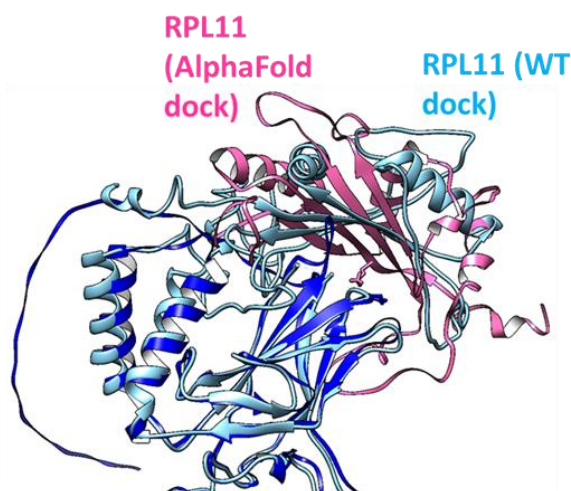
Figure 5.11 Analysing the p52/RPL11 complex generated when using the AlphaFold full length p52 predicted structure. A) The full length p52 structure predicted by AlphaFold. Dark blue represents the solved region of the protein, light blue represents predicted. B) Prediction of the AlphaFold p52/RPL11 complex as predicted by HADDOCK. C) AlphaFold p52/RPL11 structure superimposed onto the solved p52/RPL11 HADDOCK structure. D) A detailed view of the interface between p52 and RPL11 in the predicted complexes.

p52 contributing residues	RPL11 contributing residues
Lys 81	Ala 142
Asn 84	Asp 143
Lys 127	Asp 101
Glu 86	Arg 18
Asn 84	Lys 19
Pro 163	Arg 58
Arg 36	Arg 75
Pro 126	Thr 102
Ile 42	Lys 145

Table 5.6 Hydrogen bonds predicted within the AlphaFold p52/RPL11 complex

5.3. Discussion

5.3.1. Limitations

In the context of this project, there were several limitations that restricted the investigation. Firstly, the crystal structure of the 5S RNP has not been solved. The structure used in this chapter was provided by Dr Watkins and was extracted from the solved crystal structure of the human 80S ribosome (Khatter et al., 2015). With the knowledge that proteins have a dynamic structure, it is important to note that the structure of the 5S RNP bound to the ribosome is not necessarily the structure of the 5S RNP in a 'ribosome-free' state. Secondly, the only solved structure of the NF-κB subunit, p52, is in a DNA bound state and, as previously mentioned, is lacking amino acids from both the C and the N terminus.

A further limitation was found when comparing the ΔG of various iterations of the complexes. Whilst it is possible to comment on numerical differences, it is difficult to decipher the physiological relevance. It is known that the more negative the binding energy, the more stable the complex. However, the issue surfaces when comparing the ΔG of complexes containing different numbers of proteins, e.g. 5S RNP/p52 versus 5S RNP/p52/MDM2. Different proteins will contribute differently to the overall energetics of the protein complex. They contain a unique set of internal forces. So, it is possible to state which is predicted to be more energetically stable, however difficult to state whether this would have a physiological relevance e.g. competition. On the other hand, comparing the ΔG of a complex before and after mutation is more straight forward. If an increase of ≥2kcalmol^{-1} occurs following mutation, it is said that the mutation occurred in a critical portion of the interaction interface (Dehouck, 2013). Therefore, it can be said that a change in ΔG of ≥2kcalmol^{-1} is a biologically meaningful change in the value.

5.3.2. p52/RPL11 predicted to be mutually exclusive to RPL11/ribosome and RPL11/MDM2

The initial HADDOCK docking run revealed p52 binding to RPL11 within the cleft of β-pleated sheets (Figure 5.7). This is the same cleft within RPL11 that is used as the 5S RNP associates with the ribosome during ribosome biogenesis (Zheng et al., 2015). Interestingly, MDM2 also associates with RPL11 through this same set of β-pleated sheets. It is known that RPL11 binding to MDM2 is mutually exclusive to RPL11 incorporation into the ribosome due to rapidly accumulating ribosome-free 5S RNP in response to nucleolar stress (Zheng et al., 2015, Khatter et al., 2015, Pelava et al., 2016). The 'free' form of the 5S RNP leaves the cleft

of RPL11 accessible to other binding partners, such as MDM2. Due to the conformation of the RPL11/p52 complex that has been predicted by the HADDOCK software, it can be proposed that p52 binding to RPL11 relies on the same mechanism.

Further to this, it can be assumed that p52 and MDM2 are in competition for RPL11 binding, due to the nature of the interfaces alone. Taking the structures generated by the GRAMM-X software, the binding free energy of the RPL11/p52 interaction in the MDM2-containing complex was less negative than that of the 5S RNP/p52 homodimer complex (Table 5.1). This increase in ΔG value indicates the complex is less stable with the inclusion of MDM2-bound RPL11. Due to the accessibility and capability of the HADDOCK2.2 webserver, it was not possible to dock p52, MDM2 and RPL11 (van Zundert et al., 2016). Therefore, a direct comparison of p52/RPL11 and p52/MDM2/RPL11 could not be performed through HADDOCK. Further investigation could be performed utilising the 'Multi-body interface' which requires a higher level of access.

Due to the hypothesised competition between MDM2 and p52 for RPL11 binding, it can be suggested that the action of p52 outcompetes MDM2 to oppose this since the predicted strength of the p52/RPL11 interaction is higher than that seen with MDM2/RPL11. It has been shown that the MDM2/RPL11 interaction occurs to stabilise p53 in the context of cellular stress (Sloan et al., 2013a). However, if p52 outcompetes MDM2, the E3 ligase would still be able to carry out its normal function in the cell by targeting the p53 tumour suppressor for degradation. Upon analysis of the ΔG values of the p52/RPL11 predicted structure and the solved MDM2/RPL11 structure, it can be seen that the former is almost twice as energetically feasible as the latter (Table 5.4). This suggests that p52 is able to competitively bind to RPL11 and form a stronger, more stable structure. It is important to note that the solved structure of RPL11/MDM2 utilises a section of MDM2 with a length of 148 residues (Zheng et al., 2015). This contains a RING finger domain of the protein. The full length of the MDM2 protein, however, is 491 residues. Therefore, it is possible that there are discrepancies in the ΔG value due to the difference in the length of the protein. Future studies could include the use of the full length structure of MDM2 and dock the protein to RPL11 in order to study any differences in the binding free energy.

5.3.3. First 100 amino acids of p52 predicted to be critical for interaction

The use of a panel of protein interface predictors allowed the subsequent prediction of the RPL11/p52 complex to be more robust when used in tandem with the data-driven docking

style of the HADDOCK software (Figure 5.2 and Figure 5.7). Following this, the location of the critical region of p52 driving the interaction was found by creating an *in silico* truncation series. Initially, the protein was truncated to leave the N terminal domain of the Rel Homology Domain (RHD) intact (Figure 5.5). The RHD is highly conserved across the NF-κB subunits and is the site of specific DNA binding capabilities, as well as dimer formation (Williams and Gilmore, 2020). A series of truncations were created starting with the removal of the dimerization domain, called the p52-227-C truncation. It became clear that the RHD played a role in the interaction as no major differences were seen between the wild-type structure and the structure involving p52-227-C. This was supported by the insignificant change in the ΔG suggesting no change in binding affinity (Table 5.4). A portion of the RHD is responsible for DNA binding. The data predicts the ability of p52 to bind RPL11 and DNA simultaneously, due to p52 being in the DNA bound form in the solved structure and no crossover being seen between RPL11 and the DNA binding residues. Further truncations were created to remove specific secondary structure elements from the RHD of p52 aimed to leave the DNA binding region intact. The p52-184-C truncation removed the connecting chain between the halves of the RHD and one of the β sheets in the barrel (Figure 5.5C). These residues were chosen to remove because the residues appear to contact the cleft of RPL11. The p52-140-C truncation removed the helix-loop-helix element, known as the insert region, to leave the N terminal end of the RHD (Figure 5.5D). Both the p52-184-C and p52-140-C truncations showed insignificant changes to the structure of the complex. They did, however, impact the ΔG value (Table 5.4). The smaller the value, the stronger the binding affinity (Vangone and Bonvin, 2017). It must be considered that deleting large numbers of residues within the protein will have an impact on the ΔG of the protein alone and therefore the docked complex created with it. It can be assumed that the increase in ΔG reflects the instability of the truncated protein itself as opposed to an impact on binding affinity.

Finally, it was decided to remove residues 37-100 amino acids (Figure 5.5E). The prior truncations showed the requirement to preserve the N terminus of the protein. The subsequent removal of residues in the N terminus of the protein confirmed this. RPL11 was forced to dock to another binding site of p52 known to be responsible for dimerization. The predicted binding free energy of the new complex was -13.1kcalmol^{-1}. Whilst this is less energetically feasible than the wild-type (-16kcalmol^{-1}) and caused a change of greater than 2 kcalmol^{-1}, it is still predicted to be more feasible than the solved MDM2/RPL11 interaction

(-8.4kcalmol^{-1}). Thus, the software may have provided an alternate binding site for RPL11 following the N terminal truncation in the N-100-p52 structure. It is known that NF-κB forms homo- and heterodimers in the cell. No subunit will exist without a partner (Perkins, 2012). Therefore, it is highly unlikely that RPL11 would be able to bind to p52 in the location seen in Figure 5.9D.

With the removal of the first 100 amino acids causing a dramatic change in the binding interface, it reinforces that the region involved in DNA binding activity is the preferred site of interaction. From this, it can be hypothesised that the interaction could have an influence on DNA binding activity of p52. Whilst modelling this *in silico* is not possible, the influence of the interaction on DNA binding can be explored in the laboratory.

The simulated truncation series performed in Figure 5.6 and 5.9 were aimed to mirror the truncations of recombinant proteins performed by wet-lab scientists. There are pros and cons to both methods of investigation. In the laboratory, this type of study relies upon the expression of proteins using host organisms, such as *Escherichia coli*. There are many pitfalls facing recombinant protein expression, namely protein insolubility, incorrect folding, toxicity and instability (Walls and Loughran, 2011). These are, of course, detrimental to the study leading to long periods of optimisation faced by scientists. Many scientists turn to using fusion protein tags to decrease the likelihood of such setbacks. Using Chimera, however, it is possible to map endogenous truncation series. Furthermore, it is possible to make deletions that would require high level of skill and optimisation to execute in the laboratory – such as deletion in the middle of the amino acid sequence. The deletion of amino acids in Chimera does not impact the overall structure of the protein as the software relies on the static PDB structure (Pettersen et al., 2021). The use of *in silico* techniques in this chapter allowed conformational changes to downstream docking runs to be effected by the deletions alone, rather than the impact on protein folding. It is important to note that *in silico* modelling is only a prediction and must be followed by wet-lab assays. This technique, however, is able to remove the need for a scientist to perform lengthy truncation series in order to locate regions of interest within proteins.

5.3.4. E86 residue predicted to be top candidate for wet-lab mutagenesis

The discovery that the first 100 amino acids of the RHD are predicted to be critical for the p52/RPL11 interaction enabled a more focussed approach to designing mutants. In order to shortlist residues for mutagenesis, the list of predicted hydrogen bonds within the wild-type

complex was consulted. Three residues within the first 100 amino acids were predicted to form bonds and were therefore selected as targets.

Aspartic acid 94 of p52 was predicted to form a hydrogen bond with Cysteine 150 of RPL11 (Table 5.2). It was decided to change the aspartic acid residue to alanine prior to the docking run to remove the negatively charged carboxylic acid side chain. The impact of the removal of the negative charge caused a rotational shift in RPL11 binding interface. The ΔG value increased by 3.5kcalmol^{-1} (Table 5.5). In comparison to the other residues, the D94A mutation made the least impact on the conformation of the complex, however is still predicted to be within the hotspot region of the protein-protein interaction due to causing an increase in the free binding energy by more than 2 kcalmol^{-1}. There remained a large overlap in binding interface between the D94A mutant and the wild-type complex.

Lysine 90 of p52 was predicted to form a hydrogen bond with alanine 142 of RPL11 (Table 5.1). An amino acid change of lysine to glutamic acid was created to simulate a change from a positively charged and basic amino acid, to a negatively charged and acidic amino acid. For comparison, a less dramatic change was made, showing an amino acid change of lysine to asparagine removing the basic side group of lysine and replacing it with a neutral amide group. The K90N mutation increased the predicted ΔG value of the p52/RPL11 complex by a higher degree than the K90E mutation. The value increased by 3.7kcalmol^{-1} and 3.0kcalmol^{-1}, respectively (Table 5.5). Both mutations caused a similar rotational conformational change as seen in the D94A mutant (Figure 5.10). Whilst the mutations led to noticeable changes in the formation of the complex, the changes were possibly insignificant to predict the loss of the interaction. Furthermore, it was discovered that SUMOylation of K90 of p52 is critical for the phosphorylation and subsequent proteasomal processing of p52 to p100 (Vatsyayan et al., 2008). It must be considered that creating a mutation at this residue and introducing said mutation into human cell lines could make a significant repercussion upon downstream signalling. A D94 mutant could possibly cause impairment to p100 processing leaving the non-canonical pathway inactive. More specifically to this study, this would make the study of the interaction between p52 and RPL11 virtually impossible.

Finally, glutamic acid 86 was predicted to form a hydrogen bond with Lysine 19 of RPL11 (Table 5.2). Simulations of E86 mutated to both glutamic acid and alanine were performed. The E86A mutation would neutralise the charge of the residue, removing the negatively charged acidic side chain. Changing the residue to glutamine would also neutralise the

charge of the amino acid replacing the oxygen of the carboxylic acid group with an amide side chain. E86A and E86Q both increased the ΔG value by 5.0kcalmol^{-1} and 3.9kcalmol^{-1}, respectively. The E86A mutation caused the largest increase, and therefore the best disruption to the energetic stability of the p52/RPL11 complex. Both mutations shifted the binding site of RPL11 to the helix-loop-helix of p52, rather than the beta barrel shoulder of the protein (Figure 5.10). The truncations performed in Figure 5.5 showed that the helix-loop-helix was insignificant in the interaction between RPL11 and p52. Further investigation showed 15 publications referencing post translational modifications on K19 of RPL11, which contacts E86. 14 publications identify ubiquitylation of the site, and one details NEDDylation (Sundqvist et al., 2009). The Xirodimas laboratory have published several papers describing the effects that NEDDylation of lysine residues within RPL11 has on p53 activation (Mahata et al., 2012). It is proposed that treatment with the chemotherapy, Actinomycin D, leads to the rapid loss of NEDD8 from lysine residues. This includes lysine 19. The removal of the post translational modification allows RPL11 to bind to MDM2 leading to the activation of p53 and respective target genes. It should be noted that this study mutated all lysine residues on RPL11 to alanine simultaneously and did not identify K19 specifically (Sundqvist et al., 2009). It has been previously discussed that p52 and MDM2 are predicted to bind to RPL11 in the same region. If NEDDylation of lysine residues in RPL11 disrupts the interaction between RPL11 and MDM2, the same can be assumed of the p52/RPL11 interaction. This strengthens the argument that glutamic acid 86 of p52 is the strongest target site for the disruption of the RPL11/p52 complex.

Considering that the binding free energy prediction of the solved MDM2/RPL11 interaction is much less stable than that of the predicted p52-E86A/RPL11 interaction, it can be proposed that a mutation at this residue would cause RPL11 to bind to an entirely new binding site. Following the base change from glutamic acid to alanine, RPL11 contacts the helix-loop-helix of p52. This region of p52 is still within the Rel Homology Domain and is not documented to make any other contact. Therefore, unlike RPL11 binding to the dimerisation domain, this new interface is feasible. The helix-loop-helix that the E86 mutants bind to is known as the insert region (Cramer et al., 1997). This secondary structure element is predicted to bind to DNA binding proteins further suggesting the link between the p52/RPL11 complex and DNA binding activity of p52. This does, however, highlight another limitation to the molecular docking software. A protein complex will always be returned despite the ability to form in

nature. Equally, as discussed previously, the vast difference in binding free energy calculation could be due to the incomplete structure of the RPL11/MDM2 complex utilised to solve the protein structure. This solidifies the importance of follow up experimentation being carried out in the wet-laboratory to validate mutations studied in *in silico* modelling.

5.3.5. HADDOCK software most beneficial for predicting RPL11/p52 interface

Initially, the GRAMM-X software was utilised to dock the entire 5S RNP to a p52 homodimer (Figure 5.3). This software was used due to needing special access to use the higher-powered level of HADDOCK needed to predict multi-protein complex formation (van Zundert et al., 2016). Whilst the RPL11/p52 interface appears similar between the GRAMM-X and the HADDOCK software, further analysis revealed the HADDOCK predicted interaction to be more feasible (Table 5.3). Firstly, the ΔG value of the HADDOCK complex was predicted to be -16kcalmol^{-1} whereas the GRAMM-X prediction was measured to be almost half as energetically feasible (-7.8 kcalmol^{-1}). Furthermore, steric clashes predicted in the GRAMM-X complex were eliminated in the HADDOCK complex, rendering the GRAMM-X complex less feasible in a structural sense. However, it must be noted that online docking software only takes into consideration the static structure of the complex. It has been discussed that dramatic conformational changes occur when RPL11 binds to MDM2 (Zheng et al., 2015). Therefore, it must be considered that the 5S RNP would undergo significant conformational changes in the ribosome bound and ribosome free states. This would not be accounted for in the GRAMM-X software as the structure of the 5S RNP utilised in the docking run was extracted from the solved structure of the 80S ribosome. This could have contributed to the number of clashes seen in the predicted 5S RNP/p52 homodimer complex.

Following the attempt of the truncation series using GRAMM-X it became clear that the software was prioritising the RPL5/p52 interaction over the RPL11/p52 interaction. This was recognised due to the RPL5/RPL11 complex remaining the same, due to the static nature of the software, alongside RPL11 not being involved in the interface within the predicted complexes. It can be seen in Figure 5.6 that GRAMM-X is prioritising RPL5 binding. This, however, contradicts unpublished laboratory data generated by Dr Alessio Iannetti during an unbiased proteomics screen. Dr Iannetti searched for binding partners of GFP-tagged p52 and found RPL11 present in the screen. Furthermore, in a tandem mass spectrometry assay performed by the Superti-Furga laboratory, the RPL11 and p52 interaction was captured. There is no data recognising the interaction between RPL5 and p52. Whilst in Chapter 4 the

co-immunpreciptation performed demonstrated an association between RPL5 and GFP-tagged p52, this was not shown to be repeatable. Hence, the critical element of the 5S RNP that is contacted p52 is RPL11, highlighting the importance of docking software to orientate the interaction around the p52/RPL11 interface. It was decided GRAMM-X was not suitable for the investigation and HADDOCK was utilised. GRAMM-X utilises *ab initio* searches, relying on databases alone. Due to HADDOCK's data driven format, it was possible to ensure RPL11 was the priority and known interface contributing residues were utilised.

Chapter 6   Analysing the Impact of p52 Mutations Generated by *In Silico* Modelling

6.1. Introduction

6.1.1.   Protein conformational changes and DNA binding

Proteins are dynamic molecules, therefore it is unsurprising that they undergo significant conformational changes when bound to DNA (Mizuguchi and Ahmad, 2014). A DNA binding protein is required to bind to specific loci on DNA and locate binding sites amongst the entire genome (Halford and Marko, 2004). DNA is a negative molecule, therefore makes contact with positively charged amino acids (Radaeva et al., 2021). This can contribute to conformational changes of proteins during DNA binding. A wide-scale analysis of DNA binding proteins, and the subsequent conformational changes occurring, revealed these structural changes impact the stability of the protein-DNA complex (Mizuguchi and Ahmad, 2014). The analysis showed that conformational changes affect the downstream consequences of the protein-DNA interaction, such as which target genes are regulated. It was determined that the larger the conformational change detected, the more stable the protein-DNA complex. Interestingly, an early study into the conformational changes of p53 upon DNA binding suggested large changes to the protein structure (Halazonetis et al., 1993). Utilising a monoclonal antibody targeting the p53 protein, it was found that the antibody was unable to bind with p53 in a DNA bound state. Therefore, it was suggested that p53 changes conformation at both the N and C terminal ends of the protein. More recently, the DNA binding domain of p53 (p53-DBD) was analysed (Bhattacharjee et al., 2021). The DNA binding domain of p53 is not only capable of making protein-DNA contacts, but also protein-protein interactions. Therefore, through the use of relaxation dispersion NMR techniques, the presence of differential conformational states of the p53-DBD were investigated. The study demonstrated that a conformational change occurred when p53-DBD was in the DNA bound state. Further, it was determined that the DNA-bound conformation allowed the p53-DBD to contact an increased number of partner proteins. Therefore, the conformation adopted by a protein in a DNA bound state could reveal previously inaccessible interaction sites that allow further functional effects.

The growth of techniques available to measure conformational changes and DNA-protein interactions has allowed researchers to design drugs to target these types of interactions (Radaeva et al., 2021). Transcription factors make up the largest group of DNA binding proteins. Mutated transcription factors, such as p53 and NF-κB, are known to contribute to various diseases, including cancer (Lee and Young, 2013). Computer software, alongside improved experimental techniques, have identified drugs that target the previously deemed 'undruggable' interactions (Radaeva et al., 2021). The signal transducer and activator of transcription (STAT) family of transcription factors regulate cellular growth, differentiation, immunity and apoptosis (Verhoeven et al., 2020). Virtual screening programmes aided researchers to identify a compound capable of specifically binding and inhibiting STAT3-DNA interactions (Huang et al., 2014, Radaeva et al., 2021). After screening over 20,000 molecules, the software was able to isolate 57 potential candidates that would not also bind to other STAT family members. Of those, InS3-54 was predicted to be specific to STAT3 via molecular dynamics simulations. Further, the compound was determined to be the most active compared to others in the screen via luciferase assay. Therefore, the compound was tested in lung and breast cancer cell lines. InS3-54 treatment induced apoptosis as well as decreasing cell migration and invasion.

Protein-DNA interactions are difficult to target therapeutically due to the reliance on positively charged residues to mediate direct contact with the negative DNA, that the interfaces rely upon many points of contact, and they are solvent exposed (Radaeva et al., 2021). Often drugs that target transcription factors are accompanied by significant adverse effects. It is likely this is due to off-target effects (Fortune and Osheroff, 2000, Quaglio et al., 2020).

Whilst artificial intelligence and machine learning algorithms are providing an important tool for the study of DNA binding induced conformational changes, this relies upon solved crystal structures of proteins in their bound and unbound states (Radaeva et al., 2021). The issue that scientists are currently facing is that not many structures of DNA binding proteins have been solved in their unbound state. This could be as the addition of DNA stabilises the structure of the protein. As this field continues to grow with the increased capabilities of scientists to solve protein structure, there is the potential to grow the library of solved structures of unbound DNA-binding proteins.

6.1.2. Conformational changes in NF-κB during DNA binding

An early study was performed to investigate the conformational changes that occur in response to NF-κB/DNA interactions. The study utilised proteases, which are enzymes that cleave proteins at specific loci. The researchers monitored the accessibility of the cleavage sites in the unbound and DNA bound states (Matthews et al., 1995). Cleavage was followed by circular dichroism, a type of spectroscopy used to measure the type and abundance of secondary structure elements in a sample (Greenfield, 2006). In the absence of DNA, the DNA binding domain within NF-κB was cleaved by the proteases, however when bound to DNA the accessibility to the site was lost. Circular dichroism was able to determine conformational changes in both the p50 and p65 subunits bound to κB sites with a high affinity (Matthews et al., 1995). A few years later, Perkins *et al* published the interaction between the p65 subunit and Specificity protein 1 (Sp1) (Perkins et al., 1994). Sp1 is a transcription factor that activates genes that contain GC-rich binding sites in promoter regions, functioning to regulate genes involved in cellular proliferation and metastasis in cancer cells (Vizcaíno et al., 2015). However, to capture the interaction via GST pulldown, it was necessary to introduce DNA oligos into the reaction (Perkins et al., 1994). Both the preferred RelA κB site and the Sp1 site was added to the reaction mixture. This suggests a conformational change occurs within the proteins upon DNA binding to allow for further protein-protein interactions. This result reveals a similar mechanism to the paper described previously detailing the conformational change within the DNA binding domain of the p53 transcription factor (Bhattacharjee et al., 2021). Therefore, DNA binding could be a mechanism by which transcription factors regulate their interactions with partner proteins.

6.2. Results

6.2.1. Generation of mutant p52 proteins

The *in silico* analysis performed in Chapter 5 predicted glutamate 86 of p52 as a critical residue within the p52/RPL11 interface. Further, a point mutation of glutamate 86 to alanine was predicted to create a novel binding site with a lower energetic feasibility compared to wild-type (Figure 5.10 and Table 5.5). To investigate the impact of the glutamate 86 to alanine (E86A) amino acid change within the p52 protein, the mutation needed to be introduced into the GFP-p52 mammalian expression plasmid. This was achieved by designing a short strand of double stranded DNA (gBlock) to be synthesised. In order to design the mutated DNA, the plasmid backbone was studied (Figure 6.1A). The pEGFP-C2-p52 plasmid

was used as the expression plasmid and the mutant DNA strand inserted using restriction enzyme technology.

Following restriction enzyme digestion using HindIII and Kpn2I, the DNA was analysed using agarose gel electrophoresis. The agarose gel showed two distinct bands of DNA, at roughly 5000 base pairs and 1000 base pairs. During design, additional bases either side of the desired gBlock were included during synthesis. This was to allow for the creation of the sticky ends following restriction enzyme digest, allowing for subsequent ligation. To isolate the desired DNA sequence from the gBlock, the same restriction enzymes were used followed by agarose gel electrophoresis (Figure 6.1B). The mutant insert DNA from the gBlock and the 5000 base pair DNA band following plasmid digestion was excised, extracted and ligated. The ligation mixture was used to transform bacteria. Upon successful colony formation an individual colony was isolated and grown in order to extract mutant DNA. To check that the mutation was present, an identical restriction enzyme digest was performed. Subsequently, the DNA was analysed via agarose gel electrophoresis determining DNA fragments of the appropriate sized fragments were present (Figure 6.1C). Finally, Sanger Sequencing was used to confirm the successful introduction of the mutated DNA strand. The glutamate GAG codon was changed to alanine, GCG (Figure 6.1D).

A) pEGFP-C2-p52 plasmid backbone
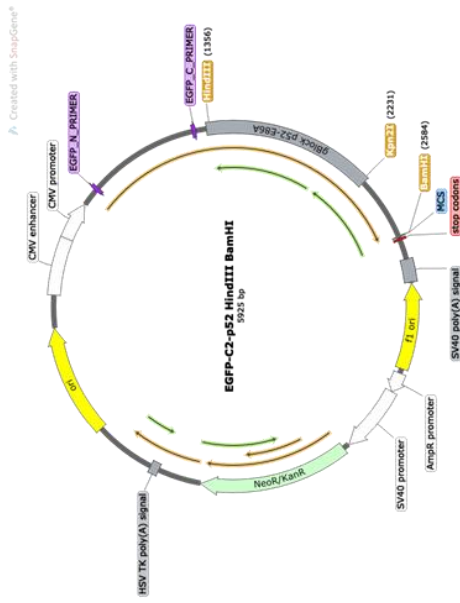
B)
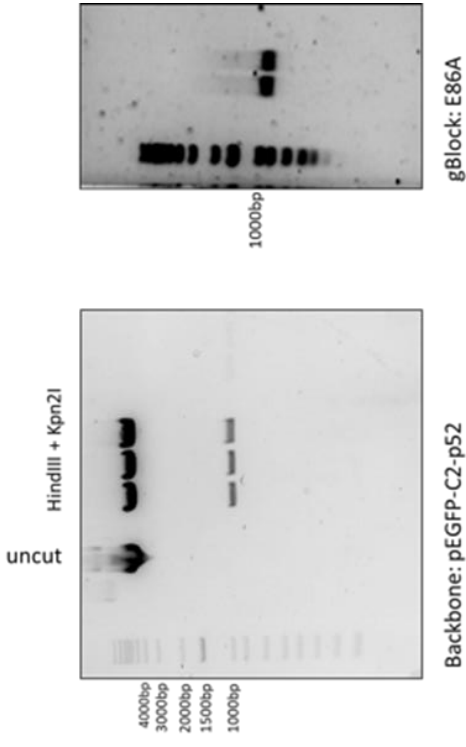
C) Ligated mutant plasmid DNA + HindIII + Kpn2I
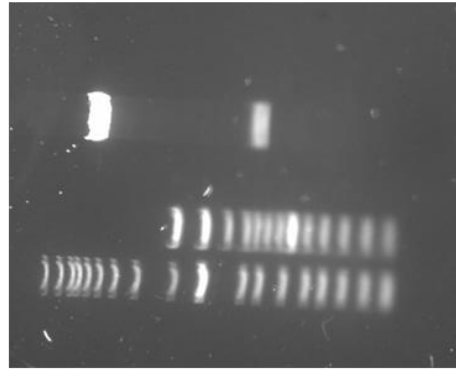
D) DNA trace of sequenced mutant plasmid DNA
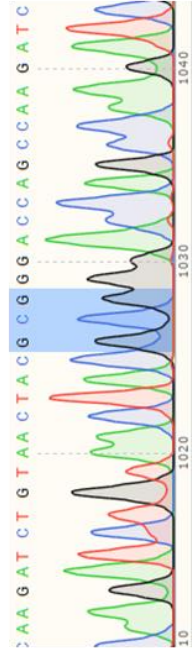
Figure 6. 1 Creation of the GFP-p52-E86A plasmid. A) The plasmid backbone of the pEGFP-C2-p52 plasmid. The wild-type p52 DNA sequence was originally cloned in using restriction enzymes, HindIII and BamHI. To insert the mutated DNA sequence, HindIII and Kpn2I restriction enzyme sites were used. B) Restriction enzyme cleavage of the plasmid backbone (left) and the dsDNA gBlock (right). Following digests DNA was run on a 1.5% agarose gel supplemented with SYBR-SAFE. C) Successfully grown p52-E86A-GFP *E. Coli* colony was subject to DNA extraction. Subsequently, DNA was digested using the HindIII and Kpn2I restriction enzymes prior to analysis on a 1.5% agarose gel. D) Sanger sequencing was using to confirm the successful insertion of the alanine codon at position 86. The GCG codon is highlighted.

6.2.2. Assessing stability of mutants

The previous figure confirmed that the mutant DNA strand was successfully inserted into the pEGFP-C2-p52 plasmid. Next, the mutant plasmid was transfected into human cell lines, U2-OS and HCT116. Mutant forms of proteins are not always well tolerated by the host cell. Therefore, the presence and stability of p52 with an E86A mutation was tested in U2-OS and HCT116 cells via western blotting. U2-OS and HCT116 cells were cultured, transfected with increasing amounts of GFP-p52 or GFP-p52-E86A plasmid DNA and harvested. Protein extraction was performed using PhosphoSafe.

Regardless of the cell line, less GFP-p52-E86A protein was detected in comparison to the wild-type (Figure 6.2A). This could indicates that either p52-E86A is less stable than wild type p52 and degraded, that there is a lack of expression from the plasmid following transfection or that the mutant protein was not efficiently extracted from cells by the PhosphoSafe buffer. Further, the western blot suggested that the HCT116 cell line tolerated the introduction of the mutant p52 plasmid better than the U2-OS cell line as more GFP-p52-E86A protein was detected in comparison to GFP-p52. Therefore, it was decided that the HCT116 cell line would be used for subsequent investigations.

It was also considered whether the decrease in presence of GFP-p52-E86A compared to GFP-p52 in the HCT116 cell lines was not due to degradation, but translocation of the protein. The extraction buffer used has a preference for extracting cytosolic proteins. Following the addition of the protein lysis buffer, cells are centrifuged at a high speed to pellet insoluble proteins as well as other unwanted cellular components. Therefore, the pellets following extraction were sonicated in 2 X Laemlli buffer and samples analysed via western blotting to visualise the protein content. It was seen that both GFP-p52 and GFP-p52-E86A was present in the pellets following cytosolic protein extraction (Figure 6.2B). Despite this, there was still less GFP-p52-E86A protein presence in the pellet analysis compared to GFP-p52. This suggests an issue with the stability of the mutant protein.
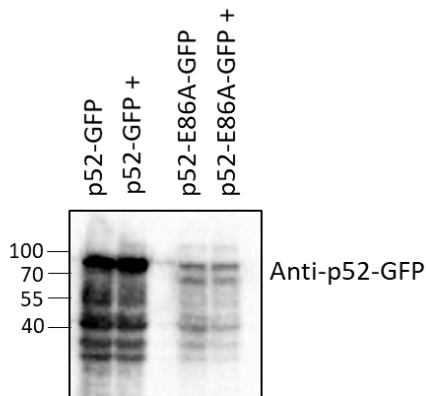
Figure 6.2 Assessing the stability of the GFP-p52-E86A protein in human cancer cell lines. A) Cell lines (as indicated) were transiently transfected with p52-GFP or p52-E86A-GFP. Cytosolic proteins were extracted using PhosoSafe lysis buffer. Following the addition of the lysis buffer, lysates were spun at a high speed to pellet nuclear, membrane associated and chromatin associated proteins. The supernatant was analysed via western blotting, developed using a BioRad ChemiDoc. B) Cell pellets described previously were boiled in 2 x Laemlli buffer prior to western blot analysis. The BioRad ChemiDoc was utilised.

6.2.3. GFP-p52-E86A associates with RPL11

A co-immunoprecipitation was performed to assess the ability of the p52-E86A mutant to bind to RPL11. To encourage the extraction of a higher concentration of nuclear proteins, alongside cytoplasmic, the salt (NaCl) concentration of the lysis buffer was increased. Increasing the NaCl concentration allows disrupts protein: DNA interactions permitting more complete nuclear protein extraction. Finally, HCT116 cells were used due to the higher presence of the mutant protein following transfection. Cells were transiently transfected with plasmids as described in the figure. Protein was extracted and GFP proteins isolated utilising the GFP Trap system. Complexes were analysed via western blotting.

The initial observation was that the input GFP-p52 sample in the cells transfected with the mutant plasmid was lower than that of the wild type p52 plasmid (Figure 6.3). The immunoprecipitation showed that p52-E86A was able to associate with RPL11. Whilst a much weaker RPL11 band is present in the p52-E86A untreated immunoprecipitation, it appeared an air bubble was transferred onto the membrane. Considering that the input sample was lower in the mutant plasmid samples, it could be suggested that the point mutation enhanced binding to RPL11. This contradicts the *in silico* modelling performed in Chapter 5.
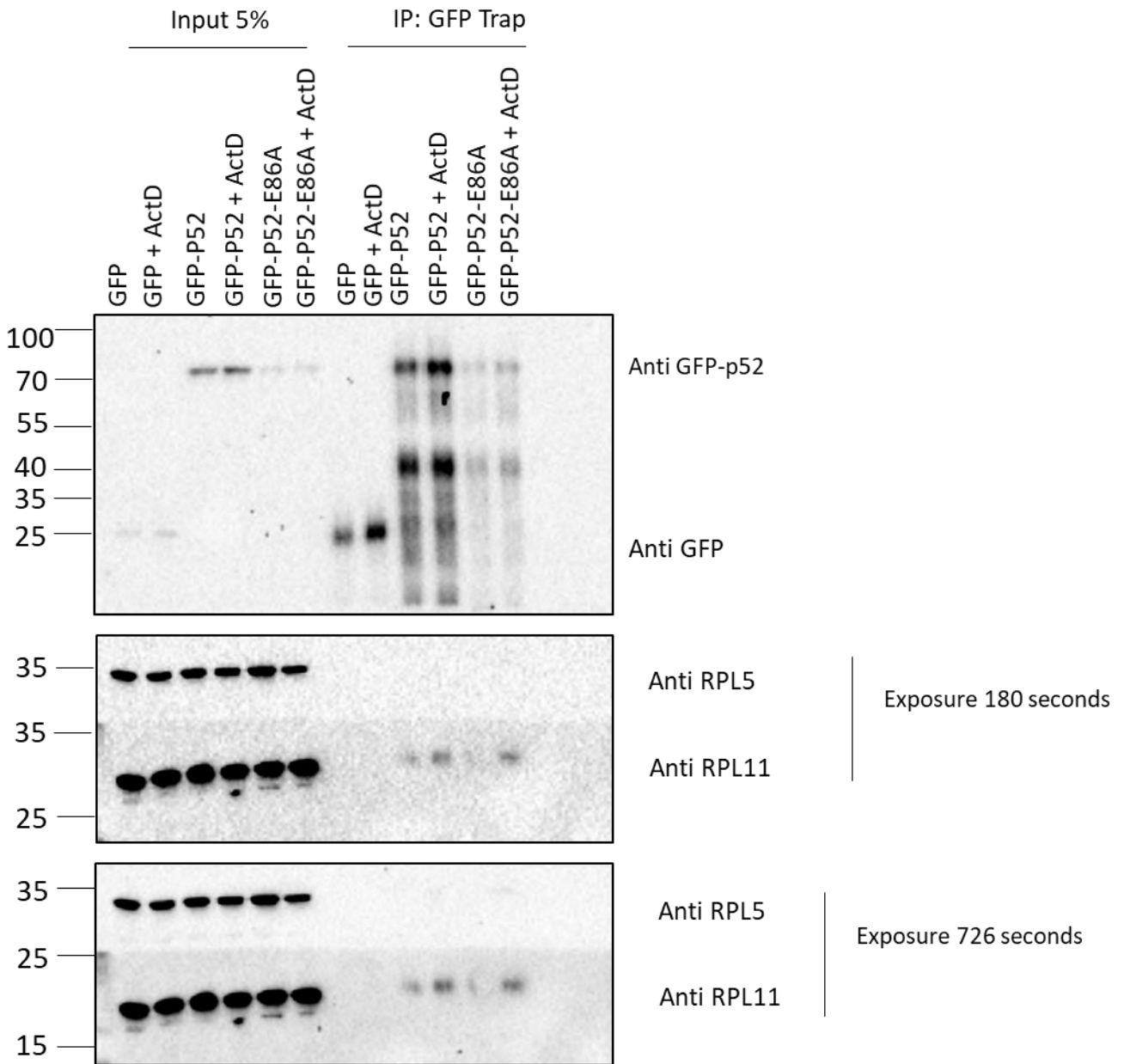
Figure 6.3 GFP-p52-E86A associates with RPL11. Co-immunprecipitation analysis was performed using HCT116 cells transiently transfected with p52-GFP and p52-E86-GFP. Western blotting analysis was subsequently performed and developed using a BioRad ChemiDoc.

6.2.4. Analysing the impact of the p52-E86A mutation on p52/RPL11 interaction in a DNA-bound state

Since the p52-E86A mutation was still capable of binding to RPL11 in cell lysates, it was important to return to the *in silico* modelling to reassess the structural analysis to see if an explanation could be provided. Whilst there are several PDB structures available for p52 homodimers, and the RelB-p52 heterodimer, they all display p52 in a DNA bound state, which was the structure used to model the interaction with RPL11. It became important to consider the conformational changes accompanied by protein-DNA contacts. Using the software, Chimera, the predicted structure of the p52-E86A/RPL11 complex was superimposed with its DNA binding site (Figure 6.4). The structure suggests that a DNA bound state would significantly impact the influence that residue 86 of p52 has on the complex. This is because interactions with DNA would likely change the overall conformation of the p52 dimer, and potentially the stability of the dimer. Furthermore, if a p52 homodimer was facilitating the p52/RPL11 complex, binding of DNA could change the accessibility of the RPL11 binding site due to other protein-protein interactions. An example would be binding of transcriptional cofactors. The prediction showed that the single amino acid change caused RPL11 to bind to the insert region (the helix-loop-helix domain) of p52-E86A. This is a different binding site in comparison to the original site on the wild-type p52 protein shown in Figure 6.4, in which RPL11 binds over the location of residue E86. The linker region is known to have a degree of flexibility to allow for DNA binding capabilities, as documented in Cramer *et al*. Thus, it was important to test the p52-E86A/RPL11 association in a DNA bound state.

p52/RPL11 predicted complex

p52/RPL11 predicted complex superimposed with DNA

p52-E86A/RPL11 predicted complex

p52-E86A/RPL11 predicted complex superimposed with DNA
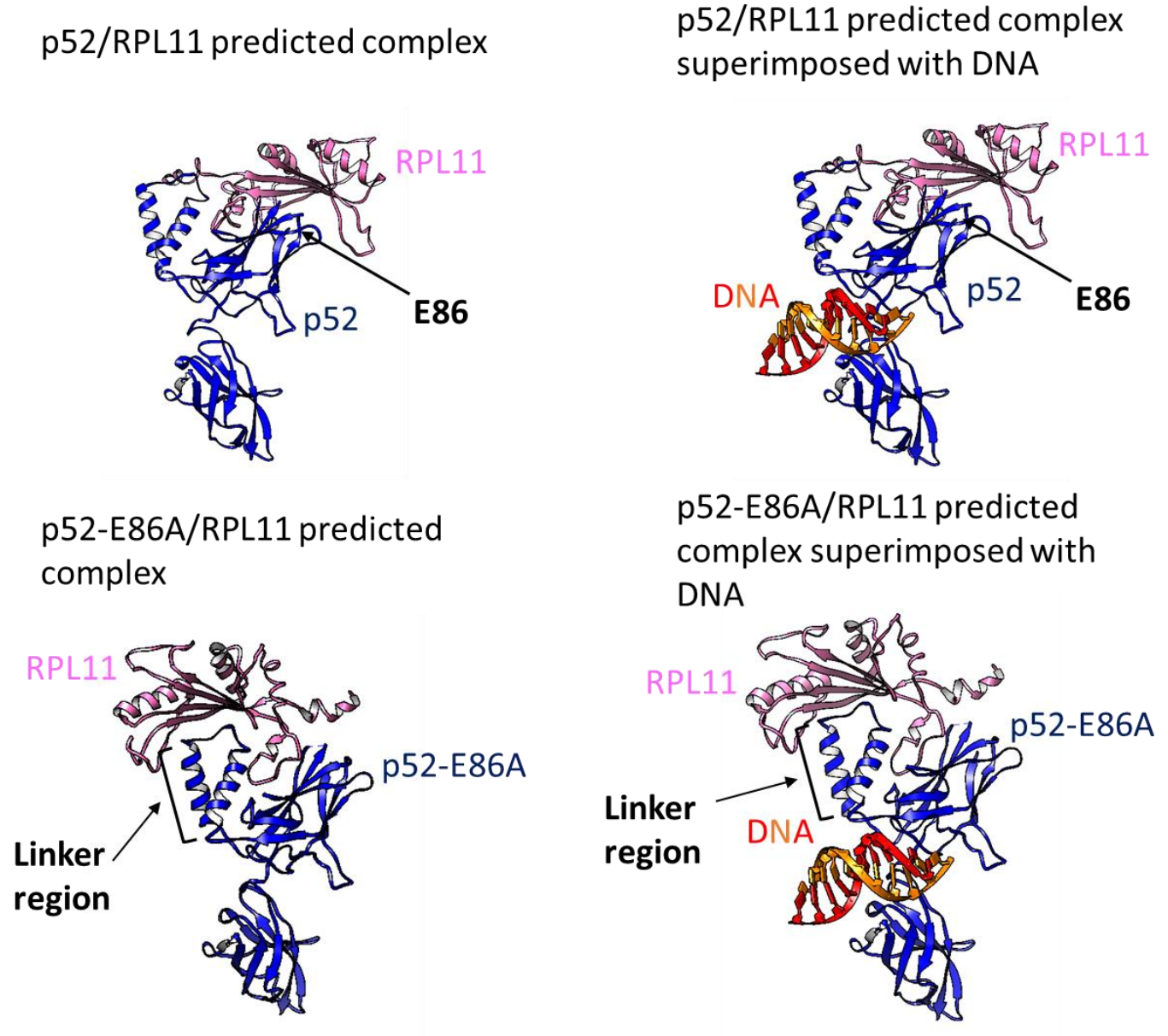
Figure 6.4 Analysis of the impact of DNA binding on the predicted p52-E86A/RPL11 structure. Structures were produced through *in silico* analysis of the p52/RPL11 and p52-E86A/RPL11 interactions. Predicted complexes were superimposed DNA from the solved crystal structure of a p52 homodimer bound to DNA (PDB ID: 1A3Q)

Further co-immunoprecipitation analysis was performed as described previously. Initially, during the incubation of the protein lysates and GFP Trap beads to isolate complexes, 20ng of a known p52 κB site was added for 90 minutes prior to elution. This was followed by a western blot. As seen in Figure 6.5A, the p52-E86A protein was capable of binding to RPL11. However, following the addition of the κB site oligo, the association between the proteins was decreased. Interestingly, in the wild-type p52 immunoprecipitation reactions, the addition of the DNA oligo appeared to enhance the binding of p52 to RPL11 (Figure 6.5A). This suggests that DNA plays an important role in this association.

Finally, to further investigate the impact that the κB site makes upon the interaction, 500ng of the DNA oligo was added overnight (Figure 6.5B). This was performed to overwhelm the lysate with DNA and encourage as many p52 molecules as possible to be in a DNA bound state. Similarly, the addition of DNA enhanced the association of GFP-p52 with RPL11. In the GFP-p52-E86A samples, the association with RPL11 was initially captured both in ActD treated and untreated samples. However, with the addition of DNA the complex was only captured when the cells were untreated. Following ActD treatment, the association of p52-E86A and RPL11 was virtually undetectable. Therefore, this strongly suggests that the E86 residue plays an important role during the interaction between RPL11 and p52 in the DNA bound state. Further, the enhancement of the p52/RPL11 interaction with the addition of a known κB oligo suggests a critical role of p52's DNA binding capabilities within the response to nucleolar stress.
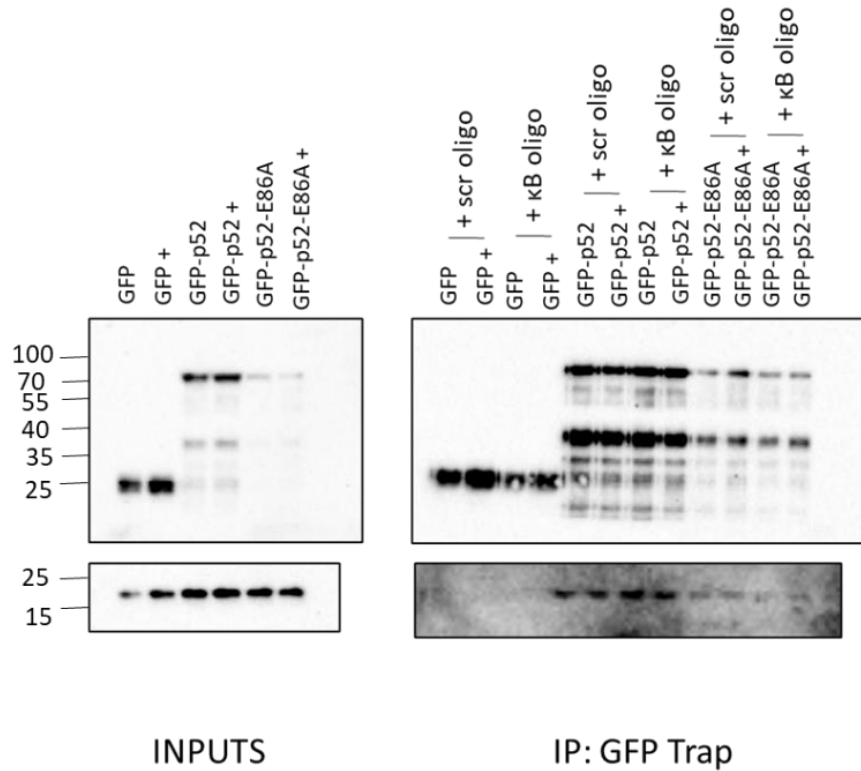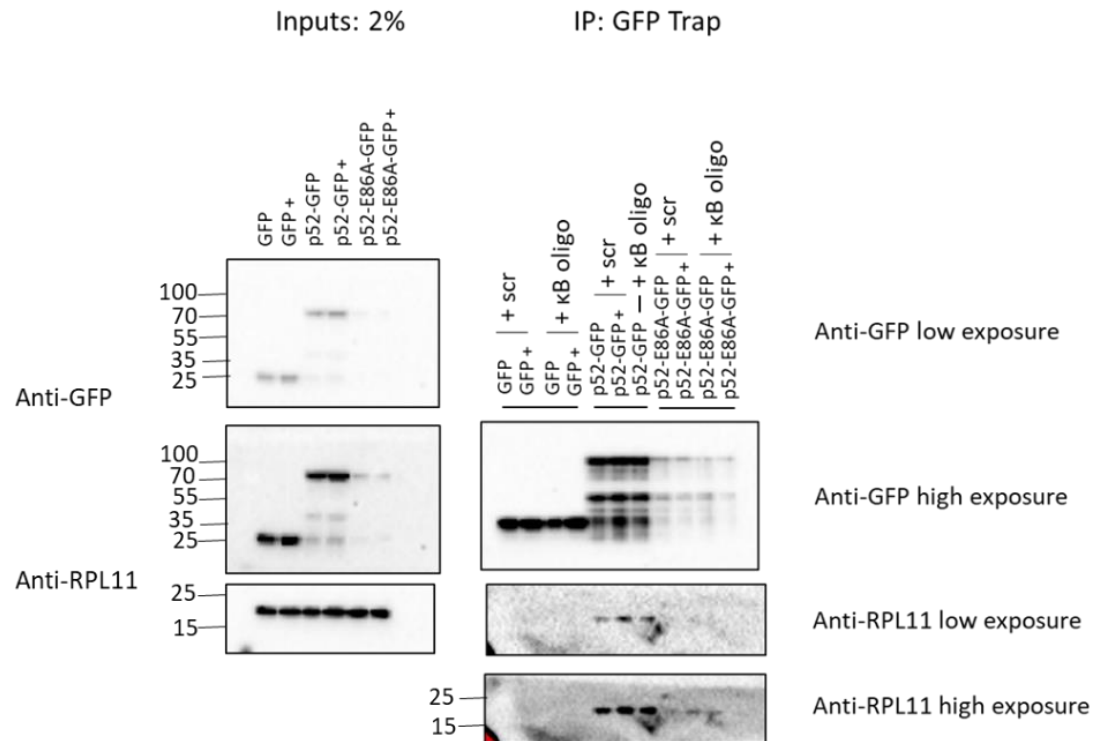
Figure 6.5 Introduction of a p52 κB site into co-immunoprecipitation experiment weakens the p52-E86A/RPL11 interaction but enhances the p52/RPL11 interaction. Co-immunoprecipitation analysis was performed on HCT116 cells transiently transfected as indicated in figure. The protein lysates were incubated with GFP-TRAP beads in the presence of known p52 κB site DNA (MHC-κB DNA), as indicated in figure. 'GFP+' or 'GFP-p52+' indicates the use of ActD treatment to stimulate ribosomal stress. ActD was added for 5 hours prior to harvest. Figure B is missing the GFP-p52 + ActD + κB oligo IP sample.

6.3. Discussion

6.3.1. Does the p52-E86A mutant impact cellular localisation of the protein?

Successful cloning of the p52-E86A mutant DNA sequence into the pEGFP-C2 plasmid backbone led to the assessment of the protein's stability in human cancer cell lines (Figure 6.2). This analysis demonstrated decreased presence of GFP-p52-E86A, in comparison to GFP-p52, following transient transfection. In comparison to the HCT116 cell line, the U2-OS cell line contained even less GFP-p52-E86A, suggesting the U2OS cell line was less tolerant of the mutant p52 protein (Figure 6.2A). The U2-OS cell line is known to rely on the p52 protein for cellular proliferation (Schumm, 2006). Therefore, the cell line could be less tolerant of the mutant p52 protein due to the reliance upon wild-type p52 to maintain normal cellular functions.

Further analysis suggested presence of nuclear, membrane or chromatin bound GFP-p52 and GFP-p52-E86A in the HCT116 cells (Figure 6.2B). It is known that mutations within protein sequences has the capability to alter stability, cellular localisation or even protein folding (Baugh et al., 2018). Even in the pellets of the cytosolic protein lysates, GFP-p52-E86A was present at a lower abundance than p52-GFP. Therefore, it is more likely that the p52-E86A protein is less stable and less tolerated in the cell lines when compared to the wild-type. One possibility of the instability could be due to the importance of the NF-κB pathway, and the NF-κB subunits, within cell biology. Therefore, if intrinsic mechanisms detect a mutant p52 protein, the cell could degrade the protein. Alternatively, the codon used during the gBlock design was GCG. This codon, coding for the amino acid alanine, is of the lowest frequency compared to other alanine codons (Quax et al., 2015). Further, the GCG codon is of a much lower frequency when compared to the original glutamate codon, GAG. This in turn can reflect tRNA abundance and thus influencing translation rates. Therefore, it is possible that p52-E86A is not translated as efficiently and an important future experiment would be to use a different alanine codon during gBlock design.

6.3.2. The relationship between the p52/RPL11 interaction and DNA binding

The initial co-immunoprecipitation performed demonstrated that the p52-E86A mutation was not sufficient to disrupt the interaction (Figure 6.3). In fact, considering the input samples it could be suggested that the mutation enhanced the interaction with RPL11.

As the p52 protein is a transcription factor, DNA binding is at the centre of the protein's function. Perkins *et al* in 1994 demonstrated that the introduction of a known κB site and Sp1 site in correct spacing and orientation to the lysate of a GST pulldown assay was necessary to capture the interaction between Sp1 and the RelA NF-κB subunit (Perkins et al., 1994). Therefore, both interacting transcription factors were required to be in the DNA bound state in order to capture the interaction. This is likely due to the conformational changes that occur when a protein binds to DNA. Therefore, the MHC-κB binding site was selected due to p52's high affinity for the site (Nijnik et al., 2003). Introduction of the κB DNA to the GFP-p52 immunoprecipitation enhanced the interaction with RPL11 in comparison to the scramble DNA (Figure 6.5). Therefore, it is suggested that p52's DNA binding activity is important for the role in the ribosomal stress response. It would be interesting to investigate the influence of a known p52 binding site within the promoter of p53 target genes, such as CCND1 encoding Cyclin D1, upon the GFP-p52/RPL11 interaction. Chromatin immunoprecipitation is a technique that measures protein-DNA interactions. It has been shown that p52 binds directly to the promoter region of p53 target genes, however indirectly via p53 to the promoter of CDKN1A (Schumm et al., 2006). It has also been shown that FLAG-tagged RPL11 is found at the promoter of CDKN1A in a p53-dependent manner (Mahata et al., 2012). This association is enhanced with ActD treatment. It could be hypothesised that if a supercomplex of p52/5S RNP/MDM2/p53 is forming, the entire complex could translocate to target genes to regulate expression. Further studies could involve measuring the dependency of RPL11 and p52 upon one another to be present at the promoter of CDKN1A. Furthermore, it would be interesting to investigate whether RPL11 is recruited to the promoter region of other p53 target genes that are known to be direct p52 target genes, such as cyclin D1.

The addition of MHC-κB DNA was sufficient to disrupt the interaction between GFP-p52-E86A and RPL11, particularly following ribosomal stress induction (Figure 6.5). This could possibly be due to a conformational change occurring during DNA binding of NF-κB subunits that changes the nature of subsequent protein-protein interactions, as alluded to by Perkins *et al* in 1994 (Perkins et al., 1994). The *in silico* modelling discussed in Chapter 5 predicted that the p52-E86A mutant would bind to the 'linker region' of the p52 protein (Cramer et al., 1997). This region is known for being modulated following DNA binding due to flexibility of the domain. Given the location of the p52-E86A/RPL11 interface, it can be hypothesised any

DNA binding induced conformational changes would impact the conformation of the linker region. The NF-κB dimers are known for adopting the 'butterfly structure' when bound to DNA (Cramer et al., 1997). This structure involves the DNA binding domain of the proteins surrounding DNA. It could be predicted that the linker region would move as a result of this (Figure 6.4). Therefore, as DNA is introduced into the co-immunoprecipitation, the p52 dimer would adopt the DNA bound conformation, potentially changing the accessibility of RPL11 to bind to the linker region of p52-E86A.

It is intriguing that κB DNA enhances the GFP-p52/RPL11 interaction but disrupts the GFP-p52-E86A/RPL11. This suggests any conformational changes within p52 that result from DNA binding strengthen the association between these proteins. This further highlights the importance of DNA binding within p52's role in the ribosomal stress response. This suggests that the RPL11/p52 complex may translocate to the promoter regions of target genes to modulate expression.

Chapter 7   Discussion

7.1. Introduction

Preliminary work produced by Dr Alessio Iannetti captured an association between the NF-κB subunit, p52, and RPL11 of the 5S RNP. This association was enhanced through stimulating ribosomal stress. Whilst the interaction had previously been captured by Dr Iannetti and documented within a proteomics study in 2004 (Bouwmeester et al., 2004), the purpose of the interaction had not been studied. In this thesis, I have investigated the role of the NF-κB subunit, p52, in the ribosomal stress response. I have further studied the interaction and shown that this is the driving force of the crosstalk between the NF-κB pathway and the 5S RNP/MDM2/p53 pathway, implicating a role for p52 in the ribosomal stress response. The data presented provides insight into a novel role for non-canonical NF-κB signalling, highlighting a tumour promoting role of p52, and this is independent of any signalling through the canonical pathway.

7.2. The emerging extra-ribosomal functions of the 5S RNP

In 2011 Malovannaya et al performed a large scale investigation into endogenous protein-protein interactions (Malovannaya et al., 2011). 3290 affinity purifications were performed from HeLa cells, a well studied cervical cancer cell line, and followed by mass spectrometry-based analysis. The NF-κB2 interactome was studied, and within that the interaction with RPL11 was identified. However, similarly to the results generated in Bouwmeester et al., an interaction with RPL5 was not captured (Bouwmeester et al., 2004). This further indicates that p52 interacts directly with RPL11, supporting the inconsistent association captured between GFP-p52 and RPL5 in Chapter 4. Whilst RPL11 itself was not immunoprecipitated by Malovannaya et al, the protein was identified as an interactor with many of the proteins that were directly investigated in the study. RPL5, on the other hand, was one of the proteins immunoprecipitated. The RPL11 interacting proteins and the RPL5 interacting proteins were cross referenced to generate a list of proteins that would represent 5S RNP interactors. The list of genes encoding predicted 5S RNP interactors was entered into the gProfiler webserver to classify the functional groups (Raudvere et al., 2019). Next, the functional groups were placed into 11 simplified categories. The total number of genes within each category was calculated and a pie chart generated (Figure 7.1). This allowed a visual representation of the

cellular processes that the 5S RNP is implicated within via crosstalk with other pathway members.

The data generated shows the two largest categories to be the DNA damage response (DDR) and the cell cycle. Therefore, it is predicted, outside of regular ribosomal functions the 5S RNP interacts with proteins involved in the two cellular processes. This supports the data generated in this thesis, which predicted the p52/RPL11 interaction to function within the DDR and cell survival in cancerous cells. Interestingly, the section relating to cells involved in cellular death is relatively small compared to others. Thus, further supporting that the 5S RNP-mediated activation of p53 does not favour apoptosis, but cell cycle arrest and subsequent DNA repair mechanisms (Lindström et al., 2022).
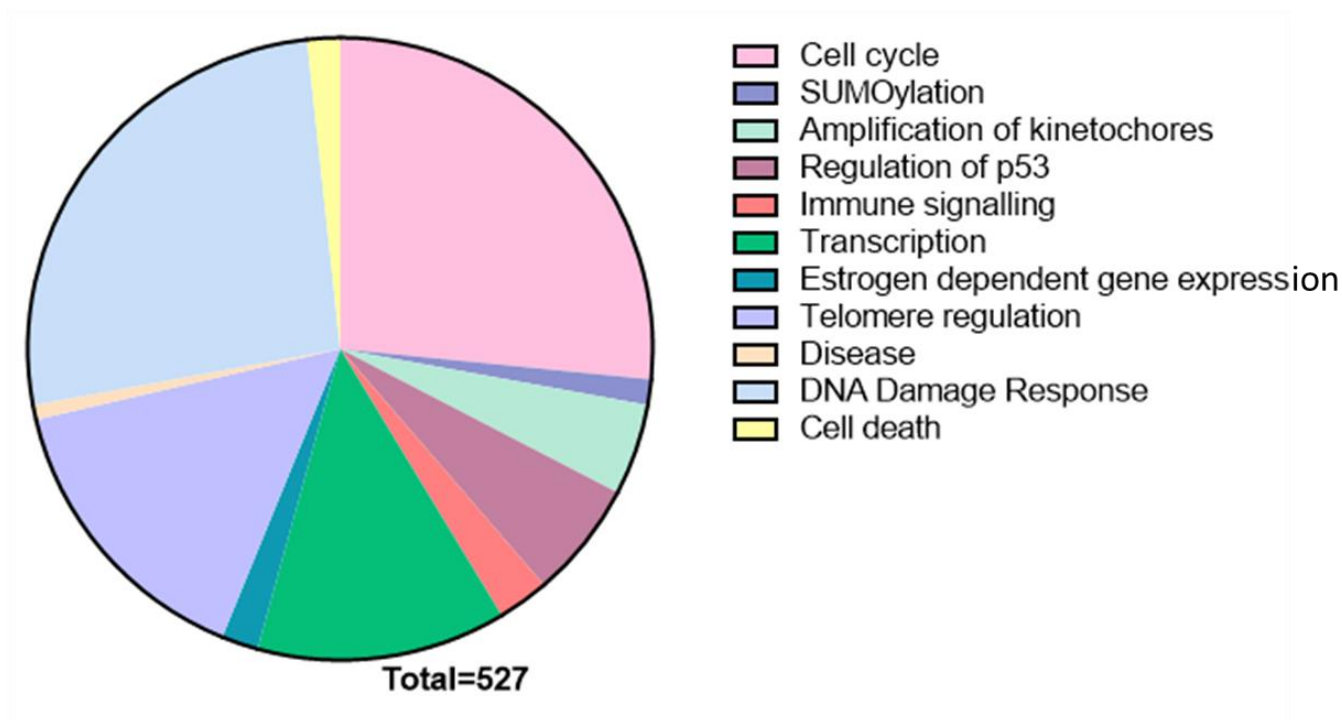
Figure 7.1 Proteins documented to interact with RPL5 and RPL11 from NURSA database. The list of interacting proteins were entered into gProfiler, a software performing functional enrichment analysis. The functional groups of the proteins were returned by the webserver. Following that, the proteins were further classified into 11 categories, detailed in the key. The total number of proteins was calculated per category and a pie chart created using GraphPad Prism 6.

7.3. p52 as a Tumour Promoter

The NF-κB family are a unique family of transcription factors through their ability to be both tumour suppressive and tumour promoting (Perkins and Gilmore, 2006). The subunits respond to the cellular environment and cellular stimuli to regulate specific subsets of target genes (Perkins, 2012). In particular, the p52 subunit has been associated with cancer cell proliferation. For example, elevated p52 protein presence in ovarian cancer cells has been linked to poor prognosis (Hufnagel et al., 2020). The data in this thesis suggests that direct interaction with RPL11 could be a mechanism by which p52 encourages cancer progression.

7.3.1. The link between p52 and cancer cell survival

The data presented in this thesis suggests that p52 plays a cell survival role in the response to ribosomal stress in cancer cell lines. The depletion of p52/p100 was sufficient to drive cell death following treatment with specific chemotherapeutic agents that cause ribosomal stress (Chapter 3). Conversely, the stable expression of GFP-p52 in U2-OS cells led to a lagged stabilisation of p53 in response to ribosomal stress. Interestingly, the p53 protein levels between GFP-p52 and GFP control cell lines were comparable by longer ActD time points, suggesting that p52 slows the response rather than having an inhibitory effect (Chapter 4). Temporal studies of p53 have shown that a slower response favours cell cycle arrest (Hafner et al., 2019). Whilst endogenous depletion of p52/p100 did not lead to increased p53 stabilisation, p53 activity and downstream signalling effects were found to increase. A cell survival relationship between p52 and p53 has been previously documented by the Perkins laboratory through the regulation of the gene, EZH2 (Iannetti et al., 2014). It was determined that p52/RelB heterodimers could suppress p53 activity through upregulation of the EZH2 gene. The study found that the repression of p53 activity led to a decline of p53-dependent senescence. The redirection of p53 activity through p52 dimer activity demonstrates the relationship between p52 and cell survival through the modulation of p53 activity.

It has been documented that p52 plays an important role in the regulation of cell cycle genes, such as genes encoding cyclin D1, and cell cycle inhibitor, p21 (Schumm et al., 2006). Therefore, p52 has been directly implicated in the regulation of cell cycle progression. Further, p52 has been linked to DNA damage repair pathways (Budke et al., 2022). The

increased cellular death markers seen in response to p52 depletion was accompanied by an increase in yH2AX, signifying double stranded DNA breaks (Podhorecka et al., 2010).

Moreover, the simultaneous increase in cell death and DNA damage coincided with the removal of cell cycle arrest markers (Chapter 3, Figure 3.12). In summary, cells lacking p52 and challenged with prolonged periods of ribosomal stress were progressing through rounds of cell cycles, possibly replicating DNA damage, thus leading to cell death. Together, these indicate that p52 has a role in quality control mechanisms within the cell cycle of U2-OS cells that contributes to cell survival.

Some similarities can be drawn between the *Nfkb2-/-* murine phenotype and the results shown in Chapter 3. The knockout mouse displays abnormal growth and development of the spleen and lymph nodes. This could be suggestive of an abnormal cell cycle and increased cellular death (Caamaño et al., 1998). On the other hand, a study showing that the p100 knockout mouse was resistant to LPS-mediated small intestinal apoptosis. The data presented in this chapter describe a context in which knocking down p100 leads to increased ActD stimulated cellular death (Papoutsopoulou et al., 2022). This therefore highlights the differences in the NF-κB response depending on cell type, cellular environment, and stimulus. Thus, the phenotype presented through this research could demonstrate a unique function of NF-κB biology which could have evolved with the onset of cancer.

p52/p100 is known to interact with proteins involved in mitosis (Ledoux et al., 2013). Research completed by Dr Katie Schumm suggested a role for p52 in mitosis, with depletion of the protein causing an increase in G2/M arrest and aberrant chromosome segregation (Schumm, 2006). This result was repeated in this study. I demonstrated that U2-OS cells transfected with a p52 siRNA could be dying through mitotic catastrophe when treated with ActD for extended time points. I propose p52 plays an important role in the successful completion of cell division through mediating DNA repair to allow cancer cells to proliferate.

7.3.2.   Is there competition between p52 and MDM2?

One possible mechanism underpinning the modulation of p53 activity via p52 is through competition with MDM2 for RPL11 binding. The western blotting analysis of U2-OS cells with overexpressed MDM2 displayed increased PARP cleavage and degradation of the p21 protein in response to nucleolar stress (Chapter 4). The removal of the cell cycle inhibitor is indicative of cellular death via aberrant cell cycle progression. Interestingly, the phenotype

was similar to the p52/p100 depleted U2-OS cells (Chapter 3). This suggests that increased cellular MDM2 could enhance the formation of more MDM2/RPL11 complexes, allowing p53 to carry out its role in cell death pathways, hence leading to the observed increase in PARP cleavage. As it has been demonstrated that a lack of p52 is associated with cellular death, it can be hypothesised that the ratio of MDM2/RPL11 and p52/RPL11 can influence the downstream signalling of p53.

It is unclear whether the competition between MDM2 and p52 for RPL11 binding is direct, as predicted in the *in silico* analysis, or allosteric. Co-immunoprecipitation analysis determined that a decrease in GFP-p52/RPL11 complexes were captured in the presence of increased MDM2 protein (Chapter 4). This implies that the increased concentration of MDM2 encourages more MDM2/RPL11 complexes, thus decreasing the abundance of p52-GFP/RPL11. This type of analysis is unable to describe the nature of the competition. MDM2 and p52 are predicted to bind RPL11 at the same site, suggesting direct competition.

Interestingly, this is also the site that RPL11 contacts the ribosome during ribosome biogenesis, suggesting the interaction between p52/RPL11 and the interactions between RPL11/ribosome, are mutually exclusive (Zheng et al., 2015, Khatter et al., 2015). The *in silico* prediction of binding energies imply that the predicted structure of the p52/RPL11 complex was more energetically feasible than the solved structure of the MDM2/RPL11 complex. However, the co-immunoprecipitation assay suggests the reverse is true. It must be noted that the co-immunoprecipitation was performed using tagged p52 and tagged MDM2, whereas the predictions used endogenous forms of the proteins. Furthermore, the PDB structures used depicted p52 in a DNA bound state and only a section of the MDM2 protein. These conditions were not replicated in the laboratory. Further co-immunoprecipitation assays demonstrated that p52 in a DNA bound state enhanced the interaction with RPL11. It would be interesting to repeat the competition analysis with p52 in the DNA bound conformation to monitor the impact of MDM2 overexpression on the p52-DNA/RPL11 complex.

During a GFP Trap co-immunoprecipitation isolating GFP-p52 complexes, it was shown that GFP-p52 could associate with both MDM2 and p53. Therefore, another hypothesis is that p52 binding changes the nature of the MDM2/RPL11 interaction, perhaps encouraging the formation of a "supercomplex". It is known that proteins are dynamic molecules that undergo conformational changes (Zacharias, 2010, Ramsey et al., 2017). It is predicted that

p52 undergoes a conformational change when bound to DNA causing a more stringent interaction with RPL11. This could influence MDM2 to stay in association with RPL11 and p53, therefore modulating the downstream effects. The competition between p52 and MDM2 could be of an allosteric nature through changing the conformation of the complex and the proteins. Therefore, altering protein-protein interactions as well as target gene regulatory mechanisms. Despite being part of the supercomplex, the E3 ligase function of MDM2 could be repressed, allowing p53 to regulate target genes, perhaps via p52-DNA contacts.

7.4. p52 as a DNA Binding Protein

The transcription factor, p52, is a DNA binding protein (Schumm et al., 2006, Iannetti et al., 2014). Therefore, it was important to investigate the role that p52 DNA binding plays within the ribosomal stress response. It is known that p52 can bind to the promoter regions of p53 target genes (Schumm, 2006). Further, it has been shown that p52 homodimers switch association with cofactor proteins in order to modulate gene expression genes during cellular stress (Rocha et al., 2003). This section will discuss the possibility that p52/RPL11 translocate to the promoter regions of p53 target genes during ribosomal stress to regulate p53 gene expression.

7.4.1. Does DNA binding modulate protein-protein interactions of p52?

In this thesis, I propose that p52 changes conformation during DNA binding which facilitates further protein-protein interactions. The DNA bound state of p52-E86A was unable to form a strong association with RPL11, however p52-E86A in the unbound state, was (Chapter 6). Therefore, it is predicted glutamate 86 of p52 makes an important connection with RPL11 during DNA binding. E86 resides in the DNA binding domain of p52, implicating the importance of this domain within the role of the p52/RPL11 association. Cramer *et al* published the crystal structure of the p52 homodimer bound to DNA (Cramer et al., 1997). The author's detailed a flexible linker region consisting of two alpha helices joined with a loop. This region was described to shift upon DNA binding. Moreover, NF-κB dimers are unique in the context of transcription factors as they utilise flexible loop regions to contact DNA. The mutant protein, p52-E86A, was predicted *in silico* to bind to this flexible loop region. The disruption of the p52-E86A complex encouraged through the addition of DNA indicates a novel conformation of p52 in the DNA bound form. As p52-E86A can interact with RPL11 in the absence of DNA, it is assumed that the conformation of the protein complex

mirrors that of the wild-type p52/RPL11 complex. Thus, it is likely that p52 undergoes a conformational change during DNA binding events, changing the accessibility and biochemistry of the protein for further interactions.

DNA binding enhanced the wild-type p52/RPL11 association. Perhaps, RPL11 has preferential binding to the novel conformation of p52 following DNA binding. Given the increased abundance of p52/RPL11 in the presence of κB DNA, it can be predicted that the complex is DNA bound during the ribosomal stress response. Mahata *et al* published that RPL11 could bind to the promoter region of p53 target genes, including the gene encoding p21 (Mahata et al., 2012). This was enhanced with ActD treatment. The p52 protein has also been documented to bind to p53 target genes. It is hypothesised that p52/RPL11 is present at the promoter regions of p53, however further chromatin immunoprecipitation studies are required to investigate this further discussed in Chapter 6).

One missing piece of information from this study is the dimer in which p52 is involved with during this response. Western blot analysis of the ribosomal stress response in cells depleted with p50 or RelA demonstrated that these proteins do not have a significant role in the response. When p52 or RelB were depleted, however, it was clear the proteins played a critical role in the stress response. Thus, p52 could be in a p52/RelB homodimer, or, this could be the action of p52 homodimers. In 2003, Rocha *et al* published that p52 homodimers switched to associate with HDAC1, as opposed to Bcl3, following UV stimulation which led to suppression of cyclin D1 gene expression (Rocha et al., 2003). The homodimers rely on cofactors of transcriptional regulation due to lacking a transactivation domain (Perkins and Gilmore, 2006). The NF-κB family are known to be sensitive to the cellular environment and alter their target gene regulation accordingly (Perkins, 2012). Certain types of cellular stress could facilitate the switch in cofactor association and downstream effects on target gene regulation. Ultraviolet radiation was documented to be an inducer of ribotoxic stress, an extreme form of ribosomal stress (Iordanov et al., 1998a). It can be speculated that p52/RPL11 containing complexes could be in association with cofactors which modulate the expression of p53 target genes following ribosomal stress. It has been demonstrated that transcription factors change their interactome when in a DNA bound state, as opposed to the unbound state (Bhattacharjee et al., 2021). Therefore, it can be predicted that p52 changes preference for protein-protein interactions when bound to DNA. The combination of the cellular environment, the conformation of p52 and the other proteins in the complex

could contribute to the preferential binding to Bcl-3 or HDAC1. An unpublished proteomics screen performed by Dr Alessio Ianneti demonstrated that GFP-p52 had an enhanced interaction with RPL11 following UV radiation, whilst the Bcl-3 association decreased. It would be interesting to investigate the abundance of HDAC1 associated with p52 following ribosomal stress induction. Further, whether depletion of the cofactors, Bcl-3 and HDAC1, alter the formation of the p52/RPL11 complex and downstream signalling effects.

7.5. Implications of p52/RPL11 in Cancer Cell Biology

The research presented describes crosstalk between non-canonical NF-κB signalling and p53 tumour suppressor signalling. Both pathways play a major role in cellular signalling and cancer cell biology (Perkins, 2012, Vousden and Prives, 2009). Further, in this context, non-canonical NF-κB is functioning to modulate and alter the p53 response to favour cancer cell survival. Evasion of apoptosis is one of the hallmarks of cancer (Hanahan and Weinberg, 2011). Aberrant growth relies upon the cell's ability to avoid cellular death mechanisms.

Cancer cells adopt this ability to proliferate, often utilising the intrinsic mechanisms in the cell to facilitate this (Williams and Stoeber, 2012). Understanding the ways in which cancer cells bypass these critical cellular pathways is key to preventing disease progression and finding new treatments. It is hypothesised that p52 plays a cell survival role during the ribosomal stress response in U2-OS and HCT116 cell lines. U2-OS cells were generated from an osteosarcoma patient, and HCT116 cells are colorectal cancer cells. The cancer cells were found to undergo cell death when treated with ribosomal stress inducing chemotherapeutics following the depletion of p52/p100 protein. This was a particularly important observation in the colorectal cancer cell line. The preferred treatment for this type of cancer in the clinic is 5-flurouracil (Cho et al., 2020). Therefore, p52 could promote resistance to the drug treatment through encouraging cell survival through direct interaction to RPL11.

Critical future experiments would be the investigation into the disruption of the p52/RPL11 interaction. Whilst the p52-E86A mutant was sufficient to weaken the interaction with RPL11 in the presence of a known κB site, further studies are required to create a mutant p52 that does not bind to RPL11. Once achieved, the mutation could be introduced using CRISPR/Cas9 gene editing. This would allow the endogenous introduction of the mutant. Cells could be cultured, treated and analysed for changes in cellular signalling and cellular fate. It could be predicted that cancer cells lacking the p52/RPL11 interaction would be more

susceptible to treatment with ribosomal stress inducing chemotherapeutics, such as ActD and 5FU.

The RPL11/MDM2 interaction has recently been investigated as a potential therapeutic target (Wang et al., 2022). A small molecular mimetic was synthesised to replicate RPL11 and bind to the appropriate binding site on the MDM2 protein. This inhibits the E3 ubiquitin ligase function of MDM2, leading to stabilisation and activation of p53. The study found that the use of the mimetic was sufficient to cause G2/M cell cycle arrest and decrease cellular proliferation of the cancer cell lines used. The study investigated the effects in HCT116 and U2-OS cells, which were the cell lines used in this project. This mirrors the effects presented in this thesis. Upon depletion of p52/p100, predicted to increase the number of MDM2/RPL11 complexes forming in response to cellular stress, led to cell cycle arrest and increased DNA damage, leading to decreased cellular proliferation and ultimately cell death. A future study could involve synthesising a short peptide to bind to the RPL11 binding site on p52 to inhibit the interaction. It is predicted that the RPL11 binding site is not within the same region as p52 contacts DNA or other NF-κB subunits during dimerization. Therefore, it is predicted that this would not cause severe adverse effects in the context of NF-κB biology. Following the binding of the peptide to p52, cells could be treated with chemotherapies that induce the 5S RNP/MDM2/p53 pathway. I hypothesise this could improve the efficiency and efficacy of the drugs, therefore could improve the burden placed upon patients undergoing these treatments.

7.6. Final Summary

The ribosomal stress response is a mechanism utilised by cells to cope with cellular stress (Sloan et al., 2013a). Ribosome biogenesis is rapidly inhibited allowing the 5S RNP to bind to and inhibit the action of E3 ligase MDM2 (Pelava et al., 2016). This allows p53 to activate and regulate target genes. The p53 tumour suppressor protein can encourage cell cycle arrest and stimulate DNA repair pathways in order to repair damage and continue cell proliferation (Vousden and Prives, 2009). On the other hand, p53 is implicated in several mechanisms of cellular death, as well as cellular senescence, in cases of overwhelming damage (Lindström et al., 2022). I propose the p52/RPL11 interaction has evolved in cancer cells to influence cellular fate in a p53 dependent manner through competition with the documented MDM2/RPL11 interaction (Figure 7.2). The association is a direct link between NF-κB signalling and ribosomal stress functioning to help cancer cells survive. Therefore, this thesis

presents a novel tumour promoting role for the NF-κB subunit, p52, through direct interaction with RPL11 of the 5S RNP, functioning to modulate p53 target gene expression following ribosomal stress.
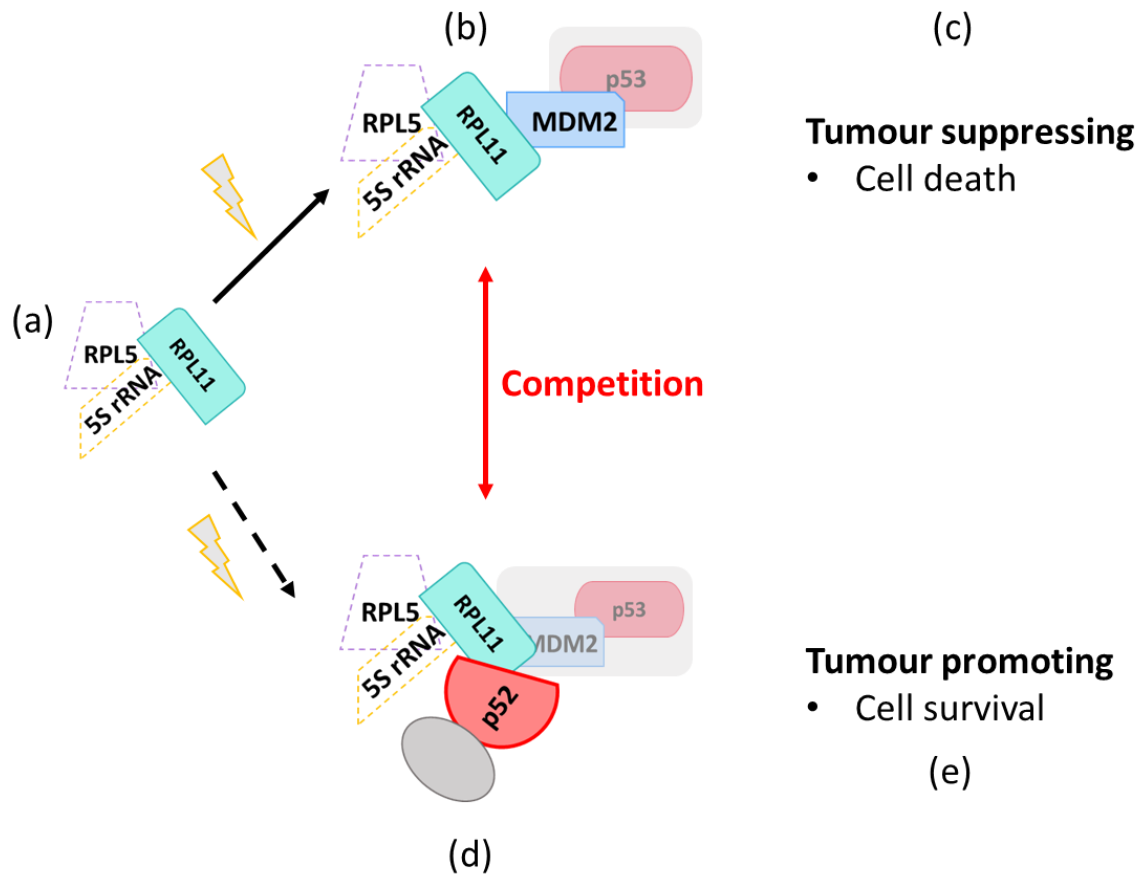
Figure 7.2 Current working hypothesis. (a) The research performed has focussed on RPL11 of the 5S RNP. However, in theory RPL11 is not stable without the other members of the complex. The data presented is inconclusive regarding the 5S rRNA and RPL5 and their involvement with p52 signalling. Therefore, the components are represented with dashed lines. (b) In response to cellular stress the 5S RNP binds to MDM2 inhibiting its function and allowing p53 to stabilise. One hypothesis is that p53 stays bound to MDM2 and the supercomplex in entirety translocates to the nucleus and binds to p53 target genes. (c) The outcome of the RPL11/MDM2 interaction is of a tumour suppressive nature, facilitating cellular death mechanisms. (d) RPL11 directly binds to p52 containing NF-κB dimers via direct interaction with p52. It is unclear whether the p52/RPL11 interaction is functioning to wholly outcompete MDM2, or whether MDM2 and possibly p53 remain part of a supercomplex to carry out regulation of p53 target genes. (e) The p52/RPL11 interaction encourages cell survival and therefore highlights a novel function of p52 as a tumour promoter.

References

ADAMS, J. M., HARRIS, A. W., PINKERT, C. A., CORCORAN, L. M., ALEXANDER, W. S., CORY, S., PALMITER, R. D. & BRINSTER, R. L. 1985. The c-myc oncogene driven by immunoglobulin enhancers induces lymphoid malignancy in transgenic mice. *Nature,* 318**,** 533-538.

ADHIKARI, A., XU, M. & CHEN, Z. J. 2007. Ubiquitin-mediated activation of TAK1 and IKK. *Oncogene,* 26**,** 3214-3226.

AHMED, K. M. & LI, J. J. 2008. NF-κB-mediated adaptive resistance to ionizing radiation. *Free Radical Biology and Medicine,* 44**,** 1-13.

AJORE, R., RAISER, D., MCCONKEY, M., JÖUD, M., BOIDOL, B., MAR, B., SAKSENA, G., WEINSTOCK, D. M., ARMSTRONG, S. & ELLIS, S. R. 2017. Deletion of ribosomal protein genes is a common vulnerability in human cancer, especially in concert with TP 53 mutations. *EMBO molecular medicine,* 9**,** 498-507.

AOUBALA, M., MURRAY-ZMIJEWSKI, F., KHOURY, M. P., FERNANDES, K., PERRIER, S., BERNARD, H., PRATS, A.-C., LANE, D. P. & BOURDON, J.-C. 2011. p53 directly transactivates Δ133p53α, regulating cell fate outcome in response to DNA damage. *Cell Death & Differentiation,* 18**,** 248-258.

ASAHARA, H., ASANUMA, M., OGAWA, N., NISHIBAYASHI, S. & INOUE, H. 1995. High DNA-binding activity of transcription factor NF-kappa B in synovial membranes of patients with rheumatoid arthritis. *Biochemistry and molecular biology international,* 37**,** 827-832.

AWASTHI, P., FOIANI, M. & KUMAR, A. 2015. ATM and ATR signaling at a glance. *Journal of cell science,* 128**,** 4255-4262.

AZER, S. A. 2018. MDM2-p53 Interactions in Human Hepatocellular Carcinoma: What Is the Role of Nutlins and New Therapeutic Options? *Journal of Clinical Medicine,* 7**,** 64.

BAI, D., ZHANG, J., LI, T., HANG, R., LIU, Y., TIAN, Y., HUANG, D., QU, L., CAO, X. & JI, J. 2016. The ATPase hCINAP regulates 18S rRNA processing and is essential for embryogenesis and tumour growth. *Nature communications,* 7**,** 12310.

BAI, X.-C., MCMULLAN, G. & SCHERES, S. H. W. 2015. How cryo-EM is revolutionizing structural biology. *Trends in Biochemical Sciences,* 40**,** 49-57.

BARTEK, J. & LUKAS, J. 2007. DNA damage checkpoints: from initiation to recovery or adaptation. *Current opinion in cell biology,* 19**,** 238-245.

BASAK, S., SHIH, V. F.-S. & HOFFMANN, A. 2008. Generation and activation of multiple dimeric transcription factors within the NF-κB signaling system. *Molecular and cellular biology,* 28**,** 3139-3150.

BASH, J., ZONG, W.-X. & GELINAS, C. 1997. c-Rel arrests the proliferation of HeLa cells and affects critical regulators of the G1/S-phase transition. *Molecular and cellular biology,* 17**,** 6526-6536.

BASU, S., NAHA, A., VEERARAGHAVAN, B., RAMAIAH, S. & ANBARASU, A. 2022. In silico structure evaluation of BAG3 and elucidating its association with bacterial infections through protein–protein and host-pathogen interaction analysis. *Journal of Cellular Biochemistry,* 123**,** 115-127.

BAUGH, E. H., KE, H., LEVINE, A. J., BONNEAU, R. A. & CHAN, C. S. 2018. Why are there hotspot mutations in the TP53 gene in human cancers? *Cell Death & Differentiation,* 25**,** 154-160.

BEG, A. A., SHA, W. C., BRONSON, R. T., GHOSH, S. & BALTIMORE, D. 1995. Embryonic lethality and liver degeneration in mice lacking the RelA component of NF-κB. *Nature,* 376**,** 167-170.

BEJERANO, G., PHEASANT, M., MAKUNIN, I., STEPHEN, S., KENT, W. J., MATTICK, J. S. & HAUSSLER, D. 2004. Ultraconserved Elements in the Human Genome. *Science,* 304**,** 1321-1325.

BERGGÅRD, T., LINSE, S. & JAMES, P. 2007. Methods for the detection and analysis of protein–protein interactions. *PROTEOMICS,* 7**,** 2833-2842.

BERK, V., ZHANG, W., PAI, R. D. & CATE, J. H. 2006. Structural basis for mRNA and tRNA positioning on the ribosome. *Proceedings of the National Academy of Sciences,* 103**,** 15830-15834.

BHATTACHARJEE, S., MUKHERJEE, S. & ROY, S. 2021. DNA-Bound p53-DNA-Binding Domain Interconverts between Multiple Conformations: Implications for Partner Protein Recognition. *The Journal of Physical Chemistry B,* 125**,** 5832-5837.

BOGAN, A. A. & THORN, K. S. 1998. Anatomy of hot spots in protein interfaces11Edited by J. Wells. *Journal of Molecular Biology,* 280**,** 1-9.

BOISVERT, F.-M., VAN KONINGSBRUGGEN, S., NAVASCUÉS, J. & LAMOND, A. I. 2007. The multifunctional nucleolus. *Nature reviews Molecular cell biology,* 8**,** 574-585.

BOISVERT, F. M. & LAMOND, A. I. 2010. p53-Dependent subcellular proteome localization following DNA damage. *Proteomics,* 10**,** 4087-4097.

BORDEIRA GASPAR, T., SÁ, A., LOPES, J. M., SOBRINHO-SIMÕES, M., SOARES, P. & VINAGRE, J. 2018. Telomere maintenance mechanisms in cancer. *Genes,* 9**,** 241.

BORIA, I., GARELLI, E., GAZDA, H. T., ASPESI, A., QUARELLO, P., PAVESI, E., FERRANTE, D., MEERPOHL, J. J., KARTAL, M. & DA COSTA, L. 2010. The ribosomal basis of Diamond-Blackfan Anemia: mutation and database update. *Human mutation,* 31**,** 1269-1279.

BOULON, S., WESTMAN, B. J., HUTTEN, S., BOISVERT, F.-M. & LAMOND, A. I. 2010. The Nucleolus under Stress. *Molecular Cell,* 40**,** 216-227.

BOUTROS, R., LOBJOIS, V. & DUCOMMUN, B. 2007. CDC25 phosphatases in cancer cells: key players? Good targets? *Nature Reviews Cancer,* 7**,** 495-507.

BOUWMEESTER, T., BAUCH, A., RUFFNER, H., ANGRAND, P. O., BERGAMINI, G., CROUGHTON, K., CRUCIAT, C., EBERHARD, D., GAGNEUR, J., GHIDELLI, S., HOPF, C., HUHSE, B., MANGANO, R., MICHON, A. M., SCHIRLE, M., SCHLEGL, J., SCHWAB, M., STEIN, M. A., BAUER, A., CASARI, G., DREWES, G., GAVIN, A. C., JACKSON, D. B., JOBERTY, G., NEUBAUER, G., RICK, J., KUSTER, B. & SUPERTI-FURGA, G. 2004. A physical and functional map of the human TNF-alpha/NF-kappa B signal transduction pathway. *Nat Cell Biol,* 6**,** 97-105.

BREN, G. D., SOLAN, N. J., MIYOSHI, H., PENNINGTON, K. N., POBST, L. J. & PAYA, C. V. 2001. Transcription of the RelB gene is regulated by NF-κB. *Oncogene,* 20**,** 7722-7733.

BROWN, J. P., WEI, W. & SEDIVY, J. M. 1997. Bypass of senescence after disruption of p21 CIP1/WAF1 gene in normal diploid human fibroblasts. *Science,* 277**,** 831-834.

BROWN, K., GERSTBERGER, S., CARLSON, L., FRANZOSO, G. & SIEBENLIST, U. 1995. Control of IκB-α Proteolysis by Site-Specific, Signal-Induced Phosphorylation. *Science,* 267**,** 1485-1488.

BRÜCKNER, A., POLGE, C., LENTZE, N., AUERBACH, D. & SCHLATTNER, U. 2009. Yeast Two-Hybrid, a Powerful Tool for Systems Biology. *International Journal of Molecular Sciences,* 10**,** 2763-2788.

BUDKE, B., ZHONG, A., SULLIVAN, K., PARK, C., GITTIN, D. I., KOUNTZ, TIMOTHY S. & CONNELL, PHILIP P. 2022. Noncanonical NF-κB factor p100/p52

regulates homologous recombination and modulates sensitivity to DNA-damaging therapy. *Nucleic Acids Research,* 50**,** 6251-6263.

BURSAĆ, S., BRDOVČAK, M. C., PFANNKUCHEN, M., ORSOLIĆ, I., GOLOMB, L., ZHU, Y., KATZ, C., DAFTUAR, L., GRABUŠIĆ, K., VUKELIĆ, I., FILIĆ, V., OREN, M., PRIVES, C. & VOLAREVIC, S. 2012. Mutual protection of ribosomal proteins L5 and L11 from degradation is essential for p53 activation upon ribosomal biogenesis stress. *Proceedings of the National Academy of Sciences of the United States of America,* 109**,** 20467-20472.

CAAMAÑO, J. H., RIZZO, C. A., DURHAM, S. K., BARTON, D. S., RAVENTÓS-SUÁREZ, C., SNAPPER, C. M. & BRAVO, R. 1998. Nuclear factor (NF)-kappa B2 (p100/p52) is required for normal splenic microarchitecture and B cell-mediated immune responses. *The Journal of experimental medicine,* 187**,** 185-196.

CAMPBELL, A. E., FERRAZ FRANCO, C., SU, L. I., CORBIN, E. K., PERKINS, S., KALYUZHNYY, A., JONES, A. R., BROWNRIDGE, P. J., PERKINS, N. D. & EYERS, C. E. 2021. Temporal modulation of the NF-κB RelA network in response to different types of DNA damage. *Biochem J,* 478**,** 533-551.

CAMPBELL, K. J., CHAPMAN, N. R. & PERKINS, N. D. 2001. UV stimulation induces nuclear factor κB (NF-κB) DNA-binding activity but not transcriptional activation. *Biochemical Society Transactions,* 29**,** 688-691.

CAO, L. & WANG, L. 2022. New covalent bonding ability for proteins. *Protein Science,* 31**,** 312-322.

CASTEDO, M., PERFETTINI, J.-L., ROUMIER, T., ANDREAU, K., MEDEMA, R. & KROEMER, G. 2004. Cell death by mitotic catastrophe: a molecular definition. *Oncogene,* 23**,** 2825-2837.

CATEZ, F., DALLA VENEZIA, N., MARCEL, V., ZORBAS, C., LAFONTAINE, D. L. J. & DIAZ, J.-J. 2019. Ribosome biogenesis: An emerging druggable pathway for cancer therapeutics. *Biochemical Pharmacology,* 159**,** 74-81.

CECI, M., GAVIRAGHI, C., GORRINI, C., SALA, L. A., OFFENHÄUSER, N., CARLO MARCHISIO, P. & BIFFO, S. 2003. Release of eIF6 (p27BBP) from the 60S subunit allows 80S ribosome assembly. *Nature,* 426**,** 579-584.

CHAISSON, M. L., BRANSTETTER, D. G., DERRY, J. M., ARMSTRONG, A. P., TOMETSKO, M. E., TAKEDA, K., AKIRA, S. & DOUGALL, W. C. 2004. Osteoclast Differentiation Is Impaired in the Absence of Inhibitor of κB Kinase α. *Journal of Biological Chemistry,* 279**,** 54841-54848.

CHAITANYA, G. V., ALEXANDER, J. S. & BABU, P. P. 2010. PARP-1 cleavage fragments: signatures of cell-death proteases in neurodegeneration. *Cell Communication and Signaling,* 8**,** 1-11.

CHANG, C.-K., LIN, S.-M., SATANGE, R., LIN, S.-C., SUN, S.-C., WU, H.-Y., KEHN-HALL, K. & HOU, M.-H. 2021. Targeting protein-protein interaction interfaces in COVID-19 drug discovery. *Computational and Structural Biotechnology Journal,* 19**,** 2246-2255.

CHANG, C. C., ZHANG, J., LOMBARDI, L., NERI, A. & DALLA-FAVERA, R. 1995. Rearranged NFKB-2 genes in lymphoid neoplasms code for constitutively active nuclear transactivators. *Molecular and Cellular Biology,* 15**,** 5180-5187.

CHANG, M., LEE, A. J., FITZPATRICK, L., ZHANG, M. & SUN, S.-C. 2009. NF-κB1 p105 Regulates T Cell Homeostasis and Prevents Chronic Inflammation1. *The Journal of Immunology,* 182**,** 3131-3138.

CHASAPIS, C. T. & SPYROULIAS, G. A. 2009. RING finger E(3) ubiquitin ligases: structure and drug discovery. *Curr Pharm Des,* 15**,** 3716-31.

CHEN, F. E. & GHOSH, G. 1999. Regulation of DNA binding by Rel/NF-κB transcription factors: structural views. *Oncogene,* 18**,** 6845-6852.

CHEN, F. E., HUANG, D.-B., CHEN, Y.-Q. & GHOSH, G. 1998. Crystal structure of p50/p65 heterodimer of transcription factor NF-κB bound to DNA. *Nature,* 391**,** 410-413.

CHEN, J. & KASTAN, M. B. 2010. 5′–3′-UTR interactions regulate p53 mRNA translation and provide a target for modulating p53 induction after DNA damage. *Genes & development,* 24**,** 2146-2156.

CHEN, Z. J. 2005. Ubiquitin signalling in the NF-κB pathway. *Nature Cell Biology,* 7**,** 758-765.

CHEN, Z. J. 2012. Ubiquitination in signaling to and activation of IKK. *Immunological Reviews,* 246**,** 95-106.

CHILDERS, M. C. & DAGGETT, V. 2017. Insights from molecular dynamics simulations for computational protein design. *Molecular Systems Design & Engineering,* 2**,** 9-33.

CHO, Y.-H., RO, E. J., YOON, J.-S., MIZUTANI, T., KANG, D.-W., PARK, J.-C., IL KIM, T., CLEVERS, H. & CHOI, K.-Y. 2020. 5-FU promotes stemness of colorectal cancer via p53-mediated WNT/β-catenin pathway activation. *Nature Communications,* 11**,** 5321.

CHOESMEL, V., BACQUEVILLE, D., ROUQUETTE, J., NOAILLAC-DEPEYRE, J., FRIBOURG, S., CRÉTIEN, A., LEBLANC, T., TCHERNIA, G., DA COSTA, L. & GLEIZES, P.-E. 2007. Impaired ribosome biogenesis in Diamond-Blackfan anemia. *Blood,* 109**,** 1275 LP-1283.

CHOONG, M. L., YANG, H., LEE, M. A. & LANE, D. P. 2009. Specific activation of the p53 pathway by low dose actinomycin D: A new route to p53 based cyclotherapy. *Cell Cycle,* 8**,** 2810-2818.

CICCIA, A. & ELLEDGE, S. J. 2010. The DNA damage response: making it safe to play with knives. *Molecular cell,* 40**,** 179-204.

CIGANDA, M. & WILLAIMS, N. 2014. Eukaryotic 5S rRNA biogenesis. 71**,** 3831-3840.

CILLUFFO, D., BARRA, V. & DI LEONARDO, A. 2020. P14ARF: The Absence that Makes the Difference. *Genes,* 11**,** 824.

CLACKSON, T. & WELLS, J. A. 1995. A hot spot of binding energy in a hormone-receptor interface. *Science,* 267**,** 383-386.

CLAUDIO, E., BROWN, K., PARK, S., WANG, H. & SIEBENLIST, U. 2002. BAFF-induced NEMO-independent processing of NF-κB2 in maturing B cells. *Nature Immunology,* 3**,** 958-965.

CMEJLA, R., CMEJLOVA, J., HANDRKOVA, H., PETRAK, J., PETRTYLOVA, K., MIHAL, V., STARY, J., CERNA, Z., JABALI, Y. & POSPISILOVA, D. 2009. Identification of mutations in the ribosomal protein L5 (RPL5) and ribosomal protein L11 (RPL11) genes in Czech patients with Diamond-Blackfan anemia. *Human Mutation,* 30**,** 321-327.

COLLINS, P. E., GRASSIA, G., COLLERAN, A., KIELY, P. A., IALENTI, A., MAFFIA, P. & CARMODY, R. J. 2015. Mapping the Interaction of B Cell Leukemia 3 (BCL-3) and Nuclear Factor κB (NF-κB) p50 Identifies a BCL-3-mimetic Anti-inflammatory Peptide *. *Journal of Biological Chemistry,* 290**,** 15687-15696.

COLLINS, P. E., KIELY, P. A. & CARMODY, R. J. 2014. Inhibition of Transcription by B Cell Leukemia 3 (Bcl-3) Protein Requires Interaction with Nuclear Factor κB (NF-κB) p50 *. *Journal of Biological Chemistry,* 289**,** 7059-7067.

COLOTTA, F., ALLAVENA, P., SICA, A., GARLANDA, C. & MANTOVANI, A. 2009. Cancer-related inflammation, the seventh hallmark of cancer: links to genetic instability. *Carcinogenesis,* 30**,** 1073-81.

CONSORTIUM, T. U. 2020. UniProt: the universal protein knowledgebase in 2021. *Nucleic Acids Research,* 49**,** D480-D489.

COOPE, H. J., ATKINSON, P. G. P., HUHSE, B., BELICH, M., JANZEN, J., HOLMAN, M. J., KLAUS, G. G. B., JOHNSTON, L. H. & LEY, S. C. 2002. CD40 regulates the processing of NF-κB2 p100 to p52. *EMBO Journal,* 21**,** 5375-5385.

CRAMER, P., LARSON, C. J., VERDINE, G. L. & MÜLLER, C. W. 1997. Structure of the human NF-κB p52 homodimer-DNA complex at 2.1 Å resolution. *The EMBO Journal,* 16**,** 7078-7090.

D'IGNAZIO, L., BATIE, M. & ROCHA, S. 2018. TNFSF14/LIGHT, a Non-Canonical NF-κB Stimulus, Induces the HIF Pathway. *Cells,* 7**,** 102-102.

DAI, M.-S., CHALLAGUNDLA, K. B., SUN, X.-X., PALAM, L. R., ZENG, S. X., WEK, R. C. & LU, H. 2012. Physical and functional interaction between ribosomal protein L11 and the tumor suppressor ARF. *The Journal of biological chemistry,* 287**,** 17120-17129.

DAI, M.-S., SEARS, R. & LU, H. 2007a. Feedback regulation of c-Myc by ribosomal protein L11. *Cell cycle (Georgetown, Tex.),* 6**,** 2735-2741.

DAI, M. S., ARNOLD, H., SUN, X. X., SEARS, R. & LU, H. 2007b. Inhibition of c-Myc activity by ribosomal protein L11. *The EMBO Journal,* 26**,** 3332 LP-3345.

DASH, B. C. & EL-DEIRY, W. S. 2005. Phosphorylation of p21 in G2/M promotes cyclin B-Cdc2 kinase activity. *Mol Cell Biol,* 25**,** 3364-87.

DAVIGNON, J.-L., HAYDER, M., BARON, M., BOYER, J.-F., CONSTANTIN, A., APPARAILLY, F., POUPOT, R. & CANTAGREL, A. 2013. Targeting monocytes/macrophages in the treatment of rheumatoid arthritis. *Rheumatology,* 52**,** 590-598.

DE LA CRUZ, J., KARBSTEIN, K. & WOOLFORD, J. L. 2015. Functions of Ribosomal Proteins in Assembly of Eukaryotic Ribosomes In Vivo. *Annual Review of Biochemistry,* 84**,** 93-129.

DEHOUCK, Y., KWASIGROCH, J. M., ROOMAN, M. & GILIS, D. 2013. BeAtMuSiC: prediction of changes in protein–protein binding affinity on mutations. *Nucleic Acids Research,* 41, 333-339.

DE VRIES, S. J. & BONVIN, A. M. J. J. 2011. CPORT: A Consensus Interface Predictor and Its Performance in Prediction-Driven Docking with HADDOCK. *PLOS ONE,* 6**,** e17695.

DE VRIES, S. J., VAN DIJK, M. & BONVIN, A. M. J. J. 2010. The HADDOCK web server for data-driven biomolecular docking. *Nature Protocols,* 5**,** 883-897.

DEAL, C. 2012. Bone loss in rheumatoid arthritis: systemic, periarticular, and focal. *Current rheumatology reports,* 14**,** 231-237.

DEGASPERI, A., BIRTWISTLE, M. R., VOLINSKY, N., RAUCH, J., KOLCH, W. & KHOLODENKO, B. N. 2014. Evaluating Strategies to Normalise Biological Replicates of Western Blot Data. *PLOS ONE,* 9**,** e87293.

DEISENROTH, C. & ZHANG, Y. 2010. Ribosome biogenesis surveillance: Probing the ribosomal protein-Mdm2-p53 pathway. *Oncogene,* 29**,** 4253-4260.

DEJARDIN, E., DROIN, N. M., DELHASE, M., HAAS, E., CAO, Y., MAKRIS, C., LI, Z.-W., KARIN, M., WARE, C. F. & GREEN, D. R. 2002. The Lymphotoxin-β Receptor Induces Different Patterns of Gene Expression via Two NF-κB Pathways. *Immunity,* 17**,** 525-535.

DELANO, W. L. 2002. Unraveling hot spots in binding interfaces: progress and challenges. *Current opinion in structural biology,* 12**,** 14-20.

DEMICCO, E. G., KAVANAGH, K. T., ROMIEU-MOUREZ, R., WANG, X., SHIN, S. R., LANDESMAN-BOLLAG, E., SELDIN, D. C. & SONENSHEIN, G. E. 2005. RelB/p52 NF-kappaB complexes rescue an early delay in mammary gland development in transgenic mice with targeted superrepressor IkappaB-alpha expression and promote carcinogenesis of the mammary gland. *Mol Cell Biol,* 25**,** 10136-47.

DI TRANI, J. M., DE CESCO, S., O'LEARY, R., PLESCIA, J., DO NASCIMENTO, C. J., MOITESSIER, N. & MITTERMAIER, A. K. 2018. Rapid measurement of inhibitor binding kinetics by isothermal titration calorimetry. *Nature Communications,* 9**,** 893.

DING, L., CAO, J., LIN, W., CHEN, H., XIONG, X., AO, H., YU, M., LIN, J. & CUI, Q. 2020. The roles of cyclin-dependent kinases in cell-cycle progression and therapeutic strategies in human breast cancer. *International journal of molecular sciences,* 21**,** 1960.

DÖPPLER, H., LIOU, G. Y. & STORZ, P. 2013. Downregulation of TRAF2 mediates NIK-induced pancreatic cancer cell proliferation and tumorigenicity. *PLoS One,* 8**,** e53676.

DOUDNA, J. A. & RATH, V. L. 2002. Structure and Function of the Eukaryotic Ribosome: The Next Frontier. *Cell,* 109**,** 153-156.

DRATWA, M., WYSOCZAŃSKA, B., ŁACINA, P., KUBIK, T. & BOGUNIA-KUBIK, K. 2020. TERT— regulation and roles in cancer formation. *Frontiers in Immunology,* 11**,** 589929.

DUCKETT, C. S., PERKINS, N. D., KOWALIK, T. F., SCHMID, R. M., HUANG, E. S., BALDWIN, A. S., JR. & NABEL, G. J. 1993. Dimerization of NF-KB2 with RelA(p65) regulates DNA binding, transcriptional activation, and inhibition by an I kappa B-alpha (MAD-3). *Mol Cell Biol,* 13**,** 1315-22.

EA, C.-K., DENG, L., XIA, Z.-P., PINEDA, G. & CHEN, Z. J. 2006. Activation of IKK by TNFα Requires Site-Specific Ubiquitination of RIP1 and Polyubiquitin Binding by NEMO. *Molecular Cell,* 22**,** 245-257.

EFTINK, M. R. 2000. Use of fluorescence spectroscopy as thermodynamics tool. *Methods in Enzymology.* Elsevier.

ELHAMAMSY, A. R., METGE, B. J., ALSHEIKH, H. A., SHEVDE, L. A. & SAMANT, R. S. 2022. Ribosome Biogenesis: A Central Player in Cancer Metastasis and Therapeutic Resistance. *Cancer Res,* 82**,** 2344-2353.

FANCELLO, L., KAMPEN, K. R., HOFMAN, I. J., VERBEECK, J. & DE KEERSMAECKER, K. 2017. The ribosomal protein gene RPL5 is a haploinsufficient tumor suppressor in multiple cancer types. *Oncotarget,* 8**,** 14462.

FERNANDEZ-LEIRO, R. & SCHERES, S. H. W. 2016. Unravelling biological macromolecules with cryo-electron microscopy. *Nature,* 537**,** 339-346.

FERREIRA, R., SCHNEEKLOTH JR, J. S., PANOV, K. I., HANNAN, K. M. & HANNAN, R. D. 2020. Targeting the RNA polymerase I transcription for cancer therapy comes of age. *Cells,* 9**,** 266.

FISCHER, M. 2017. Census and evaluation of p53 target genes. *Oncogene,* 36**,** 3943-3956.

FLITTER, W. D. & MASON, R. P. 1988. The enzymatic reduction of actinomycin D to a free radical species. *Archives of Biochemistry and Biophysics,* 267**,** 632-639.

FORTUNE, J. M. & OSHEROFF, N. 2000. Topoisomerase II as a target for anticancer drugs: when enzymes stop being nice.

FRANKLIN, D. A., LIU, S., JIN, A., CUI, P., GUO, Z., AREND, K. C., MOORMAN, N. J., HE, S., WANG, G. G., WAN, Y. Y. & ZHANG, Y. 2023. Ribosomal protein RPL11 haploinsufficiency causes anemia in mice via activation of the RP-MDM2-p53 pathway. *J Biol Chem,* 299**,** 102739.

FRANZOSO, G., BOURS, V., AZARENKO, V., PARK, S., TOMITA-YAMAGUCHI, M., KANNO, T., BROWN, K. & SIEBENLIST, U. 1993. The oncoprotein Bcl-3 can facilitate NF-kappa B-mediated transactivation by removing inhibiting p50 homodimers from select kappa B sites. *Embo j,* 12**,** 3893-901.

FRASER, C. S., BERRY, K. E., HERSHEY, J. W. & DOUDNA, J. A. 2007. eIF3j is located in the decoding center of the human 40S ribosomal subunit. *Molecular cell,* 26**,** 811-819.

FUMAGALLI, S., IVANENKOV, V. V., TENG, T. & THOMAS, G. 2012. Suprainduction of p53 by disruption of 40S and 60S ribosome biogenesis leads to the activation of a novel G2/M checkpoint. *Genes & development,* 26**,** 1028-1040.

GALLUZZI, L., VITALE, I., AARONSON, S. A., ABRAMS, J. M., ADAM, D., AGOSTINIS, P., ALNEMRI, E. S., ALTUCCI, L., AMELIO, I. & ANDREWS, D. W. 2018. Molecular mechanisms of cell death: recommendations of the Nomenclature Committee on Cell Death 2018. *Cell Death & Differentiation,* 25**,** 486-541.

GARCÍA-GARCÍA, V. A., ALAMEDA, J. P., PAGE, A. & CASANOVA, M. L. 2021. Role of NF-κB in Ageing and Age-Related Diseases: Lessons from Genetically Modified Mouse Models. *Cells,* 10**,** 1906.

GASSE, L., FLEMMING, D. & HURT, E. 2015. Coordinated ribosomal ITS2 RNA processing by the Las1 complex integrating endonuclease, polynucleotide kinase, and exonuclease activities. *Molecular cell,* 60**,** 808-815.

GAUTHIER, M. & DEGNAN, B. M. 2008. The transcription factor NF-κB in the demosponge Amphimedon queenslandica: insights on the evolutionary origin of the Rel homology domain. *Development Genes and Evolution,* 218**,** 23-32.

GEERTZ, M., SHORE, D. & MAERKL, S. J. 2012. Massively parallel measurements of molecular interaction kinetics on a microfluidic platform. *Proceedings of the National Academy of Sciences,* 109**,** 16540-16545.

GERONDAKIS, S., GRUMONT, R., GUGASYAN, R., WONG, L., ISOMURA, I., HO, W. & BANERJEE, A. 2006. Unravelling the complexities of the NF-κB signalling pathway using mouse knockout and transgenic models. *Oncogene,* 25**,** 6781-6799.

GERTZ, J., REDDY, T. E., VARLEY, K. E., GARABEDIAN, M. J. & MYERS, R. M. 2012. Genistein and bisphenol A exposure cause estrogen receptor 1 to bind thousands of sites in a cell type-specific manner. *Genome Res,* 22**,** 2153-62.

GHASSEMIFAR, S. & MENDRYSA, S. M. 2012. MDM2 antagonism by nutlin-3 induces death in human medulloblastoma cells. *Neurosci Lett,* 513**,** 106-10.

GHELLI LUSERNA DI RORÀ, A., GHETTI, M., LEDDA, L., FERRARI, A., BOCCONCELLI, M., PADELLA, A., NAPOLITANO, R., FONTANA, M. C., LIVERANI, C., IMBROGNO, E., BOCHICCHIO, M. T., PAGANELLI, M., ROBUSTELLI, V., SANOGO, S., CERCHIONE, C., FUMAGALLI, M., RONDONI, M., IMOVILLI, A., MUSURACA, G., MARTINELLI, G. & SIMONETTI, G. 2021. Exploring the ATR-CHK1 pathway in the response of doxorubicin-induced DNA damages in acute lymphoblastic leukemia cells. *Cell Biol Toxicol*.

GHOSH, G., DUYNE, G. V., GHOSH, S. & SIGLER, P. B. 1995. Structure of NF-κB p50 homodimer bound to a κB site. *Nature,* 373**,** 303-310.

GHOSH, S., MAY, M. J. & KOPP, E. B. 1998. NF-κB AND REL PROTEINS: Evolutionarily Conserved Mediators of Immune Responses. *Annual Review of Immunology,* 16**,** 225-260.

GIBSON, L. S. 2016. *The 5S RNP and the Regulation of the Tumour Suppressor, p53.* Doctor of Philosophy, Newcatle University.

GILMORE, T. D. 2006. Introduction to NF-κB: players, pathways, perspectives. *Oncogene,* 25**,** 6680-6680.

GILMORE, T. D. 2021. NF-κB and Human Cancer: What Have We Learned over the Past 35 Years? *Biomedicines,* 9**,** 889.

GILMORE, T. D. & GERONDAKIS, S. 2011. The c-Rel Transcription Factor in Development and Disease. *Genes Cancer,* 2**,** 695-711.

GILMORE, T. D. & WOLENSKI, F. S. 2012. NF-κB: where did it come from and why? *Immunological Reviews,* 246**,** 14-35.

GIONO, L. E. & MANFREDI, J. J. 2006. The p53 tumor suppressor participates in multiple cell cycle checkpoints. *Journal of Cellular Physiology,* 209**,** 13-20.

GOLDFARB, K. C. & CECH, T. R. 2017. Targeted CRISPR disruption reveals a role for RNase MRP RNA in human preribosomal RNA processing. *Genes & development,* 31**,** 59-71.

GÖÖS, H., KINNUNEN, M., SALOKAS, K., TAN, Z., LIU, X., YADAV, L., ZHANG, Q., WEI, G.-H. & VARJOSALO, M. 2022. Human transcription factor protein interaction networks. *Nature Communications,* 13**,** 766.

GREENFIELD, N. J. 2006. Using circular dichroism spectra to estimate protein secondary structure. *Nature protocols,* 1**,** 2876-2890.

GRETEN, F. R., ECKMANN, L., GRETEN, T. F., PARK, J. M., LI, Z. W., EGAN, L. J., KAGNOFF, M. F. & KARIN, M. 2004. IKKbeta links inflammation and tumorigenesis in a mouse model of colitis-associated cancer. *Cell,* 118**,** 285-96.

GULFIDAN, G., TURANLI, B., BEKLEN, H., SINHA, R. & ARGA, K. Y. 2020. Pan-cancer mapping of differential protein-protein interactions. *Scientific Reports,* 10**,** 3272.

HACKER, H. & KARIN, M. 2006. Regulation and function of IKK and IKK-related kinases. *Science's STKE,* 2006**,** re13-re13.

HAFNER, A., BULYK, M. L., JAMBHEKAR, A. & LAHAV, G. 2019. The multiple mechanisms that regulate p53 activity and cell fate. *Nature Reviews Molecular Cell Biology,* 20**,** 199-210.

HALAZONETIS, T. D., DAVIS, L. J. & KANDIL, A. N. 1993. Wild-type p53 adopts a 'mutant'-like conformation when bound to DNA. *The EMBO Journal,* 12**,** 1021-1028.

HALFORD, S. E. & MARKO, J. F. 2004. How do site-specific DNA-binding proteins find their targets? *Nucleic acids research,* 32**,** 3040-3052.

HAN, T., TONG, J., WANG, M., GAN, Y., GAO, B., CHEN, J., LIU, Y., HAO, Q. & ZHOU, X. 2022. Olaparib Induces RPL5/RPL11-Dependent p53 Activation via Nucleolar Stress. *Front Oncol,* 12**,** 821366.

HANAHAN, D. & WEINBERG, R. A. 2011. Hallmarks of cancer: the next generation. *Cell,* 144**,** 646-74.

HANNAN, K. M., SOO, P., WONG, M. S., LEE, J. K., HEIN, N., POH, P., WYSOKE, K. D., WILLIAMS, T. D., MONTELLESE, C., SMITH, L. K., AL-OBAIDI, S. J., NÚÑEZ-VILLACÍS, L., PAVY, M., HE, J.-S., PARSONS, K. M., LORING, K. E., MORRISON, T., DIESCH, J., BURGIO, G., FERREIRA, R., FENG, Z.-P., GOULD, C. M., MADHAMSHETTIWAR, P. B., FLYGARE, J., GONDA, T. J., SIMPSON, K. J., KUTAY, U., PEARSON, R. B., ENGEL, C., WATKINS, N. J., HANNAN, R. D. & GEORGE, A. J. 2022. Nuclear stabilization of p53 requires a functional nucleolar surveillance pathway. *Cell Reports,* 41**,** 111571.

HARMALKAR, A. & GRAY, J. J. 2021. Advances to tackle backbone flexibility in protein docking. *Current Opinion in Structural Biology,* 67**,** 178-186.

HAYDEN, M. S. & GHOSH, S. 2008. Shared Principles in NF-κB Signaling. *Cell,* 132**,** 344-362.

HENRAS, A. K., PLISSON-CHASTANG, C., O'DONOHUE, M. F., CHAKRABORTY, A. & GLEIZES, P. E. 2015. An overview of pre-ribosomal RNA processing in eukaryotes. *Wiley Interdisciplinary Reviews: RNA,* 6**,** 225-242.

HERNANSAIZ-BALLESTEROS, R. D., FÖLDI, C., CARDELLI, L., NAGY, L. G. & CSIKÁSZ-NAGY, A. 2021. Evolution of opposing regulatory interactions underlies the emergence of eukaryotic cell cycle checkpoints. *Scientific Reports,* 11**,** 11122.

HINDS, M. G., SMITS, C., FREDERICKS-SHORT, R., RISK, J. M., BAILEY, M., HUANG, D. C. S. & DAY, C. L. 2007. Bim, Bad and Bmf: intrinsically unstructured BH3-only proteins that undergo a localized conformational change upon binding to prosurvival Bcl-2 targets. *Cell Death & Differentiation,* 14**,** 128-136.

HINZ, M., KRAPPMANN, D., EICHTEN, A., HEDER, A., SCHEIDEREIT, C. & STRAUSS, M. 1999. NF-κB function in growth control: regulation of cyclin D1 expression and G0/G1-to-S-phase transition. *Molecular and cellular biology,* 19**,** 2690-2698.

HINZ, M. & SCHEIDEREIT, C. 2014. The IκB kinase complex in NF-κB regulation and beyond. *EMBO reports,* 15**,** 46-61.

HINZ, M., STILMANN, M., ARSLAN, S. Ç., KHANNA, K. K., DITTMAR, G. & SCHEIDEREIT, C. 2010. A cytoplasmic ATM-TRAF6-cIAP1 module links nuclear DNA damage signaling to ubiquitin-mediated NF-κB activation. *Molecular cell,* 40**,** 63-74.

HOFFMANN, A., LEVCHENKO, A., SCOTT, M. L. & BALTIMORE, D. 2002. The IkappaB-NF-kappaB signaling module: temporal control and selective gene activation. *Science,* 298**,** 1241-5.

HORN, H. & VOUSDEN, K. 2008. Cooperation between the ribosomal proteins L5 and L11 in the p53 pathway. *Oncogene,* 27**,** 5774-5784.

HU, Y., BAUD, V., OGA, T., KIM, K. I., YOSHIDA, K. & KARIN, M. 2001. IKKalpha controls formation of the epidermis independently of NF-kappaB. *Nature,* 410**,** 710-4.

HUANG, D.-B., CHEN, Y.-Q., RUETSCHE, M., PHELPS, C. B. & GHOSH, G. 2001. X-Ray Crystal Structure of Proto-Oncogene Product c-Rel Bound to the CD28 Response Element of IL-2. *Structure,* 9**,** 669-678.

HUANG, T. T., KUDO, N., YOSHIDA, M. & MIYAMOTO, S. 2000. A nuclear export signal in the N-terminal regulatory domain of IκBα controls cytoplasmic localization of inactive NF-κB/IκBα complexes. *Proceedings of the National Academy of Sciences,* 97**,** 1014-1019.

HUANG, W., DONG, Z., WANG, F., PENG, H., LIU, J.-Y. & ZHANG, J.-T. 2014. A small molecule compound targeting STAT3 DNA-binding domain inhibits cancer cell proliferation, migration, and invasion. *ACS chemical biology,* 9**,** 1188-1196.

HUANG, X., DI LIBERTO, M., CUNNINGHAM, A. F., KANG, L., CHENG, S., ELY, S., LIOU, H.-C., MACLENNAN, I. C. & CHEN-KIANG, S. 2004. Homeostatic cell-cycle control by BLyS: Induction of cell-cycle entry but not G1/S transition in opposition to p18INK4c and p27Kip1. *Proceedings of the National Academy of Sciences,* 101**,** 17789-17794.

HUFNAGEL, D. H., WILSON, A. J., SAXON, J., BLACKWELL, T. S., WATKINS, J., KHABELE, D., CRISPENS, M. A., YULL, F. E. & BEEGHLY-FADIEL, A. 2020. Expression of p52, a non-canonical NF-kappaB transcription factor, is associated with poor ovarian cancer prognosis. *Biomark Res,* 8**,** 45.

HUME, S., DIANOV, G. L. & RAMADAN, K. 2020. A unified model for the G1/S cell cycle transition. *Nucleic acids research,* 48**,** 12483-12501.

HUNTER, J., CAMPBELL, A., HANNAWAY, N., KERRIDGE, S., LULI, S., BUTTERWORTH, J., SELLIER, H., MUKHERJEE, R., DHILLON, N., SUDHINDAR, P., SHUKLA, R., BROWNRIDGE, P., BELL, H., COXHEAD, J., TAYLOR, L., LEARY, P., HASOON, M., COLLINS, I., GARRETT, M. & PERKINS, N. 2022a. Regulation of CHK1 inhibitor resistance by a c-Rel and USP1 dependent pathway. *The Biochemical journal,* 479**,** 2063-2086.

HUNTER, J. E., CAMPBELL, A. E., KERRIDGE, S., FRASER, C., HANNAWAY, N. L., LULI, S., IVANOVA, I., BROWNRIDGE, P. J., COXHEAD, J., TAYLOR, L., LEARY, P., HASOON, M. S. R., EYERS, C. E. & PERKINS, N. D. 2022b. Up-regulation of the PI3K/AKT and RHO/RAC/PAK signalling pathways in CHK1 inhibitor resistant Eμ-Myc lymphoma cells. *Biochemical Journal,* 479**,** 2131-2151.

HUXFORD, T., HUANG, D. B., MALEK, S. & GHOSH, G. 1998. The crystal structure of the IkappaBalpha/NF-kappaB complex reveals mechanisms of NF-kappaB inactivation. *Cell,* 95**,** 759-70.

IADEVAIA, V., LIU, R. & PROUD, C. G. mTORC1 signaling controls multiple steps in ribosome biogenesis. Seminars in cell & developmental biology, 2014. Elsevier, 113-120.

IANNETTI, A., LEDOUX, A. C., TUDHOPE, S. J., SELLIER, H., ZHAO, B., MOWLA, S., MOORE, A., HUMMERICH, H., GEWURZ, B. E., COCKELL, S. J., JAT, P. S., WILLMORE, E. & PERKINS, N. D. 2014. Regulation of p53 and Rb links the alternative NF-κB pathway to EZH2 expression and cell senescence. *PLoS Genet,* 10**,** e1004642.

IAPALUCCI-ESPINOZA, S. & FRANZE-FERNÁNDEZ, M. T. 1979. Effect of protein synthesis inhibitors and low concentrations of actinomycin D on ribosomal RNA synthesis. *FEBS letters.* Amsterdam, Netherlands :.

IORDANOV, M. S., PRIBNOW, D., MAGUN, J. L., DINH, T.-H., PEARSON, J. A. & MAGUN, B. E. 1998a. Ultraviolet Radiation Triggers the Ribotoxic Stress Response in Mammalian Cells *. *Journal of Biological Chemistry,* 273**,** 15794-15803.

IORDANOV, M. S., PRIBNOW, D., MAGUN, J. L., DINH, T. H., PEARSON, J. A. & MAGUN, B. E. 1998b. Ultraviolet radiation triggers the ribotoxic stress response in mammalian cells. *Journal of Biological Chemistry,* 273**,** 15794-15803.

IRAZOQUI, J. E., URBACH, J. M. & AUSUBEL, F. M. 2010. Evolution of host innate defence: insights from Caenorhabditis elegans and primitive invertebrates. *Nat Rev Immunol,* 10**,** 47-58.

ISHIKAWA, H., CARRASCO, D., CLAUDIO, E., RYSECK, R. P. & BRAVO, R. 1997. Gastric hyperplasia and increased proliferative responses of lymphocytes in mice lacking the COOH-terminal ankyrin domain of NF-kappaB2. *J Exp Med,* 186**,** 999-1014.

JACOB, S. P., FEUSIER, J. E. & CHEN, K. 2019. NFKB2 Defects. *In:* D'ELIOS, M. M. & RIZZI, M. (eds.) *Humoral Primary Immunodeficiencies.* Cham: Springer International Publishing.

JACOBS, M. D. & HARRISON, S. C. 1998. Structure of an IkappaBalpha/NF-kappaB complex. *Cell,* 95**,** 749-58.

JAMES, A., WANG, Y., RAJE, H., ROSBY, R. & DIMARIO, P. 2014. Nucleolar stress with and without p53. *Nucleus (Austin, Tex.),* 5**,** 402-426.

JANSA, P. & GRUMMT, I. 1999. Mechanism of transcription termination: PTRF interacts with the largest subunit of RNA polymerase I and dissociates paused transcription complexes from yeast and mouse. *Molecular and General Genetics MGG,* 262**,** 508-514.

JERNIGAN, K. K. & BORDENSTEIN, S. R. 2014. Ankyrin domains across the Tree of Life. *PeerJ,* 2**,** e264.

JONES, N. C., LYNN, M. L., GAUDENZ, K., SAKAI, D., AOTO, K., REY, J.-P., GLYNN, E. F., ELLINGTON, L., DU, C., DIXON, J., DIXON, M. J. & TRAINOR, P. A. 2008. Prevention of the neurocristopathy Treacher Collins syndrome through inhibition of p53 function. *Nature medicine,* 14**,** 125-133.

JONES, R. G. & THOMPSON, C. B. 2009. Tumor suppressors and cell metabolism: a recipe for cancer growth. *Genes & development,* 23**,** 537-548.

JONES, S. N., ROE, A. E., DONEHOWER, L. A. & BRADLEY, A. 1995. Rescue of embryonic lethality in Mdm2-deficient mice by absence of p53. *Nature,* 378**,** 206-208.

JOSSON, S., XU, Y., FANG, F., ST CLAIR, D. & ST CLAIR, W. 2005. RelB enhances oxidative stress response, cell survival and tumorigenicity in prostate cancer cells. *Cancer Research,* 65**,** 1128-1129.

JUMPER, J., EVANS, R., PRITZEL, A., GREEN, T., FIGURNOV, M., RONNEBERGER, O., TUNYASUVUNAKOOL, K., BATES, R., ŽÍDEK, A. & POTAPENKO, A. 2021. Highly accurate protein structure prediction with AlphaFold. *Nature,* 596**,** 583-589.

KADAKIA, S., HELMAN, S. N., BADHEY, A. K., SAMAN, M. & DUCIC, Y. 2014. Treacher Collins Syndrome: the genetics of a craniofacial disease. *International journal of pediatric otorhinolaryngology,* 78**,** 893-898.

KAESER, M. D., PEBERNARD, S. & IGGO, R. D. 2004. Regulation of p53 stability and function in HCT116 colon cancer cells. *Journal of Biological Chemistry,* 279**,** 7598-7605.

KALTSCHMIDT, B., GREINER, J., KADHIM, H. & KALTSCHMIDT, C. 2018. Subunit-Specific Role of NF-κB in Cancer. *Biomedicines,* 6**,** 44-44.

KAM-MORGAN, L. N. W., LAVOIE, T. B., SMITH-GILL, S. J. & KIRSCH, J. F. 1993. [36] Site-directed mutagenesis in analysis of protein-protein interactions. *Methods in Enzymology.* Academic Press.

KAMPEN, K. R., SULIMA, S. O., VEREECKE, S. & DE KEERSMAECKER, K. 2019. Hallmarks of ribosomopathies. *Nucleic Acids Research***,** 1-16.

KARIN, M. 1999. How NF-κB is activated: the role of the IκB kinase (IKK) complex. *Oncogene,* 18**,** 6867-6874.

KARIN, M. 2009. NF-kappaB as a critical link between inflammation and cancer. *Cold Spring Harb Perspect Biol,* 1**,** a000141.

KARIN, M., CAO, Y., GRETEN, F. R. & LI, Z.-W. 2002. NF-κB in cancer: from innocent bystander to major culprit. *Nature Reviews Cancer,* 2**,** 301-301.

KASS, S., CRAIG, N. & SOLLNER-WEBB, B. 1987. Primary processing of mammalian rRNA involves two adjacent cleavages and is not species specific. *Molecular and cellular biology,* 7**,** 2891-2898.

KASTAN, M. B. & BARTEK, J. 2004. Cell-cycle checkpoints and cancer. *Nature,* 432**,** 316-323.

KEATS, J. J., FONSECA, R., CHESI, M., SCHOP, R., BAKER, A., CHNG, W. J., VAN WIER, S., TIEDEMANN, R., SHI, C. X., SEBAG, M., BRAGGIO, E., HENRY, T., ZHU, Y. X., FOGLE, H., PRICE-TROSKA, T., AHMANN, G., MANCINI, C., BRENTS, L. A., KUMAR, S., GREIPP, P., DISPENZIERI, A., BRYANT, B., MULLIGAN, G., BRUHN, L., BARRETT, M., VALDEZ, R., TRENT, J., STEWART, A. K., CARPTEN, J. & BERGSAGEL, P. L. 2007. Promiscuous mutations activate the noncanonical NF-kappaB pathway in multiple myeloma. *Cancer Cell,* 12**,** 131-44.

KHARDE, S., CALVINO, F. R., GUMIERO, A., WILD, K. & SINNING, I. 2015. The structure of Rpf2–Rrs1 explains its role in ribosome biogenesis. *Nucleic Acids Research,* 43**,** 7083-7095.

KHATTER, H., MYASNIKOV, A. G., NATCHIAR, S. K. & KLAHOLZ, B. P. 2015. Structure of the human 80S ribosome. *Nature,* 520**,** 640-640.

KLAUCK, S., FELDER, B., KOLB-KOKOCINSKI, A., SCHUSTER, C., CHIOCCHETTI, A., SCHUPP, I., WELLENREUTHER, R., SCHMÖTZER, G., POUSTKA, F. & BREITENBACH-KOLLER, L. 2006. Mutations in the ribosomal protein gene RPL10 suggest a novel modulating disease mechanism for autism. *Molecular psychiatry,* 11**,** 1073-1084.

KOBYŁECKI, K., DRĄŻKOWSKA, K., KULIŃSKI, T. M., DZIEMBOWSKI, A. & TOMECKI, R. 2018. Elimination of 01/A'–A0 pre-rRNA processing by-product in human cells involves cooperative action of two nuclear exosome-associated nucleases: RRP6 and DIS3. *RNA,* 24**,** 1677-1692.

KOVALENKO, A., CHABLE-BESSIA, C., CANTARELLA, G., ISRAËL, A., WALLACH, D. & COURTOIS, G. 2003. The tumour suppressor CYLD negatively regulates NF-κB signalling by deubiquitination. *Nature,* 424**,** 801-805.

KOWALSMAN, N. & EISENSTEIN, M. 2006. Inherent limitations in protein–protein docking procedures. *Bioinformatics,* 23**,** 421-426.

KRESSLER, D., HURT, E. & BABLER, J. 2010. Driving ribosome assembly. *Biochimica et Biophysica Acta (BBA)-Molecular Cell Research,* 1803**,** 673-683.

KUHN, L. B., VALENTIN, S., STOJANOVIC, K., STROBL, D. C., BABUSHKU, T., WANG, Y., RAMBOLD, U., SCHEFFLER, L., GRATH, S., JOHN-ROBBERT, D., BLUM, H., FEUCHTINGER, A., BLUTKE, A., WEIH, F., KITAMURA, D., RAD, R., STROBL, L. J. & ZIMBER-STROBL, U. 2022. RelB contributes to the survival, migration and lymphomagenesis of B cells with constitutively active CD40 signaling. *Front Immunol,* 13**,** 913275.

KUNSCH, C., RUBEN, S. M. & ROSEN, C. A. 1992. Selection of optimal kappa B/Rel DNA-binding motifs: interaction of both subunits of NF-kappa B with DNA is required for transcriptional activation. *Molecular and Cellular Biology,* 12**,** 4412-4421.

KURZ, E. U., DOUGLAS, P. & LEES-MILLER, S. P. 2004. Doxorubicin Activates ATM-dependent Phosphorylation of Multiple Downstream Targets in Part through the Generation of Reactive Oxygen Species *. *Journal of Biological Chemistry,* 279**,** 53272-53281.

LAM, Y. W., LAMOND, A. I., MANN, M. & ANDERSEN, J. S. 2007. Analysis of nucleolar protein dynamics reveals the nuclear degradation of ribosomal proteins. *Curr Biol,* 17**,** 749-60.

LAMBERT, S. A., JOLMA, A., CAMPITELLI, L. F., DAS, P. K., YIN, Y., ALBU, M., CHEN, X., TAIPALE, J., HUGHES, T. R. & WEIRAUCH, M. T. 2018. The Human Transcription Factors. *Cell,* 172**,** 650-665.

LEDOUX, ADELINE C. & PERKINS, NEIL D. 2014. NF-κB and the cell cycle. *Biochemical Society Transactions,* 42**,** 76-81.

LEDOUX, A. C., SELLIER, H., GILLIES, K., IANNETTI, A., JAMES, J. & PERKINS, N. D. 2013. NFκB regulates expression of Polo-like kinase 4. *Cell Cycle,* 12**,** 3052-62.

LEE, B. M., XU, J., CLARKSON, B. K., MARTINEZ-YAMOUT, M. A., DYSON, H. J., CASE, D. A., GOTTESFELD, J. M. & WRIGHT, P. E. 2006. Induced fit and "lock and key" recognition of 5 S RNA by zinc fingers of transcription factor IIIA. *Journal of molecular biology,* 357**,** 275-291.

LEE, TONG I. & YOUNG, RICHARD A. 2013. Transcriptional Regulation and Its Misregulation in Disease. *Cell,* 152**,** 1237-1251.

LEMMENS, B. & LINDQVIST, A. 2019. DNA replication and mitotic entry: A brake model for cell cycle progression. *Journal of Cell Biology,* 218**,** 3892-3902.

LENSINK, M. F. & WODAK, S. J. 2013. Docking, scoring, and affinity prediction in CAPRI. *Proteins: Structure, Function, and Bioinformatics,* 81**,** 2082-2095.

LEONARD, B., MCCANN, J. L., STARRETT, G. J., KOSYAKOVSKY, L., LUENGAS, E. M., MOLAN, A. M., BURNS, M. B., MCDOUGLE, R. M., PARKER, P. J., BROWN, W. L. & HARRIS, R. S. 2015. The PKC/NF-κB signaling pathway induces APOBEC3B expression in multiple human cancers. *Cancer Res,* 75**,** 4538-47.

LEVY, S., AVNI, D., HARIHARAN, N., PERRY, R. P. & MEYUHAS, O. 1991. Oligopyrimidine tract at the 5'end of mammalian ribosomal protein mRNAs is required for their translational control. *Proceedings of the National Academy of Sciences,* 88**,** 3319-3323.

LI, Y., WANG, H., ZHOU, X., XIE, X., CHEN, X., JIE, Z., ZOU, Q., HU, H., ZHU, L., CHENG, X., BRIGHTBILL, H. D., WU, L. C., WANG, L. & SUN, S. C. 2016. Cell intrinsic role of NF-κB-inducing kinase in regulating T cell-mediated immune and autoimmune responses. *Sci Rep,* 6**,** 22115.

LI, Y., ZHOU, Q. L., SUN, W., CHANDRASEKHARAN, P., CHENG, H. S., YING, Z., LAKSHMANAN, M., RAJU, A., TENEN, D. G., CHENG, S. Y., CHUANG, K. H., LI, J., PRABHAKAR, S., LI, M. & TERGAONKAR, V. 2015. Non-canonical NF-κB signalling and ETS1/2 cooperatively drive C250T mutant TERT promoter activation. *Nat Cell Biol,* 17**,** 1327-38.

LI, Z.-W., CHU, W., HU, Y., DELHASE, M., DEERINCK, T., ELLISMAN, M., JOHNSON, R. & KARIN, M. 1999. The IKKβ Subunit of IκB Kinase (IKK) is Essential for Nuclear Factor κB Activation and Prevention of Apoptosis. *Journal of Experimental Medicine,* 189**,** 1839-1845.

LIANG, C., ZHANG, M. & SUN, S.-C. 2006. β-TrCP binding and processing of NF-κB2/p100 involve its phosphorylation at serines 866 and 870. *Cellular Signalling,* 18**,** 1309-1317.

LIAO, G. & SUN, S.-C. 2003. Regulation of NF-κB2/p100 processing by its nuclear shuttling. *Oncogene,* 22**,** 4868-4874.

LINDQVIST, A., RODRÍGUEZ-BRAVO, V. & MEDEMA, R. H. 2009. The decision to enter mitosis: feedback and redundancy in the mitotic entry network. *Journal of Cell Biology,* 185**,** 193-202.

LINDSTRÖM, M. S., BARTEK, J. & MAYA-MENDOZA, A. 2022. p53 at the crossroad of DNA replication and ribosome biogenesis stress pathways. *Cell Death & Differentiation,* 29**,** 972-982.

LING, L., CAO, Z. & GOEDDEL, D. V. 1998. NF-kappaB-inducing kinase activates IKK-alpha by phosphorylation of Ser-176. *Proceedings of the National Academy of Sciences of the United States of America,* 95**,** 3792-3797.

LIPTAY, S., SCHMID, R. M., NABEL, E. G. & NABEL, G. J. 1994a. Transcriptional regulation of NF-kappa B2: evidence for kappa B-mediated positive and negative autoregulation. *Molecular and cellular biology,* 14**,** 7695-7703.

LIPTAY, S., SCHMID, R. M., NABEL, E. G. & NABEL, G. J. 1994b. Transcriptional regulation of NF-kappa B2: evidence for kappa B-mediated positive and negative autoregulation. *Mol Cell Biol,* 14**,** 7695-703.

LIU, D., ZHONG, Z. & KARIN, M. 2022a. NF-κB: A Double-Edged Sword Controlling Inflammation. *Biomedicines,* 10**,** 1250.

LIU, D., ZHONG, Z. & KARIN, M. 2022b. NF-κB: A Double-Edged Sword Controlling Inflammation. *Biomedicines* [Online], 10.

LIU, J., SUDOM, A., MIN, X., CAO, Z., GAO, X., AYRES, M., LEE, F., CAO, P., JOHNSTONE, S., PLOTNIKOVA, O., WALKER, N., CHEN, G. & WANG, Z. 2012. Structure of the nuclear factor κB-inducing kinase (NIK) kinase domain reveals a constitutively active conformation. *The Journal of biological chemistry,* 287**,** 27326-27334.

LIU, T., ZHANG, L., JOO, D. & SUN, S.-C. 2017. NF-κB signaling in inflammation. *Signal Transduction and Targeted Therapy,* 2**,** 17023.

LIU, Y., HE, Y., JIN, A., TIKUNOV, A. P., ZHOU, L., TOLLINI, L. A., LESLIE, P., KIM, T.-H., LI, L. O., COLEMAN, R. A., GU, Z., CHEN, Y. Q., MACDONALD, J. M., GRAVES, L. M. & ZHANG, Y. 2014. Ribosomal protein–Mdm2–p53 pathway coordinates nutrient stress with lipid metabolism by regulating MCD and promoting fatty acid oxidation. *Proceedings of the National Academy of Sciences,* 111**,** E2414-E2422.

LLOVET, J. M., CASTET, F., HEIKENWALDER, M., MAINI, M. K., MAZZAFERRO, V., PINATO, D. J., PIKARSKY, E., ZHU, A. X. & FINN, R. S. 2022. Immunotherapies for hepatocellular carcinoma. *Nature Reviews Clinical Oncology,* 19**,** 151-172.

LUKAS, J., LUKAS, C. & BARTEK, J. 2004. Mammalian cell cycle checkpoints: signalling pathways and their organization in space and time. *DNA Repair,* 3**,** 997-1007.

LUPI, L. A., CUCIELO, M. S., SILVEIRA, H. S., GAIOTTE, L. B., CESÁRIO, R. C., SEIVA, F. R. F. & DE ALMEIDA CHUFFA, L. G. 2020. The role of Toll-like receptor 4 signaling pathway in ovarian, cervical, and endometrial cancers. *Life sciences,* 247**,** 117435.

MACALINO, S. J. Y., BASITH, S., CLAVIO, N. A. B., CHANG, H., KANG, S. & CHOI, S. 2018. Evolution of In Silico Strategies for Protein-Protein Interaction Drug Discovery. *Molecules,* 23**,** 1963.

MACIAS, E., JIN, A., DEISENROTH, C., BHAT, K., MAO, H., LINDSTRÖM, M. S. & ZHANG, Y. 2010. An ARF-independent c-MYC-activated tumor suppression pathway mediated by ribosomal protein-Mdm2 Interaction. *Cancer cell,* 18**,** 231-243.

MADRU, C., LEBARON, S., BLAUD, M., DELBOS, L., PIPOLI, J., PASMANT, E., RÉTY, S. & LEULLIOT, N. 2015. Chaperoning 5S RNA assembly. *Genes & development,* 29**,** 1432-1446.

MAHATA, B., SUNDQVIST, A. & XIRODIMAS, D. P. 2012. Recruitment of RPL11 at promoter sites of p53-regulated genes upon nucleolar stress through NEDD8 and in an Mdm2-dependent manner. *Oncogene,* 31**,** 3060-3071.

MALOVANNAYA, A., LANZ, R. B., JUNG, S. Y., BULYNKO, Y., LE, N. T., CHAN, D. W., DING, C., SHI, Y., YUCER, N., KRENCIUTE, G., KIM, B. J., LI, C., CHEN, R., LI, W., WANG, Y., O'MALLEY, B. W. & QIN, J. 2011. Analysis of the human endogenous coregulator complexome. *Cell,* 145**,** 787-99.

MANSFIELD, K. M., CARTER, N. M., NGUYEN, L., CLEVES, P. A., ALSHANBAYEVA, A., WILLIAMS, L. M., CROWDER, C., PENVOSE, A. R., FINNERTY, J. R., WEIS, V. M., SIGGERS, T. W. & GILMORE, T. D. 2017. Transcription factor NF-κB is modulated by symbiotic status in a sea anemone model of cnidarian bleaching. *Scientific Reports,* 7**,** 16025-16025.

MARINARI, B., COSTANZO, A., MARZANO, V., PICCOLELLA, E. & TUOSTO, L. 2004. CD28 delivers a unique signal leading to the selective recruitment of RelA and p52 NF-kappaB subunits on IL-8 and Bcl-xL gene promoters. *Proc Natl Acad Sci U S A,* 101**,** 6098-103.

MARTIN, I., KIM, J. W., LEE, B. D., KANG, H. C., XU, J.-C., JIA, H., STANKOWSKI, J., KIM, M.-S., ZHONG, J. & KUMAR, M. 2014. Ribosomal protein s15 phosphorylation mediates LRRK2 neurodegeneration in Parkinson's disease. *Cell,* 157**,** 472-485.

MASSOUMI, R., CHMIELARSKA, K., HENNECKE, K., PFEIFER, A. & FÄSSLER, R. 2006. Cyld inhibits tumor cell proliferation by blocking Bcl-3-dependent NF-κB signaling. *Cell,* 125**,** 665-677.

MATTHEWS, J. R., NICHOLSON, J., JAFFRAY, E., KELLY, S. M., PRICE, N. C. & HAY, R. T. 1995. Conformational changes induced by DNA binding of NF-κB. *Nucleic Acids Research,* 23**,** 3393-3402.

MAURO, V. P. & EDELMAN, G. M. 2002. The ribosome filter hypothesis. *Proc Natl Acad Sci U S A,* 99**,** 12031-6.

MAVINAHALLI, J. N., MADHUMALAR, A., BEUERMAN, R. W., LANE, D. P. & VERMA, C. 2010. Differences in the transactivation domains of p53 family members: a computational study. *BMC genomics,* 11**,** 1-17.

MCDONNELL, J. M. 2001. Surface plasmon resonance: towards an understanding of the mechanisms of biological molecular recognition. *Current opinion in chemical biology,* 5**,** 572-577.

MCGOWAN, K. A. & MASON, P. J. 2011. Animal models of Diamond Blackfan anemia. *Seminars in hematology,* 48**,** 106-116.

MCINNES, I. B. & SCHETT, G. 2011. The pathogenesis of rheumatoid arthritis. *New England Journal of Medicine,* 365**,** 2205-2219.

MERKEL, O., WACHT, N., SIFFT, E., MELCHARDT, T., HAMACHER, F., KOCHER, T., DENK, U., HOFBAUER, J. P., EGLE, A., SCHEIDELER, M., SCHLEDERER, M., STEURER, M., KENNER, L. & GREIL, R. 2012. Actinomycin D induces p53-independent cell death and prolongs survival in high-risk chronic lymphocytic leukemia. *Leukemia,* 26**,** 2508-2516.

MIZUGUCHI, K. & AHMAD, S. 2014. Conformational changes in DNA-binding proteins: Relationships with precomplex features and contributions to specificity and stability. *Proteins: Structure, Function, and Bioinformatics,* 82**,** 841-857.

MOLAVI, G., SAMADI, N. & HOSSEINGHOLI, E. Z. 2019. The roles of moonlight ribosomal proteins in the development of human cancers. *Journal of cellular physiology,* 234**,** 8327-8341.

MOLES, A., BUTTERWORTH, J. A., SANCHEZ, A., HUNTER, J. E., LESLIE, J., SELLIER, H., TINIAKOS, D., COCKELL, S. J., MANN, D. A., OAKLEY, F. & PERKINS, N. D. 2016. A RelA(p65) Thr505 phospho-site mutation reveals an important mechanism regulating NF-κB-dependent liver regeneration and cancer. *Oncogene,* 35**,** 4623-4623.

MÜLLER, I., JENNER, A., BRUCHELT, G., NIETHAMMER, D. & HALLIWELL, B. 1997. Effect of Concentration on the Cytotoxic Mechanism of Doxorubicin—Apoptosis and Oxidative DNA Damage. *Biochemical and Biophysical Research Communications,* 230**,** 254-257.

MULLINEUX, S.-T. & LAFONTAINE, D. L. J. 2012. Mapping the cleavage sites on mammalian pre-rRNAs: Where do we stand? *Biochimie,* 94**,** 1521-1532.

MULTHOFF, G., MOLLS, M. & RADONS, J. 2012. Chronic Inflammation in Cancer Development. *Frontiers in Immunology,* 2.

MURAKAMI, Y. & MIZUGUCHI, K. 2010. Applying the Naïve Bayes classifier with kernel density estimation to the prediction of protein–protein interaction sites. *Bioinformatics,* 26**,** 1841-1848.

MURRAY, J. K. & GELLMAN, S. H. 2007. Targeting protein–protein interactions: Lessons from p53/MDM2. *Peptide Science,* 88**,** 657-686.

NARLA, A. & EBERT, B. L. 2010. Ribosomopathies: human disorders of ribosome dysfunction. *Blood, The Journal of the American Society of Hematology,* 115**,** 3196-3205.

NAZAR, R. 2004. Ribosomal RNA processing and ribosome biogenesis in eukaryotes. *IUBMB life,* 56**,** 457-465.

NIJNIK, A., MOTT, R., KWIATKOWSKI, D. P. & UDALOVA, I. A. 2003. Comparing the fine specificity of DNA binding by NF-κB p50 and p52 using principal coordinates analysis. *Nucleic Acids Research,* 31**,** 1497-1501.

NILSSON, I. & HOFFMANN, I. 2000. Cell cycle regulation by the Cdc25 phosphatase family. *Progress in cell cycle research***,** 107-114.

NOOREN, I. M. A. & THORNTON, J. M. 2003a. Diversity of protein–protein interactions. *The EMBO Journal,* 22**,** 3486-3492.

NOOREN, I. M. A. & THORNTON, J. M. 2003b. Structural Characterisation and Functional Significance of Transient Protein–Protein Interactions. *Journal of Molecular Biology,* 325**,** 991-1018.

NOVACK, D. V., YIN, L., HAGEN-STAPLETON, A., SCHREIBER, R. D., GOEDDEL, D. V., ROSS, F. P. & TEITELBAUM, S. L. 2003. The IκB Function of NF-κB2 p100 Controls Stimulated Osteoclastogenesis. *Journal of Experimental Medicine,* 198**,** 771-781.

NURSE, P. 2000. A long twentieth century of the cell cycle and beyond. *Cell,* 100**,** 71-78.

O'DONOHUE, M. F., DA COSTA, L., LEZZERINI, M., UNAL, S., JORET, C., BARTELS, M., BRILSTRA, E., SCHEIJDE-VERMEULEN, M., WACHEUL, L., DE KEERSMAECKER, K., VEREECKE, S., LABARQUE, V., SABY, M., LEFEVRE, S. D., PLATON, J., MONTEL-LEHRY, N., LAUGERO, N., LACAZETTE, E., VAN GASSEN, K., HOUTKOOPER, R. H., SIMSEK-KIPER, P. O., LEBLANC, T., YARALI, N., CETINKAYA, A., AKARSU, N. A., GLEIZES, P. E., LAFONTAINE, D. L. J. & MACINNES, A. W. 2022. HEATR3 variants impair nuclear import of uL18 (RPL5) and drive Diamond-Blackfan anemia. *Blood,* 139**,** 3111-3126.

OAKLEY, T. H. & RIVERA, A. S. 2008. Genomics and the evolutionary origins of nervous system complexity. *Current Opinion in Genetics & Development,* 18**,** 479-492.

OKOROKOV, A. L., SHERMAN, M. B., PLISSON, C., GRINKEVICH, V., SIGMUNDSSON, K., SELIVANOVA, G., MILNER, J. & ORLOVA, E. V. 2006. The structure of p53 tumour

suppressor protein reveals the basis for its functional plasticity. *The EMBO Journal,* 25**,** 5191-5200.

PAEK, A. L., LIU, J. C., LOEWER, A., FORRESTER, W. C. & LAHAV, G. 2016. Cell-to-Cell Variation in p53 Dynamics Leads to Fractional Killing. *Cell,* 165**,** 631-642.

PAN, W., DENG, L., WANG, H. & WANG, V. Y. 2022. Atypical IκB Bcl3 enhances the generation of the NF-κB p52 homodimer. *Front Cell Dev Biol,* 10**,** 930619.

PANAGOPOULOS, A. & ALTMEYER, M. 2021. The Hammer and the Dance of Cell Cycle Control. *Trends in Biochemical Sciences,* 46**,** 301-314.

PANCER, Z., RAST, J. P. & DAVIDSON, E. H. 1999. Origins of immunity: transcription factors and homologues of effector genes of the vertebrate immune system expressed in sea urchin coelomocytes. *Immunogenetics,* 49**,** 773-86.

PAPOUTSOPOULOU, S., TANG, J., ELRAMLI, A. H., WILLIAMS, J. M., GUPTA, N., IKUOMOLA, F. I., SHEIBANI-TEZERJI, R., ALAM, M. T., HERNÁNDEZ-FERNAUD, J. R., CAAMAÑO, J. H., PROBERT, C. S., MULLER, W., DUCKWORTH, C. A. & PRITCHARD, D. M. 2022. Nfkb2 deficiency and its impact on plasma cells and immunoglobulin expression in murine small intestinal mucosa. *American Journal of Physiology-Gastrointestinal and Liver Physiology,* 323**,** G306-G317.

PARKER, L. L., ATHERTON-FESSLER, S. & PIWNICA-WORMS, H. 1992. p107wee1 is a dual-specificity kinase that phosphorylates p34cdc2 on tyrosine 15. *Proceedings of the National Academy of Sciences,* 89**,** 2917-2921.

PELAVA, A., SCHNEIDER, C. & WATKINS, N. J. 2016. The importance of ribosome production, and the 5S RNP-MDM2 pathway, in health and disease. *Biochemical Society Transactions,* 44**,** 1086-1090.

PELLETIER, J., THOMAS, G. & VOLAREVIĆ, S. 2017. Ribosome biogenesis in cancer: new players and therapeutic avenues. *Nature Reviews Cancer,* 18**,** 51-51.

PELTONEN, K., COLIS, L., LIU, H., TRIVEDI, R., MOUBAREK, M. S., MOORE, H. M., BAI, B., RUDEK, M. A., BIEBERICH, C. J. & LAIHO, M. 2014. A targeting modality for destruction of RNA polymerase I that possesses anticancer activity. *Cancer cell,* 25**,** 77-90.

PERKINS, N. D. 2000. The Rel/NF-κB family: friend and foe. *Trends in Biochemical Sciences,* 25**,** 434-440.

PERKINS, N. D. 2003. Oncogenes, tumor suppressors and p52 NF-κB. *Oncogene,* 22**,** 7553-7556.

PERKINS, N. D. 2012. The diverse and complex roles of NF-κB subunits in cancer. *Nature Reviews Cancer,* 12**,** 121-132.

PERKINS, N. D., AGRANOFF, A. B., PASCAL, E. & NABEL, G. J. 1994. An interaction between the DNA-binding domains of RelA(p65) and Sp1 mediates human immunodeficiency virus gene activation. *Mol Cell Biol,* 14**,** 6570-83.

PERKINS, N. D. & GILMORE, T. D. 2006. Good cop, bad cop: The different faces of NF-κB. *Cell Death and Differentiation,* 13**,** 759-772.

PERKINS, N. D., SCHMID, R. M., DUCKETT, C. S., LEUNG, K., RICE, N. R. & NABEL, G. J. 1992. Distinct combinations of NF-kappa B subunits determine the specificity of transcriptional activation. *Proceedings of the National Academy of Sciences,* 89**,** 1529-1533.

PETTERSEN, E. F., GODDARD, T. D., HUANG, C. C., MENG, E. C., COUCH, G. S., CROLL, T. I., MORRIS, J. H. & FERRIN, T. E. 2021. UCSF ChimeraX: Structure visualization for researchers, educators, and developers. *Protein Sci,* 30**,** 70-82.

PFLAUM, J., SCHLOSSER, S. & MÜLLER, M. 2014. p53 Family and Cellular Stress Responses in Cancer. *Front Oncol,* 4**,** 285.

PFLUG, K. M. & SITCHERAN, R. 2020. Targeting NF-κB-Inducing Kinase (NIK) in Immunity, Inflammation, and Cancer. *International Journal of Molecular Sciences,* 21**,** 8470.

PILLET, B., MITTERER, V., KRESSLER, D. & PERTSCHY, B. 2017. Hold on to your friends: Dedicated chaperones of ribosomal proteins: Dedicated chaperones mediate the safe transfer of ribosomal proteins to their site of pre-ribosome incorporation. *Bioessays,* 39**,** 1-12.

PODHORECKA, M., SKLADANOWSKI, A. & BOZKO, P. 2010. H2AX phosphorylation: its role in DNA damage response and cancer therapy. *Journal of nucleic acids,* 2010.

POINTER, K. B., BUDKE, B., SULLIVAN, K. & CONNELL, P. P. 2020. Targeting of Non-canonical NF-κB Factor p100/p52 Inhibits Homologous Recombination and Sensitizes Cancer Cells to DNA-damaging Therapy. *International Journal of Radiation Oncology, Biology, Physics,* 108**,** e545.

PURVIS, J. E., KARHOHS, K. W., MOCK, C., BATCHELOR, E., LOEWER, A. & LAHAV, G. 2012. P53 Dynamics Control Cell Fate. *Science,* 336**,** 1440-1444.

QING, G., QU, Z. & XIAO, G. 2005. Stabilization of basally translated NF-κB-inducing kinase (NIK) protein functions as a molecular switch of processing of NF-κB2 p100. *Journal of Biological Chemistry,* 280**,** 40578-40582.

QUAGLIO, D., INFANTE, P., DI MARCOTULLIO, L., BOTTA, B. & MORI, M. 2020. Hedgehog signaling pathway inhibitors: an updated patent review (2015–present). *Expert Opinion on Therapeutic Patents,* 30**,** 235-250.

QUAX, TESSA E. F., CLAASSENS, NICO J., SÖLL, D. & VAN DER OOST, J. 2015. Codon Bias as a Means to Fine-Tune Gene Expression. *Molecular Cell,* 59**,** 149-161.

RADAEVA, M., TON, A.-T., HSING, M., BAN, F. & CHERKASOV, A. 2021. Drugging the 'undruggable'. Therapeutic targeting of protein–DNA interactions with the use of computer-aided drug discovery methods. *Drug Discovery Today,* 26**,** 2660-2679.

RADHAKRISHNAN, S. K., GIERUT, J. & GARTEL, A. L. 2006. Multiple alternate p21 transcripts are regulated by p53 in human cells. *Oncogene,* 25**,** 1812-1815.

RAJKUMAR, S. V. 2011. Treatment of multiple myeloma. *Nature reviews Clinical oncology,* 8**,** 479-491.

RAMSEY, K. M., DEMBINSKI, H. E., CHEN, W., RICCI, C. G. & KOMIVES, E. A. 2017. DNA and IκBα Both Induce Long-Range Conformational Changes in NFκB. *Journal of Molecular Biology,* 429**,** 999-1008.

RAPE, M. & JENTSCH, S. 2004. Productive RUPture: activation of transcription factors by proteasomal processing. *Biochimica et Biophysica Acta (BBA) - Molecular Cell Research,* 1695**,** 209-213.

RAŠKA, I., KOBERNA, K., MALÍNSKÝ, J., FIDLEROVÁ, H. & MAŠATA, M. 2004. The nucleolus and transcription of ribosomal genes. *Biology of the Cell,* 96**,** 579-594.

RAUDVERE, U., KOLBERG, L., KUZMIN, I., ARAK, T., ADLER, P., PETERSON, H. & VILO, J. 2019. g:Profiler: a web server for functional enrichment analysis and conversions of gene lists (2019 update). *Nucleic Acids Research,* 47**,** W191-W198.

REITER, F., WIENERROITHER, S. & STARK, A. 2017. Combinatorial function of transcription factors and cofactors. *Current Opinion in Genetics & Development,* 43**,** 73-81.

RIABOWOL, K., DRAETTA, G., BRIZUELA, L., VANDRE, D. & BEACH, D. 1989. The cdc2 kinase is a nuclear protein that is essential for mitosis in mammalian cells. *Cell,* 57**,** 393-401.

RIVERA DEL RIO, A., VAN DER WIELEN, N., GERRITS, W. J. J., BOOM, R. M. & JANSSEN, A. E. M. 2022. In silico modelling of protein digestion: A case study on solid/liquid and blended meals. *Food Research International,* 157**,** 111271.

ROCHA, S., MARTIN, A. M., MEEK, D. W. & PERKINS, N. D. 2003. p53 Represses Cyclin D1 Transcription through Down Regulation of Bcl-3 and Inducing Increased Association

of the p52 NF-κB Subunit with Histone Deacetylase 1. *Molecular and Cellular Biology,* 23**,** 4713 LP-4727.

ROJO, F., GONZÁLEZ-PÉREZ, A., FURRIOL, J., NICOLAU, M. J., FERRER, J., BURGUÉS, O., SABBAGHI, M., GONZÁLEZ-NAVARRETE, I., CRISTOBAL, I., SERRANO, L., ZAZO, S., MADOZ, J., SERVITJA, S., TUSQUETS, I., ALBANELL, J., LLUCH, A., ROVIRA, A. & EROLES, P. 2016. Non-canonical NF-κB pathway activation predicts outcome in borderline oestrogen receptor positive breast carcinoma. *Br J Cancer,* 115**,** 322-31.

ROVILLAIN, E., MANSFIELD, L., CAETANO, C., ALVAREZ-FERNANDEZ, M., CABALLERO, O. L., MEDEMA, R. H., HUMMERICH, H. & JAT, P. S. 2011. Activation of nuclear factor-kappa B signalling promotes cellular senescence. *Oncogene,* 30**,** 2356-2366.

RUDOLPH, D., YEH, W. C., WAKEHAM, A., RUDOLPH, B., NALLAINATHAN, D., POTTER, J., ELIA, A. J. & MAK, T. W. 2000. Severe liver degeneration and lack of NF-kappaB activation in NEMO/IKKgamma-deficient mice. *Genes Dev,* 14**,** 854-62.

SATYANARAYANA, A. & KALDIS, P. 2009. Mammalian cell-cycle regulation: several Cdks, numerous cyclins and diverse compensatory mechanisms. *Oncogene,* 28**,** 2925-2939.

SAUER, M., BRETZ, A. C., BEINORAVICIUTE-KELLNER, R., BEITZINGER, M., BUREK, C., ROSENWALD, A., HARMS, G. S. & STIEWE, T. 2008. C-terminal diversity within the p53 family accounts for differences in DNA binding and transcriptional activity. *Nucleic acids research,* 36**,** 1900-1912.

SAZONOVA, E. V., PETRICHUK, S. V., KOPEINA, G. S. & ZHIVOTOVSKY, B. 2021. A link between mitotic defects and mitotic catastrophe: detection and cell fate. *Biology Direct,* 16**,** 1-11.

SCHIMMACK, G., SCHORPP, K., KUTZNER, K., GEHRING, T., BRENKE, J. K., HADIAN, K. & KRAPPMANN, D. 2017. YOD1/TRAF6 association balances p62-dependent IL-1 signaling to NF-κB. *Elife,* 6**,** e22416.

SCHMID, R. M., PERKINS, N. D., DUCKETT, C. S., ANDREWS, P. C. & NABEL, G. J. 1991. Cloning of an NF-κB subunit which stimulates HIV transcription in synergy with p65. *Nature,* 352**,** 733-736.

SCHNEIDER, G., SAUR, D., SIVEKE, J. T., FRITSCH, R., GRETEN, F. R. & SCHMID, R. M. 2006. IKKα controls p52/RelB at the skp2 gene promoter to regulate G1- to S-phase progression. *EMBO Journal,* 25**,** 3801-3812.

SCHON, O., FRIEDLER, A., BYCROFT, M., FREUND, S. M. V. & FERSHT, A. R. 2002. Molecular Mechanism of the Interaction between MDM2 and p53. *Journal of Molecular Biology,* 323**,** 491-501.

SCHREIBER, S., NIKOLAUS, S. & HAMPE, J. 1998. Activation of nuclear factor κB in inflammatory bowel disease. *Gut,* 42**,** 477-484.

SCHUMM, K. 2006. The Role of NF-κB2 in the control of cell cycle and regulation of tumour suppressor protein p53.

SCHUMM, K., ROCHA, S., CAAMANO, J. & PERKINS, N. D. 2006. Regulation of p53 tumour suppressor target gene expression by the p52 NF-κB subunit. *EMBO Journal,* 25**,** 4820-4832.

SÉE, V., RAJALA, N. K., SPILLER, D. G. & WHITE, M. R. 2004. Calcium-dependent regulation of the cell cycle via a novel MAPK–NF-κB pathway in Swiss 3T3 cells. *The Journal of cell biology,* 166**,** 661-672.

SEITZ, C. S., DENG, H., HINATA, K., LIN, Q. & KHAVARI, P. A. 2000. Nuclear factor κB subunits induce epithelial cell growth arrest. *Cancer research,* 60**,** 4085-4092.

SEN, R. & BALTIMORE, D. 1986. Inducibility of κ immunoglobulin enhancer-binding protein NF-κB by a posttranslational mechanism. *Cell,* 47**,** 921-928.

SHEEHY, A. M. & SCHLISSEL, M. S. 1999. Overexpression of RelA causes G1 arrest and apoptosis in a pro-B cell line. *Journal of Biological Chemistry,* 274**,** 8708-8716.

SHEN, P. S. 2018. The 2017 Nobel Prize in Chemistry: cryo-EM comes of age. *Analytical and Bioanalytical Chemistry,* 410**,** 2053-2057.

SHERR, C. J. 1994. G1 phase progression: cycling on cue. *Cell,* 79**,** 551-5.

SHERR, C. J. & ROBERTS, J. M. 1999. CDK inhibitors: positive and negative regulators of G1-phase progression. *Genes & development,* 13**,** 1501-1512.

SHERR, C. J. & ROBERTS, J. M. 2004. Living with or without cyclins and cyclin-dependent kinases. *Genes & development,* 18**,** 2699-2711.

SHIH, V. F.-S., TSUI, R., CALDWELL, A. & HOFFMANN, A. 2011. A single NFκB system for both canonical and non-canonical signaling. *Cell Research,* 21**,** 86-102.

SHUKLA, S., MACLENNAN, G. T., FU, P., PATEL, J., MARENGO, S. R., RESNICK, M. L. & GUPTA, S. 2004. Nuclear Factor-κB/p65 (Rel A) Is Constitutively Activated in Human Prostate Adenocarcinoma and Correlates with Disease Progression. *Neoplasia,* 6**,** 390-400.

SIEBENMORGEN, T. & ZACHARIAS, M. 2020. Computational prediction of protein–protein binding affinities. *WIREs Computational Molecular Science,* 10**,** e1448.

SLOAN, K. E., BOHNSACK, M. T., SCHNEIDER, C. & WATKINS, N. J. 2014. The roles of SSU processome components and surveillance factors in the initial processing of human ribosomal RNA. *RNA (New York, N.Y.),* 20**,** 540-550.

SLOAN, K. E., BOHNSACK, M. T. & WATKINS, N. J. 2013a. The 5S RNP Couples p53 Homeostasis to Ribosome Biogenesis and Nucleolar Stress. *Cell Reports,* 5**,** 237-247.

SLOAN, K. E., KNOX, A. A., WELLS, G. R., SCHNEIDER, C. & WATKINS, N. J. 2019. Interactions and activities of factors involved in the late stages of human 18S rRNA maturation. *RNA Biology,* 16**,** 196-210.

SLOAN, K. E., MATTIJSSEN, S., LEBARON, S., TOLLERVEY, D., PRUIJN, G. J. & WATKINS, N. J. 2013b. Both endonucleolytic and exonucleolytic cleavage mediate ITS1 removal during human ribosomal RNA processing. *Journal of Cell Biology,* 200**,** 577-588.

SLOTTA, C., SCHLÜTER, T., RUIZ-PERERA, L. M., KADHIM, H. M., TERTEL, T., HENKEL, E., HÜBNER, W., GREINER, J. F., HUSER, T. & KALTSCHMIDT, B. 2017. CRISPR/Cas9-mediated knockout of c-REL in HeLa cells results in profound defects of the cell cycle. *PloS one,* 12**,** e0182373.

SMITH, E., SOMMA, D., KERRIGAN, D., MCLNTYRE, Z., COLE, J., LIANG, K. L., KIELY, P., KEESHAN, K. & CARMODY, R. 2019. The regulation of sequence specific NF-κB DNA binding and transcription by IKKβ phosphorylation of NF-κB p50 at serine 80. *Nucleic Acids Research,* 47.

SOLT, L. A. & MAY, M. J. 2008. The IκB kinase complex: master regulator of NF-κB signaling. *Immunologic Research,* 42**,** 3-18.

SUGA, H., CHEN, Z., DE MENDOZA, A., SEBÉ-PEDRÓS, A., BROWN, M. W., KRAMER, E., CARR, M., KERNER, P., VERVOORT, M., SÁNCHEZ-PONS, N., TORRUELLA, G., DERELLE, R., MANNING, G., LANG, B. F., RUSS, C., HAAS, B. J., ROGER, A. J., NUSBAUM, C. & RUIZ-TRILLO, I. 2013. The Capsaspora genome reveals a complex unicellular prehistory of animals. *Nat Commun,* 4**,** 2325.

SUGIMOTO, M., KUO, M.-L., ROUSSEL, M. F. & SHERR, C. J. 2003. Nucleolar Arf Tumor Suppressor Inhibits Ribosomal RNA Processing. *Molecular Cell,* 11**,** 415-424.

SULLIVAN, J. C., KALAITZIDIS, D., GILMORE, T. D. & FINNERTY, J. R. 2007. Rel homology domain-containing transcription factors in the cnidarian Nematostella vectensis. *Dev Genes Evol,* 217**,** 63-72.

SUN, S.-C. 2017. The non-canonical NF-κB pathway in immunity and inflammation. *Nature reviews. Immunology,* 17**,** 545-558.

SUN, S. C. & LEY, S. C. 2008. New insights into NF-kappaB regulation and function. *Trends Immunol,* 29**,** 469-78.

SUN, X.-X., DAI, M.-S. & LU, H. 2007. 5-fluorouracil activation of p53 involves an MDM2-ribosomal protein interaction. *Journal of Biological Chemistry,* 282**,** 8052-8059.

SUNDQVIST, A., LIU, G., MIRSALIOTIS, A. & XIRODIMAS, D. P. 2009. Regulation of nucleolar signalling to p53 through NEDDylation of L11. *EMBO reports,* 10**,** 1132-1139.

SUNNY, S. & JAYARAJ, P. B. 2022. Protein–Protein Docking: Past, Present, and Future. *The Protein Journal,* 41**,** 1-26.

SUSSMAN, J. L., LIN, D., JIANG, J., MANNING, N. O., PRILUSKY, J., RITTER, O. & ABOLA, E. E. 1998. Protein Data Bank (PDB): database of three-dimensional structural information of biological macromolecules. *Acta Crystallographica Section D: Biological Crystallography,* 54**,** 1078-1084.

SWIFT, L. H. & GOLSTEYN, R. M. 2016. Chapter 22 - The Relationship Between Checkpoint Adaptation and Mitotic Catastrophe in Genomic Changes in Cancer Cells. *In:* KOVALCHUK, I. & KOVALCHUK, O. (eds.) *Genome Stability.* Boston: Academic Press.

SZKLARCZYK, D., GABLE, A. L., NASTOU, K. C., LYON, D., KIRSCH, R., PYYSALO, S., DONCHEVA, N. T., LEGEAY, M., FANG, T., BORK, P., JENSEN, L. J. & VON MERING, C. 2020. The STRING database in 2021: customizable protein–protein networks, and functional characterization of user-uploaded gene/measurement sets. *Nucleic Acids Research,* 49**,** D605-D612.

TAFFOREAU, L., ZORBAS, C., LANGHENDRIES, J.-L., MULLINEUX, S.-T., STAMATOPOULOU, V., MULLIER, R., WACHEUL, L. & LAFONTAINE, DENIS L. J. 2013. The Complexity of Human Ribosome Biogenesis Revealed by Systematic Nucleolar Screening of Pre-rRNA Processing Factors. *Molecular Cell,* 51**,** 539-551.

TAKEDA, D. Y. & DUTTA, A. 2005. DNA replication and progression through S phase. *Oncogene,* 24**,** 2827-2843.

TAM, W. F., LEE, L. H., DAVIS, L. & SEN, R. 2000. Cytoplasmic sequestration of rel proteins by IκBα requires CRM1-dependent nuclear export. *Molecular and cellular biology,* 20**,** 2269-2284.

TEGOWSKI, M. & BALDWIN, A. 2018. Noncanonical NF-κB in Cancer. *Biomedicines,* 6**,** 66-66.

THOMSON, E., FERREIRA-CERCA, S. & HURT, E. 2013. Eukaryotic ribosome biogenesis at a glance. *Journal of Cell Science,* 126**,** 4815-4821.

TOMECKI, R., SIKORSKI, P. J. & ZAKRZEWSKA-PLACZEK, M. 2017. Comparison of preribosomal RNA processing pathways in yeast, plant and human cells–focus on coordinated action of endo-and exoribonucleases. *FEBS letters,* 591**,** 1801-1850.

TRAGNI, V., PREZIUSI, F., LAERA, L., ONOFRIO, A., MERCURIO, I., TODISCO, S., VOLPICELLA, M., DE GRASSI, A. & PIERRI, C. L. 2022. Modeling SARS-CoV-2 spike/ACE2 protein–protein interactions for predicting the binding affinity of new spike variants for ACE2, and novel ACE2 structurally related human protein targets, for COVID-19 handling in the 3PM context. *EPMA Journal,* 13**,** 149-175.

TRUHLAR, S. M. E., MATHES, E., CERVANTES, C. F., GHOSH, G. & KOMIVES, E. A. 2008. Pre-folding IκBα Alters Control of NF-κB Signaling. *Journal of Molecular Biology,* 380**,** 67-82.

TUCKER, E., O'DONNELL, K., FUCHSBERGER, M., HILTON, A. A., METCALF, D., GREIG, K., SIMS, N. A., QUINN, J. M., ALEXANDER, W. S., HILTON, D. J., KILE, B. T., TARLINTON, D. M. & STARR, R. 2007. A Novel Mutation in the Nfkb2 Gene Generates an NF-κB2 "Super Repressor"1. *The Journal of Immunology,* 179**,** 7514-7522.

VACCA, A., FELLI, M. P., PALERMO, R., DI MARIO, G., CALCE, A., DI GIOVINE, M., FRATI, L., GULINO, A. & SCREPANTI, I. 2006. Notch3 and pre-TCR interaction unveils distinct NF-κB pathways in T-cell development and leukemia. *The EMBO Journal,* 25**,** 1000-1008.

VALDAR, W. S. J. & THORNTON, J. M. 2001. Protein–protein interfaces: Analysis of amino acid conservation in homodimers. *Proteins: Structure, Function, and Bioinformatics,* 42**,** 108-124.

VALENZUELA, D., CHAUDHURI, A. & MAITRA, U. 1982. Eukaryotic ribosomal subunit anti-association activity of calf liver is contained in a single polypeptide chain protein of Mr= 25,500 (eukaryotic initiation factor 6). *Journal of Biological Chemistry,* 257**,** 7712-7719.

VAN ANTWERP, D. J., MARTIN, S. J., KAFRI, T., GREEN, D. R. & VERMA, I. M. 1996. Suppression of TNF-α-Induced Apoptosis by NF-κB. *Science,* 274**,** 787-789.

VAN RIGGELEN, J., YETIL, A. & FELSHER, D. W. 2010. MYC as a regulator of ribosome biogenesis and protein synthesis. *Nature Reviews Cancer,* 10**,** 301-301.

VAN ZUNDERT, G. C. P., RODRIGUES, J., TRELLET, M., SCHMITZ, C., KASTRITIS, P. L., KARACA, E., MELQUIOND, A. S. J., VAN DIJK, M., DE VRIES, S. J. & BONVIN, A. 2016. The HADDOCK2.2 Web Server: User-Friendly Integrative Modeling of Biomolecular Complexes. *J Mol Biol,* 428**,** 720-725.

VAN UDEN, P., KENNETH, NIALL S. & ROCHA, S. 2008. Regulation of hypoxia-inducible factor-1α by NF-κB. *Biochemical Journal,* 412**,** 477-484.

VANGONE, A. & BONVIN, A. M. J. J. 2017. PRODIGY: A Contact-based Predictor of Binding Affinity in Protein-protein Complexes. *Bio-protocol,* 7**,** e2124.

VAQUERIZAS, J. M., KUMMERFELD, S. K., TEICHMANN, S. A. & LUSCOMBE, N. M. 2009. A census of human transcription factors: function, expression and evolution. *Nature Reviews Genetics,* 10**,** 252-263.

VATSYAYAN, J., QING, G., XIAO, G. & HU, J. 2008. SUMO1 modification of NF-kappaB2/p100 is essential for stimuli-induced p100 phosphorylation and processing. *EMBO reports,* 9**,** 885-890.

VERHOEVEN, Y., TILBORGHS, S., JACOBS, J., DE WAELE, J., QUATANNENS, D., DEBEN, C., PRENEN, H., PAUWELS, P., TRINH, X. B. & WOUTERS, A. The potential and controversy of targeting STAT family members in cancer. Seminars in cancer biology, 2020. Elsevier, 41-56.

VIATOUR, P., DEJARDIN, E., WARNIER, M., LAIR, F., CLAUDIO, E., BUREAU, F., MARINE, J.-C., MERVILLE, M.-P., MAURER, U. & GREEN, D. 2004a. GSK3-mediated BCL-3 phosphorylation modulates its degradation and its oncogenicity. *Molecular cell,* 16**,** 35-45.

VIATOUR, P., MERVILLE, M.-P., BOURS, V. & CHARIOT, A. 2004b. Protein Phosphorylation as a Key Mechanism for the Regulation of BCL-3 Activity. *Cell Cycle,* 3**,** 1498-1501.

VIZCAÍNO, C., MANSILLA, S. & PORTUGAL, J. 2015. Sp1 transcription factor: A long-standing target in cancer chemotherapy. *Pharmacology & Therapeutics,* 152**,** 111-124.

VOUSDEN, K. H. & PRIVES, C. 2009. Blinded by the Light: The Growing Complexity of p53. *Cell,* 137**,** 413-431.

WAKEFIELD, A., SOUKUPOVA, J., MONTAGNE, A., RANGER, J., FRENCH, R., MULLER, W. J. & CLARKSON, R. W. 2013. Bcl3 Selectively Promotes Metastasis of ERBB2-Driven Mammary TumorsBcl3 in Mammary Tumors. *Cancer research,* 73**,** 745-755.

WALLS, D. & LOUGHRAN, S. T. 2011. Tagging Recombinant Proteins to Enhance Solubility and Aid Purification. *In:* WALLS, D. & LOUGHRAN, S. T. (eds.) *Protein Chromatography: Methods and Protocols.* Totowa, NJ: Humana Press.

WANG, B., GAO, J., ZHAO, Z., ZHONG, X., CUI, H., HOU, H., ZHANG, Y., ZHENG, J., DI, J. & LIU, Y. 2022. Identification of a small-molecule RPL11 mimetic that inhibits tumor growth by targeting MDM2-p53 pathway. *Mol Med,* 28**,** 109.

WANG, M. & PESTOV, D. G. 2011. 5'-end surveillance by Xrn2 acts as a shared mechanism for mammalian pre-rRNA maturation and decay. *Nucleic acids research,* 39**,** 1811-1822.

WANG, VIVIEN Y.-F., HUANG, W., ASAGIRI, M., SPANN, N., HOFFMANN, A., GLASS, C. & GHOSH, G. 2012. The Transcriptional Specificity of NF-κB Dimers Is Coded within the κB DNA Response Elements. *Cell Reports,* 2**,** 824-839.

WANG, V. Y.-F., LI, Y., KIM, D., ZHONG, X., DU, Q., GHASSEMIAN, M. & GHOSH, G. 2017. Bcl3 Phosphorylation by Akt, Erk2, and IKK Is Required for Its Transcriptional Activity. *Molecular Cell,* 67**,** 484-497.e5.

WANG, Y., CORTEZ, D., YAZDI, P., NEFF, N., ELLEDGE, S. J. & QIN, J. 2000. BASC, a super complex of BRCA1-associated proteins involved in the recognition and repair of aberrant DNA structures. *Genes Dev,* 14**,** 927-39.

WANG, Z., SICINSKI, P., WEINBERG, R. A., ZHANG, Y. & RAVID, K. 1996. Characterization of the mouse cyclin D3 gene: exon/intron organization and promoter activity. *Genomics,* 35**,** 156-163.

WARNER, J. R. & MCINTOSH, K. B. 2009. How common are extraribosomal functions of ribosomal proteins? *Molecular cell,* 34**,** 3-11.

WEBER, H. O., SAMUEL, T., RAUCH, P. & FUNK, J. O. 2002. Human p14(ARF)-mediated cell cycle arrest strictly depends on intact p53 signaling pathways. *Oncogene,* 21**,** 3207-12.

WELLS, G. R., WEICHMANN, F., COLVIN, D., SLOAN, K. E., KUDLA, G., TOLLERVEY, D., WATKINS, N. J. & SCHNEIDER, C. 2016. The PIN domain endonuclease Utp24 cleaves pre-ribosomal RNA at two coupled sites in yeast and humans. *Nucleic acids research,* 44**,** 5399-5409.

WELLS, G. R., WEICHMANN, F., SLOAN, K. E., COLVIN, D., WATKINS, N. J. & SCHNEIDER, C. 2017. The ribosome biogenesis factor yUtp23/hUTP23 coordinates key interactions in the yeast and human pre-40S particle and hUTP23 contains an essential PIN domain. *Nucleic Acids Research,* 45**,** 4796-4809.

WELLS, J. A. 1991. [18] Systematic mutational analyses of protein-protein interfaces. *Methods in Enzymology.* Academic Press.

WESTERHEIDE, S. D., MAYO, M. W., ANEST, V., HANSON, J. L. & BALDWIN JR, A. S. 2001. The putative oncoprotein Bcl-3 induces cyclin D1 to stimulate G1 transition. *Molecular and cellular biology,* 21**,** 8428-8436.

WESTERMARCK, J., IVASKA, J. & CORTHALS, G. L. 2013. Identification of Protein Interactions Involved in Cellular Signaling. *Molecular & Cellular Proteomics,* 12**,** 1752-1763.

WILLERS, H., MCCARTHY, E. E., WU, B., WUNSCH, H., TANG, W., TAGHIAN, D. G., XIA, F. & POWELL, S. N. 2000. Dissociation of p53-mediated suppression of homologous recombination from G1/S cell cycle checkpoint control. *Oncogene,* 19**,** 632-639.

WILLIAMS, G. H. & STOEBER, K. 2012. The cell cycle and cancer. *J Pathol,* 226**,** 352-64.

WILLIAMS, L. M., FUESS, L. E., BRENNAN, J. J., MANSFIELD, K. M., SALAS-RODRIGUEZ, E., WELSH, J., AWTRY, J., BANIC, S., CHACKO, C., CHEZIAN, A., DOWERS, D., ESTRADA, F., HSIEH, Y. H., KANG, J., LI, W., MALCHIODI, Z., MALINOWSKI, J., MATUSZAK, S., MCTIGUE, T. T., MUELLER, D., NGUYEN, B., NGUYEN, M., NGUYEN, P., NGUYEN, S., NJOKU, N., PATEL, K., PELLEGRINI, W., PLIAKAS, T., QADIR, D., RYAN, E., SCHIFFER, A., THIEL, A., YUNES, S. A., SPILIOS, K. E., PINZÓN, C. J., MYDLARZ, L. D. & GILMORE, T. D. 2018. A conserved Toll-like receptor-to-NF-κB signaling pathway in the endangered coral Orbicella faveolata. *Dev Comp Immunol,* 79**,** 128-136.

WILLIAMS, L. M. & GILMORE, T. D. 2020. Looking Down on NF-κB. *Molecular and Cellular Biology,* 40**,** e00104-20.

XAVIER, R. J. & PODOLSKY, D. K. 2007. Unravelling the pathogenesis of inflammatory bowel disease. *Nature,* 448**,** 427-434.

XIAO, G., FONG, A. & SUN, S.-C. 2004. Induction of p100 Processing by NF-κB-inducing Kinase Involves Docking IκB Kinase α (IKKα) to p100 and IKKα-mediated Phosphorylation. *Journal of Biological Chemistry,* 279**,** 30099-30105.

XIAO, G., HARHAJ, E. W. & SUN, S.-C. 2001. NF-κB-Inducing Kinase Regulates the Processing of NF-κB2 p100. *Molecular Cell,* 7**,** 401-409.

XU, J., ZHOU, P., WANG, W., SUN, A. & GUO, F. 2014. RelB, together with RelA, sustains cell survival and confers proteasome inhibitor sensitivity of chronic lymphocytic leukemia cells from bone marrow. *J Mol Med (Berl),* 92**,** 77-92.

YANG, K., YANG, J. & YI, J. 2018. Nucleolar Stress: hallmarks, sensing mechanism and diseases. *Cell Stress,* 2**,** 125-140.

YANG, X. D. & SUN, S. C. 2015. Targeting signaling factors for degradation, an emerging mechanism for TRAF functions. *Immunological reviews,* 266**,** 56-71.

YAO, Z., XING, L. & BOYCE, B. F. 2009. NF-κB p100 limits TNF-induced bone resorption in mice by a TRAF3-dependent mechanism. *The Journal of clinical investigation,* 119**,** 3024-3034.

YIN, L., WU, L., WESCHE, H., ARTHUR, C. D., WHITE, J. M., GOEDDEL, D. V. & SCHREIBER, R. D. 2001. Defective lymphotoxin-beta receptor-induced NF-kappaB transcriptional activity in NIK-deficient mice. *Science,* 291**,** 2162-5.

YIN, R., FENG, B. Y., VARSHNEY, A. & PIERCE, B. G. 2022. Benchmarking AlphaFold for protein complex modeling reveals accuracy determinants. *Protein Science,* 31**,** e4379.

YU, H., LIN, L., ZHANG, Z., ZHANG, H. & HU, H. 2020. Targeting NF-κB pathway for the therapy of diseases: mechanism and clinical study. *Signal Transduction and Targeted Therapy,* 5**,** 209.

ZACHARIAS, M. 2010. Accounting for conformational changes during protein–protein docking. *Current Opinion in Structural Biology,* 20**,** 180-186.

ZHANG, H., LIU, J., DANG, Q., WANG, X., CHEN, J., LIN, X., YANG, N., DU, J., SHI, H., LIU, Y. & HAN, J. 2022. Ribosomal protein RPL5 regulates colon cancer cell proliferation and migration through MAPK/ERK signaling pathway. *BMC Mol Cell Biol,* 23**,** 48.

ZHANG, J., CLARK, K., LAWRENCE, T., PEGGIE, M. W. & COHEN, P. 2014. An unexpected twist to the activation of IKKβ: TAK1 primes IKKβ for activation by autophosphorylation. *The Biochemical journal,* 461**,** 531-537.

ZHANG, J., WARREN, M. A., SHOEMAKER, S. F. & IP, M. M. 2007. NFκB1/p50 is not required for tumor necrosis factor-stimulated growth of primary mammary epithelial cells: implications for NFκB2/p52 and RelB. *Endocrinology,* 148**,** 268-278.

ZHANG, Q., DIDONATO, J. A., KARIN, M. & MCKEITHAN, T. W. 1994. BCL3 encodes a nuclear protein which can alter the subcellular location of NF-kappa B proteins. *Mol Cell Biol,* 14**,** 3915-26.

ZHANG, Q. C., DENG, L., FISHER, M., GUAN, J., HONIG, B. & PETREY, D. 2011. PredUs: a web server for predicting protein interfaces using structural neighbors. *Nucleic Acids Res,* 39**,** W283-7.

ZHANG, S. Q., KOVALENKO, A., CANTARELLA, G. & WALLACH, D. 2000. Recruitment of the IKK signalosome to the p55 TNF receptor: RIP and A20 bind to NEMO (IKKγ) upon receptor stimulation. *Immunity,* 12**,** 301-311.

ZHANG, W., HUI, K. Y., GUSEV, A., WARNER, N., NG, S. M. E., FERGUSON, J., CHOI, M., BURBERRY, A., ABRAHAM, C., MAYER, L., DESNICK, R. J., CARDINALE, C. J.,

HAKONARSON, H., WATERMAN, M., CHOWERS, Y., KARBAN, A., BRANT, S. R., SILVERBERG, M. S., GREGERSEN, P. K., KATZ, S., LIFTON, R. P., ZHAO, H., NUÑEZ, G., PE'ER, I., PETER, I. & CHO, J. H. 2013. Extended haplotype association study in Crohn's disease identifies a novel, Ashkenazi Jewish-specific missense mutation in the NF-κB pathway gene, HEATR3. *Genes and Immunity,* 14**,** 310-316.

ZHANG, Y., HE, X., ZHAI, J., JI, B., MAN, V. H. & WANG, J. 2021. In silico binding profile characterization of SARS-CoV-2 spike protein and its mutants bound to human ACE2 receptor. *Briefings in Bioinformatics,* 22**,** bbab188.

ZHENG, J., LANG, Y., ZHANG, Q., CUI, D., SUN, H., JIANG, L., CHEN, Z., ZHANG, R., GAO, Y., TIAN, W., WU, W., TANG, J. & CHEN, Z. 2015. Structure of human MDM2 complexed with RPL11 reveals the molecular basis of p53 activation. *Genes Dev,* 29**,** 1524-34.

ZHOU, B.-B. S. & ELLEDGE, S. J. 2000. The DNA damage response: putting checkpoints in perspective. *Nature,* 408**,** 433-439.

ZHOU, X., LIAO, W.-J., LIAO, J.-M., LIAO, P. & LU, H. 2015. Ribosomal proteins: functions beyond the ribosome. *Journal of Molecular Cell Biology,* 7**,** 92-104.